Investigating the Colonisation of Voice Prostheses by *Candida albicans* Following Total Laryngectomy

Daniel R. Pentland

Thesis submitted to the University of Kent for the Degree of PhD in Cell Biology

Declaration

No part of this thesis has been submitted in support of an application for any degree or other qualification at the University of Kent, or any other University or Institution of learning.



Daniel R. Pentland

September 2019

Acknowledgements

I would like to thank Dr. Campbell Gourlay and Prof. Fritz Mühlschlegel for the opportunity to work on this PhD project and for their outstanding support and guidance. Dr. Campbell Gourlay has been an excellent mentor throughout my PhD; he has offered an enormous amount of insight, patience and encouragement. I would like to express my gratitude to him for inspiring me and making my PhD a wonderful experience.

I want to thank my friends and colleagues in the Kent Fungal Group and the School of Biosciences who have helped me in so many ways and made it a privilege to be part of this laboratory. I would also like to say a huge thank you to Hannah Chapman, who has supported me through ups and downs, listened to a ridiculous amount of practice presentations and always offered invaluable advice.

Finally, I want to thank the Kent Cancer Trust along with the University of Kent 50th Anniversary Scholarship Scheme for providing the financial support for this project.

Abstract

A total laryngectomy is a surgical procedure for the treatment of advanced laryngeal cancer. The vocal cords are removed during the procedure, leaving patients with an inability to form speech. The gold standard of speech rehabilitation involves the use of small silicone valves called voice prostheses (VPs) which are inserted into the throat. *C. albicans* is a major coloniser of VPs, often being found in polymicrobial biofilms, causing loss of device function as well as creating a reservoir for infections. As a result, VPs have to be regularly changed at great patient stress and clinical cost. In this study, we present precision antifungal-focussed treatment guidelines which significantly increase VP *in situ* lifespan from a mean of 71.9 to 192.0 days, a 2.7-fold increase, in a 20 patient cohort. In addition, we find that the high CO_2 environment of the throat (due to the CO_2 content of exhaled breath) increases the biofilm-forming capacity of *C. albicans*. All stages of biofilm growth (attachment, maturation and dispersal) are enhanced in 5% CO_2 and this is accompanied by increased antifungal tolerance; providing a possible explanation for the success of *C. albicans* in the VP niche. Finally, we explore potential treatment options for high CO_2 biofilms, identifying the glycolytic inhibitor 2-deoxyglucose as a promising candidate. Overall, our study characterises a clinically relevant CO_2-mediated increase in *C. albicans* biofilm formation which could influence future biofilm studies and therapeutic discovery.

Abbreviations

2-DG	2-deoxyglucose
AFR	amyloid forming region
Als	agglutinin-like sequence
ATG	antifungal treatment guidelines
ATP	adenosine triphosphate
C. albicans	*Candida albicans*
C. dubliniensis	*Candida dubliniensis*
C. elegans	*Caenorhabditis elegans*
C. glabrata	*Candida glabrata*
C. krusei	*Candida krusei*
C. parapsilosis	*Candida parapsilosis*
C. tropicalis	*Candida tropicalis*
cAMP	cyclic adenosine monophosphate
CFSTR	continuous flow stirred tank reactor
CFU	colony forming unit
CO_2	carbon dioxide
CSLM	confocal scanning laser microscopy
DBS	donor bovine serum
DMSO	dimethyl sulfoxide
DNA	deoxyribonucleic acid
ECM	extracellular matrix
eDNA	extracellular DNA
EKHUFT	East Kent Hospitals University Foundation Trust
ERCC	external RNA controls consortium
EV	extracellular vesicles
FBS	foetal bovine serum
FDR	false discovery rate
FITC	fluorescein isothiocyanate
GAP	GTPase activating protein
GEF	guanosine exchange factor
GO	gene ontology
GPI	glycophosphatidylinositol
GSEA	gene set enrichment analysis
GTP	guanosine triphosphate
H_2O	water
HSGs	hyphal-specific genes
MAPK	mitogen activated protein kinase
MDT	multidisciplinary team
MIC	minimum inhibitory concentration

MQ	milliQ
mRNA	messenger ribonucleic acid
NHS	National Health Service
OD	optical density
OPC	oropharyngeal candidiasis
P. aeruginosa	*Pseudomonas aeruginosa*
PBC	peptide binding cavity
PBS	phosphate-buffered saline
PCA	principal component analysis
PCR	polymerase chain reaction
PDMS	polydimethylsiloxane
PFR	plug flow reactor
PKA	protein kinase A
RA	Ras association
RHE	reconstituted human epithelia
RIN	RNA integrity number
RNA	ribonucleic acid
rpm	rotations per minute
RPMI-1640	Roswell Park Memorial Institute 1640 (media)
S. aureus	*Staphylococcus aureus*
S. cerevisiae	*Saccharomyces cerevisiae*
SMIC	sessile minimum inhibitory concentration
TEP	tracheoesophageal puncture
TFKO	transcription factor knockout
VP	voice prosthesis
VVC	vulvovaginal candidiasis
YPD	yeast extract peptone dextrose

Contents

Abbreviations iv

1 Introduction 2

1.1 *Candida albicans* 2

1.1.1 Genetics of *C. albicans* 3

1.1.2 Life cycle of *C. albicans* 4

1.1.3 Pathogenicity of *C. albicans* 8

1.1.4 Iron homeostasis in *C. albicans* 10

1.1.4.1 *C. albicans* iron acquisition mechanisms 11

1.1.4.2 Regulation of *C. albicans* iron homeostasis 14

1.2 *Candida albicans* Morphogenesis and Signalling Pathways 17

1.2.1 The Ras1-Cyr1-PKA pathway 18

1.2.2 The MAP kinase pathway 24

1.2.3 Alternative pathways driving the yeast-to-hyphae switch 25

1.2.4 Negative regulation of the yeast-to-hyphae switch 26

1.3 *Candida albicans* Biofilms 27

1.3.1 Stages of *C. albicans* biofilm formation 28

1.3.2 Regulation of *C. albicans* biofilm formation 31

1.3.3 Antimicrobial tolerance within *C. albicans* biofilms 36

1.3.4 Current treatment strategies for *C. albicans* biofilms 42

1.3.5 Models used to study biofilms 44

1.4 Laryngeal Cancer, Laryngectomies and Voice Prostheses 48

1.4.1 Laryngectomies and voice prostheses 49

1.4.2 Microbial colonisation of voice prostheses 51

1.4.3 Current strategies for the prevention of microbial colonisation of voice prostheses 53

1.5 Aims of this Study 56

2 Paper 1 – Precision antifungal treatment significantly extends voice prosthesis lifespan in patients following total laryngectomy 57

2.1 Author Contributions 58

2.2 Abstract 60

2.3 Introduction 61

2.4 Materials and Methods 66

2.4.1 Patient cohort and voice prostheses 66

2.4.2 Microorganism isolation and identification 66

2.4.3 MALDI-ToF mass spectrometry identification of microorganisms 67

2.4.4 Antifungal sensitivity testing 67

2.4.5 Antibacterial sensitivity testing 68

2.4.6 Scanning electron microscopy (SEM) of voice prosthesis surfaces 68

2.4.7 Atomic force microscopy (AFM) of voice prosthesis surfaces 68

2.4.8 *Candida* strains and growth media 69

2.4.9 *In vitro* biofilm growth assays 69

2.4.10 Biofilm quantification via XTT assay 70

2.4.11 Antifungal treatment of biofilms 71

2.4.12 Mixed species biofilm competition assays 71

2.4.13 Biofilm composition analysis via chromogenic agar 72

2.4.14 Analysis of voice prosthesis lifespans 72

2.4.15 Treatment guideline approval 73

2.4.16 Study approval 73

2.5 Results 74

2.5.1 Analysis of bacterial species found on early failing voice prostheses 74

2.5.2 Analysis of fungal species found on early failing voice prostheses 77

2.5.3 Co-isolation frequencies of different species from early failing voice prostheses 79

2.5.4 Factors promoting microbial colonisation of voice prostheses 81

2.5.5 *C. parapsilosis* does not have a competitive advantage over *C. albicans* in biofilm establishment 84

2.5.6 Antimicrobial sensitivity of clinical isolates 85

2.5.7 Antifungal sensitivity of *C. albicans* clinical isolates within biofilms 90

2.5.8 Development and clinical testing of antifungal treatment guidelines (ATG) to extend VP lifespan 92

2.6 Discussion 99

2.6.1 *C. albicans* is the most prevalent fungi isolated from early failing VPs 99

2.6.2 Antifungal sensitivity testing of biofilm-associated cells 102

2.6.3 Precision antifungal treatment guidelines significantly increase VP Lifespans 103

2.7 Supplementary Materials 106

3 Paper 2 – CO_2 enhances *Candida albicans* biofilm formation and reveals novel approaches to their inhibition 112

3.1 Author Contributions 113

3.2 Abstract 114

3.3 Introduction 115

3.4 Materials and Methods 120

3.4.1 *Candida* strains and growth media 120

3.4.2 *In vitro* biofilm growth assays 120

3.4.3 Biofilm quantification via XTT assay 121

3.4.4 *C. albicans* transcription factor knockout (TFKO) screen 121

3.4.5 Iron starvation of *C. albicans* biofilms 121

3.4.6 Preparation of PDMS-coated microscope slides 122

3.4.7 Preparation of *C. albicans* biofilms on silicone coated slides for microscopy 123

3.4.8 Confocal scanning laser microscopy (CSLM) of *C. albicans* biofilms on silicone slides 123

3.4.9 RNA isolation from *C. albicans* biofilms 124

3.4.10 Library Preparation and RNA Sequencing 125

3.4.11 Analysis of RNA-Seq data 126

3.4.12 Gene Set Enrichment Analysis of transcription profiles 126

3.4.13 Antifungal treatment of *C. albicans* biofilms 127

3.4.14 *C. albicans* attachment assay 128

3.4.15 2-deoxyglucose (2-DG) treatment of *C. albicans* biofilms 128

3.4.16 *C. albicans* biofilm dispersion assay 128

3.5 Results 130

3.5.1 High CO_2 increases *C. albicans* biofilm growth 130

3.5.2 Analysis of the effect of CO_2 on phases of *C. albicans* biofilm growth 132

3.5.3 Identification of the regulatory mechanisms that govern CO_2

acceleration of *C. albicans* biofilm formation 135

3.5.4 Transcriptome analysis of *C. albicans* biofilms grown in high and low CO_2 142

3.5.5 CO_2 elevation enhances azole tolerance in *C. albicans* biofilms 149

3.5.6 Precision approaches to overcome CO_2 acceleration of *C. albicans* biofilm formation 151

3.6 Discussion 154

3.6.1 Physiological CO_2 levels increase *C. albicans* biofilm formation 154

3.6.2 *C. albicans* biofilms grown in 5% CO_2 exhibit increased drug tolerance ... 157

3.6.3 CO_2 and iron homeostasis in *C. albicans* biofilms 158

3.7 Supplementary Materials 162

4 Discussion 175

4.1 Polymicrobial Nature of Voice Prosthesis Biofilms 175

4.2 Physiological Levels of CO_2 (5%) Enhance the Biofilm-Forming Ability of *Candida albicans* 180

4.2.1 The effect of high CO_2 on *C. albicans* biofilm growth relies on the adenylate cyclase Cyr1 182

4.2.2 CO_2 and iron homeostasis in *C. albicans* biofilms 184

4.3 Potential Therapeutic Options to Combat *Candida albicans* Biofilms 187

4.4 *Candida albicans* Biofilm Formation on Other Medical-Implant Devices 189

4.5 Future Investigations 190

References 192

Appendix 1 – Quality control analysis of RNA-Seq reads 217

Appendix 2 – Ranked GSEA gene set lists 223

Introduction

1.0 Introduction

Modern medicine has seen an increase in the development and use of indwelling medical devices such as voice prostheses (VPs), catheters, dentures, tracheostomy tubes and many others. The use of such devices, on either a temporary or permanent basis, has prolonged and improved the quality of life for numerous patients. However, a common complication surrounding the use of indwelling devices is their susceptibility to colonisation by microorganisms, often leading to device failure as well as providing a reservoir of potential pathogens. Indeed, it has been estimated that 60-70% of nosocomial infections are associated with medical devices [1]. Colonisation of an indwelling medical device normally requires device removal sometimes accompanied with antimicrobial therapy, making medical device management and infection prevention very expensive. A variety of microorganisms, both bacterial and fungal, have been observed to colonise medical devices. For instance, *Staphylococcus aureus* and *Staphylococcus epidermidis* commonly colonise central venous catheters [2], while *Escherichia coli* is a prevalent coloniser of urinary catheters [3]. *Candida* species, particularly *Candida albicans*, are widespread fungal colonisers of many medical devices including voice prostheses, central venous catheters, dentures, tracheostomy tubes, and urinary catheters [4].

1.1 *Candida albicans*

C. albicans is a member of the *Saccharomycetaceae* family of ascomycete fungi and is distantly related to the prototypical yeast species *Saccharomyces cerevisiae* [5]. *C. albicans* is a commensal organism located on the mucosal surfaces of the oral cavity, gastrointestinal tract and genitourinary tract of most healthy individuals [6][7]. Despite being a commensal

organism, it is also an opportunistic pathogen [6][8]; in fact, it is the most widespread of all the human fungal pathogens [9]. Infection with *C. albicans* is particularly a problem among immunocompromised individuals or persons with implanted medical devices such as catheters or voice prostheses [10][11].

1.1.1 Genetics of *C. albicans*

C. albicans has a diploid genome of approximately 32Mb which is divided between eight pairs of chromosomes [12]. Within this diploid genome there are several genes which have homologues in *S. cerevisiae*, however, there are also numerous other genes with no *S. cerevisiae* homologues [6]. These genes with no obvious *S. cerevisiae* homolog are thought to be promising candidate genes essential for human interactions. This is because the majority of *S. cerevisiae* strains are not able to adhere to, or invade, human tissues. The products of these genes, especially those of genes which also do not have human homologues, could represent favourable targets for antifungal therapies [6].

An unusual characteristic of the *C. albicans* genome is the fact that the CUG codon encodes serine instead of leucine [13]. Species which have this abnormality within their genetic code are grouped into the CUG clade. Alongside *C. albicans* in this clade are other pathogenic *Candida* species such as *Candida parapsilosis* and *Candida tropicalis* [14].

It has been reported that clinical isolates of *C. albicans* exhibit a variable karyotype [15]. This phenomenon was first described by Magee and Magee in 1987 [12]. Changes in karyotype have been proposed as a mechanism to survive in conditions of stress, for instance, strains of *C. albicans* growing on L-sorbose often lose one of their chromosome 5s. Upon return to a

glucose-containing medium, the remaining chromosome 5 is replicated, restoring the number of chromosomes to normal [16]. Likewise, strains which are resistant to fluconazole (a triazole antifungal often used to treat *C. albicans* infections) tend to have higher occurrence of loss of chromosome 4 or gain of chromosome 3 [17]. Janbon, G. et al. suggest that the genome of *C. albicans* contains a reservoir of genes whose expression is governed by chromosome number [16]. These genes could regulate crucial functions, such as alternative carbon source utilisation, which become necessary under certain stress conditions.

1.1.2 Life cycle of *C. albicans*

Candida albicans was traditionally considered to be asexual, only existing as an obligate diploid [18]. However, it has now been discovered that mating occurs between diploid mating type-like (*MTL*) **a** and α strains in this organism, producing an **a**/α tetraploid product [18]. While this is similar to the mating program in *Saccharomyces cerevisiae* (two haploid mating types; **a** and α which combine to generate an **a**/α diploid product) [19] it differs in several key respects.

Mating in *C. albicans* is reliant on a reversible phenotypic switch between two states termed 'white' and 'opaque'. Only the 'opaque' state is capable of mating efficiently; 'opaque' cells have been demonstrated to mate approximately 10^6 fold more readily than 'white' cells [20]. 'White' cells are fairly round and form white, dome-shaped colonies on solid agar, they also express a specific set of genes. In contrast, 'opaque' cells tend to be larger and more oblong, forming darker colonies which grow flatter against solid agar. 'Opaque' cells also express a specific set of genes which differ from those expressed in 'white' cells [21].

This unusual mating program involving a reversible phenotypic switch hitherto seems to be unique to *C. albicans* as well as the very closely related fungal species *Candida dubliniensis* [22]. It appears that 'white' cells are better suited for growth and survival within a mammalian host; 'opaque' cells are unstable at temperatures above 35°C and primarily colonise skin [23]. Therefore, it is likely this unusual mating program has evolved to allow *Candida albicans* to survive the variety of environments within a mammalian host while still being able to produce mating-competent cells [20].

Only *C. albicans* cells which are homozygous at the *MTL* locus (**a**/**a** or α/α) are capable of reversibly switching between 'white' and 'opaque' states, and are thus capable of efficient mating [18]. This is because two homeodomain proteins called Mtla1 and Mtlα2, encoded by the *MTLa* and *MTLα* alleles respectively (Figure 1.1), work together to inhibit white-opaque switching [20]. These proteins are both present in *MTL* heterozygous cells (**a**/α) and thus white-opaque switching cannot occur, only one of these two proteins is present in *MTL* homozygous cells, meaning white-opaque switching is not suppressed and mating (between **a**/**a** cells and α/α cells) can take place. Since the *MTL* locus controls both white-opaque switching and the mating type of *C. albicans* cells, it ensures switching only occurs in mating-competent cells, i.e. does not occur in *MTL* heterozygous cells since these cells are not capable of mating anyway [24]. It is important to note that only certain *C. albicans* strains, such as strain WO-1, exhibit efficient white-opaque switching; the common laboratory strain CAl4 does not switch (it is fixed in the 'white' state) because it is *MTL* heterozygous [20]. It has however been demonstrated that CAl4 **a** and α strains, generated from directed mutagenesis of the *MTLα1* and *MTLα2* or *MTLa1* genes respectively, are capable of white-opaque switching and subsequent mating [20].

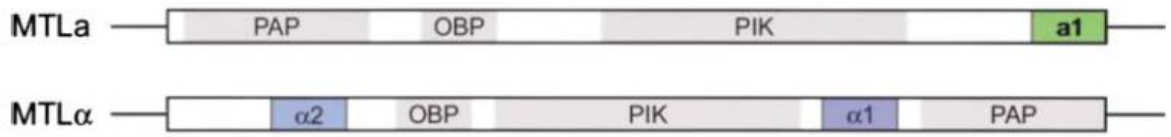


Figure 1.1: The Mating-type like (*MTL*) locus of *Candida albicans*. The *MTLa* allele is made up of 8746 base pairs and encodes four different proteins, the Mtla1 protein (gene abbreviated to a1 in the figure) is an important homeodomain protein associated with white-opaque switching. The *MTLα* allele is made up of 8861 base pairs and encodes five different proteins, the homeodomain protein Mtlα2 and another transcriptional regulatory protein Mtlα1 (gene abbreviated to α2 and α1 respectively in the figure) are also crucial in white-opaque switching. **Key:** PAP – poly(A) polymerase, PIK – phosphatidyl inositol kinase, OBP – protein with similar sequences to oxysterol binding proteins. *Figure adapted from Figure 1 in Miller, M. et al.* [20].

In the life cycle of *Saccharomyces cerevisiae*, the **a**/α diploid product of mating returns to a haploid state through meiosis [19]. However, there does not appear to be a meiosis step in the life cycles of *Candida* species, despite the presence of a number of genes in the genome which are homologous to genes involved in meiosis in *S. cerevisiae* [24]. Instead, the tetraploid *Candida albicans* offspring employs a parasexual mechanism to return to a normal diploid state [24]. This involves the random and cooperative loss of chromosomes, resulting in genetically varied progeny with a range of phenotypes [18].

Furthermore, Forche, A. *et al.* discovered that, although meiosis does not occur in *Candida albicans*, recombination between homologous chromosomes does. The recombination relies upon Spo11, a highly conserved protein which is responsible for the formation of double-strand DNA breaks during conventional meiosis in eukaryotes. This genetic recombination carried out by Spo11 during the parasexual cycle of *Candida albicans* is likely to have evolved to increase genetic diversity without the need for meiosis [18].

A key trait of *C. albicans* is its ability to grow as a biofilm upon both biotic and abiotic surfaces (see Section 1.3); this is crucial to the success of *C. albicans* in colonising medical devices such as voice prostheses. *MTL* homozygous 'opaque' cells only form very thin and fragile biofilms [25], whereas *MTL* homozygous 'white' cells form robust biofilms with similar architecture to *MTL* heterozygous biofilms [26]. Despite the similar architecture, *MTL* homozygous 'white' biofilms display unique pathogenic characteristics. **a**/α biofilms are impermeable to molecules ranging from 300Da to 140kDa, impenetrable to polymorphonuclear leukocytes, and tolerant to antifungals. However, the opposite is true for **a**/**a** or α/α biofilms [26]. Clinically this implies biofilms composed of mating-competent cells could be easier to treat and may not persist in the host as long as **a**/α biofilms. Consistent with this, natural *C. albicans* **a**/α strains exhibit increased virulence and competitive fitness in a mouse model for systemic infection compared to their spontaneous *MTL* homozygous offspring [27].

Interestingly, biofilm formation is regulated by different signalling pathways in *MTL* homozygous and heterozygous cells. **a**/α biofilms are regulated by the Ras1-Cyr1-PKA pathway (see Section 1.2.1) whereas **a**/**a** and α/α biofilms are regulated by the MAP kinase pathway (see Section 1.2.2) [26]. The MAP kinase pathway also regulates the pheromone response during mating and it has been shown that α-pheromone induces 'white' **a**/**a** cells to attach to plastic and silicone surfaces and promotes biofilm maturation [25]. Moreover, the addition of 10% of 'opaque' cells (in a 50:50 ratio of **a**/**a** and α/α) to majority *MTL* homozygous 'white' cells increases biofilm development by up to 59% [25]. It has been hypothesised that biofilms mostly composed of 'white' cells facilitate the mating between minority 'opaque' cells embedded in the matrix by protecting pheromone gradients that direct chemotropism

during the mating process. This could be the reason 'white' cells respond to mating pheromones even though they themselves cannot efficiently mate [25].

1.1.3 Pathogenicity of *C. albicans*

As previously stated, *C. albicans* is the most widespread, and hence the most important, of all the human fungal pathogens [9]. Although it is normally a harmless member of normal human microflora (it is present on the skin and mucosal surfaces of 30-70% of healthy individuals) [28], it can opportunistically cause infection. *Candida albicans* infections are primarily a problem among immunocompromised persons such as HIV/AIDS patients or in hospital patients who have indwelling medical devices such as catheters [6]. The eradication of other competing commensals following antibiotic treatment can also cause people to become susceptible to *Candida* infections [6]. Furthermore, it is well documented that *Candida* species, particularly *C. albicans*, form biofilms on voice prostheses in total laryngectomy patients [10].

The infections caused by *C. albicans* range from superficial infection of mucosal surfaces (commonly referred to as candidiasis) to a full systemic infection called candidaemia which can advance to disseminated candidiasis whereupon fungal growths can occur within internal organs such the kidney, heart and brain [6]. The most well-known candidiasis infection is pseudomembranous candidiasis, more commonly referred to as thrush. The symptoms include white spots which, upon removal, reveal a region of inflammation in the underlying membrane. These infections frequently affect mucosal membranes of the vagina, oropharynx, oesophagus and intestine [5]. A particularly prevalent form of pseudomembranous candidiasis is vulvovaginal candidiasis (VVC) which by some estimations

may affect as many as 75% of women at some point during their life time [5]. Another well described pseudomembranous candidiasis is oral-pharyngeal candidiasis (OPC). This form of candidiasis is especially a problem in immunocompromised individuals; it is extremely common amongst AIDS patients, so much so that the onset of OPC is regarded as a marker of AIDS development in HIV patients [29].

Superficial mucosal surface infections can be readily treated with a range of antifungals. For example, VVC is usually successfully treated with azole antifungals like fluconazole and albaconazole [5]. However, candidaemia is extremely dangerous and can be fatal; even after treatment with first line antifungals such as fluconazole, it is still linked to a high mortality rate [30]. As with many *C. albicans* infections, weakened immune defences are a significant risk factor for developing candidaemia. In healthy individuals, neutrophils provide suitable defence against *C. albicans* in the blood. As such, neutropenia, either as a result of particular blood cancers or treatment with immunosuppressants, significantly increases the risk of developing candidaemia. Furthermore, damage to the mucosa of the gastrointestinal tract, for example due to surgery, is also a risk factor as it enables the spread of *C. albicans* living in the gastrointestinal tract [31]. The symptoms of candidaemia range from fever and chills which do not abate following antibiotic treatment to severe sepsis or septic shock similar to that of bacterial septicaemia [5]. However, sometimes there is a lack of precise symptoms which is a major reason for the high mortality since diagnosis may occur too late for antifungal therapies [32]. It has been reported that even a delay of as little as 12-24 hours can double mortality rate [33]. Due to this, it has become common practice to prophylactically administer antifungals after any event which is likely to increase the risk of candidaemia, such as after abdominal surgery or bone marrow transplants [5].

Although the majority of cases of candidiasis and candidaemia are caused by *C. albicans*, there are other species within the *Candida* genus which are also pathogenic in humans. These include *Candida glabrata, Candida tropicalis, Candida dubliniensis and Candida parapsilosis*. *Candida* species have increasingly become associated with nosocomial infections [8]; in fact, *Candida albicans* is recognised as the fourth most common cause of all hospital-acquired infections in the USA [6].

1.1.4 Iron homeostasis in *C. albicans*

C. albicans is able to colonise a wide range of niches within the host, both as a commensal and a pathogen, all with highly variable micronutrient availabilities. Iron is an essential micronutrient for virtually all life on Earth; it is required in the form of haem and iron-sulphur clusters for the activity of several cellular proteins, such as enzymes involved in amino acid biosynthesis, complexes of the mitochondrial electron transport chain, and enzymes involved with lipid biosynthesis [34]. Despite being so essential, high-iron levels result in cellular toxicity due to the production of reactive oxygen species via the Fenton reaction [35].

Bioavailable iron is found at extremely low concentrations in the blood (approximately 10^{-15}nM Fe^{3+}) [36] but is highly abundant in the gastrointestinal tract [37]. Mammalian hosts actively sequester iron through its binding to several proteins (see below), thus limiting its bioavailability to potential pathogens. This process is termed 'nutritional immunity' and forms an important part of host defences against pathogenic microorganisms [38]. Consequently, an ability to acquire sufficient amounts of iron from the host sequestration molecules is a prerequisite for a microorganism to become pathogenic. This is even more complex for

microorganisms which can be both commensal and virulent since they have to survive in both high- and low-iron environments. The opportunistic pathogen *C. albicans* has therefore evolved mechanisms to obtain sufficient iron in iron-scarce environments (as an invasive pathogen in the blood or tissues), while protecting against iron-toxicity in surroundings where iron is plentiful (as a commensal in the gastrointestinal tract) [39].

1.1.4.1 *C. albicans* iron acquisition mechanisms

C. albicans possesses an array of iron-uptake machinery; including direct acquisition from host proteins/molecules, a reductive iron-uptake system similar to that in *S. cerevisiae* of free or chelated Fe^{3+}, and a siderophore import system.

Upon entry into the free iron-poor environment of the blood, *C. albicans* is able to acquire iron directly from haemoglobin molecules where the majority of the bloodstream iron is found. *C. albicans* has been observed to lyse erythrocytes, releasing the haemoglobin [40]. After which a *C. albicans* cell surface receptor, Rbt5, binds to the haemoglobin [41] and internalises it via endocytosis as Rbt5-haemoglobin complexes [42]. The haem oxygenase Hmx1 is required to release the haemoglobin-bound ferrous iron within the cell [43] (Figure 1.2).

The small amount of extracellular non-haemoglobin bound iron in the blood is bound by an iron-chelating glycoprotein called transferrin, and this serves as the major iron delivery system for the host [44]. *C. albicans* has exhibited utilisation of host transferrin as a source of iron *in vitro* [45]. Certain pathogenic bacteria, such as those from the *Neisseriaceae* and *Pasteurellacea* families, possess a specific transferrin receptor (composed of the proteins

TbpA and TbpB) [46]. It is unclear whether *C. albicans* has a similar mechanism for transferrin usage, although the fact direct contact with transferrin is required suggests it probably does. The ferric iron (Fe^{3+}) obtained from the transferrin enters the *C. albicans* cells via a reductive iron-uptake system highly conserved with that of *S. cerevisiae* [45]. Ferric reductases, Cfl1 and Cfl95, in the plasma membrane reduce the Fe^{3+} to Fe^{2+} [47]. This Fe^{2+} is then oxidised back to Fe^{3+} by a multicopper ferroxidase, e.g. Fet31, which is complexed to an iron permease called Ftr1 that transports the Fe^{3+} into the cell [48]. The activity and proper assembly of the multicopper ferroxidase enzymes with the iron permeases relies on Cu^{2+} which is supplied by the intracellular copper transporter Ccc2 [49] (Figure 1.2).

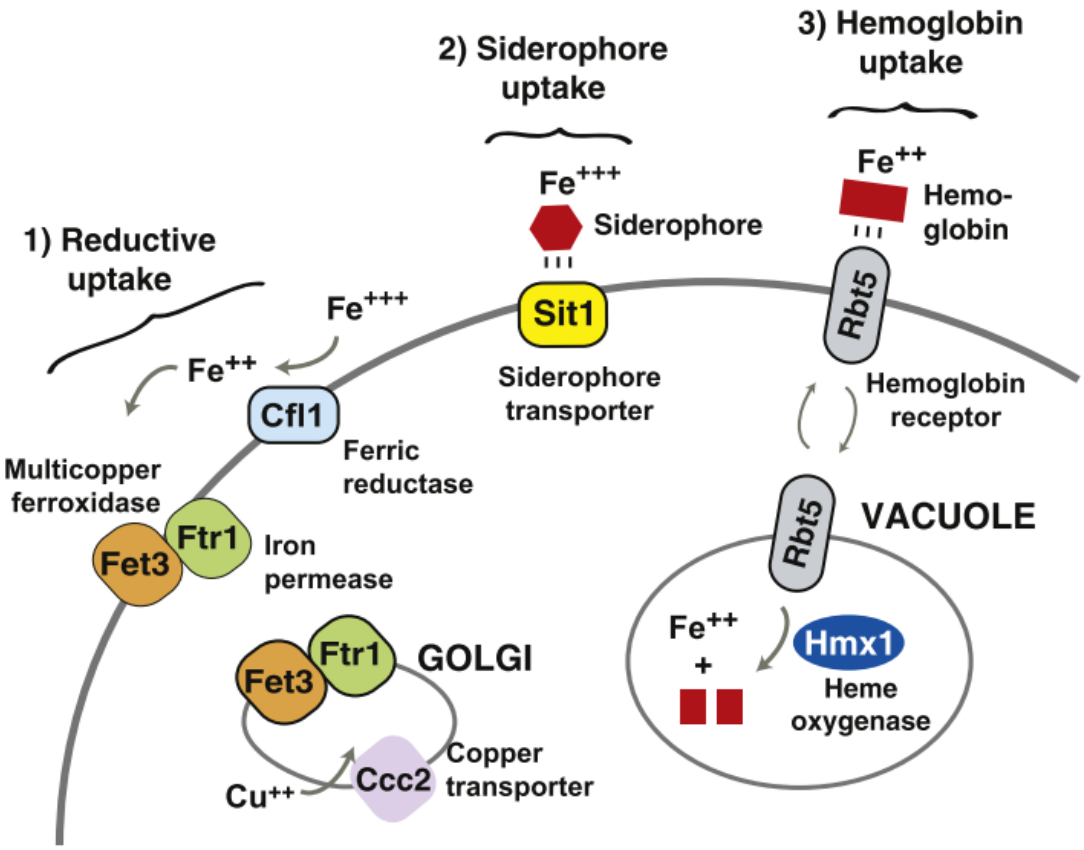


Figure 1.2: The three pathways of iron-acquisition in *C. albicans*. The reductive uptake pathway is responsible for the uptake of soluble Fe^{3+} in the environment as well as that obtained from ferritin and transferrin. Siderophore uptake involves the uptake of small Fe^{3+} chelators called siderophores. Haemoglobin uptake enables *C. albicans* to utilise Fe^{2+} from host haemoglobin molecules. *Figure taken from Figure 1 in Chen, C. et al.* [56].

Within host tissues the majority of iron is bound to the protein ferritin. *C. albicans* is able to obtain iron from directly ferritin *in vitro*, either from exogenously provided ferritin or from epithelial cells in culture, in a mechanism involving the cell-surface adhesin Als3 [50]. Als3 is a hyphal-specific protein which accumulates ferritin on the surface of hyphal *C. albicans* cells. Yeast-form cells are unable to bind ferritin, meaning the yeast-to-hyphal switch is crucial for the use of ferritin-derived iron [50]. After ferritin aggregation, *C. albicans* was observed to acidify culture media to dissociate Fe^{3+} from the ferritin, likely by destabilising its tertiary structure [50]. The dissociated Fe^{3+} enters the fungal cell using the same reductive iron-uptake system detailed above [50] (Figure 1.2). As discussed in Section 1.4.2, Als3 also plays major roles in *C. albicans* cell adhesion and biofilm formation, suggesting this single protein is responsible for multiple virulence attributes and provides a link between virulence and iron acquisition. Indeed, an *als3Δ/Δ* null mutant displayed severely attenuated virulence in a RHE oral candidiasis model [51], however, had wild-type virulence levels in a murine bloodstream infection model [52].

The final method of iron acquisition by *C. albicans* involves siderophore uptake (Figure 1.2). Siderophores are small high-affinity Fe^{3+} chelators which several pathogenic bacteria and fungi synthesise to scavenge iron from their environment [53]. *C. albicans* is quite unusual in that it possesses a siderophore importer, Sit1 [54], but its genome does not encode the known fungal siderophore biosynthetic enzymes [55]. Thus, *C. albicans* is able to utilise exogenous siderophores [54], such as those synthesised by other microorganisms, but does not appear to produce its own. Siderophore activity seems to be more important for *C. albicans* iron acquisition within host tissues as a *sit1Δ/Δ* null mutant has reduced virulence in a RHE infection model but not in a murine bloodstream infection model [54].

1.1.4.2 Regulation of iron homeostasis in *C. albicans*

In order to obtain sufficient iron in iron-limiting environments while at the same time protecting from iron-toxicity in iron-replete surroundings, *C. albicans* must be able to quickly and robustly switch from aggressive iron-uptake to significantly reducing or halting it altogether and vice versa. Unsurprisingly, this switch is under very tight control both at a transcriptional and post-translational level.

A transcriptional regulatory network composed of the transcription factors Sfu1 and Sef1, along with the CCAAT-binding HAP complex precisely regulates iron homeostatic genes in response to surrounding iron levels [56][57]. In low-iron environments, such as that of the bloodstream, the expression of *SEF1* is increased, the Sef1 transcription factor in turn upregulates components of all three of the major *C. albicans* iron-uptake pathways (haemoglobin uptake, reductive iron uptake, and siderophore uptake) [56]. The increase in *SEF1* expression relies upon indirect control by the HAP complex via the transcriptional repressor *SFU1* which represses *SEF1* and iron-uptake genes. Upon iron-deprivation, the expression of the HAP complex component gene *HAP43* (*CAP2*) is elevated [57]. The genes for the other HAP complex components, *HAP2* and *HAP3* (*HAP32*), are also upregulated, and the expression of *HAP5* maintained, in a Hap43-dependent manner. The four components; Hap43, Hap2, Hap3 and Hap5 come together to form the HAP complex which is responsible for the repression of *SFU1* and iron-utilisation genes [57]. In this way, the transcriptional repressor HAP complex is able to indirectly activate iron-uptake pathways. Sef1 also directly activates *HAP43* in a positive-feedback loop [56]. Under iron-replete conditions, the HAP complex is not active [57], meaning Sfu1 is able to repress *SEF1* and hence reduce the expression of iron-uptake genes [56].

In addition to the transcriptional control, Sef1 is also subject to post-translational control in a circuit with Sfu1 (functioning in a transcriptional-independent role) and the cyclin-dependent kinase Ssn3 [58] (Figure 1.3). In iron-replete environments, Sfu1, in addition to acting as a transcriptional repressor as detailed above, forms a complex with Sef1 in the cytoplasm. This prevents Sef1 entering the nucleus and leads to its degradation, thus allowing Sef1 activity to be rapidly halted when *C. albicans* cells have sufficient iron in order to avoid iron-related toxicity [58]. Conversely, in iron-deplete environments Sef1 forms a different complex with Ssn3, resulting in its phosphorylation, nuclear localisation and transcriptional activity [58] (Figure 1.3).

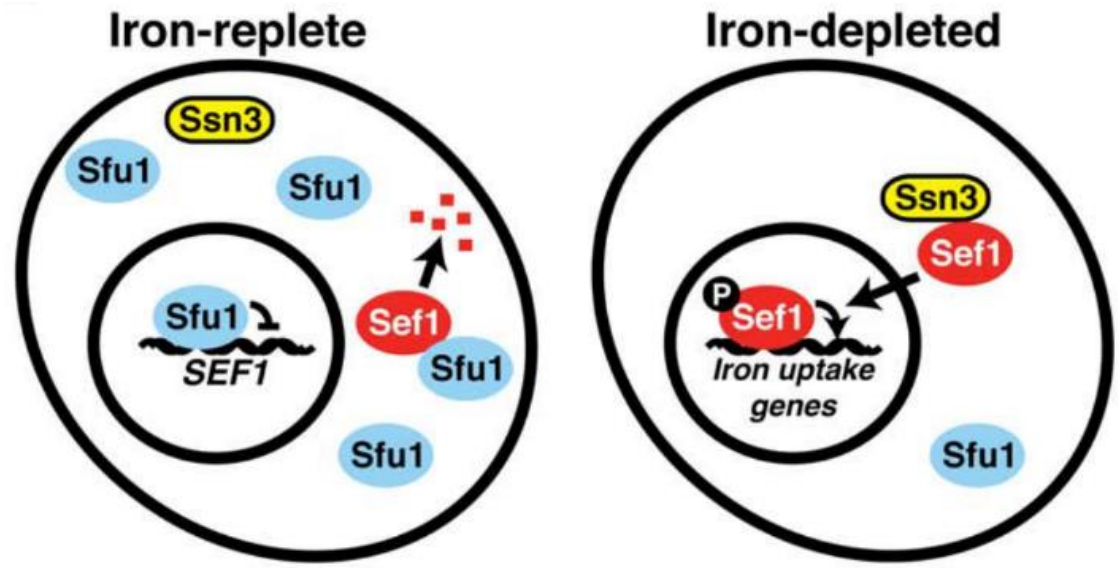


Figure 1.3: Post-translational control of Sef1 by Sfu1 and Ssn3. In iron-replete media, Sef1 is sequestered in the cytoplasm by Sfu1 where it is degraded. In iron-deplete media, Sef1 is phosphorylated by Ssn3, promoting its stabilisation and translocation into the nucleus where it can active iron-uptake genes. *Figure adapted from Figure 4 in Chen, C. et al.* [58].

Overall, Sef1 protects against iron-limitation while Sfu1 protects against iron-toxicity, and due to these opposing roles they have differing roles in virulence. For instance, Sef1 is required for virulence and survival in the bloodstream; a *sef1Δ/Δ* mutant exhibited a significant virulence defect in a murine intravenous infection model but a *sfu1Δ/Δ* mutant did not [56]. Likewise, in a competitive fitness mouse infection model for persistence in host tissues, the *sef1Δ/Δ* mutant was significantly outcompeted by the wild-type. However, the *sfu1Δ/Δ* mutant displayed a significant competitive advantage against the wild-type, presumably due to an increased ability to take up extracellular iron [56]. Both Sef1 and Sfu1 appear to contribute to commensalism since in a murine gastrointestinal infection model (which mimics commensalism) both null mutants displayed significant competitive defects compared to wild-type. The *sfu1Δ/Δ* mutant showed the most pronounced effect, possibly indicating that Sfu1 is the most important for commensalism [56]. Consistent with this, Pande, K. *et al.* discovered that passage of *C. albicans* through the murine gastrointestinal tract elicited a phenotypic switch to a novel commensal cell type which the authors called GUT (Gastrointestinally-InduCed Transition) [59]. These GUT cells have enhanced fitness within the murine gastrointestinal tract and exhibited increased transcript levels of *SFU1* with decreased transcript levels of *SEF1* and iron-uptake genes, consistent with the relative abundance of iron in the GI tract [59].

These murine model experiments demonstrate the clear link between iron homeostasis and *C. albicans* virulence. This link extends beyond Sef1-mediated iron uptake in low-iron host niches; Als3 for instance has key direct roles in virulence in addition to its function in iron-acquisition. It has even been argued that *C. albicans* uses the iron-status of its surroundings

to identify where it is in the mammalian host and thus whether it should express virulence or commensal factors [39].

1.2 *Candida albicans* Morphogenesis and Signalling Pathways

An important aspect of *C. albicans* biology, in terms of pathogenesis, is its ability undergo morphogenesis from a yeast, to pseudohyphal or hyphal forms in response to environmental cues (Figure 1.4). The virulence of *C. albicans* is closely linked with the capacity to switch between these forms; hyphal *C. albicans* cells are frequently located at sites of tissue invasion, and moreover, cells which are unable to readily form hyphae exhibit reduced virulence [6]. In particular, other *Candida* species which do not commonly produce true hyphae are not often isolated from human tissues, implying a decreased virulence. However, as strains that are incapable of growing in the yeast form also have less virulence it has been proposed that both the yeast and hyphal forms play important roles during infection [60][61]. For instance, hyphal cells express specific cell wall proteins, such as Hwp1 [62], which enable attachment to human tissues and subsequent tissue invasion. Other hyphal cell wall proteins, for example Hyr1 [63], also contribute to the avoidance of neutrophil- and macrophage-mediated phagocytosis. On the other hand, yeast cells seem to be crucial for dissemination into the bloodstream and the creation of a systemic infection [28][64].

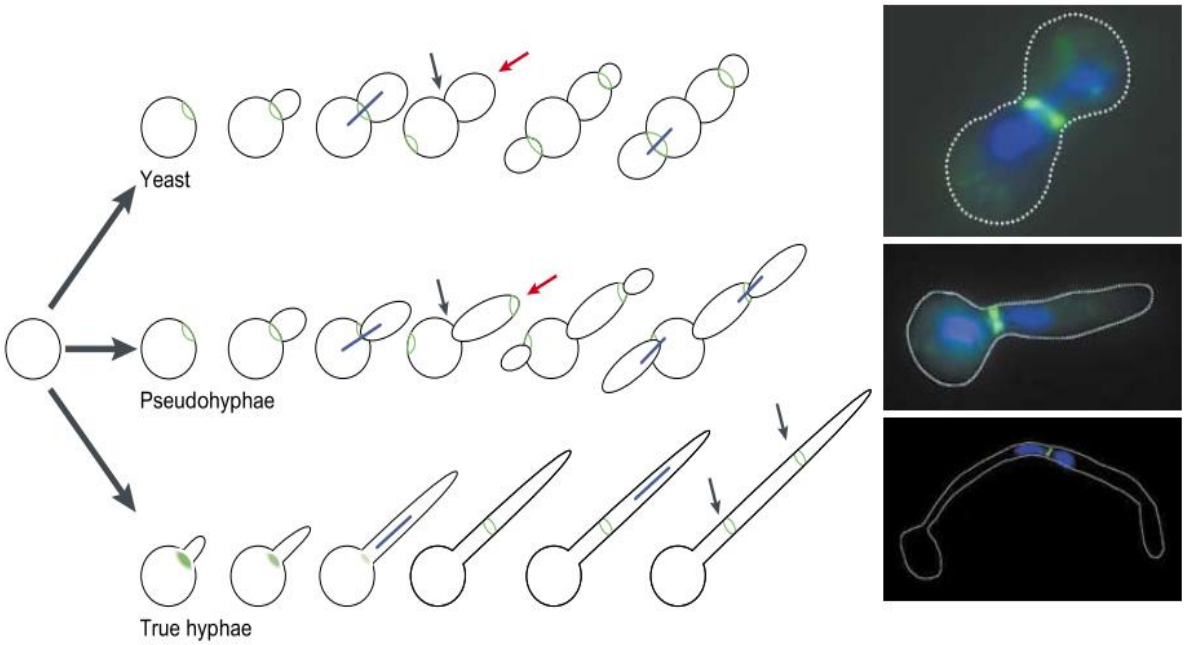


Figure 1.4: The three different morphological forms of *Candida albicans*. Yeast cells have a rounded shape and can bud and separate from each other. Pseudohyphal cells are more elongated and remained attached to each other at a constricted site called the septation site. It is believed that the branching growth pattern of pseudohyphal cells enables acquisition of nutrients that are away from the parental colony. Hyphal cells are very long and polarised with no noticeable constrictions between cells. The elongating structure from the round yeast cell when it is induced into true hyphal growth is called a germ tube. The blue lines in the diagram represent the nucleus in each cell morphology and the green bands represent the septin rings which form at the boundary between the mother and daughter cells. *Figure adapted from Box 1 in Berman, J. et al.* [6].

1.2.1 The Ras1-Cyr1-PKA pathway

There are several signalling pathways which induce the *C. albicans* morphogenic switch by transducing environmental signals from the exterior to the interior of the cell (Figure 1.5), including the Ras1-Cyr1-protein kinase A and the mitogen-activated protein kinase (MAPK) pathways [6]. Ras signalling is crucial to the integration of environmental cues with morphogenesis and *C. albicans* possesses two Ras genes - *RAS1* and *RAS2*, which encode the small GTPase Ras1 and a highly divergent Ras-like protein termed Ras2 [65]. The importance of Ras1 signalling to the virulence of *C. albicans* is demonstrated by the fact that mutants

which lack Ras1 are defective in their ability to undergo hyphal transition and exhibit reduced virulence in mouse infection models [66]. Ras signalling is now known to mediate the induction of hyphal growth in response to a variety of environmental cues including growth at 37°C (via alleviation of Hsp90-mediated repression of the Ras1-Cyr1-PKA pathway) [67][68], exposure to high levels of CO_2 [69], N-acetylglucosamine [70] and serum exposure [71].

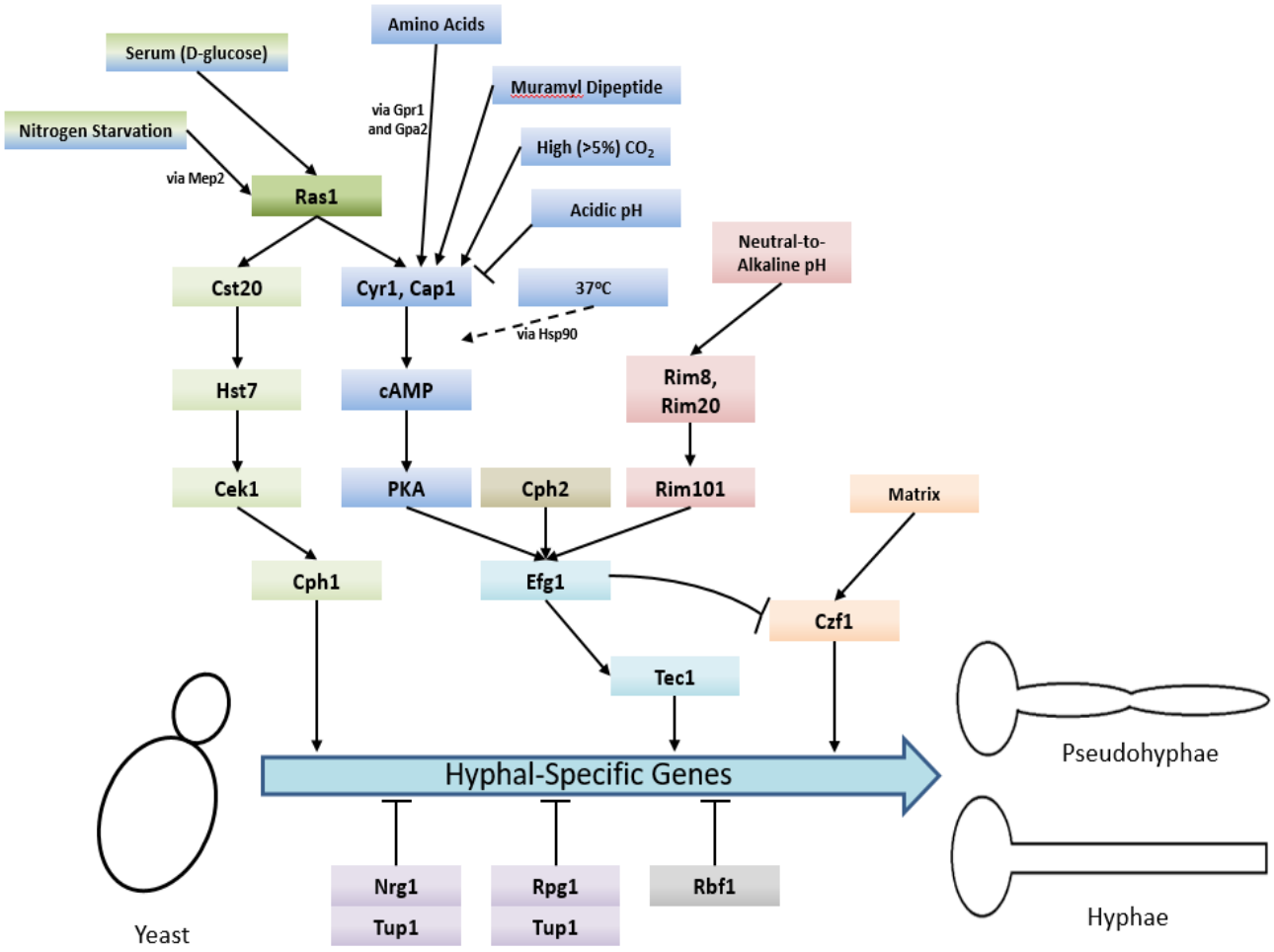


Figure 1.5: Summary of the signalling pathways and stimuli which regulate the yeast-to-hyphae morphogenic switch in *Candida albicans*. Several different pathways are responsible for inducing the yeast-to-hyphae switch: MAP kinase pathway (green), Cyr1-PKA pathway (blue), pH response pathway (red), and matrix response pathway (orange). There are also two pathways which negatively regulate the switch: Tup1-Nrg1-Rpg1 pathway (purple) and Rbf1 pathway (grey). The environmental conditions which engage the different signalling pathways to regulate the yeast-to-hyphae morphogenic switch are also indicated.

Upon activation, Ras1 directly interacts with and activates Cyr1 (the *C. albicans* adenylate cyclase), causing an increase in the production of the second messenger cAMP [66]. cAMP causes the derepression of two isoforms of protein kinase A (PKA) by triggering the dissociation of the PKA regulatory subunit (Bcy1) from the catalytic subunits (Tpk1 or Tpk2). The activation of PKA stimulates several processes within the cell including the yeast-to-hyphae switch [28]. PKA is believed to phosphorylate the transcription factor Efg1 on threonine-206, thereby activating it and resulting in the expression of HSGs [72]. The Tpk1 and Tpk2 isoforms have some redundant functions in *C. albicans*, however, they have also been demonstrated to have specific roles. For instance, Tpk1 is necessary for the formation of hyphae on solid media but not in liquid media, while the opposite is true for Tpk2. Tpk2 is also required for agar invasion but Tpk1 is not [73]. Moreover, Tpk2 seems to play more of a role in biofilm formation as a *tpk2Δ/Δ* mutant exhibited attenuated adhesion to a polystyrene surface and hence formed less dense biofilms [74]. A recent phosphoproteomic study using *tpk1Δ/Δ*, *tpk2Δ/Δ*, and a *tpk1Δ/Δtpk2Δ/Δ* double mutant identified 31 predicted Tpk1-specific phosphorylation sites and 27 predicted Tpk2-specific sites. Cell wall, membrane and signalling-related proteins were enriched in the Tpk1-specific targets, whereas filamentation and transporter-related proteins were enriched in the Tpk2-specific targets. This study also found 68 predicted Tpk-redundant phosphorylation sites [75].

A number of environmental signals promote the yeast-to-hyphae switch via the Ras1-Cyr1-PKA pathway. Some of these signals, including CO_2 interface directly with the Cyr1 adenylate cyclase to activate it [69]. CO_2 is able to do this because, unlike most signalling molecules, it is able to enter the cell by simple diffusion and is maintained in the cell as HCO_3^- via conversion by a carbonic anhydrase encoded by *NCE103* [69]. It has recently been discovered that the

expression of *NCE103* is controlled in response to CO_2 availability by the bZIP transcription factor Rca1; Rca1 is regulated in a CO_2-dependent manner by the Sch9 kinase via a cascade mediated by lipid/Pkh1/2 signalling [76]. A lysine residue at position 1373 is critical for CO_2 activation of Cyr1. This lysine residue is located in the C-terminal catalytic domain and makes up a receptor site which detects increased HCO_3^- levels [77], leading to increased cAMP production and activation of PKA filamentation [69]. The response of *C. albicans* to CO_2 is of interest because within a mammalian host, the levels of CO_2 are approximately 150x that of normal air (~5% compared to 0.03%). It could be the case that high levels of CO_2, such as those found within the upper respiratory tract (where voice prostheses are located), may promote *C. albicans* colonisation. However, it is interesting to note that other pathogenic *Candida* species, including *C. dubliniensis*, *C. glabrata*, *C. parapsilosis* and *C. krusei*, do not undergo the yeast-to-hyphae transition in response to elevated CO_2 [78]. Although this does not rule out the fact that the adenylate cyclase of the latter species is activated by carbon dioxide/bicarbonate; the physiological significance of CO_2 sensing with regards to *Candida* infection remains to be determined.

Furthermore, it appears that CO_2 is used as a communication molecule in *C. albicans* biomasses. In addition to the host-derived CO_2, microorganisms themselves produce and secrete metabolic CO_2 into their immediate microenvironment. It was observed by Hall, R. *et al*. that in *C. albicans* biomasses, metabolic CO_2 initially provides HCO_3^- as a metabolic intermediate, thereby supporting growth, but eventually accumulates to sufficient levels to induce filamentous growth via activation of Cyr1 [77]. Given the well-known connection between *C. albicans* morphogenesis and virulence, along with the fact that *C. albicans* cells are often found in mixed biofilms on medical devices such as voice prosthesis, it would seem

likely that this new found role of metabolically derived CO_2 contributes to pathogenicity by increasing host tissue invasion via morphogenic switching (Figure 1.6) as well as supporting biofilm establishment and maintenance.

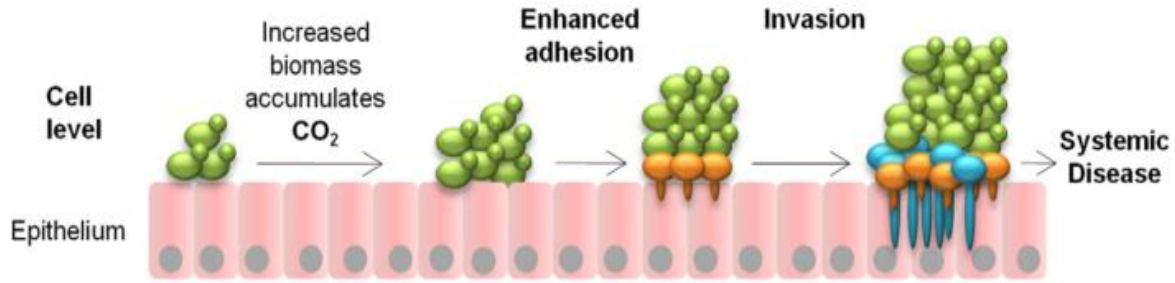


Figure 1.6: Model for how metabolic CO_2 signalling may contribute to the pathogenicity of *Candida albicans*. Cells proliferate on the epithelial surface, the fungal growth results in pockets of elevated CO_2 at the bottom of the biomass. This elevated CO_2 induces cells to undergo the yeast-to-hyphae switch, promoting hyphal growth and thus increasing the surface adherence of the cells. At the same time, protruding hyphae detect a range of host environmental signals including serum, pH, and more CO_2, further enhancing filamentation and subsequent tissue invasion. *Figure adapted from Figure 7 in Hall, R. et al.* [77].

Muramyl dipeptide (MDP), the minimal biologically active subunit of bacterial peptidoglycan, also induces *C. albicans* filamentation by acting directly upon Cyr1 [79]. A further signal which can cause morphogenesis through direct interaction with Cyr1 are amino acids. Amino acids, when in the presence of glucose, activate Cyr1 via upstream signalling through the G-protein coupled receptor Gpr1 and its Gα protein Gpa2 [80]. Upon its activation by Gpr1, Gpa2 is believed to bind to a Gα domain on the Cyr1 adenylate cyclase thereby activating it [80]. This binding of Gpa2 to a fungal adenylate cyclase Gα domain has been demonstrated in fission yeast [81] but it is yet to be proved experimentally in *C. albicans*.

In contrast, acidic pH causes a reduction in signalling through the Ras1-Cyr1-PKA pathway via a Ras1-independent downregulation of Cyr1 activity [82]. *C. albicans* cells grown at pH 4 in hyphae-inducing conditions do not form hyphae, instead remaining as yeast or pseudohyphal cells and this is not reliant upon Ras1. It has also been observed that low extracellular pH results in fast and sustained decreases in intracellular pH which potentially contributes to reduced cAMP signalling through the reduction of intracellular bicarbonate levels [82].

The yeast-to-hyphae switch in response to exposure to serum relies on Ras1 signalling upstream of Cyr1 [71]. The component of serum principally responsible for the induction of hyphal growth is D-glucose which is able to activate both the Ras1-Cyr1-PKA pathway and the MAP-kinase pathway [71][83]. The precise mechanism of Ras1 activation by D-glucose in *C. albicans* remains to be elucidated but in *S. cerevisiae* it depends on both an intracellular phosphorylated form of D-glucose and a G-protein coupled receptor Gpr1 with its Gα protein Gpa2 [84]. Gpr1-type receptors have been characterised in *C. albicans* [80] and so a similar mechanism for Ras1 activation may exist in this pathogen. However, deletion of either CaGpr1 or CaGpa2 had no effect on D-glucose-mediated cAMP signalling, but deletion of CaCdc25 (the *C. albicans* Ras1 GEF) or CaRas1 eliminated this signalling [80]. These findings indicate Ras1 activation via Cdc25 is the primary mechanism by which D-glucose induces morphogenesis. The response of *C. albicans* to D-glucose is of physiological relevance because links between candida infection and hyperglycaemia [85] as well as insulin-dependent diabetes mellitus [86] have been reported. Moreover, *C. albicans* cells have increased tolerance to oxidative and cationic stresses upon exposure to levels of glucose that may be found in the bloodstream [87].

The CaRas2 protein contains several variations in conserved motifs typically thought to be critical for Ras-related activities and is thus considered an unusual Ras protein. Sequence alignment using BLAST has shown that the *C. albicans* Ras2 protein only has 25%-30% identity with all other fungal Ras proteins in the database except a Ras-like protein only found in *Candida dubliniensis* (80% identity) [88]. When *RAS2* is deleted in a *ras1Δ/Δ* background, intracellular cAMP levels are restored to approximately 30% of wild type levels (*ras1Δ/Δ* mutant has a 20x reduction in cAMP). Ras1 and Ras2 may therefore exhibit antagonistic roles in *C. albicans* [88]. This is intriguing since the deletion of *RAS2* in a *ras1Δ/Δ* background results in a significantly increased defect in hyphal morphogenesis. Nevertheless as *ras2Δ/Δ* mutants themselves exhibit normal hyphal development [88] the role of Ras2 in morphogenesis and pathogenesis in *C. albicans* has yet to be elucidated.

1.2.2 The MAP kinase pathway

Ras1 has also been shown to regulate hyphal transition in response to other environmental cues, such as nitrogen starvation [89], via MAP kinase signalling. As with the Cyr1/PKA pathway, the regulatory MAP kinase cascade is also activated by Ras1 [66] and consist of the kinases Cst20, Hst7 and Cek1 [90][91][92][93][94]. Ras1/MAPK signalling culminates in the phosphorylation and activation of the transcription factor Cph1, which in turn promotes the expression of hyphal-specific genes (HSGs) [80] such as Als3 (adhesin) [95], Hwp1 (invasin) [62], Hyr1 (host immune response modulator) [63], and Hgc1 (hyphal-specific cyclin) [96] (Figure 1.5). It has been shown that inactivation of the Ras1-Cyr1-PKA pathway inhibits filamentous growth in the majority of usual hyphae-inducing conditions, however, inactivation of the MAP kinase pathway only prevents filamentous growth in only a specific subset of conditions [91].

1.2.3 Alternative pathways driving the yeast-to-hyphae switch

Although Ras1-Cyr1-PKA and MAP kinase signalling are the major pathways responsible for promoting the yeast-to-hyphae switch, there are also several other pathways which drive *C. albicans* morphogenesis under certain environmental conditions. For instance, the Rim101 pathway induces the transition of yeast-to-hyphae in response to extracellular pH levels. At an alkaline pH, a number of proteins, including Rim8, stimulate the proteolytic cleavage of the carboxyl terminus of the zinc-finger transcription factor Rim101. This truncated version of Rim101 activates the expression of alkaline-specific genes and represses acid-induced genes. It also results in the activation of HSGs, stimulating the yeast-to-hyphae switch (Figure 1.5). Surprisingly, the presence of the Rim101 pathway is not required for growth at either alkaline or acidic pH *in vitro*. However, it has been demonstrated that it is essential for a number of host-pathogen interactions and thus can be considered extremely important *in vivo* for the pathogenicity of *C. albicans* [97]. Furthermore, *C. albicans* cells embedded in a matrix are stimulated to switch to hyphal growth via a pathway involving the transcription factor Czf1 (Figure 1.5). It has been speculated that the ability of *C. albicans* to switch to hyphal growth in response to embedded conditions may be important in promoting invasion of the fungal cells into host tissues [98].

Genotoxic stress resulting in perturbations in the normal cell cycle can cause also a yeast-to-hyphae switch in *C. albicans*. For instance, mutations which prevent DNA damage repair or DNA replication pathways are capable to prompting filamentous growth. These situations will activate the DNA damage/replication checkpoints, in turn activating the Rad53 checkpoint kinase which plays a key role in promoting hyphal growth [99]. Moreover, it has been observed that reactive oxygen species, such as those produced from hydrogen peroxide

released by phagocytic cells also stimulates hyphal growth through Rad53 signalling [100].

1.2.4 Negative regulation of the yeast-to-hyphae switch

In addition to the signalling pathways which drive the yeast-to-hyphae switch, there are also negative regulators that are controlled by Ras signalling (Figure 1.5). Hyphal-specific genes are repressed by the global-repressor Tup1 [101] via the specific DNA-binding proteins Nrg1 [102][103] and Rfg1 [104]; the deletions of each of these three proteins results in *C. albicans* cells which are constitutively hyphal even under non-hyphal inducing conditions [101][102][103][104]. Approximately half of the genes found to be upregulated during hyphal development in response to 37^{o}C and serum are repressed by Tup1 and Nrg1 or Rfg1, suggesting that repression removal is a crucial step in the yeast-to-hyphae switch [105]. Consistently, it has been found that hyphal-inducing conditions such as serum exposure and growth at 37^{o}C cause a reduction in the expression levels of *NRG1*, leading to the conclusion that one way in which repression of hyphal-specific genes is overcome during the yeast-to-hyphae switch is via down-regulation of the repressors [103]. Ras1-Cyr1-PKA pathway activation results in the prompt but short-term removal of Nrg1 from the promoters of hyphal-specific genes. The maintenance of this repression elimination, and hence hyphal development, is achieved through the subsequent recruitment of the Hda1 histone deacetylase which deacetylates a subunit of NuA4 histone acetyltransferase, causing it to also be removed from the promoter. This results in the coiling of the portion of the promoter containing the Nrg1 binding site, preventing the re-binding of Nrg1. It is important to note the removal of Nrg1 is an absolute prerequisite for the Hda1 recruitment [106].

1.3 *Candida albicans* Biofilms

Biofilms are structured communities of microorganisms which are attached to either a living or non-living surface. The cells are often encased within a matrix of self-made extracellular polymeric substance (EPS); this EPS is composed of DNA [107][108], lipids [107], proteins [107][109] and polysaccharides [107]. Medically, biofilms are of particular importance because it is thought that a significant percentage of human microbial infections include biofilm formation [110][111][112]. Indeed, estimates from the National Institutes of Health suggest pathogenic biofilms (bacterial and fungal) are responsible for up to 80% of all microbial infections in the US [113].

Moreover, cells which reside within biofilms have distinctive phenotypes compared to planktonic cells, for example, they exhibit increased tolerance to antibiotic and antifungal drugs. It has been estimated that bacteria, for example *Pseudomonas aeruginosa* (*P. aeruginosa*), residing within a biofilm are 10-1000x more tolerant to antibiotics than their planktonic counterparts [114]. While *C. albicans* biofilm cells are more tolerant to antifungals including fluconazole, nystatin and amphotericin B [115]. The reasons for this increased tolerance are complex but include the presence of an extracellular matrix reducing the ability of antimicrobial agents to reach the cells [116][117], metabolic differences (such as modulation of glycolysis, ergosterol biosynthesis and mitochondrial respiration) [118] inherent to biofilms and upregulation of efflux pumps [119]. *C. albicans* biofilms are usually composed of a mixture of morphological forms; typically yeast, pseudohyphal and true hyphal cells are all present within a mature biofilm [8][115][120].

1.3.1 Stages of *Candida albicans* biofilm formation

The formation of a biofilm is the result of a very precise and complex series of events that are divided into distinct stages; attachment, initiation, maturation and dispersion (Figure 1.7).

Attachment: The first step in biofilm formation, and hence the colonisation of a surface, is the initial attachment of cells to that surface [120]. At the beginning of this stage, the majority of *C. albicans* cells are yeast form [115]. Both nonspecific factors, such as cell surface hydrophobicity and electrostatic forces, and specific factors, such as adhesins on the yeast cell surface binding to precise ligands on the substratum to be colonised, are responsible for the preliminary attachment of *C. albicans* cells [120]. The adhesins, such as members of the agglutinin-like sequence (Als) family (Als1-7 and Als9), are glycosylphosphatidylinositol (GPI) anchored cell wall proteins. The Als adhesins possess a folded N-terminal domain required for protein-ligand interaction, a 600-1000 residue serine/threonine-rich tandem domain, and a C-terminal peptide which covalently bonds GPI [121]. The N-terminal domain contains a peptide binding cavity (PBC) which can accommodate the final 6 peptides in the C-terminals of a variety of proteins, with a salt bridge being formed between the C-terminal carboxylic acid group and a positively charged invariant lysine at the end of the PBC [122]. In this way the adhesins are capable of binding numerous structurally unrelated ligands. Mechanisms underlying *C. albicans* attachment to abiotic surfaces are not fully understood but are likely to involve the PBC binding to adsorbed proteins, as well as possibly involving hydrophobic interactions since an *als1Δ/Δals3Δ/Δ* double mutant exhibited significantly reduced interaction with a hydrophobic AFM tip [123]. After attachment, the *C. albicans* cells form a basal layer which functions to anchor the biofilm to the surface as it matures.

Initiation: Approximately 3-6 hours after the initial attachment, pseudohyphal and hyphal cells start forming from the proliferating yeast-form cells [8]. After around 11 hours, colonies of *C. albicans* cells begin to appear as thick tracks over the surface being colonised [115]. This step in biofilm development is characterised by the appearance of extracellular material covering the *C. albicans* colonies. Communities of *C. albicans* continue to grow and secrete a matrix of self-made EPS composed of DNA (5%) [107][108], lipids (15%) [107], proteins (55%) [107][109] and polysaccharides (25%) [107].

Maturation: The maturation phase of biofilm growth lasts between 24-48 hours [120]. Colonies of *C. albicans* continue to grow and secrete EPS, increasing the amount of extracellular material encasing the biofilm [115]. This extracellular matrix serves as a physical barrier to the surrounding environment and also contributes to the structural integrity of the biofilm, protecting it from mechanical disruption. Mature biofilms possess a complex 3D structure which is thought to signify the optimum spatial arrangement to allow nutrient influx, waste disposal, and the founding of microniches within the biofilm. For instance, microcolonies within a mature biofilm are separated by water channels which enable the circulation of nutrients throughout the biofilm. Typically, a mature *C. albicans* biofilm comprises a thin layer of yeast cells which attaches a thicker layer of yeast, pseudohyphal and hyphal cells to the substratum [124].

Dispersion: The final stage of biofilm development is the dispersal stage during which yeast-form cells bud off from hyphal cells within a mature biofilm and disperse in order to establish additional biofilms elsewhere [115][125]. In actuality, *C. albicans* biofilms disperse yeast-form cells during all stages of growth with greater dispersion occurring once the biofilm has

reached maturity [126]. Interestingly, the yeast-form cells emerging from mature biofilms have distinct characteristics compared to typical planktonic yeast cells. The dispersed cells display enhanced adherence, increased propensity to filament, and increased biofilm forming capability. Overall, this contributes to increased pathogenicity in a mouse model of blood disseminated candidiasis [126]. The dispersed biofilm cells are fully-equipped with key virulence factors to cause the dissemination of infection.

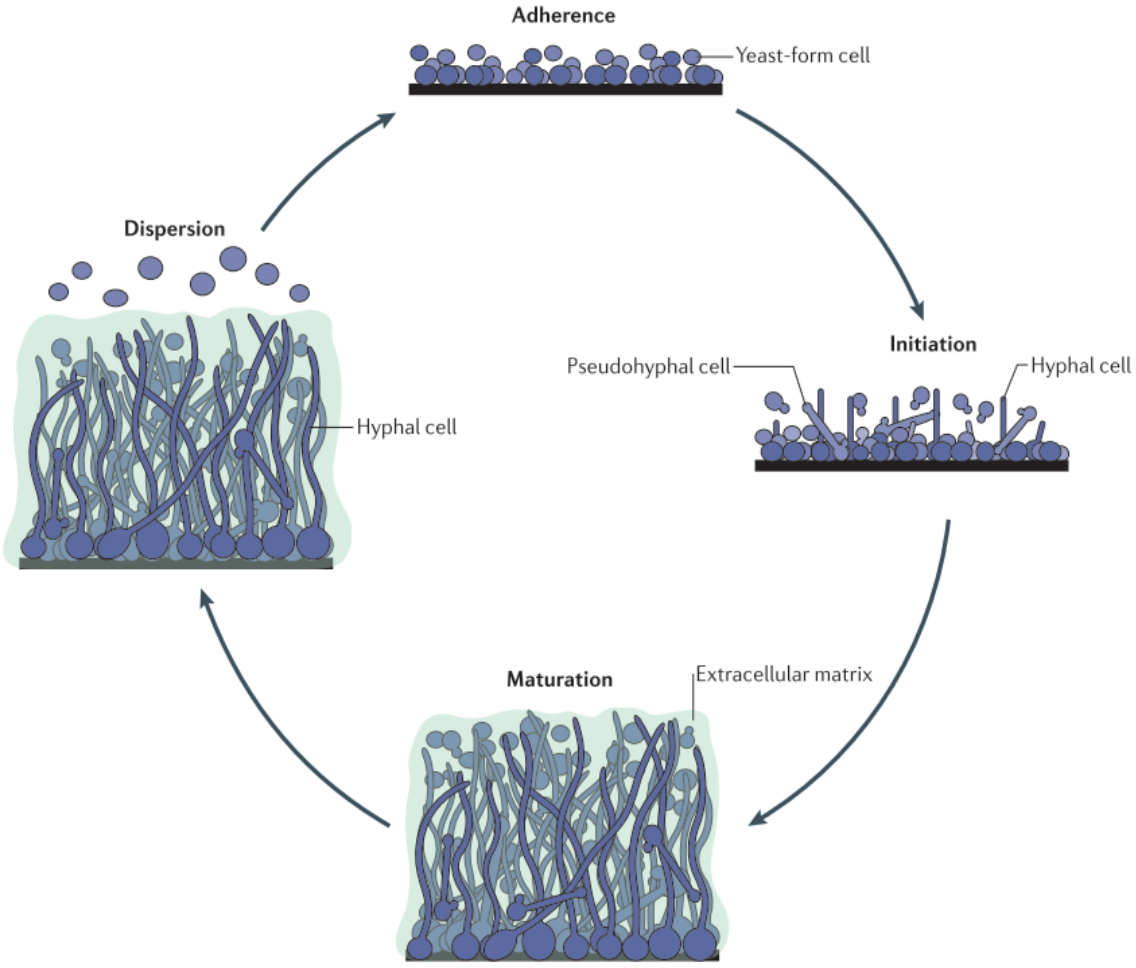


Figure 1.7: Stages of *Candida albicans* biofilm formation. Biofilm formation in *C. albicans* follows four clearly defined stages: cells attach to a surface in the yeast-form, they begin to proliferate and produce extracellular matrix while undergoing the yeast-to-hyphal switch, this continues for 24-48 hours to produce the mature biofilm, before finally dispersing yeast-form cells to establish new biofilms elsewhere. *Figure adapted from Figure 1 in Lohse, M. et al.* [125].

1.3.2 Regulation of *Candida albicans* biofilm formation

C. albicans biofilm formation is an exceedingly complex process involving very tightly regulated, interwoven signalling pathways centrally controlled by a set of nine transcription factors; Bcr1, Brg1, Efg1, Tec1, Ndt80, Rob1, Flo8, Rfx2 and Gal4 [127][128]. These nine essential regulators are subject to autoregulation (Figure 1.8) and coordinate the expression of over a 1000 target genes upregulated during biofilm formation [127].

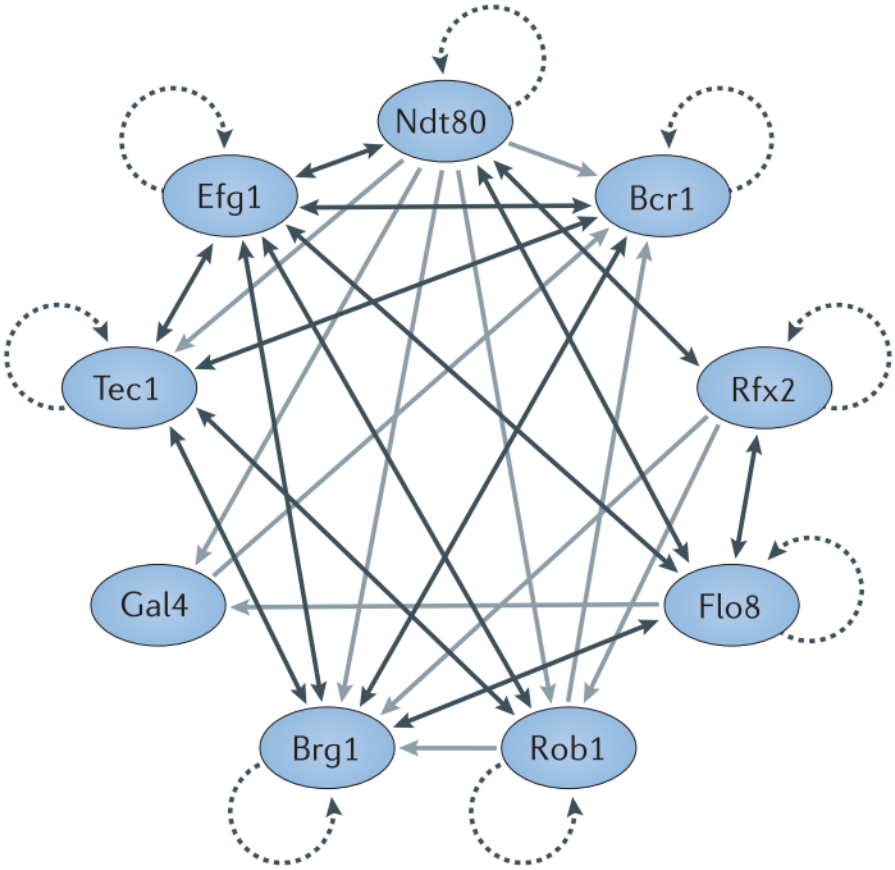


Figure 1.8: The nine core transcription factors which form a highly interconnected network to control *Candida albicans* biofilm formation. All of these transcription factors, apart from Gal4, are subject to autoregulation. Direct binding interactions where the transcription factors regulate each other are specified by double-headed arrows, and binding interactions where one transcription factor regulates the other are specified by single-headed arrows. This highlights the complexity of the regulation of *C. albicans* biofilm formation. *Figure taken from Figure 2 in Lohse, M. et al.* [125].

Interestingly, the nine 'core' transcription factors have been shown to function during different developmental stages within *C. albicans* biofilms [128][129]. Governing key processes such as initial attachment, matrix deposition and dispersal. Thus, positive regulators downstream of the 'core' also show stage specificity in their function, for example adhesins such as the Als family are predominantly upregulated in early stage biofilms [130] (Figure 1.9).

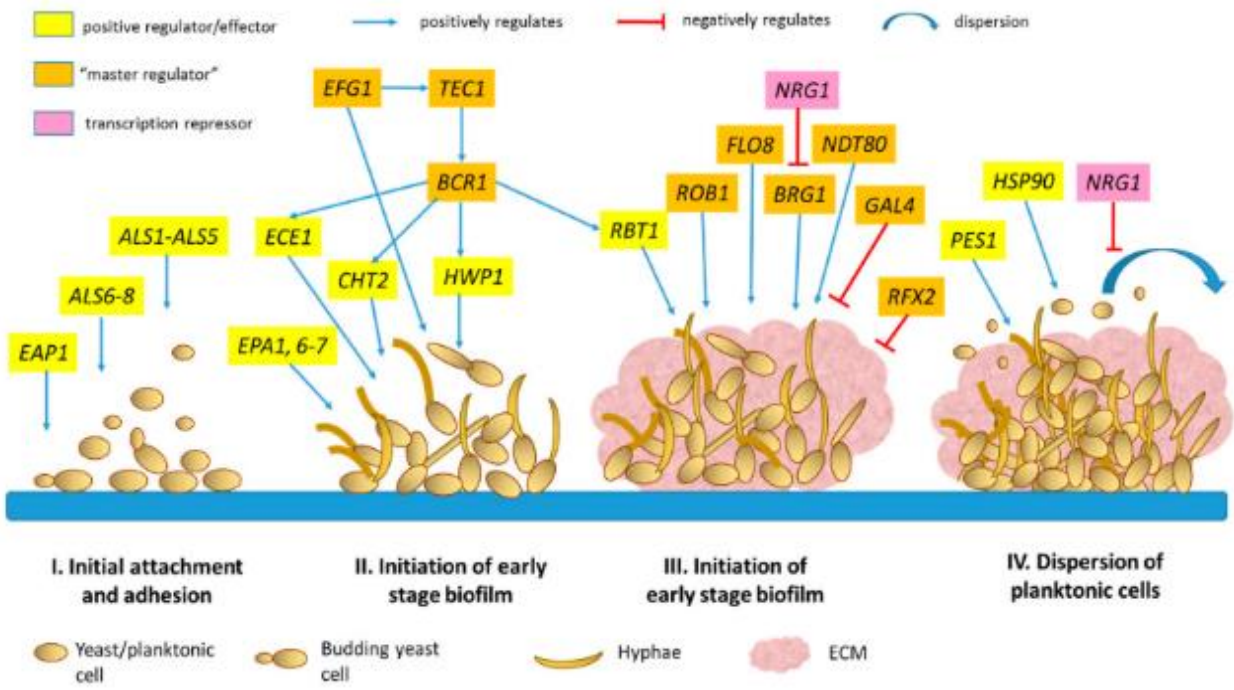


Figure 1.9: The stages of *C. albicans* biofilm formation and the transcription factor network which controls it. The master regulators have been demonstrated to primarily function within different stages of *C. albicans* biofilm growth. Other positive regulators also function at different time points, with the majority of the adhesins functioning in the earlier stages. *Figure taken from Figure 1 in Chong, P. et al.* [129].

The transcription regulator Bcr1 has important roles in the attachment of *C. albicans* cells to a surface to initiate biofilm formation, as well as the cell-cell attachments which maintain architectural integrity during maturation. The *bcr1Δ/Δ* mutant is unable to form biofilms and

also cannot switch to hyphal growth under certain conditions. However, when present within mixed biofilms formed using wild-type cells, *bcr1Δ/Δ* mutant cells produce lots of hyphae [131]. These hyphal cells are unable to adhere to surfaces and initiate biofilm formation, thus the Bcr1 transcription factor is required to impart some function on hyphal cells vital to biofilm development. In fact, Bcr1 upregulates at least 11 genes encoding cell wall proteins, including the adhesins Als1, Als3, and Hwp1 which have been shown to have critical roles in biofilm formation [127][132][133][134]. This is not the whole story however, since more than thirty transcription factors (including Bcr1) have been shown to be necessary for adherence [135]. Moreover, Fox, E. P. *et al.* demonstrated that different sets of adhesins are upregulated in early and late biofilms, adding further complexity to this field [128]. Additional work needs to be conducted to fully understand the intricacies of biofilm adherence.

Extracellular matrix (ECM) deposition is a hallmark of biofilm growth but knowledge is currently limited on the regulation of this process, as well as the exact purpose of all the components. Mass spectrometry has identified over 500 proteins in the matrix, the majority of which are enzymes. Intriguingly, several of these enzymes do not possess traditional export sequences and so it's questionable if they are actively secreted, instead likely coming from lysed cells within the biofilm [107]. It has been proposed that these extracellular enzymes may digest cellular components to provide nutrients to *C. albicans* cells in the maturing biofilm. They may also have roles in promoting the dispersal phase of biofilm growth while also protecting biofilm cells from host immune cells. However, these hypotheses are yet to be experimentally validated [107][125]. Extracellular DNA (eDNA) is another key component of the biofilm ECM. In bacterial biofilms, eDNA contributes to several aspects of biofilm formation ranging from adhesion to structural stability and antimicrobial tolerance [136]. *P.*

aeruginosa biofilms disperse upon treatment with DNase [137]. It is likely that eDNA plays similar roles in *C. albicans* biofilms, indeed, Martins, M. *et al.* demonstrated that eDNA is present at all stages of *C. albicans* biofilm growth and DNase treatment reduces overall biofilm biomass in latter phases of development [108].

Two transcription factors called Zap1 and Rlm1 have been identified as having roles in the regulation of ECM deposition. Zap1 is a negative regulator of two glucoamylases, Gca1 and Gca2, which are involved in β-1,3-glucan biosynthesis, a major component of the biofilm matrix that has been linked to biofilm-associated drug tolerance [116][117]. Consequently, a *zap1Δ/Δ* mutant has been shown to have increased matrix production [138]. Furthermore, a group of alcohol dehydrogenases regulated by Zap1 including Adh5, Csh1 and Ifd6, have been reported to have functions in matrix deposition. It has been proposed that these alcohol dehydrogenases create aryl and acyl alcohols which function as quorum-sensing molecules which control several biofilm maturation events [138]. Rlm1 functions in a pathway with the glucan synthase Fks1 to regulate the production of cell wall and ECM β-1,3-glucan during *C. albicans* biofilm growth, and a *rlm1Δ/Δ* mutant has decreased matrix production resulting in reduced antifungal tolerance [139].

It has recently been published that extracellular vesicles (EVs) produced within *C. albicans* biofilms have a crucial role in ECM deposition and thus antimicrobial tolerance. Mutants lacking key components of the endosomal sorting complexes required for transport (ESCRT) pathway have reduced biofilm EV production along with reduced matrix glucan and mannan levels. The authors proposed that EVs have a direct role in matrix biogenesis, since the addition of wild-type vesicles to mutant biofilms resulted in the restoration of matrix

polysaccharide levels and antimicrobial tolerance. This suggests that the EVs are delivering functionally-relevant cargo which is actively contributing to ECM production [140].

Another key aspect of *C. albicans* biofilm growth is the formation of hyphal cells. Hyphal cells are required for biofilm formation because the expression of several cell surface adhesins, such as Hwp1 and Eap1, is highly upregulated during hyphal growth. These adhesins are required for attachment (both cell-cell and cell-surface) during biofilm maturation, and as a result it means Ras signalling is strongly linked to the development of biofilms [141]. It was discovered by Ramage, G. *et al*. that the hyphal-defective mutant *efg1Δ/Δ* (as well as *efg1Δ/Δ cph1Δ/Δ*) is unable to form biofilms [142]. Rather than the true basal layer which wild-type *C. albicans* cells form, these mutants only produce very few surface-attached cells. Despite this, strangely, the surface-attached mutant cells have no susceptibility to fluconazole and limited susceptibility to amphotericin B [142]. These are important observations because it appears as though simple surface-adhesion is sufficient to induce the antifungal tolerance characteristic of cells in biofilms; this tolerance does not require biofilm maturation [115].

Dispersion is the final stage in *C. albicans* biofilm formation and, as with all other aspects of biofilm growth, is a highly regulated process. The transcription factor Nrg1 (see Section 1.3.4), whose degradation is inhibited by the *C. albicans* quorum-sensing molecule farnesol [143], has been shown to promote biofilm cell dispersion [144]. Conversely, the transcription factor Ume6 negatively regulates dispersion with overexpression of the *UME6* gene reducing biofilm cell distribution [126]. A histone deacetylase complex composed of four core members (Set3, Hos2, Snt1, and Sif2) has also been revealed to be required for dispersion, possibly through being recruited to particular genes by Nrg1 [145]. Environmental factors such as nutrient

availability have been suggested to affect dispersion, and some experimental evidence points to biofilm dispersal increasing in rich media compared to nutrient-poor media [146]. The precise molecular mechanisms behind these dispersal responses to the environment are yet to be elucidated.

1.3.3 Antimicrobial tolerance within *C. albicans* biofilms

A principal, and perhaps the most medically relevant, phenotype of biofilms is that they exhibit increased antimicrobial tolerance compared to planktonic cells. Some fungal biofilms can be up to 20000-fold more tolerant to antifungals by some estimations [147]. The repertoire of antifungals for the treatment of fungal infections is significantly lower than that of antibiotics for bacterial infections. The development of novel antifungals is hindered by the eukaryotic nature of fungal cells and hence the large similarities to host mammalian cells. Thus, clinicians are limited in the range of treatment options available, particularly if the fungal pathogen displays tolerance or resistance. Potential host toxicity of these antifungals is also a major issue and long-term usage antifungals such as fluconazole is associated with adverse effects in the host [148]. Currently, there are 5 classes of antifungals; azoles, polyenes, echinocandins, allylamines, and pyrimidine analogs [149]. *C. albicans* employs a variety of mechanisms to increase its tolerance to these antifungals; some of these mechanisms are shared between planktonic and biofilm cells but others are specific to the biofilm scenario.

Azoles: Azoles such as fluconazole and miconazole are primarily fungistatic and function by inhibiting the lanosterol 14α-demethylase enzyme in the ergosterol biosynthetic pathway [150][151]. Ergosterol is unique to fungi; it is the main constituent of the fungal cell

membrane and functions to regulate membrane fluidity, asymmetry, and hence its integrity [152].

One mechanism *C. albicans* biofilms use to increase tolerance to fluconazole is by increasing the expression of the *ERG* genes which encode the components of the ergosterol biosynthetic pathway. This causes changes in azole target levels, often resulting in a failure of the antifungal to efficiently eradicate the pathogen [153]. A study by Borecká-Melkusová, S. *et al*. showed that the *ERG9* and *ERG11* (encodes lanosterol 14α-demethylase) genes were upregulated in *C. albicans* biofilms following treatment with fluconazole. The *ERG3* gene was also upregulated during biofilm growth independently fluconazole treatment [154]. Additionally, Nailis *et al*. reported significant increases in *ERG1*, *ERG3*, *ERG11* and *ERG25* gene expression in mature *C. albicans* biofilms after fluconazole treatment [155]. Contrary to this, a whole transcriptome analysis found no significantly altered gene expression in mature *C. albicans* biofilms after fluconazole treatment [156]. However, this could be explained by another mechanism which *C. albicans* biofilms use to increase tolerance – β-1,3-glucan in the ECM binds to azoles [157] (as well as other antifungals such as amphotericin B [156]). When in a biofilm, the cell wall of *C. albicans* undergoes architectural changes, increasing its β-1,3-glucan content. In addition, β-1,3-glucan is also secreted and forms a major component of the biofilm ECM [157]. It could be that once a biofilm is sufficiently mature, the cell walls and ECM prevents certain drugs even reaching the cells.

A further mechanism of azole tolerance is the upregulation of drug efflux pumps within biofilm-associated cells [158]. Two groups of efflux pumps have been associated with azole resistance in *C. albicans*; the Cdr1 and Cdr2 pumps (ATP-binding cassette (ABC) transporters

encoded by the *CDR1* and *CDR2* genes) and the Mdr pumps (major facilitator (MF) superfamily encoded by the *MDR* genes) [159]. An additional member of the MF superfamily encoded by *FLU1* has also been implicated in fluconazole resistance [160]. *In vitro* studies have shown expression of *CDR1*, *CDR2*, *MDR1* and *FLU1* is increased in *C. albicans* biofilm cells compared to planktonic cells [158][161]. This has also been confirmed *in vivo* [130]. However, it has been argued these drug efflux pumps probably only play a major role in antifungal tolerance in the early stages of biofilm formation. Drug efflux pump gene expression increases in as little as 15 minutes of initial attachment to a surface [158] but decreases as *C. albicans* biofilms mature [161]. This is intriguing since tolerance usually increases as biofilms age. Furthermore, it has been shown that knockout mutants of *CDR1*, *CDR2*, and *MDR1* are sensitive to azoles planktonically and in early stage biofilms but maintain tolerance within late stage biofilms, indicating these drug efflux pumps are not necessary for the azole tolerance of mature biofilms [161][162].

Polyenes: Polyenes such as amphotericin B and nystatin function by binding to ergosterol in the fungal cell membrane. Upon binding, transmembrane pores are formed which induce the leakage of electrolytes and cytoplasmic contents, resulting in cell death [153].

Similar to the azoles, *C. albicans* biofilms can resist polyene treatment by alterations in gene expression. Significant increases in *SKN1*, *KRE1* and *ERG1* expression have been observed in mature biofilms upon addition of amphotericin B [155]. This is consistent with a report of a small population of highly amphotericin B tolerant biofilm-associated yeast-form cells which had significant upregulation of *ERG25*, *SKN1*, and *KRE1* [163]. *SKN1* and *KRE1* encode proteins involved in β-1,6-glucan biosynthesis (another component of fungal cell walls and ECM) and

restructuring of the glucan portion of cell walls has been associated with transient amphotericin B tolerance [164]. The authors proposed that a synergistic effect of the alteration of cell wall β-1,6-glucan content along with ergosterol changes is responsible for the increased tolerance, and these mechanisms were activated by the biofilm environment [163]. In addition, amphotericin B is bound by β-1,3-glucan and so can be sequestered in the biofilm ECM similar to azoles [156]. Consistent with this, *C. albicans* biofilms grown under flow have greater matrix deposition than statically grown biofilms and are significantly more tolerant to amphotericin B [165].

Echinocandins: Echinocandins such as caspofungin function by inhibiting the β-1,3-glucan synthase enzyme Fks1 [166], preventing the incorporation of β-1,3-glucan in the cell walls of *C. albicans* cells as well as in the ECM of biofilms. In comparison to the other antifungal classes discussed here, echinocandins possess a reasonably good efficacy against *Candida* biofilms *in vitro* [167][168] and *in vivo* [169]. Notably, since the Fks1 enzyme isn't found within mammalian cells, echinocandins display low levels of host toxicity. However, their use is fairly limited, predominantly being used for invasive candidiasis, as they are expensive and have a high molecular weight meaning they have to be administered intravenously [149].

Allylamines: Like the azoles, allylamines target ergosterol biosynthesis. They do this by inhibiting the squalene oxidase enzyme in the ergosterol biosynthetic pathway [153].

Pyrimidine analogs: Pyrimidine analogs such as 5-flucytosine function by disrupting fungal DNA and RNA synthesis [170]. It becomes an active antifungal upon being converted into 5-fluorouracil by cytosine deaminase, a fungal-specific enzyme [171]. 5-fluorouracil cannot be

used as an antifungal itself since it is highly toxic to mammalian cells and poorly taken up by fungal cells [170].

In addition to the tolerance mechanisms specific to each drug class, there are a variety general biofilm mechanisms which increase tolerance to several of the antifungals. Firstly, simply the fact that biofilms have a high cell density enables a certain level of antimicrobial tolerance; resuspended biofilm cells retain tolerance but are more susceptible when diluted [162]. This mechanism is not specific to biofilms as high planktonic cell densities (1×10^8 cells/ml) also exhibit increased tolerance to azoles and amphotericin B compared to lower densities (1×10^3 cells/ml) [162].

Additionally, the presence of persister cells within *C. albicans* biofilms contributes to their tolerance against a variety of antifungals. Persister cells are thought to be metabolically dormant phenotypic variants, as oppose to mutants, which can resist antimicrobial concentrations much higher than the usual MICs [172]. LaFleur *et al*. observed a biphasic killing pattern of *C. albicans* biofilms when treated with amphotericin B and/or the antiseptic chlorhexidine, suggesting the presence of a subpopulation of highly tolerant cells [172]. Importantly, the biofilm defective mutant *efg1Δ/cph1Δ* gives rise to persisters, showing the formation and tolerance of persister cells is not reliant on the development of a mature biofilm, instead simply occurring as a result of attaching to a surface. Furthermore, drug efflux does not account for persister cell survival since a mutant lacking the drug efflux pumps Cdr1, Cdr2, Mdr1 and Flu1 exhibits the same biofilm killing profile with the same amphotericin B and chlorhexidine MICs as wild type [172]. It is also important to note that persister cell production appears to be strain specific in *C. albicans* as GDH2346 forms persisters but

SC5314 does not [173], indicating persister cells are one of many reasons for *C. albicans* biofilm tolerance.

The presence of an extracellular matrix is a crucial feature of biofilms which contributes to tolerance to several antifungals; including azoles, polyenes, echinocandins and pyrimidine analogs [117]. *C. albicans* biofilms with a more extensive matrix, such as those grown under flow conditions, exhibit higher tolerances than those with less matrix material [165]. As previously mentioned, β-1,3-glucan in the ECM is able to bind to fluconazole [157] and amphotericin B [156], potentially reducing their penetration into biofilms. Furthermore, the cell walls of biofilm-associated cells are up to 2x thicker and contain more β-1,3-glucan than those of planktonic cells [157], resulting in them being able to bind 4-5x more fluconazole per cell wall [117]. Biofilms of a β-1,3-glucan synthase heterozygous knockout mutant (*FKS1/fks1Δ*), which have a 30% reduction in β-1,3-glucan content, exhibited higher susceptibility to the pyrimidine analog 5-flucytosine and the echinocandin andulafungin than wild-type [117]. Further evidence for the important role of the ECM in biofilm tolerance comes from the fact that mutants lacking the glucan transferase genes *BGL2* and *PHR1*, and the exoglucanase gene *XOG1*, have increased sensitivity to fluconazole specifically when in a biofilm. These enzymes are predicted to be in the ECM and are critical for the delivery and accumulation of β-1,3-glucan in the matrix.

From the above discussion it is clear that antimicrobial tolerance within *C. albicans* biofilms is complex and cannot be attributed to a single mechanism. While all the mechanisms described here have been shown to contribute to biofilm tolerance in several growth scenarios, they are probably not all utilised in every situation. The precise mechanisms of tolerance are likely

to be dependent on the experimental set-up used to grow the biofilms. For example, biofilms which are grown under flow conditions have a significantly different structure [174][175] and exhibit altered antifungal tolerance patterns from static biofilms [165][175]. Moreover, there appears to be contradiction between some studies; Nailis *et al.* found several *ERG* genes upregulated in mature biofilms after fluconazole treatment [155], whereas Vediyappan *et al*. concluded there were no significantly differentially expressed genes upon fluconazole treatment [156]. However, this could be due to the different experimental model systems used to grow the biofilms in the first place. This means that biofilms formed under different conditions *in vivo* are likely to have different tolerances as well as different mechanisms used to achieve these.

1.3.4 Current treatment strategies for *C. albicans* biofilms

Due to the high level of antimicrobial tolerance exhibited by *C. albicans* biofilms and the plethora of mechanisms used to achieve this, current treatment strategies are limited. There are presently no biofilm-specific therapeutics available, however, there has been some success using the currently available antifungals often in combinations with other compounds.

Echinocandins such as caspofungin and micafungin have displayed efficacy against *in vitro C. albicans* and *C. parapsilosis* biofilms [167]. This is likely due to their mode of action; inhibiting the synthesis of the major cell wall and ECM component β-1,3-glucan which has been implicated in biofilm-related antifungal tolerance. Liposomal formulations of the polyene amphotericin B have also been demonstrated to rapidly (95% biofilm killing in 12h) kill *C. albicans* biofilms *in vitro* in a dose-dependent manner [176]. This study also found

caspofungin to be effective against *C. albicans* biofilms [176]. Furthermore, liposomal amphotericin B has been observed to be effective at treating a catheter-associated biofilms in an *in vivo* rabbit model [177].

Combination therapy of traditional antifungals with other compounds seems to be an appealing option for *C. albicans* biofilm treatment. The hope being that treatment concentrations of antifungals, many of which have associated side-effects and host toxicity, can be reduced and still be effective. For instance, the combination of fluconazole and the antibiotic doxycycline significantly reduced the sessile minimum inhibitory concentration (SMIC) of fluconazole from 64-512μg/ml to 1-16μg/ml against biofilm-associated *C. albicans* cells. This combination was even effective against planktonic cells of strains known to be fluconazole-resistant [178].

Combinations of antifungals with painkillers such as aspirin have also had some success against *C. albicans* biofilms. Aspirin has shown efficacy against *Candida* biofilms on its own, although only at concentrations above those typically used for therapeutic effects in humans which limits its clinical use [179]. However, combination of amphotericin B and aspirin, at clinically relevant concentrations, reduced amphotericin B MIC values against *C. albicans* and *C. parapsilosis* biofilms *in vitro* [180]. In addition, administration of caspofungin after pre-treatment with the painkiller diclofenac significantly reduced *C. albicans* biofilm growth on an *in vivo* rat catheter model compared to treatment with each drug alone [181]. This may be due to a diclofenac-mediated increase in membrane permeability, diclofenac treatment has also been shown to reduce the expression level of genes downstream of the Ras1-Cyr1-PKA pathway including *EFG1* and hyphal-specific genes *ALS1, ALS3, HWP1* and *ECE1* which have

important roles in biofilm formation (Figure 1.9) [182]. The authors of the *in vivo* rat catheter study propose that coating medical devices with diclofenac, together with using traditional antifungals, could be a potential treatment strategy to eradicate *C. albicans* biofilms [181].

Treatment of *C. albicans* biofilms with miconazole has been shown to induce the intracellular production of superoxide radicals. *SOD5* and *SOD6* genes, encoding the superoxide dismutase enzymes Sod5 and Sod6 which rapidly convert toxic superoxide into molecular oxygen, were upregulated following miconazole treatment. The addition of the Sod inhibitor N,N'-diethyldithiocarbamate (DDC) increased the fungicidal activity of miconazole against *C. albicans* biofilms [183].

Finally, some recent studies have focussed on the use of more unusual compounds in the treatment of *C. albicans* biofilms. Yan, Y. *et al.* identified the Chinese herbal medicine component shikonin as being able to inhibit the formation and break up mature *C. albicans* biofilms [184]. Shikonin treatment also reduced fungal burden in a murine VVC model. Similar to diclofenac treatment, shikonin treatment resulted in the downregulation of hyphal- and biofilm-related genes such as *EFG1*, *ALS1, ALS3, HWP1* and *ECE1* as well as upregulation of negative hyphal regulators *TUP1* and *NRG1* [184]. An additional study showed polyphenol extracts from green tea elicited a dose-dependent inhibition of *C. albicans* biofilm formation [185].

1.3.5 Models used to study biofilms

There are numerous methods/models used to grow biofilms both *in vitro* and *in vivo*. One of the most frequently used *in vitro* model systems are microtiter plate-based models in which

biofilms are either grown on the bottom and walls of the wells on a plate (often a 96-well plate), or on a removable surface placed within the wells (often a silicone disc/square in a 12/24-well plate) [186] (Figure 1.10). Microtiter plate-based models are closed systems i.e. there is no addition/subtraction of material to/from the wells throughout the course of the experiment. As a result, the microenvironment within the wells will alter during the experiment (nutrients will diminish, waste products will accumulate, etc.). These model systems are widely used due to their low cost, efficiency because a large number of tests can be performed simultaneously, and the fact that these systems are excellent for screening purposes [187].

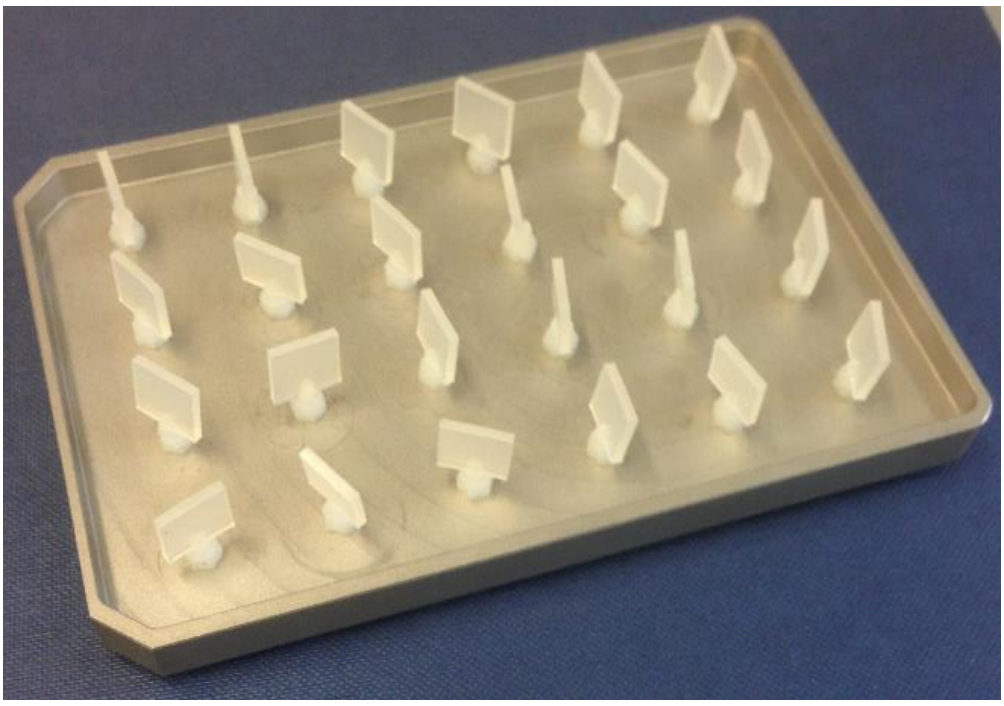


Figure: 1.10: The *in vitro* biofilm model used within this study. Biofilms were grown on 1cm^2 silicone squares which mimic the surface of the voice prosthesis. They were placed in modified 24-well plate lids so that they protrude into RPMI media containing *C. albicans* cells when placed on a 24-well plate. This enables easy washing and quantification of growth without disruption of the biofilm by transferring to new plates containing PBS or XTT reagent (see Materials and Methods).

Another method for growing biofilms *in vitro* is the flow displacement biofilm model system. In this system, growth medium is continually added, and waste-products removed, from the experimental system. There are two general groups of flow displacement systems: the 'continuous flow stirred tank reactor' (CFSTR) and the 'plug flow reactor' (PFR) [186]. A CFSTR system is operated at a steady state i.e. growth medium is added at the same rate as waste is removed, thus nutrient/waste concentrations stay the same. When dilution rate is higher than the growth rate (doubling time) of a microorganism, planktonic cells are washed away only leaving behind cells attached to a surface that will grow into a biofilm. A PFR system consists of the growth medium being added at one end and flowing through the reactor as a 'plug' to the other, mixing only occurs by diffusion in a radial direction. Unlike a CFSTR system, a PFR system is not stirred, meaning conditions change gradually through the reactor. In a CFSTR system, conditions are constant throughout [186].

A further method for *in vitro* biofilm growth is a cell-culture-based system. These model systems often use human cell lines in order to replicate *in vivo* conditions *in vitro*. For instance, models of oral and vaginal candidiasis have been produced, these use reconstituted human epithelia (RHE) as the surface upon which *C. albicans* forms a biofilm. These models do have limitations however because commensal microflora and cell-mediated immune responses are not present [186]. As previously discussed, *C. albicans* not only causes superficial candidiasis infections, but can also cause serious systemic infections. With this in mind, another type of *in vitro* biofilm model has been developed which investigates the ability of the different morphogenic forms of *C. albicans* to adhere to endothelium under flow conditions similar to those found in blood vessels [188]. Glass slides are covered with immortalised human microvascular endothelial cells (HMEC-1 cell line) and placed in a parallel plate flow chamber,

a suspension of *C. albicans* cells then flows through the chamber. With this model it was discovered that *C. albicans* cells in the yeast form adhere more readily to endothelial cells than filamentous forms do. This contrasts to the findings of other assays which used static conditions [186].

Microfluidic devices are yet another model used to study biofilm growth. They are extremely useful pieces of equipment because it is possible to use them to generate biofilms under conditions which are physiologically relevant, such as physiological flow rates and low fluid-to-cell ratios. The channels within microfluidic devices are typically very small (50-500µm wide, 30-250µm deep, 5-40mm long) and this small size allows microscopic analysis of any biofilms grown at a single-cell resolution. Environmental conditions can also be precisely regulated in microfluidic devices [189].

Although a lot can be learned from *in vitro* biofilm growth models, it is also necessary to study biofilm growth *in vivo*. These *in vivo* biofilm models are typically carried out in either *Caenorhabditis elegans* worms or, if a vertebrate model is required, in murine animals. Investigations using *C. elegans* as a model system have typically focused on bacterial biofilm formation and have allowed the identification of both bacterial and host genes which are required for bacterial adhesion and Biofilm growth. *In vivo* studies of *C. albicans* biofilms are usually conducted in murine animal models, primarily to examine biofilm formation as a result of implanted medical devices such as catheters [186]. These animal models have been used to investigate the *in vivo* susceptibility and molecular response of *C. albicans* biofilms to several antifungal compounds (such as fluconazole and caspofungin) [190], to increase understanding of the molecular basis of *C. albicans* biofilm formation, and to study the role

of specific adhesins (such as Eap1) in biofilm formation [191]. Animal models also provide an insight into the changes in gene expression in biofilms *in vivo* over time [130].

1.4 Laryngeal Cancer, Laryngectomies and Voice Prostheses

Head and neck cancer is the sixth most common cancer worldwide and the eighth most common cancer in the UK with 650,000 new cases (12,000 in the UK) and 350,000 deaths (4,000 in the UK) attributed to it each year worldwide [192][193]. Laryngeal malignancy is the most frequent head and neck cancer, making up 26.2% of newly diagnosed male cases and 13.1% of female cases in the UK [193]. Approximately 12,000 people are diagnosed with laryngeal cancer each year in the United States [194].

Laryngeal malignancy is treated with radiotherapy if it is diagnosed at an early stage, however, at later stages treatment involves surgery often in conjunction with radiotherapy [194]. Unfortunately, the majority of head and neck cancers are diagnosed at an advanced stage; 62% of new diagnoses in Northern Ireland are at Stage III or IV (Stage IV alone accounts for 45%) [193]. This means many cases of laryngeal cancer have to be treated with a surgical procedure known as a laryngectomy after which the patient relies on the use of an indwelling medical device called a voice prosthesis to form speech. It has been estimated that there are currently 50,000–60,000 laryngectomees living in the United States [194].

As with all indwelling medical devices, the surface of a voice prosthesis provides an environment for the growth of microorganisms sequestered away from the host's immune system. This ultimately leads to the failure of the device and can also be a source of potentially harmful infections [195][196]. Thus, voice prostheses need to be regularly changed,

contributing to much inconvenience and stress to the patient as well as financial cost to medical institutions. Management and prevention of microorganism growth on voice prostheses is crucial to increasing the lifespan of these devices, and an understanding of biological pathways which microorganisms utilise during colonisation is critical to this.

1.4.1 Laryngectomies and Voice Prostheses

A laryngectomy involves the partial or total removal of the larynx, along with surrounding lymph nodes, and results in the alteration of the upper airway anatomy (Figure 1.11) [197]. This surgery is often used to treat laryngeal or hypopharyngeal cancers, with the precise surgery approach dependent on the stage of the cancer; earlier stage cancers can be treated with a partial laryngectomy to remove only the affected part of the larynx, whereas patients with advanced stage cancer will have their entire larynx removed [194].

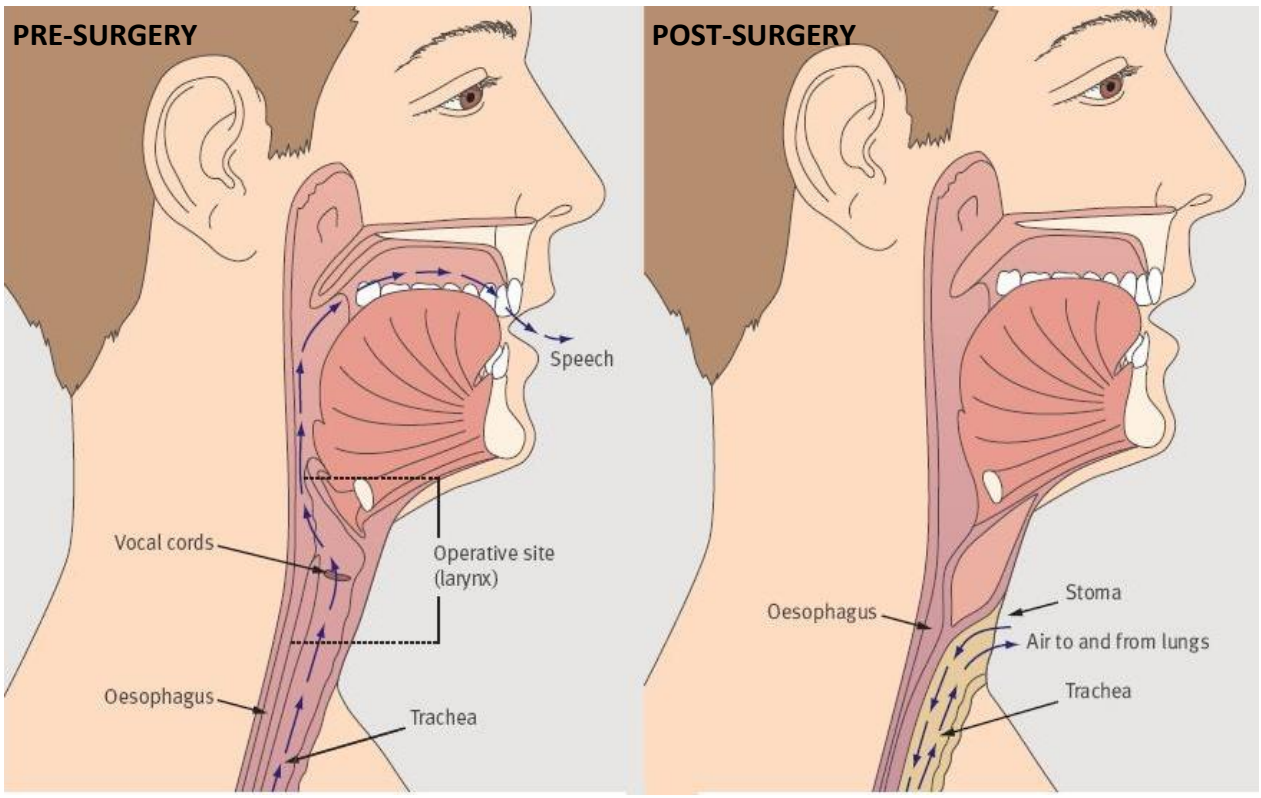


Figure 1.11: Upper airway anatomy before and after total laryngectomy. A total laryngectomy removes the larynx, including the vocal cords, and separates the trachea from the oesophagus and the mouth. After the operation, the patient breathes through a hole at the base of the neck called a stoma.

Following the surgery, the patient will no longer be able to breathe through their mouth or nose, instead breathing through a hole at the base of the neck called a stoma [197]. Furthermore, as the vocal cords are located within the larynx (Figure 1.11), most total laryngectomy patients are no longer able to form speech on their own. There are three major methods which 85-90% of laryngectomees employ to achieve speech; oesophageal speech, artificial larynx speech and tracheoesophageal speech [194]. Oesophageal speech involves creating vibrations to mimic speech using air emitted from the oesophagus. This method of speaking can be advantageous because it does not rely on additional devices, however, it does take time to learn and proves difficult to achieve. Artificial larynx speech involves using an external electrical device (called an artificial larynx) which produces vibrations when held on the cheek or under the chin. These vibrations are then modulated by the patient's mouth to generate speech. This method tends to be used in the short-term following a laryngectomy operation before the patient learns one of the other techniques [194].

The gold standard for speech rehabilitation is tracheoesophageal speech which requires the use of a small silicone valve known as a voice prosthesis [198] (Figure 1.12). The voice prosthesis (VP) is inserted into a hole called the tracheoesophageal puncture (TEP) made by the surgeon behind the stoma between the trachea and the oesophagus. It is made up of a one-way valve surrounded by a flange to prevent the TEP from closing and functions to direct air from the trachea into the oesophagus while inhibiting foods and liquids flowing through to the lungs. Air is forced through the voice prosthesis by covering the stoma with a finger, and this redirected air causes the top of the oesophagus to vibrate which can be modulated by the mouth to create speech [194].

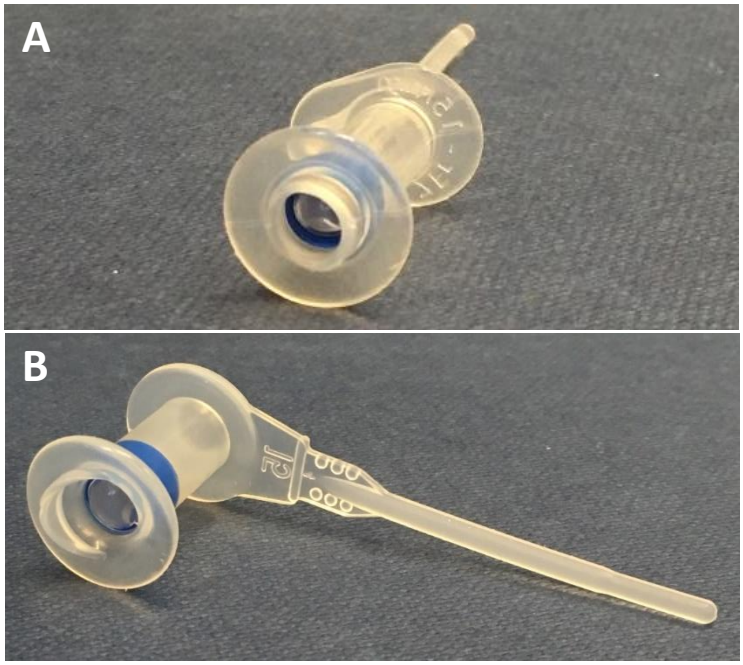


Figure 1.12: Two types of voice prostheses commonly used for speech rehabilitation following total laryngectomy. (A) The Provox Vega voice prostheses. **(B)** The Provox 2 voice prostheses.

1.4.2 Microbial colonisation of voice prostheses

Although VPs produce the best results in terms of voice quality, they also pose a major problem. The silicone of the prostheses, as with many synthetic materials of indwelling medical devices, is readily colonised by microorganisms. The foods, liquids and saliva [199] which begin to coat the silicone surface of the VP, along with the high humidity and approximate 37^{o}C temperature in the oesophagus, provide the perfect environment for microbe attachment and growth as a biofilm [10]. These microbes range from bacteria to fungi, with both often being found together in a mixed community. *Streptococcal* species such as *Streptococcus mitis* and *Streptococcus sobrinus*, *Staphylococcal* species such as *Staphylococcus aureus* [200], and *Pseudomonas aeruginosa* [201] are the major bacterial microorganisms frequently isolated from voice prostheses. *Candida* species, particularly *Candida albicans*, *Candida glabrata*, and *Candida tropicalis*, are the primary fungal

microorganisms which grow on VPs in a biofilm and ultimately cause the devices to fail [202]. The exact microbial composition on a particular voice prostheses is influenced by several factors including patient diet, lifestyle and the voice prostheses management regime to which they subscribe [10]. This is highlighted by a study conducted in India by Sayed *et al.* which found a different microbial landscape compared to similar European studies [201].

Device failure is predominantly attributed to 'leakage' caused by microorganism biomass preventing the valve fully closing, hindering the VP function and hence resulting in the replacement of the device [192][195]. Moreover, the microbial colonisation also acts as a reservoir from which potential pathogens can cause infection such as pneumonia if the voice prosthesis remains in the body for too long [196]. The mean VP lifespan is highly variable across different studies and has been reported as being between 120 and 200 days [201][203], after which it needs to be replaced in an invasive procedure.

C. albicans is the most prevalent fungal coloniser of a VP surface and as such a significant number of device failures are associated with the presence of *C. albicans* [202][204][205]. Since fungal cells have a larger biomass than bacterial cells, it has been hypothesised that the fungal cells directly contribute to voice prosthesis failure due to valve 'leakage' more than bacterial cells. Although the importance of the role the bacterial cells play should not be underestimated. Consequently, this study focuses on the *C. albicans* colonisation of voice prostheses and the factors, such as CO_2 concentration, which influence it.

1.4.3 Current strategies for the prevention of microbial colonisation of voice prostheses

Due to the inherent tolerance of biofilms to perturbations and treatments (see Section 1.3.3), there have been limited treatment strategies for prolonging VP *in situ* lifespan which has resulted in some intuitive approaches. These treatment approaches to prevent microbial colonisation of VPs broadly fall within two categories: modifications to the silicone surface itself or prophylactic treatments (for example with antifungals) and dietary recommendations [10].

Voice prosthesis silicone surface modifications: Several studies have focussed on the coating of silicone VPs with a thin-layer of metal. A gold or titanium coating (<100nm) did not affect the physical properties of the VP or cause any difference in speech quality [206]. However, further evidence is required to determine if this approach leads to decrease in biofilm formation. Promising results have been observed by coating Groningen button VPs with a palladium/tin salt mixture which significantly attenuated biofilm formation compared to uncoated VPs [207]. The Blom-Singer Advantage is a commercially available VP which contains 7% silver oxide in the valve. In a 33 patient cohort with particularly early failing VPs, the Blom-Singer Advantage exhibited a significantly increased mean lifespan *in situ* compared to other indwelling VPs such as the Provox 2 (36 days to 110 days) [208].

Hydrophobicity has been shown to influence biofilm formation on VPs *in vivo* [209]. Therefore, studies have been carried out to determine if the addition of hydrophobic fluorocarbons, such as fluoro-alkylsiloxanes, to the silicone surface can reduce microbial colonisation. Coating a silicone surface with long chain fluoro-alkylsiloxanes reduced microbial adherence and also increased the rate of detachment of microbes which did

manage to attach [210]. The benefit of fluorocarbon coating is very reliant on the fluorocarbon chain length as short chain (1 fluorocarbon unit) perfluoro-alkylsiloxane actually increased microbial colonisation *in vivo* whereas long chain (8 fluorocarbon units) perfluoro-alkylsiloxane reduced it [211].

Finally, covalently adding quaternary ammonium salts to the silicone surface has been proposed to prevent microbial VP colonisation. Antibacterial activity of silicone coated with quaternary ammonium salts against both Gram-positive and Gram-negative species has been demonstrated *in vitro* and *in vivo* [212]. Quaternary ammonium salts also reduced the number of viable yeast and bacteria in an artificial throat mixed biofilm VP model [213].

Prophylactic treatments and dietary recommendations: The effects of bacteria with probiotic attributes, such as *Lactobacilli* and some *Streptococcal* species, on biofilm formation have been investigated. Exposure of biofilms grown in an artificial throat model to suspensions of the probiotic *Lactococcus lactis* 53 and *Streptococcus thermophilus* B strains reduced CFU of both bacteria and yeasts on Groningen and Provox 2 VPs compared to untreated controls [214]. Biosurfactants released by *S. thermophilus* B inhibit the adhesion of *Candida* species to silicone rubber [215]. Certain dietary modifications to increase a patient's probiotic intake have also been proposed to have beneficial effects of the *in situ* lifespans of VPs. For instance, the consumption of buttermilk has been widely regarded as prolonging the function of VPs; in an artificial throat model which mimicked buttermilk ingestion, biofilm formation on Groningen button VPs was almost completely prevented [216].

The use of antifungal agents to 'decontaminate' the oropharynx has been considered to enhance the lifespan of VPs. Historically, the use Amphotericin B lozenges [217] and buccal bioadhesive slow-release Miconazole nitrate tablets [218] to reduce oropharyngeal fungal burden have resulted in increases in voice prosthesis lifespans. However, the Amphotericin B lozenges and Miconazole tablets have since been discontinued by the pharmaceutical company [10]. Overall, there is little evidence that oral administration of antifungals prolongs VP lifespan and there is also a concern that prophylactic antifungal use may contribute to the emergence of resistant strains.

Finally, there have been some promising results investigating the use of synthetic salivary peptides, which exhibit bactericidal and fungicidal activity and are active against antifungal resistant *Candida* strains [219], to increase VP lifespan. Synthetic peptides dhvar4 and dhvar5, which are analogs of human histatin-5, were studied in an artificial throat VP model to determine their effect on VP biofilm integrity. Dhvar4 had no significant effect on mixed biofilms growing on Groningen button VPs, on the other hand, dhvar5 significantly reduced both bacteria and yeast numbers [220]. Intriguingly, airflow resistance through the VP valve, a hallmark of biofilm growth on these devices, remained high during dhvar5 treatment. Treatment with the mucolytic N-acetylcysteine removed most of the extracellular matrix (ECM) and decreased airflow resistance. This prompted the authors to conclude that VP lifespans are not only dictated by cell growth itself but also by the extent of biofilm ECM deposition [220]. These results raise important questions about which biofilm attribute (cell densities or ECM production) should be focussed on when developing treatment strategies.

Overall, there have been some promising results in various studies investigating different strategies to prevent polymicrobial biofilm formation and thus increase VP lifespan. However, there has been limited success in translating these studies into effective clinical treatments and as such average VP lifespan has not increased significantly in the last 10 years [221].

1.5 Aims of this Study

The colonisation of voice prostheses by microorganisms such as *Candida albicans* and their subsequent removal is a significant burden to total laryngectomy patients. Despite numerous attempts, voice prosthesis lifespans have not significantly increased over the last 10 years and according to some studies may even be lower than originally thought [221]. *Candida albicans* is the primary fungal microbe consistently found on failed voice prostheses [202] and significantly contributes to their failure. Here, we further investigate the microbial landscape on failed voice prostheses while exploring treatment strategies, principally prophylactic antifungal application directly on VP surfaces, to increase VP *in situ* lifespan. We focus on the effect of physiologically relevant concentrations of CO_2 (5%) [222] on biofilm formation in *C. albicans* to gain insights into its success in the VP scenario which could prove useful in the development of novel antifungal treatments in the future. We also hope that our findings will be more widely applicable to *C. albicans* infections in high CO_2 niches within the host, many of which involve biofilm formation [113].

Chapter 2 – Precision antifungal treatment significantly extends voice prosthesis lifespan in patients following total laryngectomy

Daniel R. Pentland[1], Sarah Stevens[2], Leila Williams[2], Mark Baker[2], Carolyn McCall[2], Viktorija Makarovaite[1], Alistair Balfour[2], Friedrich A. Mühlschlegel[3], Campbell W. Gourlay[1*]

[1]Kent Fungal Group, School of Biosciences, University of Kent, Kent, CT2 9HY, UK

[2]East Kent Hospitals University NHS Foundation Trust, Kent, UK

[3]Laboratoire National de Santé, Dudelange, L-3555, Luxembourg

[*]Author for correspondence

2.1 Author Contributions

All authors are members of a multidisciplinary team (MDT) at Canterbury Hospital, Canterbury, Kent.

I (Daniel R. Pentland) wrote this paper in its entirety. Microorganism identification from early failing voice prostheses and initial antimicrobial sensitivity testing was carried out by Dr. Mark Baker at the William Harvey Hospital, Ashford, Kent. I was responsible for the full analysis of this microbiology data and the conclusions drawn. I also carried out all the experiments detailed within this paper.

Throughout my PhD, as a member of the MDT at Canterbury Hospital, I met with other members every 3 months where I discussed, advised and was involved in both the formulation and the implementation of the novel VP antifungal treatment guidelines detailed in the paper. Together with Sarah Stevens and Leila Williams, I collated anonymised VP lifespan data for before and after antifungal treatment guidelines implementation. I was then responsible for the statistical analyses of this data presented in the paper.

Finally, I have disseminated this research through presentations at both public lectures and professional conferences:

1. **July 2016 – British Yeast Group (University of Swansea, UK)**

   Poster and oral presentation – 'Investigating the Colonisation of Voice Prostheses by *Candida albicans*'

2. **January 2017 – Kent Cancer Trust Annual Public Lecture (University of Kent, UK)**

   Oral presentation – 'A Multi-Disciplinary (MDT) Approach to Combat Biofilm Formation on Voice Prostheses'

3. **May 2017 – Molecular Mechanisms of Host-Pathogen Interactions and Virulence in Human Fungal Pathogens (Nice, France)**

   Poster – 'Investigating the Colonisation of Voice Prostheses by *Candida albicans*'

4. **September 2017 – British Yeast Group (University of Kent, UK)**

   Poster – 'Investigating the Colonisation of Voice Prostheses by *Candida albicans*'

5. **March 2018 – Advanced Laryngectomy: Rehabilitation and Surgical Voice Restoration Course (Imperial College London, UK)**

   Oral presentation – '*Candida*: The Facts. What it is, What it Does, and How to Control it'

6. **June 2018 – British Yeast Group (University of Leicester, UK)**

   Oral presentation – 'Investigating the Effects of High CO_2 on *Candida albicans* Biofilm Formation'

2.2 Abstract

Surgical voice restoration, which involves the use of a small silicone voice prosthesis (VP), is the gold standard for speech rehabilitation following total laryngectomy, a common treatment for advanced laryngeal cancer. Reported VP lifespans within patients are highly variable and the devices have to be changed on a regular basis, resulting in frequent clinician visits and increased medical costs. Multi-species biofilms comprised of both bacterial and fungal microorganisms easily colonise VPs, leading to loss of device function as well as creating a reservoir for infections. Through studying the biofilm composition on 159 early failing VPs from 48 total laryngectomy patients, we have confirmed that *Candida* species, particularly *Candida albicans*, are the predominant fungal species colonising early failing VPs. We also find that *Staphylococcus aureus* is the most common bacterial coloniser within our patient cohort. In addition, we present a 20 patient study of a novel antifungal focussed treatment strategy which significantly increases VP *in situ* lifespan from a mean of 71.9 to 192.0 days, a 2.7-fold increase. Our treatment guidelines represent a significant advance in both our understanding of voice prosthesis failure and a new effective method to increase voice prosthesis lifespan.

2.3 Introduction

Head and neck cancer is the sixth most common cancer worldwide and the eighth most common cancer in the UK with 650,000 new cases (12,000 in the UK) and 350,000 deaths (4,000 in the UK) attributed to it each year worldwide [192][193]. Laryngeal malignancy is the most frequent head and neck cancer, making up 26.2% of newly diagnosed male cases and 13.1% of female cases in the UK [193]. Approximately 12,000 people are diagnosed with laryngeal cancer each year in the United States [194].

Laryngeal malignancy is treated with radiotherapy if it is diagnosed at an early stage, however, at later stages treatment involves surgery often in conjunction with radiotherapy [194]. The majority of head and neck cancers are diagnosed at an advanced stage; for example 62% of new diagnoses in Northern Ireland are reported to be at Stage III or IV (Stage IV alone accounts for 45%) [193]. Late diagnosis means that many cases of laryngeal cancer have to undergo a partial or total laryngectomy. It has been estimated that there are currently 50,000–60,000 people who have had a laryngectomy living in the United States [194].

Following a total laryngectomy, the patient will no longer be able to breathe through their mouth or nose, instead breathing through a hole at the base of the neck called a tracheostoma (stoma) [197]. Furthermore, as the vocal cords are located within the larynx, most total laryngectomy patients are no longer able to form speech on their own. There are three major methods which 85-90% of laryngectomees employ to achieve speech; oesophageal speech, artificial larynx speech (use of a handheld device called an electrolarynx) and tracheoesophageal speech [194]. The gold standard for speech rehabilitation is tracheoesophageal speech which requires the use of a small silicone valve known as a voice

prosthesis (VP) [198]. The voice prosthesis is inserted into a tracheoesophageal puncture (TEP): a surgically-created puncture which is made behind the stoma between the trachea and the oesophagus. A VP is made up of a one-way valve within a central barrel with an anterior (tracheal) flange and a posterior (oesophageal) flange which serve to retain it within the tracheoesophageal wall. The VP functions to direct air from the trachea into the oesophagus during speech while inhibiting passage of food and liquid to the lungs. Air is forced through the voice prosthesis by covering the stoma, and this redirected air is modulated by the mouth to create speech [194].

Voice prostheses are susceptible to colonisation by microbial biofilms [223]. Such contamination may be enhanced by the environment of the oesophagus e.g. foods, liquids (including saliva), humidity and constant temperature [10][199], and device failure has been attributed to such microbial growth as it can prevent valve closure [224][225] and thereby allow leakage of oesophageal contents into the airway. A loss of valve functionality can also lead to reduced airflow for speech and requires replacement of the device [192][195]. Moreover, the microbial colonisation may act as a reservoir of potential pathogens which may lead to life-threatening infections such as pneumonia [196]. The mean VP lifespan is highly variable across different studies and has historically been reported as being between 120 and 200 days [201][203]. However, a recent large-scale study which analysed the lifespan of 3648 VPs reported an average of 86 days [221].

A number of strategies have been proposed to increase VP lifespan, such as the use of magnets to support the closing of the valve [226] and the incorporation of compounds, for example silver oxide, within the VP material to prevent microbe colonisation [227]. VPs

containing magnets such as the Provox ActiValve have been shown to have longer *in situ* lifespans than other models [221][228]. However, the overall levels of success with these approaches has been variable and importantly the average VP device lifespan has not significantly increased over the last 10 years [221].

Co-colonisation of VPs by bacterial and fungal species is commonly reported. *Streptococcal* species (e.g. *Streptococcus mitis* and *Streptococcus sobrinus*), *Staphylococcal* species (e.g. *Staphylococcus aureus*) [200], and *Pseudomonas aeruginosa* [201] are among the major bacterial microorganisms frequently isolated from voice prostheses. *Candida* species, particularly *Candida albicans*, *Candida glabrata*, and *Candida tropicalis*, are the primary fungal microorganisms isolated from VPs [202]. Microorganisms, such as *C. albicans*, colonise VPs by growing as biofilms. Biofilms are structured communities of microorganisms which are attached to either a living or non-living surface. The cells are often encased within an extracellular matrix composed of DNA [107][108], lipids [107], proteins [107][109] and polysaccharides [107]. Medically, biofilms are of particular importance because it is thought that a significant percentage of human microbial infections include biofilm formation [110][111][112]. Furthermore, cells within biofilms can be up to 1000x more tolerant to antimicrobial treatment than their planktonic counterparts [114][115].

The exact microbial composition on any particular voice prostheses is influenced by several factors including patient diet, lifestyle and the voice prosthesis management regime to which they subscribe [10]. This is highlighted by a study conducted in India [201] which found a different microbial landscape with much higher numbers of *P. aeruginosa*, to that described in similar European studies [204]. *C. albicans* is the most prevalent fungal coloniser of a voice

prosthesis surface and thus a significant number of device failures correlate with the presence of *C. albicans* [202][204]. It is a commensal yeast that is found on the mucosal surfaces of the oral cavity, gastrointestinal tract and genitourinary tract of most healthy individuals [6][7]. *C. albicans* is a dimorphic fungus and biofilm formation of this organism involves a switch from growing in the typical budding yeast form to a filamentous hyphal form. This switch in morphology is also closely related to the shift from growing as a commensal organism to becoming pathogenic, since the hyphal form can invade human tissue [6]. Hyphal *C. albicans* cells express specific cell wall proteins, such as Als1 and Hwp1, which enable attachment to surfaces (and between cells) during biofilm maturation [132][133]. The yeast-to-hyphae switch is driven by a variety of environmental stimuli, including growth at 37^{o}C [67][68], exposure to high levels of CO_2 [69], and serum exposure [71].

Despite being a commensal organism, it is also an opportunistic pathogen [6][8]; in fact, it is the most widespread of all the human fungal pathogens [9]. The infections caused by *C. albicans* range from superficial infection of mucosal surfaces (commonly referred to as candidiasis) to a full systemic infection called candidaemia which can advance to disseminated candidiasis whereupon fungal growths can occur within internal organs such the kidney, heart and brain [6]. The other fungal species which commonly colonise voice prostheses, such as *C. glabrata*, *C. tropicalis* and *C. parapsilosis*, also cause infections [229][230][231][232] and have been increasingly associated with nosocomial infections [8].

Here we characterise the microflora found on early failing voice prosthesis from 48 patients within Kent (South East UK) over a 5-year period (2011-2016). We observe that multi-species biofilms form in most cases with *C. albicans* and *S. aureus* being the most prevalent. We

demonstrate that the high CO_2 environment experienced in the airway promotes *C. albicans* biofilm formation on VPs, providing an explanation for its prevalence. We devised a strategy to tackle yeast contamination that involved the directed application of antifungals verified to be most effective in drug sensitivity assays of clinical isolates. We report results from a 20 patient study that verifies antifungal treatment as an effective approach to VP lifespan extension. Over 8 years, this study documented voice prosthesis *in situ* lifespan, both before and after implementation of the antifungal treatment guidelines. Statistical analyses confirmed that the treatment guidelines significantly increased voice prosthesis lifespan within the patient cohort. Our guidelines represent a significant advance in both our understanding of VP failure and a new effective method to increase VP lifespan.

2.4 Materials and Methods

2.4.1 Patient cohort and voice prostheses

Biofilms from a total of 159 voice prostheses from 48 patients were analysed for microorganism composition. All prostheses were removed from patients attending one of the three main acute hospital sites within East Kent, UK: William Harvey Hospital, Ashford; Canterbury Hospital, Canterbury; Queen Elizabeth the Queen Mother Hospital, Margate. 38 of these patients had multiple voice prosthesis failures and were followed as part of the *Candida* management guideline impact study, which documented the voice prosthesis lifespans before and after implementation of the treatment guidelines.

2.4.2 Microorganism isolation and identification

To determine which microorganisms were present, a failed voice prosthesis was removed from the patient and sealed in a sterile pot. Upon receipt at the microbiology laboratory, the voice prosthesis was added to 2ml saline solution along with glass beads and vortexed at 2500rpm for 30 seconds. The resulting suspension was plated on chromogenic agar to preliminarily distinguish species. 50µl of the suspension was also plated on Sabouraud Dextrose Agar (SDA) plates (Oxoid, CM0041) containing 100µg/ml chloramphenicol (Oxoid, SR0078) to promote the growth of fungal species while inhibiting bacterial growth. Chromogenic agar and SDA plates were incubated for 48 hours at 37^{o}C. Bacterial colonies were then picked from the chromogenic plates and fungal colonies were picked from the SDA plates, species were identified using matrix assisted laser desorption ionisation time-of-flight mass spectrometry (MALDI-ToF).

2.4.3 MALDI-ToF mass spectrometry identification of microorganisms

MALDI-ToF mass spectrometry was used to identify species isolated from failed voice prostheses within this study. Fungal and bacterial colonies were picked and applied to a steel MALDI target plate before being overlaid with an α-cyano-4-hydroxycinnamic acid (4-HCCA) matrix (Sigma-Aldrich, 70990) [233]. MALDI-ToF mass spectrometry was performed using a Bruker MALDI Biotyper (Bruker) as per the manufacturer's instructions. The resulting mass spectra were compared to a reference database for identification using the MBT Compass and MBT Explorer Software along with the MBT Compass Library which comprises approximately 2750 species from 471 microorganism genera.

2.4.4 Antifungal sensitivity testing

Antifungal sensitivity testing was performed using the Fungitest™ commercial testing kit (BioRad, 60780) as per the manufacturer's instructions. Briefly, isolated colonies were selected from culture plates (see Microorganism isolation and identification) and suspended in 3ml sterile distilled water. This suspension was then used to inoculate 3ml of RPMI-1640 media to a density of 10^3 CFU/ml and 100µl of this resulting suspension was placed in each well of the Fungitest™ plate. The Fungitest™ plates were incubated for 48 hours at 37°C, at which point the fungal growth was measured via a colorimetric readout (blue = no growth, pink = growth). Isolates were assigned sensitive, intermediate or resistant based upon the European Committee on Antimicrobial Sensitivity Testing (EUCAST) breakpoint recommendations for each antifungal and/or species [234].

2.4.5 Antibacterial sensitivity testing

Antibacterial sensitivity testing was carried out to determine the minimum inhibitory concentrations (MICs) of clinically commonly used antibiotics. The sensitivity testing was performed using a standard broth microdilution procedure in accordance with the International Standard ISO 20776-1 method (detailed at: https://www.iso.org/obp/ui/#iso:std:iso:20776:-1:ed-2:v1:en) as recommended by EUCAST [235]. Isolates were assigned sensitive, intermediate or resistant based upon the EUCAST breakpoint recommendations for each antibiotic and/or species [236].

2.4.6 Scanning electron microscopy (SEM) of voices prosthesis surfaces

Segments were taken from the valve and flange of a Provox Vega voice prosthesis and mounted onto 12.5mm aluminium SEM specimen stubs (Agar Scientific, AGG301) with superglue. The surfaces were imaged at ambient temperature with a Hitachi S-3400N scanning electron microscope, using the variable pressure scanning electron microscopy (VP-SEM) mode with a chamber pressure of 30Pa and accelerating voltage of 10kV. The backscattered electron (BSE) detector in conjunction with the energy dispersive X-ray spectroscopy (EDS) detector was used throughout with a working distance of 10mm. The acquisition software was Oxford Instruments INCA and images were exported directly from this.

2.4.7 Atomic force microscopy (AFM) of voice prosthesis surfaces

Segments were taken from the valve and flange of a Provox Vega voice prosthesis and mounted onto 15mm AFM specimen discs (Agar Scientific, F7003) with superglue. These surfaces were imaged at ambient temperature using a Bruker Multimode 8 scanning probe

microscope with a Nanoscope V controller, using the ScanAsyst peak-force tapping mode with a 50µm x 50µm scan area and a 700nm scan height. SCANASYST-AIR (Bruker) silicon nitride cantilevers (tip height of 2.5-8.0µm, nominal tip radius of 2nm) with a nominal spring constant of 0.4N/m and a resonance frequency of 70kHz were used throughout. The image acquisition software was Nanoscope 8.15 R3sr5 and the processing software was Nanoscope Analysis.

2.4.8 *Candida* strains and growth media

Candida strains (Table S3) were routinely grown at 30°C in yeast peptone dextrose (YPD) media (2% peptone (BD Bacto), 2% D-glucose (Fisher Scientific), 1% yeast extract (BD Bacto)). For the biofilm growth assays, *Candida* biofilms were grown at 37°C in RPMI-1640 media (Sigma-Aldrich, R8755) supplemented with 80µg/ml uridine (Sigma-Aldrich, U3750). *Candida* strains were maintained in YPD + 20% glycerol at -80°C for long-term storage and revived at 30°C on YPD + 2% Technical Agar (Oxoid) plates.

2.4.9 *In vitro* biofilm growth assays

C. albicans biofilms were grown on a PDMS silicone elastomer (Provincial Rubber, S1). The silicone was cut into 1cm^2 squares and placed in clips in a modified 24-well plate lid (Academic Centre for Dentistry Amsterdam, AAA-model – Figure S1) so they could be suspended in media within a sterile 24-well plate (Greiner Bio-one, CELLSTAR, 662160). Silicone squares were incubated in 1ml 50% Donor Bovine Serum (DBS) (Gibco, 16030074) for 30 min at 30°C, then washed twice with 1ml Phosphate-Buffered Saline (PBS – 137mM NaCl, 2.7mM KCl, 10mM Na_2HPO_4, 1.8mM KH_2PO_4, pH 7.4) to remove excess DBS. *Candida* strains were inoculated into a test tube containing 5ml YPD media and placed in a 30°C orbital shaking incubator with constant shaking at 180rpm for 18h. OD_{600} measurements were taken and a

volume of overnight culture corresponding to OD_{600} = 1.0 (3 x 10^7 CFU/ml) was removed. These cells were pelleted by centrifugation at 4000rpm for 5 min at which point the supernatant was discarded. The resultant pellet was re-suspended in 5ml PBS to wash and centrifuged again at 4000rpm for 5 min. The PBS supernatant was discarded and the pellet re-suspended in fresh PBS (at an OD_{600} of 1.0). The OD_{600} 1.0 standard cell suspension was added to wells (1ml per well) in a pre-sterilised 24-well plate and the lid with the silicone squares attached was placed on top so the silicone squares protruded into the cell suspension. These plates were then incubated at 37°C (in either 0.03% CO_2 or 5% CO_2) without shaking for 90 min to allow cell attachment to the silicone. After the attachment phase, the silicone squares were washed twice with 1ml PBS to remove any unattached cells and transferred to 1ml RPMI-1640 media (Sigma-Aldrich, R8755). They were then incubated at 37°C (in either 0.03% CO_2 or 5% CO_2) without shaking for up to 48 h to allow biofilm maturation. Growth of biofilms on the surface of a sterile VP was conducted using the same protocol.

2.4.10 Biofilm quantification via XTT assay

Biofilm growth was quantified using an XTT assay [237]. Biofilms were washed twice with 1ml PBS to remove any planktonic cells before proceeding to quantification. After washing, the biofilms were transferred to a new pre-sterilised 24-well plate (Greiner Bio-one, CELLSTAR, 662160) containing 30µg/ml XTT labelling reagent (Roche, 11465015001) and incubated at 37°C for 4h. After incubation, the biofilms were removed from the 24-well plate and the absorbance of the remaining XTT labelling reagent was measured at 492nm using a BMG LABTECH FLUOstar Omega plate reader machine.

2.4.11 Antifungal treatment of biofilms

Biofilms were seeded on silicone elastomer sections as described above and grown in RPMI-1640 for 24h at 37°C. The biofilms were then transferred to fresh RPMI-1640 media containing an antifungal, either; Fluconazole, Miconazole or Nystatin to represent those used in the clinical guidelines (Figure S4). Fluconazole (Santa Cruz Biotechnology, sc-205698) was made as a 50mg/ml stock solution in ethanol and diluted in RPMI-1640 final concentrations of 32µg/ml and 128µg/ml. Miconazole (Santa Cruz Biotechnology, sc-205753) was made as a 50mg/ml stock solution in DMSO and also diluted in RPMI-1640 to final concentrations of 32µg/ml and 128µg/ml. Nystatin (Santa Cruz Biotechnology, sc-212431) was made as a 5mg/ml stock solution in DMSO and diluted in RPMI-1640 to final concentrations of 2µg/ml and 8µg/ml. Drug vehicle controls (0.25% ethanol for Fluconazole, 0.25% DMSO for Miconazole and 0.15% DMSO for Nystatin) were used to ensure the solvents were not affecting biofilm growth. The biofilms matured in the RPMI-1640 media containing the select antifungal for a further 24h at 37°C in both 0.03% and 5% CO_2 before proceeding to quantification via the XTT assay. Experiments were performed in biological and technical triplicate.

2.4.12 Mixed species biofilm competition assays

Biofilms were set up as described previously, except that for mixed biofilms *C. albicans* and *C. parapsilosis* clinical isolate overnight cultures were each counted and adjusted to $1.5x10^7$ CFU/ml to give a $3x10^7$ CFU/ml overall inoculum (equivalent to OD_{600} of 1.0) for the 90 min attachment phase. After attachment, the silicone squares were washed twice with 1ml PBS to remove any unattached cells and transferred to 1ml RPMI-1640 media (Sigma-Aldrich, R8755). They were then incubated at 37°C in both 0.03% CO_2 or 5% CO_2 without shaking for

48h to allow biofilm maturation before proceeding to quantification via the XTT assay. Experiment was performed in biological and technical triplicate.

2.4.13 Biofilm composition analysis via chromogenic agar

Silicone squares with biofilms on them were dropped into 2ml PBS and vortexed for 10 seconds at 2500rpm to release the biofilm cells from the surface. The resulting biofilm cell suspension was plated on Candida Ident. Agar (Fluka Analytical, 94382) in triplicate (200µl per plate). The chromogenic agar plates were incubated at 30^{o}C for 48h, at which point photographs of the plates were taken. *C. albicans* colonies appeared green and *C. parapsilosis* colonies stayed white on the Candida Ident Agar plates.

2.4.14 Analysis of voice prosthesis lifespans

Voice prosthesis lifespans of patients living in East Kent, UK were investigated over the course of 8 years (2010-2018). In total, 38 patients had their voice prosthesis lifespan documented. However, 18 patients were removed from further analysis due to a lack of adherence to the guidelines, moving out of the hospital catchment area resulting in incomplete data entries, incomparable data (e.g. changes in voice prosthesis type or width), or simply not enough voice prostheses failures/changes for statistical analysis within the time period. The voice prosthesis lifespans of the remaining 20 patients, before and after the implementation of our treatment guidelines, were analysed using the Online Application for Survival Analysis 2 (OASIS 2) platform [238]. In total, 143 voice prostheses before and 176 after implementation of the guidelines were included in this study. Kaplan-Meier survival curves were plotted and log-rank tests performed to statistically compare device lifespans before and after the treatment guidelines. Wilcoxon Signed-Rank tests were also carried out to determine if the

guidelines effect was significant when taking into account the inherent differences in device lifespan from patient to patient. For all analyses, the significance level (α) was 0.05.

2.4.15 Treatment guideline approval

Treatment guidelines for the treatment of voice prostheses with antifungal drugs were approved by the East Kent Hospital University Foundation Trust (EKHUFT) Voice Prosthesis Infection Management Multi-disciplinary team (MDT), EKHUFT Antimicrobial Stewardship Group, EKHUFT Drugs and Therapeutics Committee, EKHUFT ENT Audit Group, and EKHUFT Adult Speech and Language Therapy Service, East Kent Prescribing Group.

2.4.16 Study approval

The collection and identification of microorganisms on early failing voice prosthesis study was approved by the University of Kent Research Ethics and Governance Committee.

The voice prosthesis lifespan study was approved by the EKHUFT Research and Innovation Department in accordance with the Department of Health's Research Governance Framework for Health and Social Care and EKHUFT Research and Innovation policy. The EKHUFT Research and Development reference number for this project is 2018/GAP/20. This study was also approved by the University of Kent Research Ethics and Governance Committee.

2.5 Results

We conducted a study to determine the most common fungal and bacterial species found upon failed voice prostheses. Our study cohort comprised 48 patients (41 males and 7 females) within the National Health Service catchment area of East Kent, UK, who had a total of 159 early failed voice prostheses sent for microbial analysis between them over the five-year period of the study. The mean age of the patient cohort at the start of the study was 69.5 years (age range = 35 – 90 years). The microbial composition of biofilms on the failed voice prosthetic surfaces was analysed by initial culturing on chromogenic agar followed by matrix assisted laser desorption ionisation time-of-flight mass spectrometry (MALDI-ToF). Bacterial and fungal species were usually found together on early failing VPs suggesting a prevalence for mixed species biofilm formation as previously described [204].

2.5.1 Analysis of bacterial species found on early failing voice prostheses

S. aureus was the most frequently isolated bacterial species (Figure 1B), being found on multiple early failing VP (Figure 2.1B and 2.1C). This finding is in line with previous studies that also identified *S. aureus* as the prevalent bacterial organism found within VP biofilms [200][239]**.** However, *S. aureus* was one of several *Staphylococcal* species identified, the others being identified at lower frequencies included *Staphylococcus epidermidis* and *Staphylococcus schleiferi* (Figure 2.1B and 2.1C). We also identified the *S. aureus* strain methicillin-resistant *S. aureus* (MRSA) on 5 VPs and counted these separately from the rest of the *S. aureus* isolates (Figure 2.1B and 2.1C). These 5 VPs all came from the same patient, suggesting there are likely patient-specific reasons for this colonisation. *P. aeruginosa* was the second most frequent bacterial species found on early failing VPs (Figure 2.1B and 2.1C). Previous studies have also identified *P. aeruginosa* as a prevalent bacterial species found

within VP biofilms [201]. Several *Streptococcus* species were also identified, but at a low frequency, including *Streptococcus milleri*, *Streptococcus mitis,* and *Streptococcus intermedius* (Supplementary Table S2.1).

It is worth noting that the same bacterial species were frequently isolated from sequential VPs removed from the same patient implicating a common pattern of biofilm establishment. In total, 30 of 38 patients (78.9%) had the same bacterial species present on at least 2 voice prostheses.

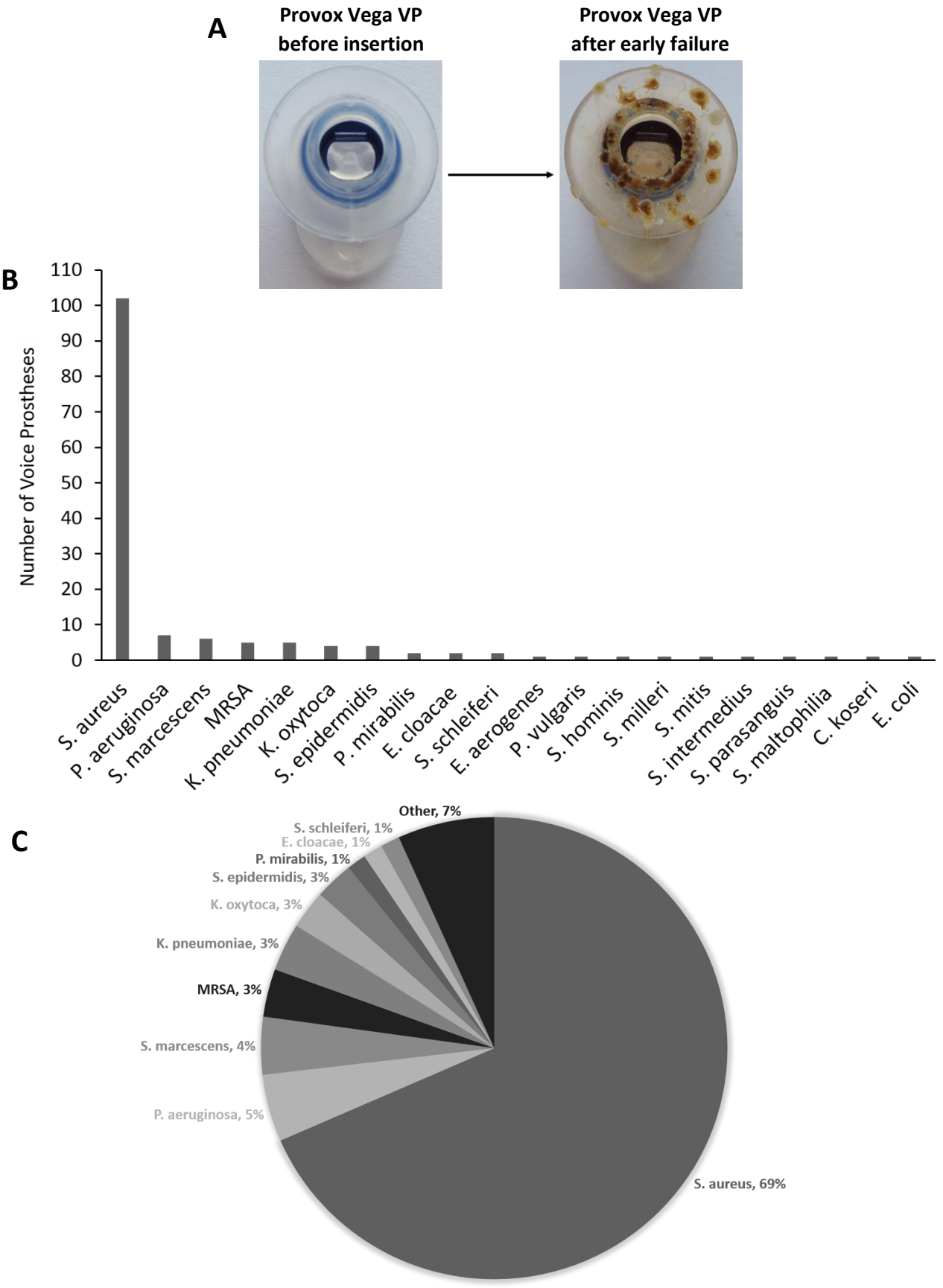


Figure 2.1: The range and distribution of bacterial species found on voice prostheses within this study. **(A)** An example of a failed voice prosthesis removed from a patient. Note the ring of colonisation on the prosthesis hood around the valve mechanism. **(B)** Bar graph representation of absolute numbers of times each bacterial species was isolated from 159 early failing VPs. **(C)** Pie chart representation of percentage of total bacteria isolated from 159 early failing VPs.

2.5.2 Analysis of fungal species found on early failing voice prostheses

Yeast species were commonly isolated from early failing VPs. Within the 159 voice prostheses, 107 (67.3%) were colonised by a single yeast species, 37 (23.3%) were colonised by multiple yeast species, and just 15 (9.4%) showed no yeast species presence. Interestingly, the three VPs without yeast colonisation came from the same patient, and represented 100% of their failed voice prostheses. In total, 178 yeast isolates were identified and 168 (94.4%) of these were *Candida* species, the remaining 10 fungal isolates were made up of *Saccharomyces cerevisiae* (8) and *Pichia manshurica* (2). *S. cerevisiae* and *P. manshurica* isolates were normally found alongside *Candida* species (62.5% and 100% respectively). The most frequently isolated yeast species was *C. albicans* (Figure 2.2). This is in line with previous studies which identified *C. albicans* as the yeast species most commonly found on VPs [202][204][240]. The non-*albicans Candida* isolates constituted 44.4% of all fungal isolates, with *Candida glabrata* being the most common of these (Supplementary Table S2.2).

As had been observed for bacteria, the same fungal species were frequently isolated from multiple early failing VPs from the same patient. In total, 38 of the 48 patients had more than one voice prosthesis failure during the course of the study and 29 (76.3%) of these had the same fungal species on at least 2 VPs (25 of these also had the same bacterial species on at least 2 voice prostheses). The most commonly reoccurring fungal species was *C. albicans*, being found on multiple VPs within 18 patients.

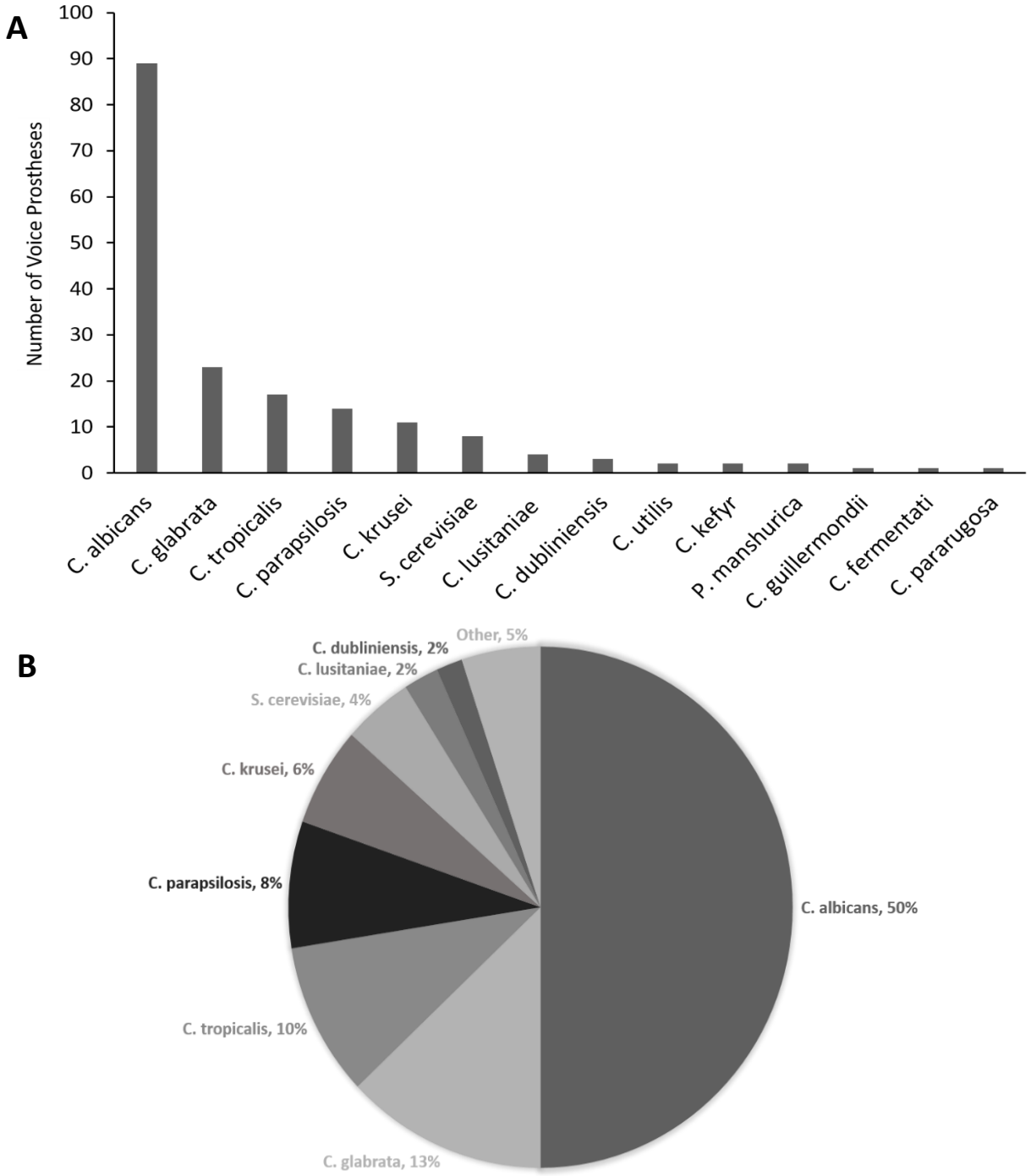


Figure 2.2: The range and distribution of fungal species found on voice prostheses within this study. **(A)** Bar graph representation of absolute numbers of times each yeast species was isolated from 159 early failing VPs. **(B)** Pie chart representation of percentage of total yeast isolated from 159 early failing VPs.

2.5.3 Co-isolation frequencies of different species from early failing voice prostheses

Fungal and bacterial species were often found together on VPs, 134 (84.3%) of the early failing VPs had at least one species of each present. The two most numerous species in this study, *S. aureus* and *C. albicans*, were the most commonly co-isolated, being found together on 60 VPs (Table 2.1). This may simply be due to the fact they were the two most prevalent species on voice prostheses in this study. However, it has previously been demonstrated that these two organisms have a synergistic advantage within the biofilm scenario [241][242]. Thus, it is likely these two microorganisms also have a synergistic relationship on VPs. Furthermore, other *Candida* species were frequently isolated alongside *S. aureus* (Table 2.1), again possibly indicating a relationship between fungal and bacterial species. Other bacterial species such as *P. aeruginosa* and *S. marcescens* were co-isolated with *C. albicans* the majority of the time; 57.1% and 83.3% respectively (Table 2.1). It was very rare for only fungal species to be present; only 10 (6.3%) VPs harboured solely fungal species and all of these were either the first or second voice prosthesis failure of their respective patients. After a second failure, there was never solely fungal species present. The significance of this, if any, is yet to be determined.

The two most commonly co-isolated fungal species were *C. albicans* and *C. glabrata* which were isolated together on 17 VPs; on 73.9% of VPs where *C. glabrata* was present, *C. albicans* was also co-isolated (Table 2.1). *C. krusei* was co-isolated with *C. albicans* 63.6% of the time. Interestingly, *C. parapsilosis* was seldom co-isolated with other *Candida* species; of the 14 VPs which harboured *C. parapsilosis*, only 1 also had other *Candida* species (*C. albicans* and *C. krusei* on the same VP) present (Table 2.1).

Species	*C. albicans*	*C. glabrata*	*C. tropicalis*	*C. parapsilosis*	*C. krusei*	*S. aureus*	*P. aeruginosa*	*S. marcescens*
C. albicans		17 (**19.1%**)	1 (**1.1%**)	1 (**1.1%**)	7 (**7.9%**)	60 (**67.4%**)	4 (**4.5%**)	5 (**5.6%**)
C. glabrata	17 (**73.9%**)		2 (**8.7%**)	0	0	19 (**82.6%**)	1 (**4.3%**)	0
C. tropicalis	1 (**5.9%**)	2 (**11.8%**)		0	0	12 (**70.6%**)	0	0
C. parapsilosis	1 (**7.1%**)	0	0		1 (**7.1%**)	7 (**50.0%**)	2 (**14.3%**)	0
C. krusei	7 (**63.6%**)	0	0	1 (**9.1%**)		9 (**81.8%**)	2 (**18.2%**)	1 (**9.1%**)
S. aureus	60 (**58.8%**)	19 (**18.6%**)	12 (**11.8%**)	7 (**6.9%**)	9 (**8.8%**)		5 (**4.9%**)	2 (**2.0%**)
P. aeruginosa	4 (**57.1%**)	1 (**14.3%**)	0	2 (**28.6%**)	2 (**28.6%**)	5 (**71.4%**)		0
S. marcescens	5 (**83.3%**)	0	0	0	1 (**16.7%**)	2 (**33.3%**)	0	

Table 2.1: Number of voice prostheses upon which the most commonly isolated species in this study were found together. Percentages indicate the relative frequencies of the underlined species (within the same row) being co-isolated with each of the other species.

2.5.4 Factors promoting microbial colonisation of voice prostheses

Examination of early failing VPs often suggested an uneven distribution of microbial growth across the device surface (Figure 2.1A). We investigated surface topography using atomic force and scanning electron microscopy as roughness has been shown to be an important driver of colonisation [243][244]. The prosthesis hood and oesophageal flange of the device exhibited a significantly rougher topography than the valve which appeared smooth using these high resolution techniques (Figures 2.3B and 2.3C). The roughness of the oesophageal flange was particularly evident in the AFM 3D plot of its surface (Figure 2.3D). In line with previous studies, this may suggest that the flange, specifically the valve-flange interface, provides a more likely site for initial attachment [224]. This proposition is also consistent with our observations that failed voice prostheses often exhibit heavy colonisation on the prosthesis hood and oesophageal flange (Figure 2.1A), particularly at the rougher inner edge where the prosthesis hood interfaces with the valve (Figure 2.3Bii).

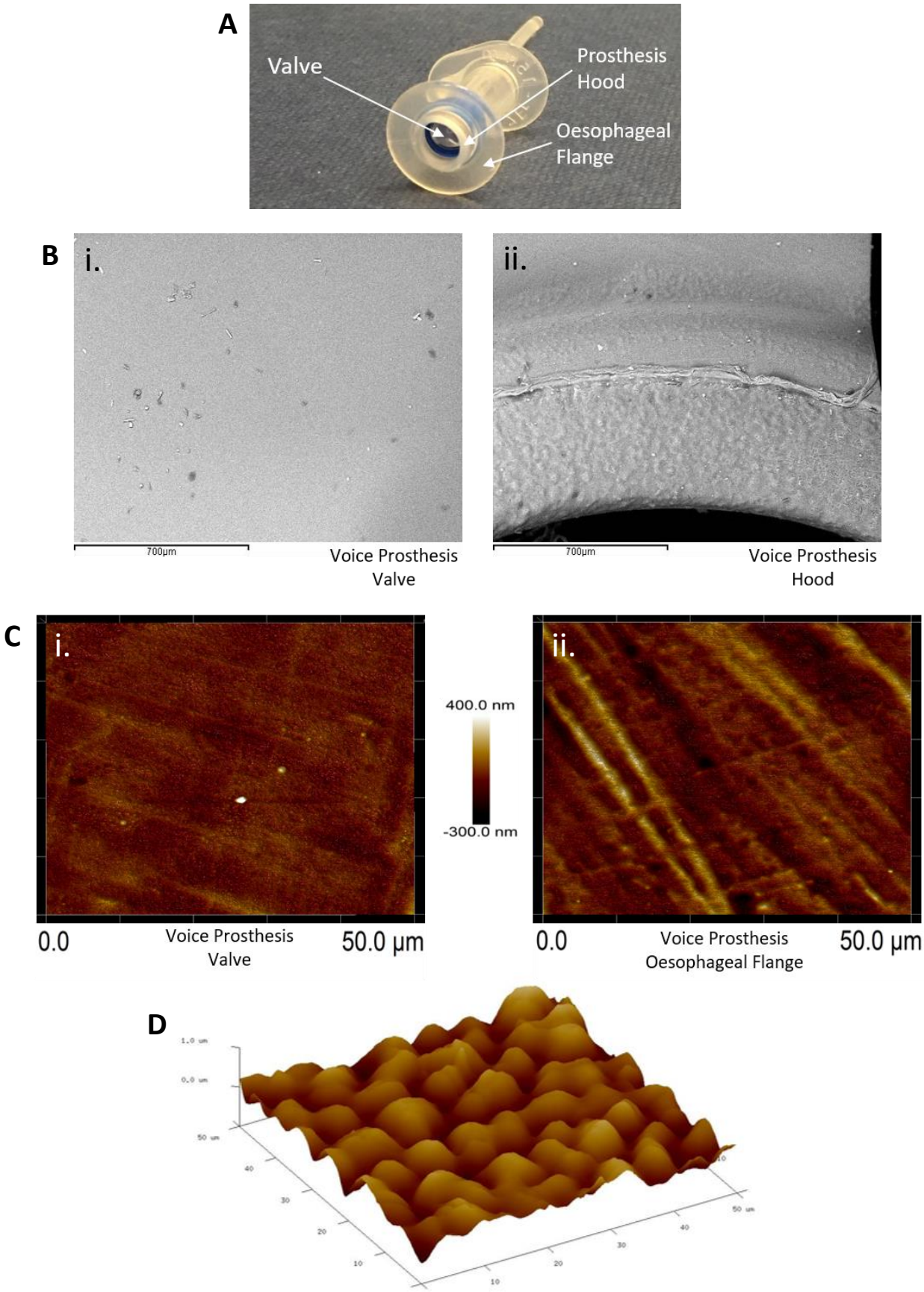


Figure 2.3: Atomic force and scanning electron microscopy surface topography of the valve and oesophageal flange of the Provox Vega voice prosthesis. (A) The Provox Vega voice prosthesis. **(B)** SEM images of the **(i)** valve and **(ii)** inner-side of the prosthesis hood were taken at x120 magnification. The scale bars represent 700µm. **(C)** AFM images of the **(i)** valve and **(ii)** oesophageal flange were taken of 50µm x 50µm surface areas with a scan height of 700nm. **(D)** AFM 3D plot of a 50µm x 50µm area of the oesophageal flange. Z-axis is 0–1µm. Several images were taken and representative examples are presented.

Environmental factors may also contribute to microbial contamination and early failure of voice prostheses. High CO_2 levels promote the *C. albicans* yeast-to-hyphae switch via the Ras1-Cyr1-PKA pathway [69]. This morphogenic switch is associated with *C. albicans* virulence [6] as well as being required for biofilm formation [142]. Due to the high CO_2 levels (~5%) experienced in the airway as a result of exhaled breath [245], we contemplated whether CO_2 could be exerting an effect on *C. albicans* biofilm formation in the VP scenario. Indeed, when seeded onto a voice prosthetic surface, *C. albicans* has increased biofilm growth in 5% CO_2 after 24h than in atmospheric air (Figure 2.4). This offers an explanation as to why *C. albicans* is such a prevalent coloniser of early failing VPs, as the valve mechanism and parts of the oesophageal flange will be bathed in exhaled air during voice production.

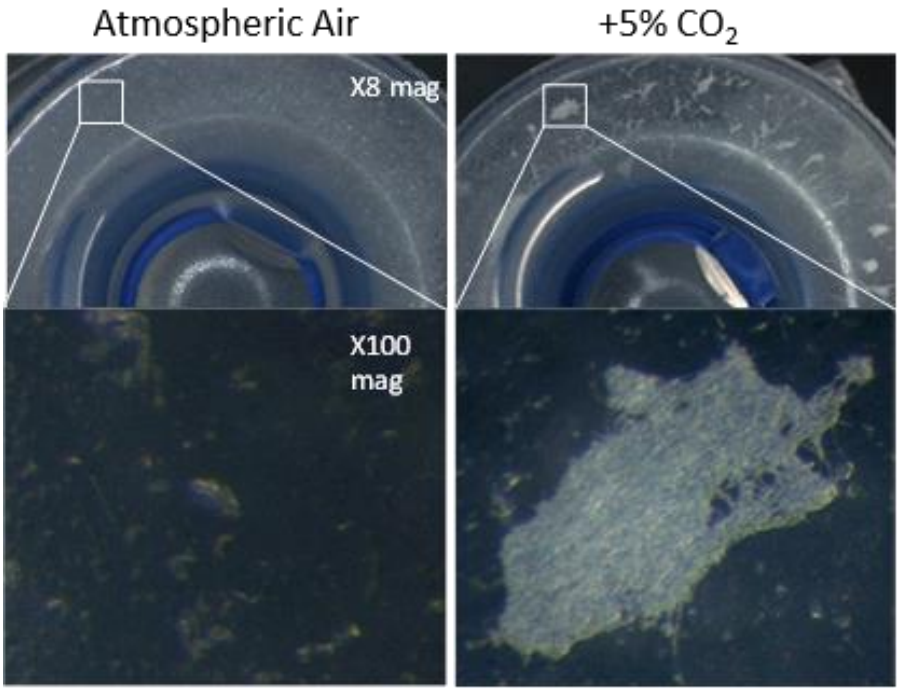


Figure 2.4: *C. albicans* biofilm forming on the flange of a voice prosthesis *in vitro* in both atmospheric air and elevated CO_2 conditions. *C. albicans* biofilm formation was assessed on a Provox Vega VP at 37°C under atmospheric air and elevated CO_2 conditions that mimic exhaled breath. Images were collected after 24h at x8 and x100 magnification. The experiment was repeated three times and representative images are presented.

2.5.5 *C. parapsilosis* does not have a competitive advantage over *C. albicans* in biofilm establishment

We observed that *Candida parapsilosis* was rarely co-isolated with another *Candida* species. Of the 14 VPs which harboured *C. parapsilosis*, only 1 also had another *Candida* species present. This is a stark contrast to other *Candida* species, such as *C. glabrata* which was found on 23 VPs, 19 of which also had additional *Candida* species (Table 2.1). This led us to investigate whether *C. parapsilosis* exhibited a competitive advantage over *C. albicans* with regards to biofilm growth. A *C. parapsilosis* clinical isolate found as the sole yeast species on a failed VP was selected for this investigation. Biofilms were seeded using equal cell numbers of the *C. albicans* and *C. parapsilosis* clinical isolates either alone or in combination and incubated for 48h to mature. Overall biofilm growth was analysed by measuring the metabolic activity of the biofilms using the XTT colorimetric assay which gives a colour readout that correlates well with cell number [237] (Figure 2.5). The proportions of *C. albicans* and *C. parapsilosis* cells were then analysed by removing biofilms from the silicone surface and plating the resulting cell suspension on chromogenic agar (Supplementary Figure S2.2). Strikingly, while the *C. albicans* G-3065 clinical isolate was able to form a robust biofilm on the silicone surface, the *C. parapsilosis* G10402 clinical isolate was not (Figure 2.5). Moreover, when these two clinical isolates were seeded together, the resultant biofilm was composed primarily of *C. albicans* cells (Supplementary Figure S2.2). In addition, while *C. albicans* biofilms were significantly increased ($p < 0.01$) when grown in the presence of increased CO_2 this was not observed for *C. parapsilosis*. These data suggest that the identification of *C. parapsilosis* in isolation on failed VPs may not arise from a competitive advantage over *C. albicans*, however, further experiments are required to be certain.

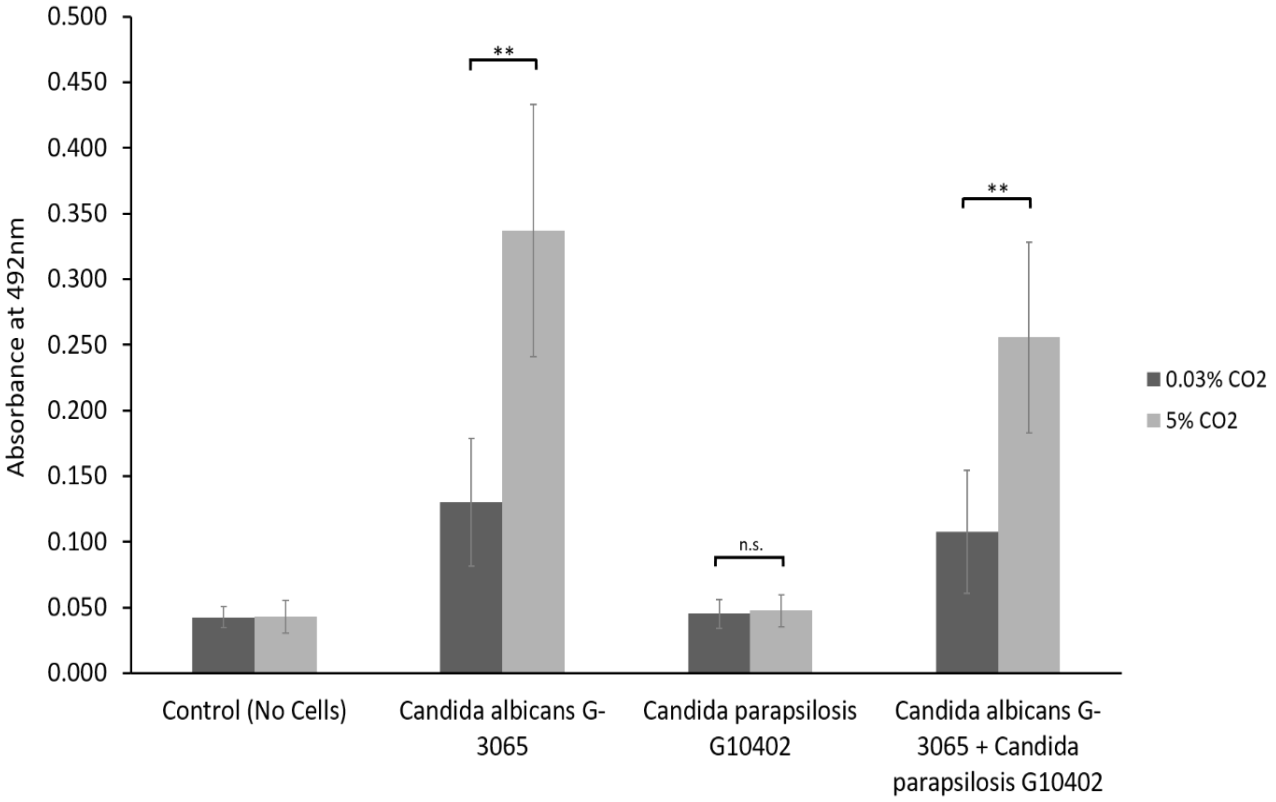


Figure 2.5: *In vitro* biofilm assay using *C. albicans* and *C. parapsilosis* early failing VP clinical isolates. Biofilms were seeded and grown for 48h to mature before quantification using the XTT assay. The *C. albicans* G-3065 clinical isolate makes bigger biofilms than the *C. parapsilosis* G10402 clinical isolate, and this biofilm formation is influenced by CO_2 concentration. The graph represents three independent experiments each containing triplicates, error bars denote Standard Deviation. Paired two-tail t-tests were carried out: *p<0.05, **p<0.01, ***p<0.001, n.s. = not significant.

2.5.6 Antimicrobial sensitivity of clinical isolates

Antibacterial sensitivities (sensitive, intermediate or resistant) were assigned based upon EUCAST breakpoint recommendations for each antibiotic in each particular species [236]. The sensitivities of the five most common bacterial species found on early failing VP to an example antibiotic from the five major antibiotic classes [246] are reported (Table 2.2). Only 10 (8.5%) of the most common bacterial isolates tested for sensitivity against the β-lactam antibiotic Amoxicillin were judged to be sensitive, and these were all *S. aureus* isolates. All of the *P.*

aeruginosa, *S. marcescens*, MRSA, and *K. pneumoniae* isolates tested for Amoxicillin sensitivity were resistant. 76 (74.5%) were deemed to be sensitive to the macrolide Erythromycin, with a significant number of *S. aureus* isolates being found to be resistant. The majority of the common bacterial isolates were sensitive to the fluoroquinolone Ciprofloxacin with 111 (93.3%) being judged as sensitive, however, all of the MRSA isolates tested were resistant to Ciprofloxacin. Likewise, a high number of isolates were sensitive to the tetracycline Tetracycline (104 – 87.4%), but this antibiotic did not exhibit good activity against the *P. aeruginosa* and *S. marcescens* isolates with 5 (83.3%) of both species being resistant. Finally, 115 (96.6%) of the common bacterial isolates tested were sensitive to the aminoglycoside Gentamicin, this was in fact the most effective antibiotic tested in this study (Table 2.2).

Species	Total Number of Isolates Tested	Number of Isolates in Each Category (%)		
		Sensitive	Intermediate	Resistant
Amoxicillin				
Staphylococcus aureus	96	10 (10.4)	0	76 (79.2)
Pseudomonas aeruginosa	6	0	0	6 (100)
Serratia marcescens	6	0	0	6 (100)
MRSA	5	0	0	5 (100)
Klebsiella pneumoniae	5	0	0	5 (100)
Total	**118**	**10 (8.5)**	**0**	**98 (83.1)**
Erythromycin				
Staphylococcus aureus	97	71 (73.2)	1 (1.0)	25 (25.8)
Pseudomonas aeruginosa	0	-	-	-
Serratia marcescens	0	-	-	-
MRSA	5	5 (100)	0	0
Klebsiella pneumoniae	0	-	-	-
Total	**102**	**76 (74.5)**	**1 (1.0)**	**25 (24.5)**
Ciprofloxacin				
Staphylococcus aureus	97	95 (97.9)	0	1 (1.0)
Pseudomonas aeruginosa	6	5 (83.3)	0	1 (16.7)
Serratia marcescens	6	6 (100)	0	0
MRSA	5	0	0	5 (100)
Klebsiella pneumoniae	5	5 (100)	0	0
Total	**119**	**111 (93.3)**	**0**	**7 (5.9)**
Tetracycline				
Staphylococcus aureus	97	95 (97.9)	0	2 (2.1)
Pseudomonas aeruginosa	6	0	0	5 (83.3)
Serratia marcescens	6	0	1 (16.7)	5 (83.3)
MRSA	5	5 (100)	0	0
Klebsiella pneumoniae	5	4 (80)	0	1 (20)
Total	**119**	**104 (87.4)**	**1 (0.8)**	**13 (10.9)**
Gentamicin				
Staphylococcus aureus	97	93 (95.9)	0	4 (4.1)
Pseudomonas aeruginosa	6	6 (100)	0	0
Serratia marcescens	6	6 (100)	0	0
MRSA	5	5 (100)	0	0
Klebsiella pneumoniae	5	5 (100)	0	0
Total	**119**	**115 (96.6)**	**0**	**4 (3.4)**

Table 2.2: Antibiotic sensitivity of the five most common bacterial species isolated from early failing VPs. The number of sensitive, intermediate and resistant isolates based upon EUCAST breakpoint recommendations [47] are given for the five most commonly isolated bacterial species.

Antifungal sensitivity testing was performed using the Fungitest™ commercial testing kit (see Materials and Methods). Sensitivities (sensitive, intermediate or resistant) were assigned based upon EUCAST breakpoint recommendations for each antifungal in each particular species [234]. The majority of the fungal isolates from the voice prostheses were sensitive to Fluconazole, Miconazole and Nystatin (Table 2.3); three commonly used antifungals in the clinical setting. Of the 168 *Candida* isolates, 155 were tested for Fluconazole sensitivity and 139 of these were found to be sensitive (89.7%). Moreover, 123 of the *Candida* isolates were tested for Miconazole sensitivity and 107 were sensitive (87.0%). Finally, 129 of the *Candida* isolates were tested for Nystatin sensitivity and 126 of these were found to be sensitive (97.7%). Nystatin therefore appeared to be the most effective antifungal with regards to inhibition of growth of *Candida* species obtained from early failing VPs in this patient cohort.

Species	Total Number of Isolates Tested	Number of Isolates in Each Category (%)		
		Sensitive	Intermediate	Resistant
Fluconazole				
Candida albicans	83	81 (97.6)	2 (2.4)	0
Candida glabrata	23	21 (91.3)	2 (8.7)	0
Candida tropicalis	15	15 (100)	0	0
Candida parapsilosis	14	12 (85.8)	0	2 (14.3)
Candida krusei	9	1 (11.1)	2 (22.2)	6 (66.7)
Total	**144**	**130 (90.3)**	**6 (4.2)**	**8 (5.5)**
Miconazole				
Candida albicans	62	59 (95.1)	3 (4.9)	0
Candida glabrata	19	19 (100)	0	0
Candida tropicalis	13	7 (53.9)	6 (46.1)	0
Candida parapsilosis	9	4 (44.4)	4 (44.4)	1 (11.1)
Candida krusei	9	8 (88.9)	1 (11.1)	0
Total	**112**	**97 (86.6)**	**14 (12.5)**	**1 (0.9)**
Nystatin				
Candida albicans	65	64 (98.5)	0	1 (1.6)
Candida glabrata	20	18 (90.0)	1 (5.0)	1 (5.0)
Candida tropicalis	15	15 (100)	0	0
Candida parapsilosis	9	9 (100)	0	0
Candida krusei	9	9 (100)	0	0
Total	**118**	**115 (97.4)**	**1 (0.9)**	**2 (1.7)**

Table 2.3: Antifungal sensitivity of the five most common *Candida* species isolated from early failing VPs. The number of sensitive, intermediate and resistant isolates based upon EUCAST breakpoint recommendations [45] are given for the five most commonly isolated yeast species.

2.5.7 Antifungal sensitivity of *C. albicans* clinical isolates within biofilms

It has been established that biofilm-associated cells are commonly more tolerant to antimicrobials than their planktonic counterparts [115]. As laboratory based sensitivities are based upon planktonic growth we investigated whether *C. albicans* isolates obtained from early failing VPs demonstrated antifungal tolerance when grown as a biofilm on a silicone surface. Biofilms were seeded and grown for 24h before the addition of antifungals, after which they were grown for an additional 24h to observe the effect of drug application. Antifungal concentrations were selected based upon previously reported MIC values for these antifungals against *C. albicans* biofilms [115]. Due to the previously observed effect of high CO_2 concentration increasing *C. albicans* biofilm growth (Figures 2.4 and 2.5), we also sought to investigate whether CO_2 level had any influence on the activity of the antifungals.

Overall, the clinical isolates displayed higher tolerances to Fluconazole and Miconazole compared to Nystatin (Table 2.4). Moreover, this azole tolerance was significantly increased in biofilms grown in high CO_2 environments (Supplementary Figures S2.3 and S2.4). For instance, G-8424 biofilms grown in 0.03% CO_2 had an average decrease in XTT activity of 59% relative to the untreated control upon treatment with 32μg/ml Fluconazole ($p < 0.001$), whereas there was no significant decrease in relative XTT activity in the 5% CO_2 G-8424 biofilms (Table 2.4 and Supplementary Figure S2.3). This is also true for the 128μg/ml Miconazole treatments in all three isolates (Table 2.4 and Supplementary Figure S2.4). Furthermore, despite the fact that 0.03% and 5% CO_2 G-1625 biofilms both displayed significant decreases in relative XTT activity upon Fluconazole treatment, the relative XTT activity is still significantly higher ($p < 0.05$) in the biofilms grown in 5% CO_2 (Supplementary Figure S2.3). Nystatin sensitivities were generally independent of CO_2 concentration (Figure

2.6). The G-3065 and G-8424 clinical isolate biofilms were more tolerant to Fluconazole and Miconazole than the G-1625 isolate, however, all isolate biofilms exhibited good sensitivity to Nystatin (Table 2.4). Based on these data, we conclude that Nystatin is the most potent against *C. albicans* biofilms on silicone surfaces and also offers the greatest protection against the CO_2 biofilm activation. However, Fluconazole and Miconazole are still both efficacious against some isolates.

Antifungal	*C. albicans* G-3065		*C. albicans* G-8424		*C. albicans* G-1625	
	0.03% CO_2	5% CO_2	0.03% CO_2	5% CO_2	0.03% CO_2	5% CO_2
Fluconazole						
32µg/ml						
128µg/ml						
Miconazole						
32µg/ml						
128µg/ml						
Nystatin						
2µg/ml						
8µg/ml						

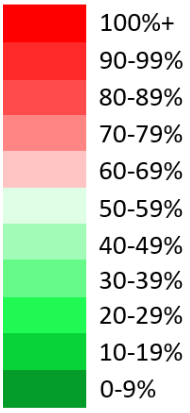


Table 2.4: Antifungal sensitivity of biofilms of three *C. albicans* clinical isolates from early failing VPs. Action of antifungals was measured via the percentage XTT assay activity relative to untreated in both 0.03% and 5% CO_2.

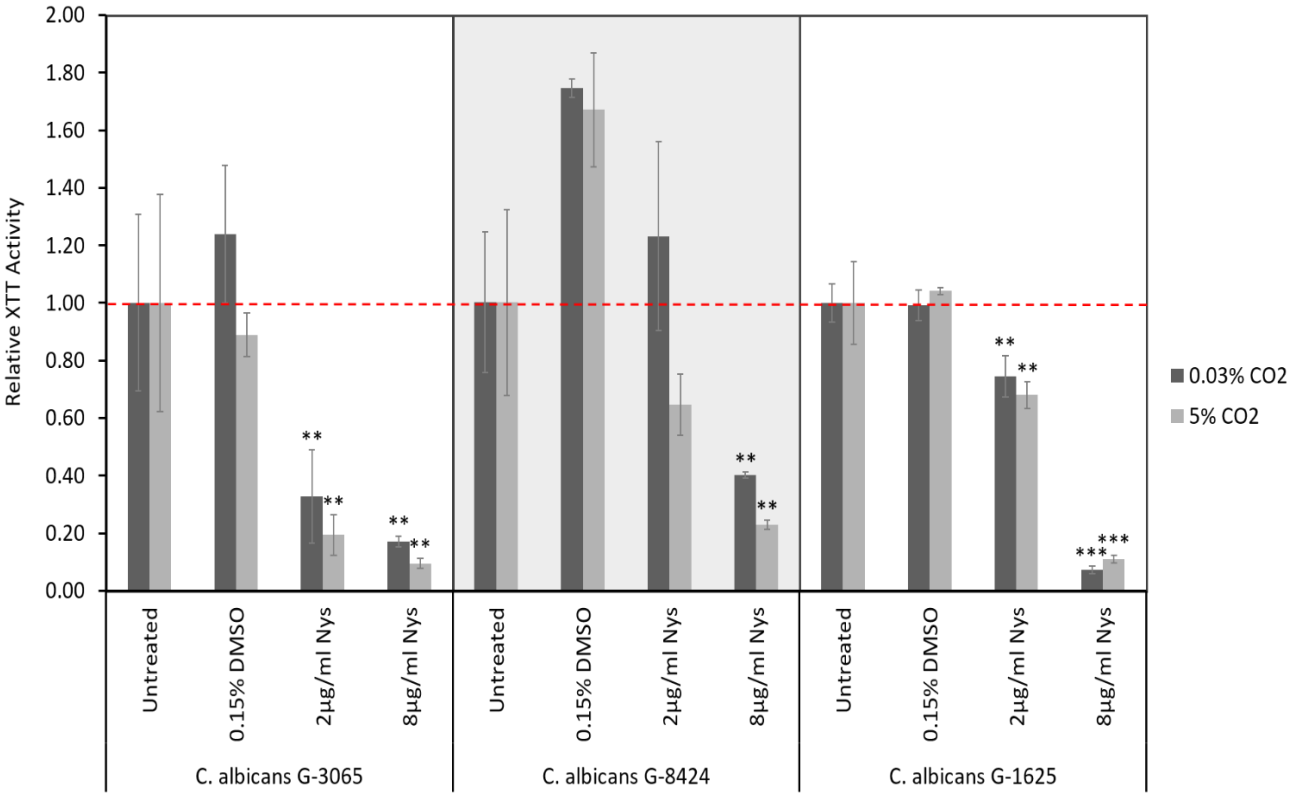


Figure 2.6: Nystatin sensitivities of *C. albicans* clinical isolate biofilms. Biofilms were seeded and grown for 24 hours before addition of Nystatin, they were then grown for a further 24 hours before quantification using the XTT assay. The relative XTT activity is presented with the 0.03% and 5% CO_2 biofilms normalised to the 0.03% and 5% CO_2 untreated controls respectively. This prevents the general higher growth of 5% CO_2 biofilms impacting the analysis. Graphs represent three independent experiments each containing triplicates, error bars denote Standard Deviation. Two-way ANOVAs followed by a Tukey test for multiple comparisons were carried out: *p<0.05, **p<0.01, ***p<0.001. Stars directly above the bars indicate a significant difference to untreated in the same CO_2 environment, for clarity only comparisons which were statistically significant have been indicated on the graphs.

2.5.8 Development and clinical testing of antifungal treatment guidelines (ATG) to extend VP lifespan

Although VP biofilms are likely to be formed from several species we hypothesised that an antifungal approach to reduce colonisation would be effective in extending device lifespan. The rationale behind this was based primarily upon the likelihood that yeast contamination

would contribute significant biomass that is more likely to impair valve function. In addition, we have observed that the elevated CO_2 environment in which a VP sits promotes biofilm growth of the most commonly isolated yeast, *C. albicans*. As other commonly isolated bacteria, such as *S. aureus* and *P. aeruginosa* have been reported to use *Candida* hyphae as a scaffold to attach to during biofilm formation [247], it may be the case that antifungal treatment also attenuates the bacterial colonisation.

The antifungal drugs selected for treatment were chosen based upon safety and the fungal sensitivity data (Tables 2.3 and 2.4), with Nystatin being demonstrated to be the most effective as it had the lowest levels of resistance (Table 2.3) along with being reported as having few side effects and no drug interactions [248]. Previous studies have also identified that most non-*albicans Candida* species have higher azole MICs [249][250], whereas all *Candida* species have low *in vitro* nystatin MICs [251]. Moreover, *C. albicans* sensitivity to Nystatin when in a biofilm appears to be unaffected by CO_2 level (Figure 2.6).

Our antifungal voice prosthesis management pathway involves determining the identity and antimicrobial sensitivities of microorganisms present on a failed VP. Based on the antifungal sensitivities of the colonising fungal species, a course of antifungals (most commonly Nystatin) is suggested and prescribed for topical application directly to the VP (brushed through it with a voice prosthesis cleaning brush). Fluconazole may be prescribed for oral use if tissue granulation is present around the TEP. Subsequent VP lifespans should be carefully monitored to determine if treatment is having a positive effect on device lifespan and accompanying microbiology analysis conducted to assess the emergence of antifungal resistance. If Nystatin does not improve device lifespan sufficiently then Miconazole gel

applied directly to the voice prosthesis is the next treatment option after Nystatin, depending on the results of sensitivity testing. Any patients that do not observe a VP lifespan increase are referred to the managing multi-disciplinary team (MDT) for discussion and recommendations on further treatment options. The treatment guidelines are briefly summarised in Figure 2.8C, described in detail in Supplementary Figure S2.5 and found with an additional information document at http://southkentcoast.referralsupport.co.uk/wp-content/uploads/2019/04/Clinical-guidelines-for-the-management-of-early-voice-prostheses-failure-associated-with-Candida-infection-EKPG-Oct-2016.pdf.

To test the effectiveness of our antifungal approach to managing early voice prosthesis failure associated with *Candida* colonisation, VP data from 38 patients was assessed. VP lifespan data from the patient cohort before and after their placement on the ATG was assessed. Over the course of the study, 18 patients were removed from further analysis because of either; known lack of adherence to the ATG, moving out of the hospital catchment area resulting in incomplete data entries, a change in voice prosthesis type or width or insufficient VP replacement data. This left 20 patients with complete VP lifespan data entries before and after guideline implementation on which to conduct statistical analyses.

Throughout the 8 year course of the study, the lifespan of 319 voice prostheses (143 before and 176 after guidelines) across the 20 patient cohort were analysed. These 319 voice prostheses represented all the VP changes for the 20 patients when the removed VP was replaced by the same model of the same width. This ensured there were no external factors such as VP surface/surface area influencing the results. We also included all changes and not just those specifically attributed to the presence of *Candida* growth to remove bias.

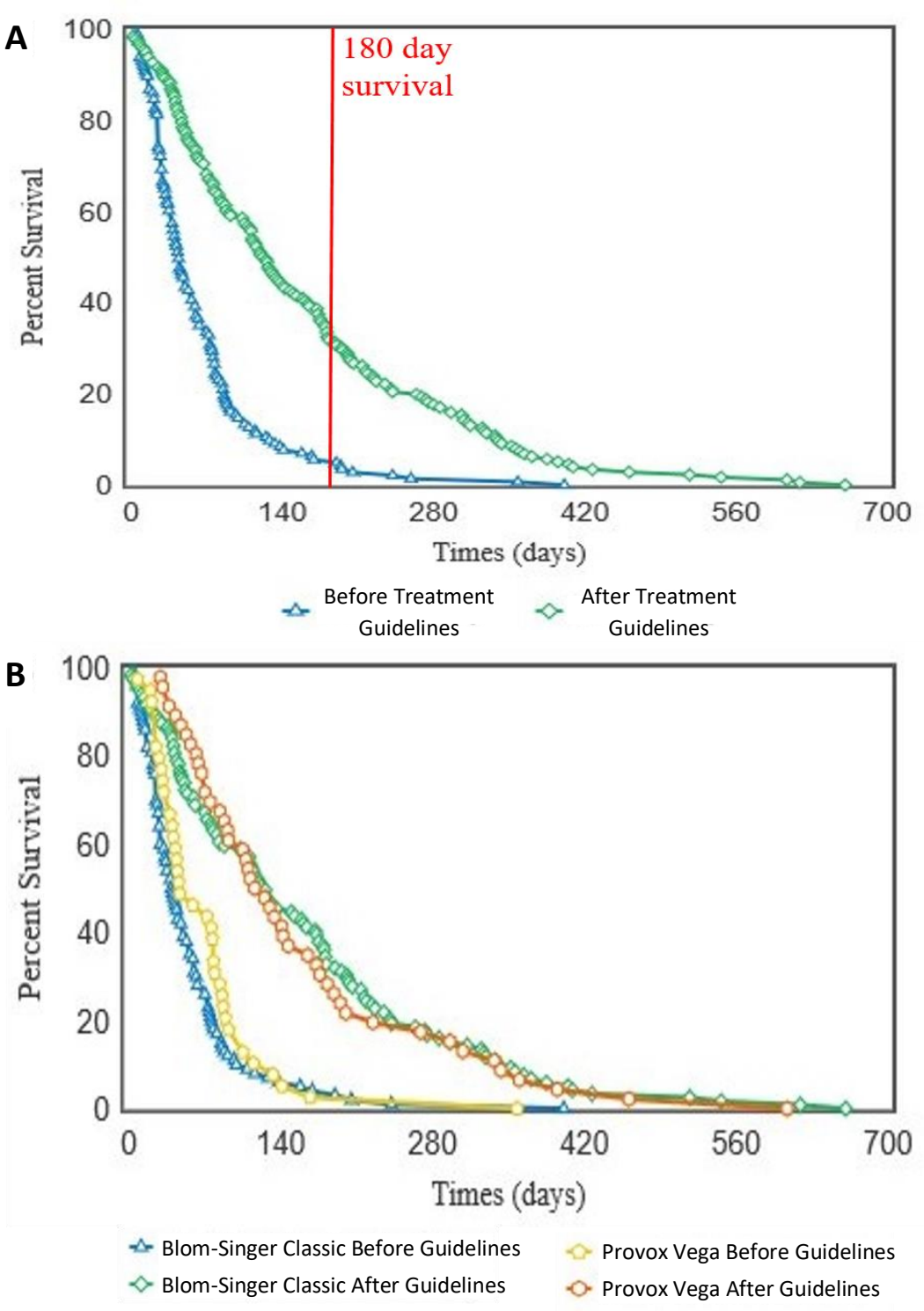


Figure 2.7: Kaplan-Meier survival curves showing the voice prosthesis *in situ* lifespans before and after implementation of our antifungal treatment pathway. (A) Device lifespans were documented before and after implementation of the ATG. Kaplan-Meier survival curves were plotted using the OASIS2 online platform [49] and a log-rank test was used to compare the survival curves: $p<0.001$. Red line is at 180 days lifespan which we targeted as the ideal lifespan to achieve. **(B)** After lifespan analysis across all devices was performed, the lifespans were categorised into groups depending on which VP model a patient was using. Kaplan-Meier survival curves were again plotted using the OASIS2 online platform [49] and log-rank tests were used to compare them: Blom-Singer Classic, Before vs. After; $p<0.001$. Provox Vega, Before vs. After; $p<0.001$.

Overall, implementation of the ATG resulted in a significant ($p < 0.001$) increase in VP lifespan within our patient cohort (Figure 2.7A). Importantly, this lifespan increase was not dependent on VP manufacturer/model as both the Blom-Singer Classic and the Provox Vega (the two most common VPs in this study) had similar lifespan increases (Figure 2.7B). It is also important to highlight that the lifespans of these two VP models were not significantly different to one another either before or after the treatment guidelines implementation (Figure 2.7B). The mean voice prostheses lifespan before guideline implementation was 71.9 days (range = 4-401 days) and this increased to 192.0 days (range = 2-661 days) after implementation of the antifungal management pathway, representing an average 270% increase in lifespan (Figure 2.8B).

Although there was variation in average post guideline VP lifespan increase between patients, the majority of the patients in our cohort experienced an overall increase in device lifespan (Figure 2.8A). Two patients did not exhibit an increase in VP lifespan, instead having a slight decrease of -2.4 days and -45.5 days respectively (Figure 2.8A). However, these two patients had long-lived voice prostheses on average (97.1 days and 193.3 days respectively) in comparison with the rest of the cohort prior to the introduction of the new antifungal clinical guidelines. This is particularly evident for patient 16 whose voice prostheses were already lasting longer than the post treatment guidelines mean lifespan across all patients. Thus, the treatment guidelines are likely of most benefit to patients who are experiencing early failing voice prostheses.

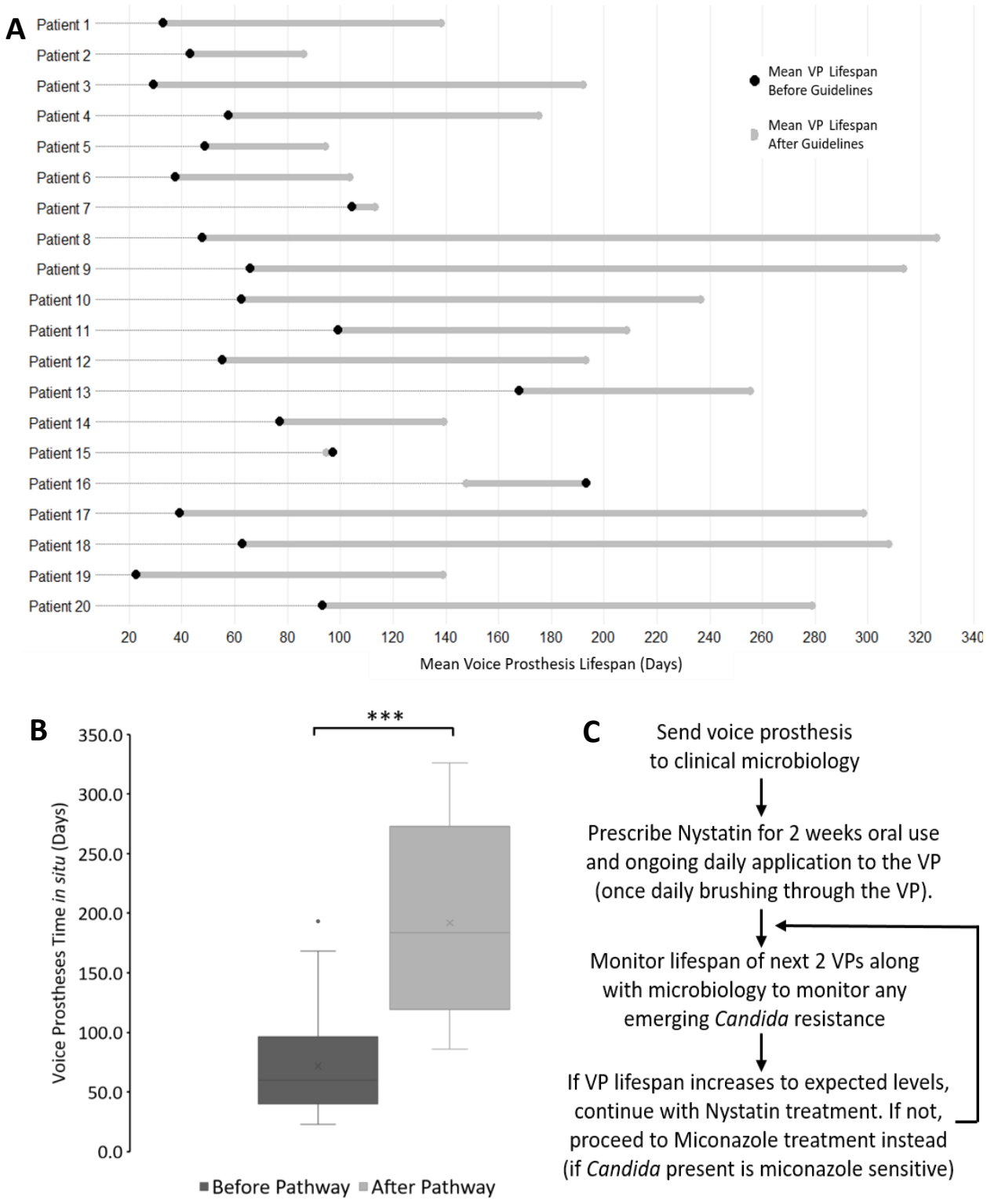


Figure 2.8: The antifungal treatment guidelines along with its effects on voice prosthesis lifespan within each patient. (A) Dumbbell chart representation of the mean VP lifespan difference after guideline implementation for each of the 20 patients. **(B)** Box plot representation of VP *in situ* lifespans before and after guideline implementation, Wilcoxon Signed-Rank test: ***p<0.001. **(C)** Summary of the treatment pathway. As of January 2019, this management pathway has been distributed to 34 different speech and language therapy centres (32 in the UK, 2 internationally) upon request.

Although we did not identify any cases of resistance to antifungal application, our MDT have applied a 6 months (180 days) limit before VP change. This length of time was chosen primarily to reduce the possibility of development of antifungal resistance amongst the colonising *Candida* species and also to ensure that the VP remains structurally sound. Before ATG use only 8 VPs (5.6%) reached this target across all 20 patients, while post-ATG 63 VPs (35.8%) lasted at least 180 days (Figure 2.7A). It is worth noting that after the treatment guidelines were implemented, several VPs were being routinely changed because they had been *in situ* for >6 months and not because they had actually failed.

2.6 Discussion

2.6.1 *C. albicans* is the most prevalent fungi isolated from early failing VPs

The colonisation of VP by microorganisms, specifically *Candida* species, resulting in their degradation and failure has long been documented [217]. However, whether the presence of *Candida* led directly to early failure and whether antifungal treatment would provide an effective option for prevention of early failure has not previously been tested. Our analysis of the colonising organisms found on failed VPs is in line with previous investigations in that a number of bacterial and *Candida* species are present.

We found that *Candida albicans* is the most prevalent fungal microorganism found on failed voice prostheses. Buijssen, K. *et al*. found that *C. albicans* was the most common fungal species, being present in 77% of biofilms from failed voice prostheses, *C. tropicalis* was second with 52% and *C. glabrata* third with 46% [204]. Likewise, in a 2002 study conducted by Bauters, T. *et al*. *C. albicans* was also the most common, being identifed in 41.4% of voice prosthesis biofilms, followed by *C. glabrata* (33.1%) and *C. krusei* (15.9%) [202]. In our study, *C. albicans* was found on 56.0% of voice prostheses while *C. glabrata* (14.5%) and *C. tropicalis* (10.7%) were the second and third most commonly found fungal species respectively. *C. glabrata* and *C. tropicalis* were found here with much lower frequency than observed by Bujissen, K. *et al.* [204]. This could reflect a difference in the identification methods used, different patient demographics or lifestyles. Different lifestyles and dietary habits have previously been suggested to have an impact on the microbial colonisation of voice prostheses. For instance, a study conducted in India by Sayed, S. *et al.* found a different microbial picture on voice prostheses compared to European studies that may be attributed to the very different patient lifestyles and geographical location [201]. *C. glabrata* was

isolated from only 9.1% failed VPs in the Indian study [201]; a much lower frequency than in the European studies discussed above [202][204], although not too dissimilar to our study (14.5% VPs with *C. glabrata*). In addition, Sayed, S. *et al.* identified *P. aeruginosa* on 63.6% failed VPs [201] whereas Bujissen, K. *et al.* did not find this species at all [204] and we identified *P. aeruginosa* on only 4.4% VPs. Moreover, Chaturvedi, P. *et al*. found that in the Indian scenario, *C. tropicalis* was the most prevalent fungal species colonising voice prostheses [205]. The high consumption of dairy products such as yoghurt and buttermilk in India has been proposed to influence biofilm growth on voice prostheses. The presence of *Streptococcus thermophilus* and *Lactobacillus* in yoghurt may reduce biofilm formation [215][252], while the high lactoferrin content in buttermilk (also found in saliva) has antibacterial and antifungal properties against organisms such as *C. albicans* and *Streptococcus mutans* [253][254][255].

Our study found *S. aureus* as the most prevalent bacterial species on failed voice prostheses, present on 64.2% of voice prostheses, often in combination with one or more *Candida* species. This was expected since *S. aureus* is a member of the normal oral and perioral microbiota [256]. Moreover, it is the third most commonly isolated organism with *C. albicans* in poly-microbial infections (a significant proportion of which are nosocomial infections) [257]. Synergistic relationships between *S. aureus* and *C. albicans* have previously been documented. *S. aureus* is poor at forming biofilms on its own, however, it has been suggested that the hyphal *C. albicans* cells provide a scaffold on which the *S. aureus* cells can attach within a poly-microbial biofilm [247]. This may well be the scenario in the mixed biofilms on the failed VPs and offers an explanation as to why these two microorganisms are frequently on the same device. The attachment of *S. aureus* to *C. albicans* could also be a mechanism

which the bacteria uses to invade human tissues and disseminate infection, being carried on the hyphae as they penetrate the epithelial layers [258]. Within a mixed biofilm, *S. aureus* cells also become coated in *C. albicans* matrix material, enhancing its antibiotic tolerance [241]. Furthermore, *S. aureus* and *C. albicans* mixed biofilms can withstand higher shear stresses than pure *C. albicans* biofilms [242]. Given the high frequency that these two microorganisms are found together, along with the synergy they have been previously shown to exhibit, their inter-species relationship in the voice prosthesis setting should not be underestimated. The potential impact of this relationship is highlighted by the fact co-infection results in increased mortality in mouse models than either microorganism alone [259][260].

In addition to the large numbers of *S. aureus* isolates, several other bacterial species were identified on voice prostheses in this study, including *P. aeruginosa* (4.4% of VPs) and *S. marcescens* (3.8% of VPs). The study performed by Sayed, S. *et al.* in India concluded *P. aeruginosa* was the most common bacterial species on voice prostheses [201]. It is likely, as the authors of the Indian study also proposed, that the differences in ratios of microorganisms identified in studies of this nature are due to the different geographical areas and the varied patient lifestyles within them (see above).

We investigated whether *C. parapsilosis* possesses any competitive advantage over *C. albicans*, demonstrating that *C. albicans* is able to outcompete *C. parapsilosis* and form the majority of mixed mature biofilms *in vitro*. This was surprising based on our epidemiological observations; there must be other factors contributing to the success of *C. parapsilosis in vivo*, such as patient diet, flora, and lifestyle, which we were unable to mimic in our *in vitro* assay.

C. parapsilosis is adept at forming biofilms [261], however, its biofilms tend to be composed primarily of yeast-form cells and have a thinner, less structured overall organisation compared to *C. albicans* biofilms [237]. Moreover, unlike other *Candida* species, the biofilm-forming ability of *C. parapsilosis* is strain specific [261] so it could be that the G10402 clinical isolate we used is a poor producer of biofilms when it is the sole organism. The explanation behind the apparent competitive fitness against other fungal species on voice prostheses *in vivo* remains a mystery. Although, it should be highlighted that the microorganism identification methods used in this study were qualitative not quantitative. Thus, despite the presence of *C. parapsilosis* on 14 of the voice prostheses, it may not have formed a significant proportion of these biofilms.

2.6.2 Antifungal sensitivity testing of biofilm-associated cells

Within clinical settings, drug sensitivity tests on isolates are routinely carried out on planktonic cells (as we have done in this study). However, our azole and Nystatin biofilm sensitivity results highlight a potential need to also conduct antimicrobial sensitivity tests on biofilm cells. It is well-known that biofilm-associated cells have increased tolerance to antimicrobial agents [153], and it has been estimated by the National Institutes of Health that pathogenic biofilms (bacterial and fungal) are responsible for up to 80% of all microbial infections in the US [113]. Therefore, testing antimicrobial sensitivity of isolates while they are growing as biofilms may be more representative of the scenario within patients and certainly more representative of medical device colonisation such as that of VPs. We observed an increase in tolerance to the azoles Fluconazole and Miconazole in *C. albicans* biofilms grown in high CO_2 environments. Again, demonstrating discrepancy between traditional sensitivity testing methods and the clinical scenario. This tolerance increase could be due to

several reasons including the increased expression of drug efflux pumps as well as a possible increase in matrix deposition displayed by biofilms grown in high CO_2, both of which have been associated with biofilm antimicrobial tolerance [157][159][161].

2.6.3 Precision antifungal treatment guidelines significantly increase voice prostheses lifespans

We have demonstrated that the lifespan of voice prostheses can be significantly increased by focusing on the prevention/management of the *Candida* colonisation, without directly treating the bacterial colonisation. We decided upon this approach based on several reasons. Firstly, due to the larger size of yeast cells compared to bacterial cells, we theorised that yeast contamination would contribute significant biomass that may impair valve function. Combined with our observation that the elevated CO_2 environment may promote *Candida* biofilm formation, we thought the *Candida* colonisation could be the principal cause of voice prosthesis failure. Secondly, *C. albicans* is particularly adept at degrading silicone rubber [204]. Finally, there is a substantial level of agreement across several different studies that *Candida* species, particularly *C. albicans*, are the predominant fungal species found on voice prostheses [202][204][205]. The picture is not as consistent in regards to bacterial species with some studies finding *Pseudomonas aeruginosa* as the most common bacteria [201], some finding Lactobacilli as the most common [262], and others finding *Staphylococcus aureus* as the predominant species (this study). Therefore, we proposed a treatment focusing on the *Candida* colonisation would likely be more wide-ranging than an equivalent bacterial treatment pathway.

To our knowledge, this is the first long-term study of the effect of a voice prosthesis management regime that advises topical application of antifungals directly on the device surface. Historically, the use of Amphotericin B lozenges [217] and buccal bioadhesive slow-release Miconazole nitrate tablets [218] to reduce oropharyngeal fungal burden have resulted in increases in voice prosthesis lifespans. However, these studies did not investigate the use of antifungals directly on the VP surface. Furthermore, the Amphotericin B lozenges and the buccal bioadhesive Miconazole tablets have since been discontinued by the pharmaceutical company [10]. More recently, much of the focus on enhancing voice prosthesis lifespans *in situ* has been on the designs of the voice prostheses themselves. Provox released the ActiValve model for patients which have experienced particularly early failing voice prostheses [226], and this model does have a significantly increased lifespan compared to traditional voice prostheses [228].

Prior to implementation of our voice prostheses antifungal treatment guidelines, the average *in situ* lifespan of voice prostheses within our patient cohort was 71.9 days. This is similar to a recent large-scale study of voice prosthesis lifespans in the U.S. by Lewin *et al.* which found an average lifespan of 86 days [221]. While being slightly less than a study by Kress *et al*. which found an average lifespan of 108 days [228]. The average device lifespan within our patient cohort increased to 192.0 days after clinicians started following the management guidelines – a 2.7-fold increase. The actual lifespan of voice prostheses post guidelines implementation may be higher than the 192.0 days reported here, as we recommended the clinicians change some voice prostheses prophylactically after 6 months (180 days) *in situ*. This ensures there is no emerging antifungal resistance as well as no structural deterioration of the device due to mechanical stress and the constant application of antifungals.

In conclusion, *C. albicans* is the most prevalent fungal species found on failed voice prostheses. We have demonstrated that directed application of topical antifungals onto the voice prosthesis surface to combat fungal colonisation results in significantly extended voice prosthesis lifespans. As of January 2019, our voice prosthesis treatment guidelines have been distributed to 34 centres (32 in the UK and 2 internationally). We hope to collaborate with these centres in the future to continue evolving our treatment guidelines and further analyse their impact.

2.7 Supplementary Materials

Species	Isolation Frequency from 159 Voice Prostheses	
	Number	Percentage
Staphylococcus aureus	102	64.2
Pseudomonas aeruginosa	7	4.4
Serratia marcescens	6	3.8
MRSA	5	3.1
Klebsiella pneumoniae	5	3.1
Klebsiella oxytoca	4	2.5
Staphylococcus epidermidis	4	2.5
Proteus mirabilis	2	1.3
Enterobacter cloacae	2	1.3
Staphylococcus schleiferi	2	1.3
Enterobacter aerogenes	1	0.6
Proteus vulgaris	1	0.6
Staphylococcus hominis	1	0.6
Streptococcus milleri	1	0.6
Streptococcus mitis	1	0.6
Streptococcus intermedius	1	0.6
Streptococcus parasanguis	1	0.6
Stenotrophomonas maltophilia	1	0.6
Citrobacter koseri	1	0.6
Escherichia coli	1	0.6

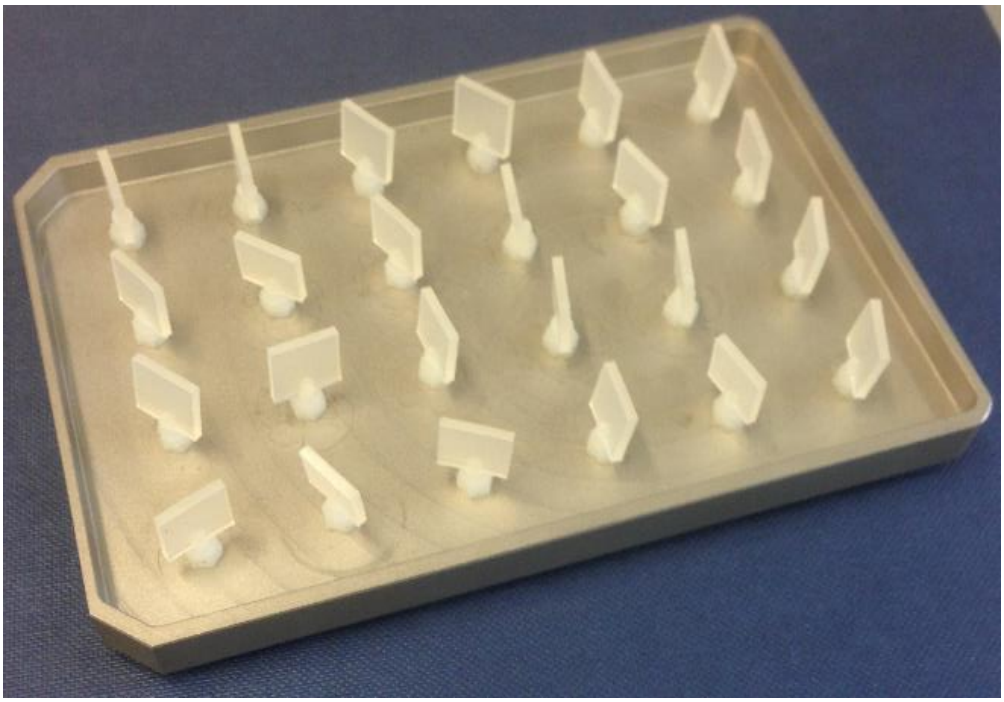
Supplementary Table S2.1: Distribution of bacterial species on 159 voice prostheses. Number is the absolute number of voice prostheses upon which the particular species was found.

Species	Isolation Frequency from 159 Voice Prostheses	
	Number	Percentage
Candida albicans	89	56.0
Candida glabrata	23	14.5
Candida tropicalis	17	10.7
Candida parapsilosis	14	8.8
Candida krusei	11	6.9
Saccharomyces cerevisiae	8	5.0
Candida lusitaniae	4	2.5
Candida dubliniensis	3	1.9
Candida utilis	2	1.3
Candida kefyr	2	1.3
Pichia manshurica	2	1.3
Candida guillermondii	1	0.6
Candida fermentati	1	0.6
Candida pararugosa	1	0.6

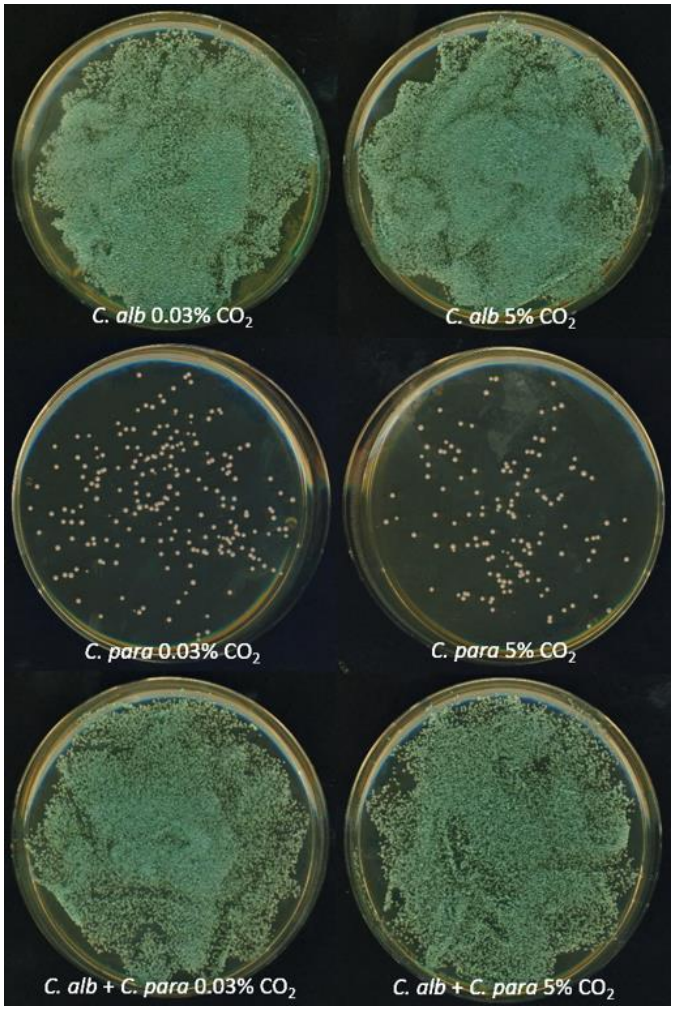
Supplementary Table S2.2: Distribution of fungal species on 159 voice prostheses. Number is the absolute number of voice prostheses upon which the particular species was found.

Strain	Species	Genotype/Parent	Source
G-3065	*C. albicans*	Clinical Isolate	Failed Voice Prosthesis
G-8424	*C. albicans*	Clinical Isolate	Failed Voice Prosthesis
G-1625	*C. albicans*	Clinical Isolate	Failed Voice Prosthesis
G10402	*C. parapsilosis*	Clinical Isolate	Failed Voice Prosthesis

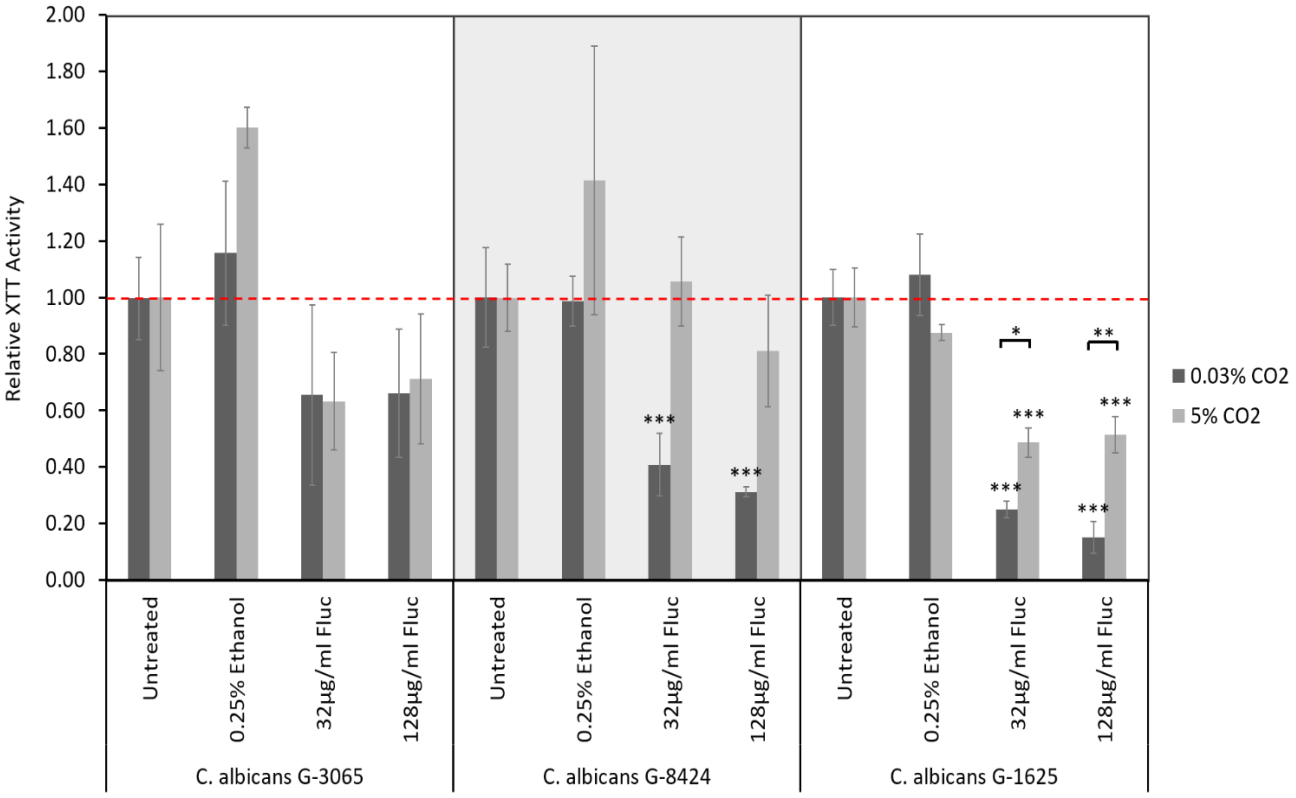
Supplementary Table S2.3: *Candida* strains used within this study.



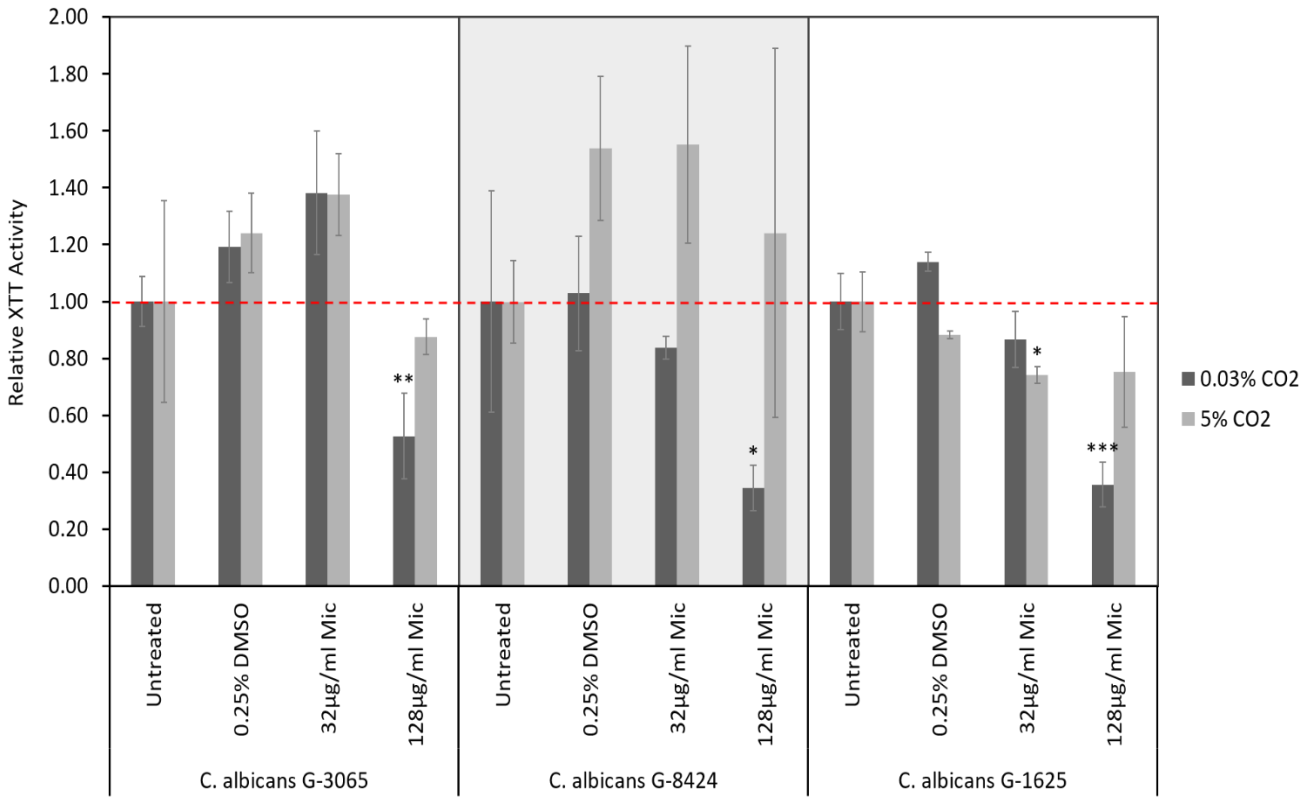
Supplementary Figure S2.1: The *in vitro* biofilm model used within this study. Biofilms were grown on 1cm^2 silicone squares which mimic the surface of the voice prosthesis. They were placed in modified 24-well plate lids so that they protrude into RPMI-1640 media containing *C. albicans* cells when placed on a 24-well plate. This enables easy washing and quantification of growth without disruption of the biofilm by transferring to new plates containing PBS or XTT reagent (see Materials and Methods).



Supplementary Figure S2.2: Chromogenic agar of *C. albicans* (G-3065) and *C. parapsilosis* (G10402) clinical isolate biofilms. Although they did not mature into a full biofilm, *C. parapsilosis* cells did attach to the silicone surface. The majority of the *C. albicans* and *C. parapsilosis* mixed biofilms are made up of *C. albicans* cells. Green colonies: *C. albicans*, white colonies: *C. parapsilosis*.



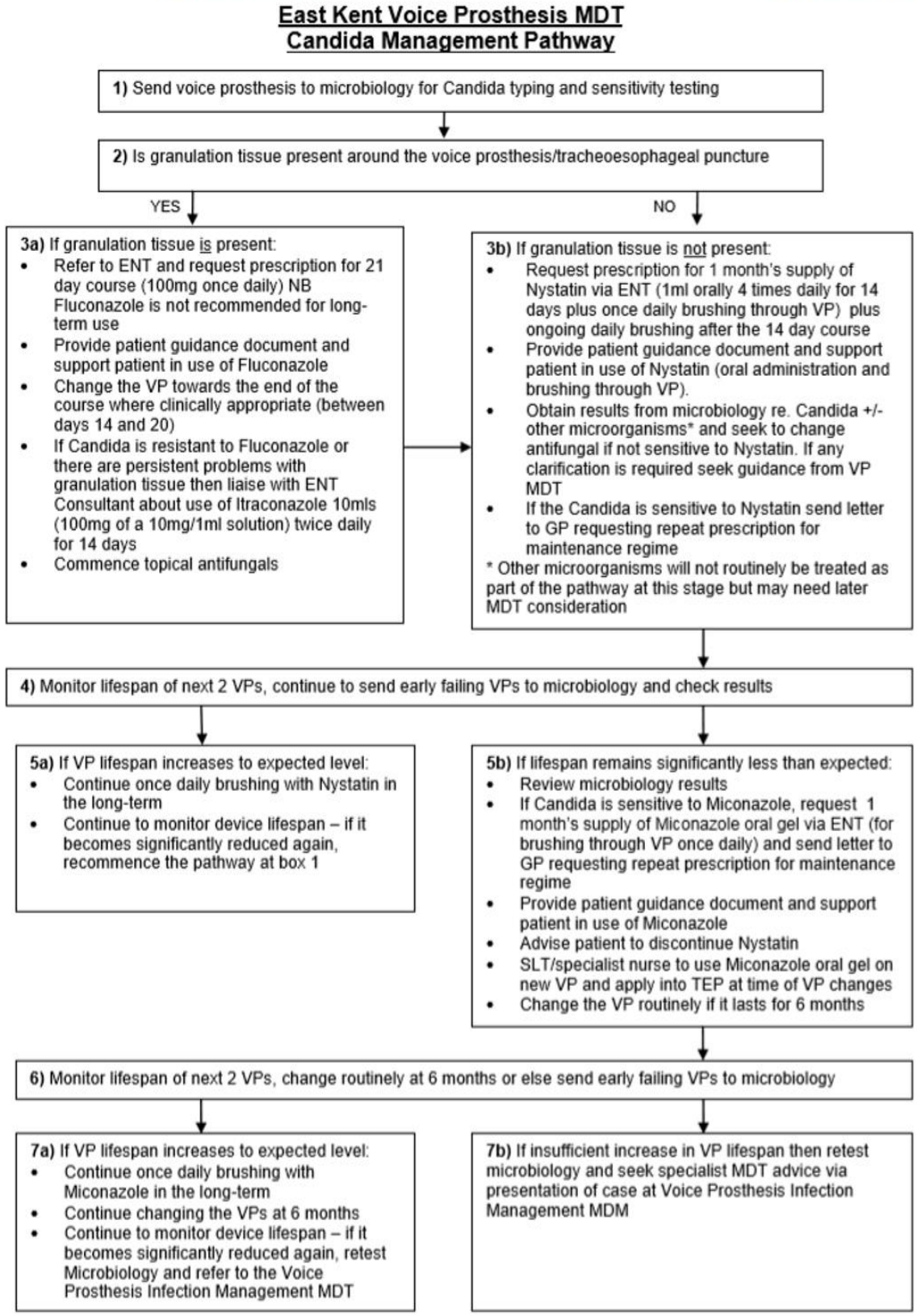
Supplementary Figure S2.3: Fluconazole sensitivities of *C. albicans* clinical isolate biofilms. Biofilms were seeded and grown for 24 hours before addition of Fluconazole, they were then grown for a further 24 hours before quantification using the XTT assay. The relative XTT activity is presented with the 0.03% and 5% CO_2 biofilms normalised to the 0.03% and 5% CO_2 untreated controls respectively. This prevents the general higher growth of 5% CO_2 biofilms impacting the analysis. Graphs represent three independent experiments each containing triplicates, error bars denote Standard Deviation. Two-way ANOVAs followed by a Tukey test for multiple comparisons were carried out: *p<0.05, **p<0.01, ***p<0.001. Stars directly above the bars indicate a significant difference to untreated in the same CO_2 environment.



Supplementary Figure S2.4: Miconazole sensitivities of *C. albicans* clinical isolate biofilms. Biofilms were seeded and grown for 24 hours before addition of Miconazole, they were then grown for a further 24 hours before quantification using the XTT assay. The relative XTT activity is presented with the 0.03% and 5% CO_2 biofilms normalised to the 0.03% and 5% CO_2 untreated controls respectively. This prevents the general higher growth of 5% CO_2 biofilms impacting the analysis. Graphs represent three independent experiments each containing triplicates, error bars denote Standard Deviation. Two-way ANOVAs followed by a Tukey test for multiple comparisons were carried out: *p<0.05, **p<0.01, ***p<0.001. Stars directly above the bars indicate a significant difference to untreated in the same CO_2 environment.

East Kent Hospitals University NHS
NHS Foundation Trust

Kent Community Health NHS
NHS Foundation Trust



Supplementary Figure S2.5: Detailed voice prosthesis management guidelines. As of January 2019, this management pathway has been distributed to 34 different speech and language therapy centres (32 in the UK, 2 internationally) upon request.

Chapter 3 – CO_2 enhances *Candida albicans* biofilm formation and reveals novel approaches to their inhibition

Daniel R. Pentland[1], Friedrich A. Muhlschlegel[2], Campbell W. Gourlay[1*]

[1]Kent Fungal Group, School of Biosciences, University of Kent, Kent, CT2 9HY, UK

[2]Laboratoire National de Santé, Dudelange, L-3555, Luxembourg

*Author for correspondence

3.1 Author Contributions

I (Daniel R. Pentland) wrote this paper in its entirety and carried out all the experiments detailed herein. I was responsible for the statistical analyses and presentation of the data along with the conclusions drawn. In addition, I have disseminated this research through presentations at professional conferences:

1. **July 2016 – British Yeast Group (University of Swansea, UK)**

   Poster and oral presentation – 'Investigating the Colonisation of Voice Prostheses by *Candida albicans*'

2. **May 2017 – Molecular Mechanisms of Host-Pathogen Interactions and Virulence in Human Fungal Pathogens (Nice, France)**

   Poster – 'Investigating the Colonisation of Voice Prostheses by *Candida albicans*'

3. **September 2017 – British Yeast Group (University of Kent, UK)**

   Poster – 'Investigating the Colonisation of Voice Prostheses by *Candida albicans*'

4. **June 2018 – British Yeast Group (University of Leicester, UK)**

   Oral presentation – 'Investigating the Effects of High CO_2 on *Candida albicans* Biofilm Formation'

3.2 Abstract

C. albicans is the predominant fungal pathogen worldwide with its ability to form biofilms crucial to its success as well as enabling it to be a prevalent coloniser of medical devices. *C. albicans* is a dimorphic yeast, existing in both budding yeast and filamentous hyphal forms, and the capacity to switch between these forms is extremely important to its biofilm producing proficiency. CO_2 concentrations in mammalian hosts are more than 150x that in the atmosphere (5% vs. 0.03%) and it has been well established that 5% CO_2 stimulates the yeast-to-hyphal morphogenic switch via the Ras1-Cyr1-PKA pathway. However, until now the effect of high CO_2 on *C. albicans* biofilm growth was unknown. Here, we show that 5% CO_2 enhances each stage of the *C. albicans* biofilm forming process; from attachment through maturation to dispersion, and this is accompanied by an increased tolerance to azoles and iron sequestration. We find that elevated CO_2 leads to an increase in expression of glucose transporters and that treatment with the glycolytic inhibitor 2-deoxyglucose (2-DG) is equally effective in both 0.03% and 5% CO_2 environments. This suggests that 2-DG maybe repurposed as an anti-biofilm compound for use under conditions of elevated CO_2. We also observe that *C. albicans* biofilm growth is reliant upon the adenylate cyclase Cyr1 but elevation of CO_2 can override the requirement for Ras1. Transcriptome analysis reveals key biofilm formation pathways governed by the central biofilm regulators Efg1, Brg1, Bcr1 and Ndt80 are upregulated in *C. albicans* biofilms grown in 5% CO_2 compared to those in atmospheric (0.03%) CO_2. We thus characterise a 5% CO_2-mediated increase in *C. albicans* biofilm formation which could have important clinical implications for the prevention/treatment of *C. albicans* biofilms.

3.3 Introduction

C. albicans is a commensal yeast located on the mucosal surfaces of the oral cavity, gastrointestinal tract and genitourinary tract of most healthy individuals [6][7]. Despite being a commensal organism, it is also an opportunistic pathogen [6][8]; in fact, it is the most widespread of all the human fungal pathogens [9] and is the fourth most common cause of hospital-acquired infections in the USA [6]. Infection with *C. albicans* is a particular problem among immunocompromised individuals or persons with implanted medical devices such as catheters or voice prostheses [10][11]. *C. albicans* can readily colonise medical devices and grow on their surfaces, isolated from the host immune system, as biofilms [4].

Biofilms are structured communities of microorganisms attached to a surface. The cells are often encased within an extracellular matrix (ECM) which is commonly comprised of DNA [107][108], lipids [107], proteins [107][109] and polysaccharides [107]. *C. albicans* is able to form biofilms on both abiotic and biotic surfaces and biofilm-associated cells are considerably more tolerant to traditional antifungals when compared to planktonic cells [147]. The reasons for this increased tolerance are complex but include; the presence of an ECM which can act as a barrier to prevent antimicrobial agents to reaching the cells [116][117], the presence of metabolically dormant persister cells inherent to biofilms [172], and the upregulation of drug efflux pumps [119]. A significant percentage of human microbial infections arise from, or are, mediated via the formation of a biofilm [110][111][112], and this, combined the limited treatment options available, means the ability of *C. albicans* to grow as a biofilm is of particular medical interest.

C. albicans is a dimorphic fungus, meaning it has the ability to undergo a morphogenetic switch from a yeast, to pseudohyphal or hyphal forms in response to environmental cues. The virulence of *C. albicans* is closely linked with the capacity to switch between these forms; hyphal *C. albicans* cells are frequently located at sites of tissue invasion, and cells which are unable to readily form hyphae exhibit reduced virulence [6]. This yeast-to-hyphal switch is critical in the biofilm formation process as hyphal cells express a number of specific cell surface adhesins which enable cell-cell attachment as well as cell-surface attachment during biofilm maturation [134]. These adhesins, such as the agglutinin-like sequence (Als) protein family which consists of 8 members (Als1-7 and Als9), possess a folded N-terminal domain required for protein-ligand interaction, a 600-1000 residue serine/threonine-rich tandem domain, and a C-terminal peptide which covalently bonds to glycosylphosphatidylinositol (GPI) to anchor the adhesin in the fungal cell wall [121]. The Als proteins also contain an amyloid forming region (AFR) in the N-terminal domain [263] which interacts with AFRs of other Als proteins. This results in the formation of large molecular weight clusters of Als proteins on the fungal cell wall called nanodomains which can bind multivalent ligands with high avidity [264]. These nanodomains form in response to forces applied to the adhesin molecules, such as that created under laminar flow, which cause the AFR to unfold and facilitate Als molecule aggregation [265][266]. Nanodomains strengthen adhesion and support the structure of mature biofilms [267].

C. albicans biofilm formation is a complex process involving tightly regulated, interwoven signalling pathways centrally controlled by a set of nine transcription factors; Bcr1, Brg1, Efg1, Flo8, Gal4, Ndt80, Rob1, Rfx2 and Tec1. These nine essential regulators function at different stages throughout *C. albicans* biofilm formation [129] and coordinate the expression of over

a 1000 target genes upregulated during biofilm formation [127]. *C. albicans* biofilm formation can divided into distinct stages that are governed by programmes of gene expression; attachment, initiation, maturation and dispersion. The attachment stage involves the initial attachment of *C. albicans* cells, primarily in the yeast-form [115], to a surface [120]. Both nonspecific factors, such as cell surface hydrophobicity and electrostatic forces, and specific factors, such as adhesins on the yeast cell surface binding to precise ligands on the substratum to be colonised, are responsible for the preliminary attachment [120]. Approximately 3-6 hours after the initial attachment, pseudohyphal and hyphal cells start forming from the proliferating yeast-form cells [8]. This initiation step is characterised by the appearance of extracellular material. The maturation phase of biofilm growth lasts between 24-48 hours [120]. Colonies of *C. albicans* continue to grow and secrete ECM, increasing the amount of material encasing the biofilm [115]. The final stage of biofilm development is the dispersal stage during which yeast-form cells bud off from hyphal cells within a mature biofilm and disperse in order to establish additional biofilms elsewhere [115][125]. The yeast-form cells emerging from mature biofilms have distinct characteristics compared to typical planktonic yeast cells; with enhanced adherence, an increased propensity to filament, and increased biofilm forming capability [126].

Elevated CO_2 levels, as found in a number physiologically relevant scenarios such as in exhaled breath or hypercapnia, have been shown to promote the yeast-to-hyphal switch in *C. albicans*. CO_2 is converted to bicarbonate ions HCO_3^- by the enzyme carbonic anhydrase which in turn activate the adenylate cyclase Cyr1, resulting in increased cAMP levels and the PKA dependent activation of hyphal specific genes [69]. The yeast-to-hyphal switch is critical to the biofilm maturation process of *C. albicans* [142], as well as being important to its virulence

[6]. Therefore, it has been hypothesised that high CO_2 could drive *C. albicans* biofilm formation and increase its propensity to cause infection. The effect of CO_2 is particularly important within the context of biofilm development on voice prostheses (VPs) since these devices are situated in the throat of patients where they are consistently exposed to high CO_2 (5%) levels during exhalation. If CO_2 does play a role in *C. albicans* biofilm maturation it could offer a possible explanation as to why *C. albicans* is found in such high frequencies on failed voice prostheses. In addition as it has been estimated that as many as 80% of all microbial infections directly or indirectly involve pathogenic biofilms [113] and that CO_2 content within the blood is also elevated (46mmHg and 40mmHg for venous and arterial blood respectively versus 0.3mmHg found in atmospheric air) [222][268]. Thus, the work presented here could be more widely applicable to bloodstream infections and biofilm formation within the body.

Here we demonstrate that high CO_2 concentration (5%) increases *C. albicans* biofilm formation on silicone surfaces. Transcriptome analysis reveals that several core biofilm regulatory pathways, including those governed by Efg1, Bcr1, Brg1, and Ndt80, are upregulated in *C. albicans* biofilms grown in 5% CO_2. We also demonstrate that a high CO_2 environment results in increased tolerance of biofilms to azole antifungals, as well as enhanced dispersal of cells from mature biofilms. Moreover, a transcription factor knockout (TFKO) library screen demonstrated transcription factors involved in the acquisition of iron, such as the HAP transcription factors Hap43, Hap2, Hap3 and Hap5, to be important for *C. albicans* biofilm formation on a silicone surface in atmospheric CO_2 conditions. However, high CO_2 was able to overcome the requirement for HAP transcription factor activity and enable *C. albicans* biofilms to forage for essential metabolites to support growth. Overall, we propose that *C. albicans* has adapted to utilise the high CO_2 environment found in the host to promote

its ability to colonise and to compete for nutrition. Our analysis reveals new approaches that can be taken to prevent *C. albicans* biofilm formation in high CO_2 environments that pave the way for new therapeutic approaches to treat these highly drug tolerant structures.

3.4 Materials and Methods

3.4.1 *Candida* strains and growth media

Candida strains (Supplementary Table S3.1) were routinely grown at 30°C in yeast peptone dextrose (YPD) media (2% peptone (BD Bacto), 2% D-glucose (Fisher Scientific), 1% yeast extract (BD Bacto)). For biofilm growth assays, *Candida* biofilms were grown at 37°C in RPMI-1640 media (Sigma-Aldrich, R8755) supplemented with 80µg/ml uridine (Sigma-Aldrich, U3750) if required.

3.4.2 *In vitro* biofilm growth assays

C. albicans biofilms were grown on a PDMS silicone elastomer (Provincial Rubber, S1). The silicone was cut into 1cm^2 squares and placed in clips in a modified 24-well plate lid (Academic Centre for Dentistry Amsterdam, AAA-model) so they could be suspended in media within a 24-well plate. Silicone squares were incubated in 1ml 50% Donor Bovine Serum (DBS) (Gibco, 16030074) for 30 minutes at 30°C, then washed twice with 1ml Phosphate-Buffered Saline (PBS – 137mM NaCl, 2.7mM KCl, 10mM Na_2HPO_4, 1.8mM KH_2PO_4, pH 7.4) to remove excess DBS. *Candida* strains were inoculated into a test tube containing 5ml YPD media and placed in a 30°C orbital shaking incubator with constant shaking at 180rpm for 18h. OD_{600} measurements were taken and a volume of overnight culture corresponding to OD_{600} = 1.0 (3 x 10^7 CFU/ml) was removed. These cells were pelleted by centrifugation at 4000rpm for 5 min at which point the supernatant was discarded. The resultant pellet was resuspended in 5ml PBS to wash and centrifuged again at 4000rpm for 5 min. The PBS supernatant was discarded and the pellet re-suspended in fresh PBS (at an OD_{600} of 1.0). The OD_{600} 1.0 standard cell suspension was added to wells (1ml per well) in a pre-sterilised 24-well plate (Greiner Bio-one, CELLSTAR, 662160) and the lid with the silicone squares attached was placed on top so

the silicone squares protrude into the cell suspension. These plates were then incubated at 37°C (in either 0.03% CO_2 or 5% CO_2) without shaking for 90 min to allow cell attachment to the silicone. After the attachment phase, the silicone squares were washed twice with 1ml PBS to remove any unattached cells and transferred to 1ml RPMI-1640 media (Sigma-Aldrich, R8755). They were then incubated at 37°C (in either 0.03% CO_2 or 5% CO_2) without shaking for 48h to allow biofilm maturation.

3.4.3 Biofilm quantification via XTT assay

Biofilm growth was quantified using an XTT assay [237]. Biofilms were washed twice with 1ml PBS to remove any planktonic cells before proceeding to quantification. After washing, the biofilms were transferred to a new pre-sterilised 24-well plate (Greiner Bio-one, CELLSTAR, 662160) containing 30µg/ml XTT labelling reagent (Roche, 11465015001) and incubated at 37°C for 4h. After incubation, the biofilms were removed from the 24-well plate and the absorbance of the remaining XTT labelling reagent was measured at 492nm using a BMG LABTECH FLUOstar Omega plate reader machine.

3.4.4 *C. albicans* transcription factor knockout (TFKO) screen

Biofilms using mutants from a *C. albicans* TFKO library [269] were seeded and grown for 48h on a PDMS silicone elastomer (Provincial Rubber, S1) as described above. Biofilm growth was quantified using the XTT assay. Experiments were performed in biological triplicate.

3.4.5 Iron starvation of *C. albicans* biofilms

Biofilms were set up as described previously except they were incubated at 37°C in either 0.03% CO_2 or 5% CO_2 for 48h in RPMI-1640 containing varying concentrations of the Fe^{2+}

chelator 3-(2-Pyridyl)-5,6-diphenyl-1,2,4-triazine-p,p'-disulfonic acid monosodium salt hydrate (Ferrozine – Sigma-Aldrich, 160601) or the Fe^{3+} chelator Deferasirox (Cambridge Bioscience, CAY16753-5). Ferrozine was made as a 100mM stock solution in sterile MQ H_2O and diluted in RPMI-1640 to final concentrations of 250-500µM. Deferasirox was made as a 20mg/ml stock solution in DMSO and diluted in RPMI-1640 to final concentrations of 70-210µg/ml. A 1% DMSO vehicle control was included in the experiment. Final biofilms were quantified using the XTT assay. Ferrozine experiments were performed in 6 biological replicates each in technical triplicate. Deferasirox experiments were performed in biological duplicate and technical triplicate.

3.4.6 Preparation of PDMS-coated microscope slides

To prepare PDMS for coating microscope slides 16g (6.16×10^{-4} mol) silanol-terminated PDMS (cSt 1000, M_W 26000, from Fluorochem Ltd.) and 0.26g (12.48×10^{-4} mol, 1:4 stoichiometric ratio) cross-linking agent tetraethyl orthosilicate (TEOS – Sigma-Aldrich, 131903) were mixed at 3500rpm for 60 secs using a DAC 150FV2-K speedmixer. At this point, 720µl tin(II) ethylhexanoate (Sigma-Aldrich, S3252) made up at a concentration of 0.6M in toluene was added as a catalyst and the mix spun for a further 60 secs at 3500rpm. The elastomer mixture was then doctor bladed onto microscope slides using an automatic precision film applicator MTCX4 (Mtv-Messtechnik – blade width = 70mm, thickness adjustability 0-3000µm). The doctor blade height was set 10µm higher than the thickness of the microscope slide. The elastomer mix was poured over the top of the slide (with a bias towards the side of the microscope slide closest to the doctor blade), and then the doctor blade is moved at a constant speed over the substrate. The microscope slide was then air cured for 2h before being heat cured for 18h in a 70°C oven.

3.4.7 Preparation of *C. albicans* biofilms on silicone coated slides for microscopy

Biofilms were grown directly on microscope slides that had been pre-coated with a PDMS silicone polymer (see above) for confocal imaging. Biofilms were grown with a prefabricated well. PDMS-coated microscope slides were incubated with 400µl 50% Donor Bovine Serum (DBS) (Gibco, 16030074) in the wells for 30 min at 30°C and washed twice with 400µl PBS. *C. albicans* overnight cultures were grown in YPD at 30°C and washed in PBS as described previously. 400µl of the OD_{600} 1.0 standard cell suspension was added to the wells and incubated at 37°C (in either 0.03% CO_2 or 5% CO_2) without shaking for 90 min to allow cell attachment to the silicone surface of the microscope slide. After the attachment phase, the microscope slides were washed twice with 400µl PBS to remove any unattached cells and then incubated at 37°C with 400µl RPMI-1640 media in the wells for 6h, 24h or 48h (in either 0.03% CO_2 or 5% CO_2). Biofilms were washed twice with 400µl PBS and then incubated in the dark for 45 min at 30°C in 400µl PBS containing 50µg/ml ConA-FITC (Sigma-Aldrich, C7642) and 20µM FUN-1 (Invitrogen Molecular Probes, F7030). After incubation with the dyes, the stained biofilms were washed again with 400µl PBS to remove any residual dye. The well was removed and 2 drops of ProLong™ Diamond Antifade Mountant (Invitrogen, P36965) was added to each stained biofilm. A cover slip was placed on top and the microscope slides were incubated in the dark at room temperature overnight to allow the mountant to cure.

3.4.8 Confocal scanning laser microscopy (CSLM) of *C. albicans* biofilms on silicone slides

Stained biofilms grown on silicone coated slides were imaged using a Zeiss LSM880/Elyra/Axio Observer.Z1 Confocal Microscope (Carl Zeiss Inc.) using the 488nm argon and the 561nm DP55 lasers. Images of the green (ConA-FITC) and the red (FUN-1) were taken simultaneously using a multitrack mode. Z-stacks were taken using the inbuilt 'optimal' settings to determine

the optimal intervals (typically 1.5-2.0µm slices) based upon sample thickness and magnification. The 20x and oil-immersion 40x objective lenses were used throughout. The image acquisition software used was ZENBlack and the image processing software was ZENBlue.

3.4.9 RNA isolation from *C. albicans* biofilms

Total RNA was extracted in biological triplicate per condition (0.03% and 5% CO_2) using the E.Z.N.A.™ Yeast RNA Kit (Omega Bio-Tek, R6870-01) as per the manufacturer's instructions with a few modifications. Specifically, *C. albicans* CAI-4 biofilms were seeded and grown in 0.03% and 5% CO_2 as described for *in vitro* biofilm growth assays. Mature biofilms were washed twice with 1ml ice-cold PBS to remove any planktonic cells. Biofilm cells were harvested by transferring silicone squares upon which the biofilms were growing into 5ml cold SE buffer/2-mercaptoethanol (provided in the E.Z.N.A.™ Yeast RNA Kit) and vortexing at 2500rpm for 1 min. The resulting biofilm cell suspension was pelleted by centrifugation at 4000rpm for 10 min at 4°C. The supernatant was discarded and the cells re-suspended in fresh 1ml cold SE buffer/2-mercaptoethanol, this cell suspension was transferred to a 2ml Eppendorf tube. The cell suspension was centrifuged again for 10 min at 4°C, the supernatant discarded and the pellet re-suspended in 480µl fresh SE buffer/2-mercaptoethanol. The biofilm cell suspension was incubated with 80µl lyticase stock solution (5000units/ml in SE buffer) at 30°C for 90 min. The resulting spheroplasts were pelleted by centrifugation at 2900rpm for 10 min at 4°C and the supernatant aspirated and discarded. The spheroplasts were gently re-suspended in 350µl YRL buffer/2-mercaptoethanol (provided in the E.Z.N.A.™ Yeast RNA Kit). The rest of the RNA extraction proceeded as per the manufacturer's instructions including the optional DNase digestion step. RNA was eluted in 30µl DEPC water,

the concentration and purity established using a NanoDrop ND-1000 spectrophotometer (NanoDrop Technologies) and stored at -80^{o}C.

3.4.10 Library Preparation and RNA Sequencing

RNA samples were sent to the Centre for Genome Enabled Biology and Medicine (Aberdeen, UK) for library preparation and sequencing. Before library preparation, the quality and quantification of RNA samples were evaluated with TapeStation (Agilent) and Qubit (Thermal Fisher). Samples with a minimum RIN of 8.0 proceeded to library preparation. The input of RNA was based on the specifically measured RNA concentration by Qubit. The mRNA-Seq libraries were prepared using TruSeq™ Stranded mRNA Sample Preparation Kit (Illumina) according to the manufacturer's instructions. Briefly, Poly-A RNA were purified from 500ng of total RNA with 1ul (1:100) ERCC spike (Thermal Fisher) as an internal control using RNA purification oligo(dT) beads, fragmented and retrotranscribed using random primers. Complementary-DNAs were end-repaired, and 3-adenylated, indexed adapters were then ligated. 15 cycles of PCR amplification were performed, and the PCR products were cleaned up with AMPure beads (Beckman Coulter). Libraries were validated for quality on Agilent DNA1000 Kit and quantified with the qPCR NGS Library Quantification kit (Roche). The final libraries were equimolar pooled and sequenced using the High Output 1X75 kit on the Illumina NextSeq500 platform producing 75bp single-end reads. For each library a depth 50-70M reads were generated.

3.4.11 Analysis of RNA-Seq data

Analysis of RNA-Seq data was performed using the Galaxy web platform [270]. The quality of the RNA sequencing reads was checked using FastQC v0.11.5 [271] with default settings. Low

quality ends (Phred score < 20) and any adaptor sequences were trimmed using TrimGalore! v0.4.3 [272]. Reads which became shorter than 40bp after trimming were removed from further analysis. After trimming, 97.7% of initial reads remained and the quality was checked again using FastQC v0.11.5 [271] to ensure the trimming had worked correctly. There were no Poly-A reads (more than 90% of the bases equal A), ambiguous reads (containing N) or low quality reads (more than 50% of the bases with a Phred score < 25). After processing, the mean Phred score per read was 35. Processed reads were aligned with the reference *C. albicans* genome SC5314 version A21-s02-m09-r10 using HISAT2 v2.1.0 [273] with single-end reads and reverse strand settings (rest of the settings were default). After alignment, the number of mapped reads which overlapped CDS features in the genome (using the *C. albicans_SC5314_version_A21-s02-m09-r10_features.gtf* annotation file [274]) were determined using htseq-count v0.9.1 [275] with default settings. Reads aligning to multiple positions or overlapping more than one gene were discarded, counting only reads mapping unambiguously to a single gene. Differential gene expression analysis between conditions (0.03% and 5% CO_2) was performed using DESeq2 v1.18.1 [276] with default settings.

3.4.12 Gene Set Enrichment Analysis of transcription profiles

Downstream analysis of RNA Sequencing data was performed using the PreRanked tool of Gene Set Enrichment Analysis (GSEA; Broad Institute) [277] which compares a pre-ranked significantly differentially expressed gene list to a functional gene set database. False discovery rate (FDR) q-values were calculated based upon 1000 permutations. The gene set database used was assembled by Sellam, A. *et al*. as described in [278], which is based upon experimental analyses from published studies, Gene Ontology (GO) term categories curated by the *Candida* Genome Database [279] and protein-protein interaction information derived

from *Saccharomyces cerevisiae* data curated by the *Saccharomyces* Genome Database [280]. Gene set networks were generated in Cytoscape 3.7.1 (Available at: https://cytoscape.org/) [281] using the EnrichmentMap plug-in (Available at: http://apps.cytoscape.org/apps/enrichmentmap). Gene expression heat maps based on GO term categories were created using the Pheatmap package in R Studio.

3.4.13 Antifungal treatment of *C. albicans* biofilms

Biofilms were set up as described previously and grown in RPMI-1640 for 24h at 37°C. The biofilms were then transferred to fresh RPMI-1640 media containing a select antifungal. Three antifungals were tested; fluconazole, miconazole and nystatin. Fluconazole (Santa Cruz Biotechnology, sc-205698) was made as a 50mg/ml stock solution in ethanol and diluted in RPMI-1640 final concentrations ranging from 8-256µg/ml. Miconazole (Santa Cruz Biotechnology, sc-205753) was made as a 50mg/ml stock solution in DMSO and also diluted in RPMI-1640 to final concentrations ranging from 8-256µg/ml. Nystatin (Santa Cruz Biotechnology, sc-212431) was made as a 5mg/ml stock solution in DMSO and diluted in RPMI-1640 to final concentrations ranging from 1-8µg/ml. Drug vehicle controls (0.5% ethanol for Fluconazole, 0.5% DMSO for Miconazole and Nystatin) were used in all cases. The biofilms matured in the RPMI-1640 media containing the select antifungal for a further 24h at 37°C in both 0.03% and 5% CO_2 before proceeding to quantification via the XTT assay. Experiments were performed in biological and technical triplicate.

3.4.14 *C. albicans* attachment assay

CAI-4 cells were seeded onto silicone-coated microscope slide for 90 min as described previously for growing biofilms for confocal microscopy, except here an OD_{600} of 0.1 was used instead of 1.0 and the silicone-coated microscope slides were not pre-incubated with DBS. The slide surface was washed twice with 400µl PBS to remove any unattached cells. Images were taken using a Leica DMR fitted with a Leica DFC9000 GT camera using a 20x objective lens and brightfield settings. The image acquisition software used was the Leica Application Suite X package. Using identical microscope settings throughout, five images were taken of each of three biological replicates in both 0.03% and 5% CO_2 and the cells per image counted using the 'Cell Counter' function in ImageJ.

3.4.15 2-deoxyglucose (2-DG) treatment of *C. albicans* biofilms

Biofilms were set up as described previously except they were incubated at 37°C in either 0.03% CO_2 or 5% CO_2 for 48h in RPMI-1640 containing varying concentrations of 2-DG. 2-DG (Sigma-Aldrich, D6134) was made up as a 20% stock solution in sterile MQ H_2O and diluted in RPMI-1640 to final concentrations of 0.25-1%. Biofilms were quantified using XTT assays and images were also taken. Experiments were performed in biological and technical triplicate.

3.4.16 *C. albicans* biofilm dispersion assay

Biofilms were set up as described previously and grown in RPMI-1640 for 48h at 37°C. The spent media, containing dispersed cells, was sonicated at amplitude 4µm for 10 secs to separate clumps of hyphal cells (previous work in our lab has demonstrated these sonication settings do not affect viability). After sonication, the dispersed cells were diluted 1 in 10 and 200µl of this suspension was plated on YPD agar plates in triplicate. YPD plates were

incubated for 48h at 37^{o}C to allow colonies to form, at which point the number of colonies were manually counted using a Stuart Scientific Colony Counter. Experiments were performed in biological and technical triplicate.

3.5 Results

3.5.1 High CO_2 enhances *C. albicans* biofilm growth

C. albicans biofilms were seeded and grown on silicone in both levels found in exhaled air (5%) and normal air (0.03%) CO_2 conditions for 24 and 48 hours. Biofilms were quantified using the XTT assay which acts as a readout of cell number [237]. After 24 hours of growth, both CAI4pSM2 and SN152 *C. albicans* strains assayed exhibited a significantly higher cell number within biofilms grown in a 5% CO_2 environment compared to 0.03% CO_2. However, after 48 hours, cell numbers within biofilms grown in both CO_2 conditions appeared equal (Figure 3.1A). Biofilms formed from clinical isolates isolated from failed voice prostheses displayed a similar effect with significantly higher cell numbers within biofilms grown in 5% CO_2. Interestingly, although cell number appeared equivalent at 48h, the resultant biofilm mass appeared noticeably larger in biofilms grown under elevated CO_2 conditions (Figure 3.1B). This CO_2-mediated increase in biofilm growth is specific to the biofilm scenario as planktonic *C. albicans* cells exhibited no significant difference in growth rate in RPMI-1640 between 0.03% and 5% CO_2 environments (data not shown).

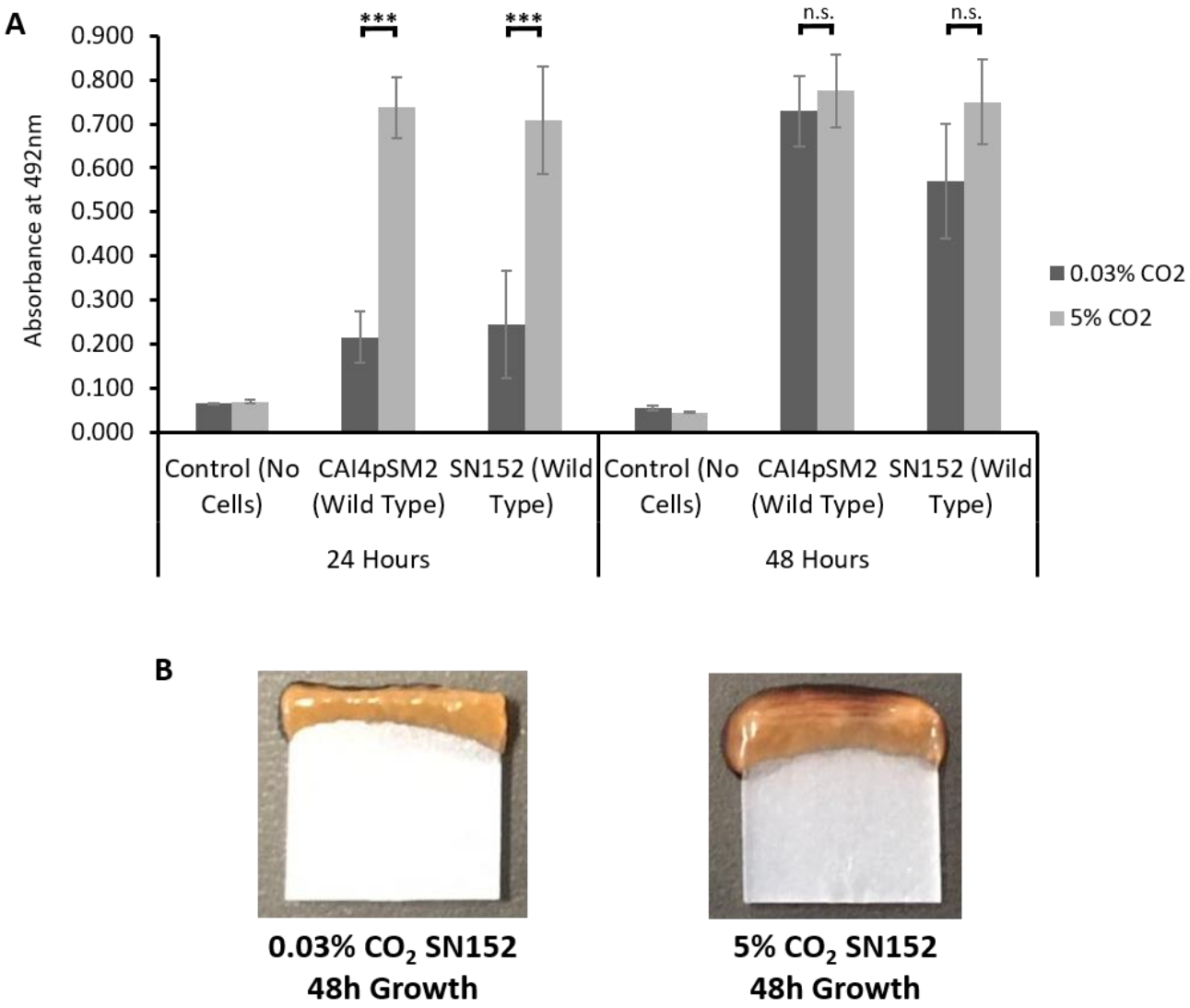


Figure 3.1: The effect of high CO_2 (5%) on *C. albicans* biofilm formation. (A) Biofilm growth assay using two laboratory strains. Biofilms were seeded and grown for 24h or 48h, the resulting biofilms were quantified using the XTT assay. Control wells with no cells were set up as media controls to monitor for contamination as well as to ensure there was no reaction of the silicone squares with the XTT reagents. The graph represents three biological replicates each containing technical triplicates, error bars denote Standard Deviation. Paired two-tail t-tests were carried out: *p<0.05, **p<0.01, ***p<0.001, n.s. = not significant. **(B)** Representative images of SN152 biofilms grown in 0.03% and 5% CO_2 for 48h (red coloration due to XTT assay).

3.5.2 Analysis of the effects of CO_2 on phases of *C. albicans* biofilm growth

We sought to determine which phases of biofilm growth were influenced by CO_2 elevation. To investigate the attachment phase *C. albicans* cells were seeded for 90 min onto silicone-coated microscope slides under 0.03% CO_2 or 5% CO_2 levels. We observed that exposure to elevated CO_2 led to a significant increase in the number of cells that attached to silicone (mean of 2108 cells in 0.03% vs. a mean of 7033 cells in 5% CO_2) (Figure 3.2A). Cells also appeared to attach as larger aggregations in 5% CO_2 when compared to those in 0.03% CO_2 (Supplementary Figures S3.1A and B) indicating that both cell-substrate and cell-cell attachments may be enhanced.

Confocal scanning laser microscopy (CSLM) was used to investigate the effects of CO_2 on biofilm growth during maturation. *C. albicans* biofilms were seeded on silicone-coated microscope slides and images were taken at 6h, 24h and 48h of growth under either 0.03% or 5% CO_2 growth conditions (Figure 3.2B). Biofilm images are displayed as maximum intensity ortho-projections of Z-stacks to give a view of the overall structures of the biofilms. Green fluorescence resulted from ConA conjugated to FITC (green) binding to the polysaccharides in the cell wall. Red fluorescence was due to FUN-1 forming aggregates in the cytoplasm of metabolically active cells. After 6h growth in 0.03% CO_2, the majority of cells were found in the yeast form with some visibly initiating hyphae. In comparison, biofilms grown in 5% CO_2 appeared to consist of a high proportion of hyphal cells, were visibly denser and had begun to exhibit an ordered structure in the Z-plane (Figure 3.2B). After 24h growth in 0.03% CO_2, biofilms were progressing through the maturation stage with the appearance numerous hyphal cells. However, the 5% CO_2 biofilms displayed a fully mature biofilm organisation displaying hyphal cells organised in a brush-like structure above a basal layer of yeast cells

(Figure 3.2B). At 48h, biofilms grown in both 0.03% and 5% CO_2 appeared as dense mature structures, however, biofilms grown under elevated CO_2 were generally deeper (Figure 3.2B).

Dispersion is the final stage of biofilm formation, we therefore investigated whether CO_2 elevation resulted in increased levels of cell shedding. We routinely observed that spent RPMI-1640 media isolated after biofilm growth in 5% CO_2 contained more cells than that of taken from biofilms grown in 0.03% CO_2 (Supplementary Figure S3.2A). We quantified this by seeding and growing *C. albicans* biofilms for 48h in 0.03% and 5% CO_2 and conducting colony forming unit (CFU) assays using the spent RPMI-1640 media (Figure 3.2C and Supplementary Figure S3.2B). Our results showed an approximate four-fold increase in cell number released from mature biofilms when grown under elevated CO_2 conditions, consistent with an increase in dispersal. Overall, these data demonstrate that the elevation of CO_2 enhances each stage of the *C. albicans* biofilm forming process, from attachment through maturation to dispersion.

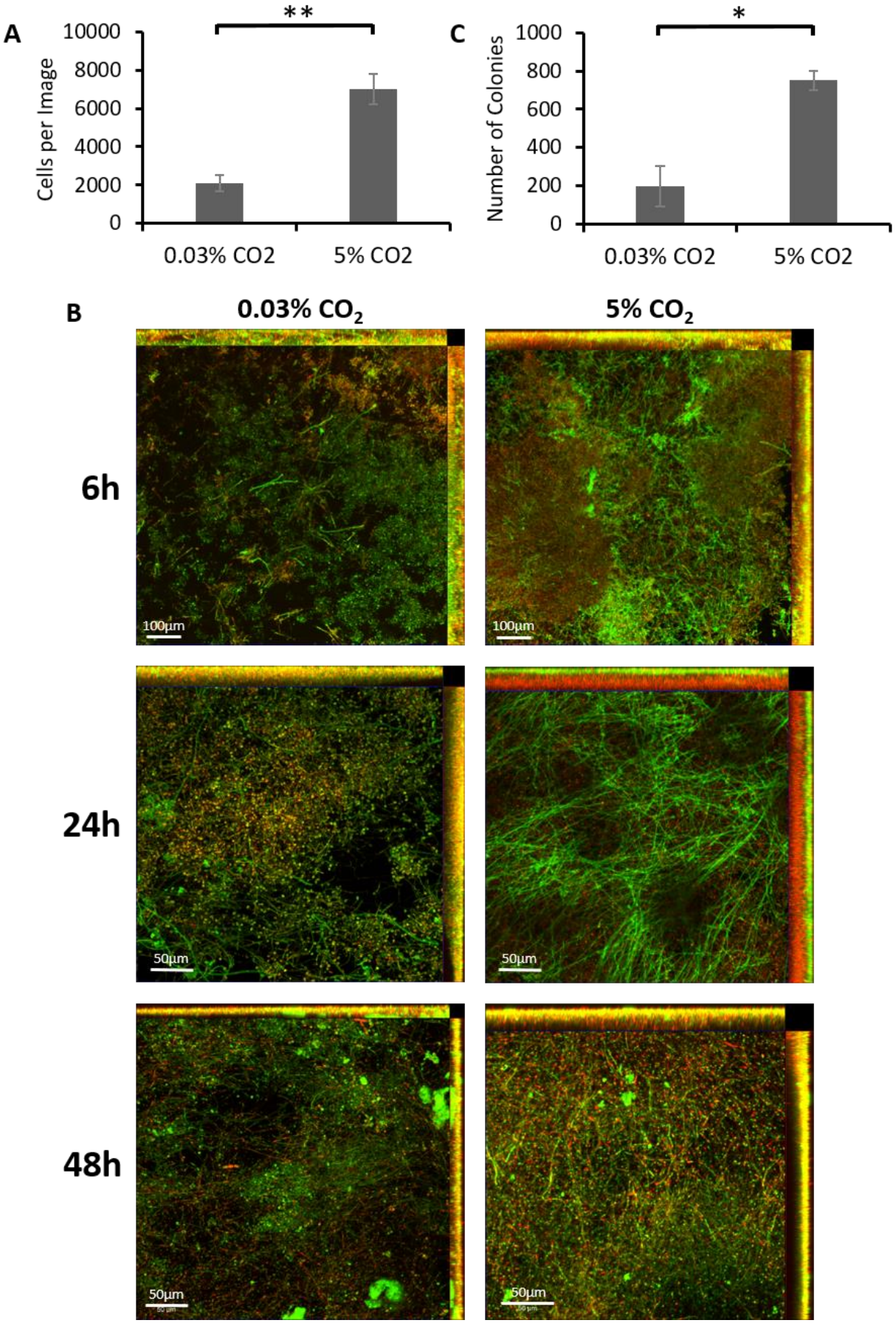

A
**
Cells per Image
10000
8000
6000
4000
2000
0
0.03% CO2
5% CO2
C
*
Number of Colonies
1000
800
600
400
200
0
0.03% CO2
5% CO2
B
0.03% CO2
5% CO2
6h
24h
48h
100µm
100µm
50µm
50µm
50µm
50µm

Figure 3.2: The effects of high CO_2 (5%) on different stages of *C. albicans* biofilm growth. (A) Attachment: *C. albicans* CAI-4 cells were seeded onto silicone-coated microscope slides in 0.03% or 5% CO_2 and images taken at 20x objective magnification (Supplementary Figure S2). Cells per image were counted using the 'Cell Counter' function in ImageJ and the mean number of cells per image in the two conditions were calculated across three biological replicates (five images per replicate). A paired two-tail t-test was carried out: **p<0.01. Error bars denote Standard Deviation. **(B)** Maturation: Biofilms were seeded on silicone-coated microscope slide and grown for 6h, 24h and 48h. Biofilms were stained with ConA-FITC (green) and FUN-1 (red). Images were taken using 20x and 40x objective magnifications. Experiments were repeated in triplicate and representative images are presented. **(C)** Dispersion: Mean number of colonies per plate from a 1:10 dilution of the spent RPMI-1640 media after 48h biofilm growth in 0.03% and 5% CO_2. Graph represents three biological replicates each containing technical triplicates, error bars denote Standard Deviation. A paired two-tail t-test was carried out: *p<0.05.

3.5.3 Identification of the regulatory mechanisms that govern CO_2 acceleration of *C. albicans* biofilm formation

CO_2 is sensed by *C. albicans* cells, in the form of bicarbonate ions (HCO_3^-), via the adenylate cyclase Cyr1 (Cdc35) [69] within the context of the Ras-cAMP-PKA pathway. We investigated whether CO_2 elevation may drive biofilm formation via the same mechanism. We conducted biofilm growth assays using *C. albicans* mutants lacking key components of the Ras1-Cyr1-PKA pathway; *ras1Δ/Δ*, *cdc35Δ/Δ*, *CDC35*$^{\Delta RA}$ (adenylate cyclase missing the Ras1 interacting domain), *tpk1Δ/Δ* (missing a catalytic subunit isoform of PKA), and *tpk2Δ/Δ* (missing the other catalytic subunit isoform of PKA). Biofilm formation was quantified via XTT assay after 48h and compared to an isogenic wild type control. The *ras1Δ/Δ* mutant displayed significantly attenuated biofilm growth in 0.03% CO_2 but this was rescued to wild type levels in 5% CO_2 (Figure 3.3A), indicating that Ras1 function is dispensable for biofilm formation under conditions of elevated CO_2. The *cdc35Δ/Δ* and *CDC35*$^{\Delta RA}$ mutants both exhibited significantly reduced biofilm growth when grown under either atmospheric or elevated CO_2 conditions (Figure 3.3A). Conversely, both *tpk1Δ/Δ* and *tpk2Δ/Δ* mutants exhibited biofilm growth

equivalent to the wild type under both CO_2 conditions (Figure 3.3A). Taken together, this data implies the CO_2-mediated effect on *C. albicans* biofilm growth is reliant on Cyr1 but can bypass a requirement for Ras1 and that the PKA isoforms Tpk1 and Tpk2 are functionally redundant with respect to cAMP activation of the biofilm programme. Our findings are however consistent with the adenylate cyclase Cyr1 as a key CO_2 sensor in the enhanced biofilm growth observed under elevated CO_2 conditions.

To investigate the molecular basis of the activation of *C. albicans* biofilm formation in 5% CO_2, we conducted a screen of a transcription factor knockout (TFKO) library [269] containing 146 mutants each lacking a non-essential transcription factor for biofilm-forming ability. This screen identified 121 deletions that had no effect upon biofilm formation in either CO_2 condition (Supplementary Figure S3.3). The screen identified 21 transcription factors which, upon their deletion, resulted in attenuated biofilm formation (Supplementary Table S3.2). Specifically, 5 TFKO mutants (*tup1Δ/Δ*, *sef1Δ/Δ*, *swi4Δ/Δ*, *pho4Δ/Δ* and *efg1Δ/Δ*) had diminished biofilm growth in both 0.03% and 5% CO_2, 12 had reduced biofilm formation only in 0.03% CO_2 (*hap2Δ/Δ*, *rbf1Δ/Δ*, *rob1Δ/Δ*, *fgr15Δ/Δ*, *dal81Δ/Δ*, *mig1Δ/Δ*, *brg1Δ/Δ*, *C4_00260WΔ/Δ*, *zcf27Δ/Δ*, *C1_13880CΔ/Δ*, *crz1Δ/Δ*, and *hap43Δ/Δ*), and 4 TFKOs had reduced biofilm formation only in 5% CO_2 (*leu3Δ/Δ*, *mbp1Δ/Δ*, *bas1Δ/Δ*, and *try6Δ/Δ*) (Supplementary Table S3.2 and Supplementary Figure S3.3). Intriguingly, 3 additional mutants, *zcf17Δ/Δ*, *zcf30Δ/Δ* and *mac1Δ/Δ*, displayed increased biofilm growth in 0.03% CO_2 but no significant difference in 5% CO_2.

We performed gene ontology enrichment analysis on the genes encoding the 24 transcription factors whose loss impacted upon biofilm growth to group them according to biological

processes. This revealed that 6 of these transcription factors – Brg1, Dal81, Efg1, Leu3, Rob1 and Try6 – were already known to be involved in the regulation of single-species biofilm formation within *C. albicans* (Supplementary Table S3.2). Interestingly, out of these, only the *efg1Δ/Δ* mutant exhibited attenuated biofilm growth in both 0.03% and 5% CO_2. The *brg1Δ/Δ*, *dal81Δ/Δ*, and *rob1Δ/Δ* mutants had significantly reduced biofilm growth in 0.03% CO_2 but this was rescued in the 5% CO_2 environment (Supplementary Table S3.2), possibly indicating a redundancy of these when cells are exposed to high CO_2. This important finding suggests that CO_2 elevation can bypass the requirement for some of the key transcriptional regulators of biofilm formation (Figure 3.3B). The *leu3Δ/Δ* and *try6Δ/Δ* mutants had significantly reduced biofilm growth in 5% CO_2 but no significant difference in 0.03% CO_2.

Moreover, 8 of the transcription factors – Brg1, Crz1, Efg1, Mac1, Mig1, Rob1, Zcf27, Zcf30 – are associated with the positive regulation of filamentous growth and Tup1 is involved in the negative regulation of filamentous growth. *C. albicans* biofilm formation is strongly linked with the yeast-to-hyphal switch, with mutants unable to perform this switch have previously been shown to be deficient in biofilm growth [142]. Our results are consistent with this, demonstrating that perturbation of the hyphal programme in *C. albicans* can have significant impacts on biofilm growth on silicone surfaces.

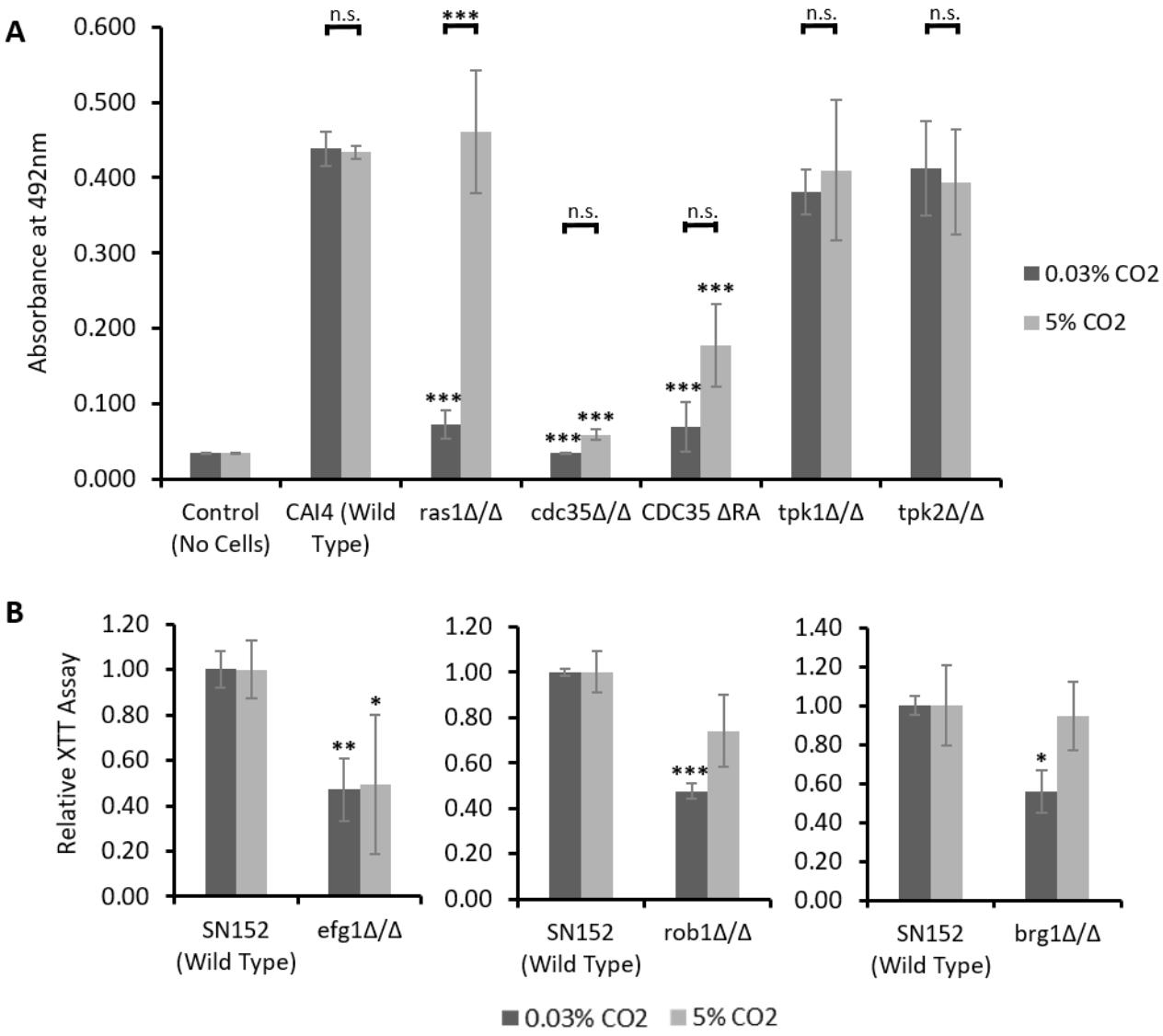
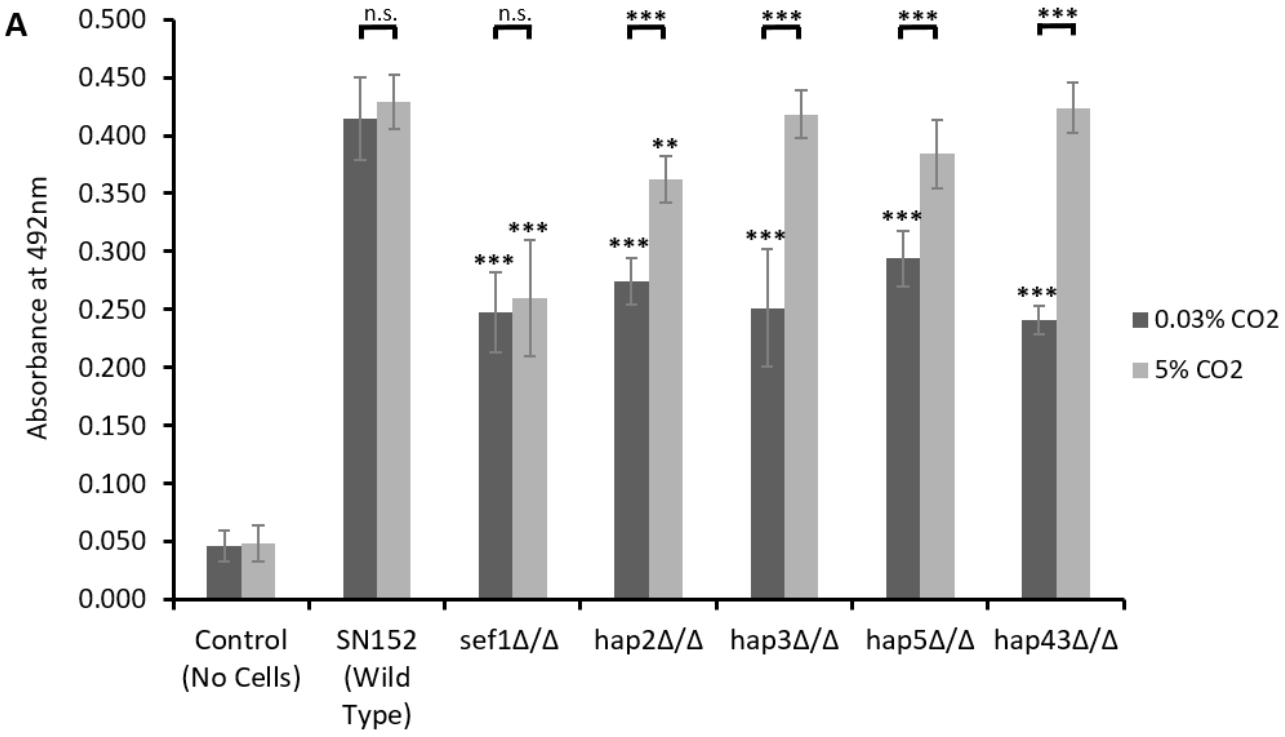


Figure 3.3: Biofilm growth assays of *C. albicans* Ras1-Cyr1-PKA pathway and central biofilm regulator null mutants. Mutants were seeded and grown as biofilms for 48h before XTT quantification. **(A)** Graph represents three biological replicates each containing technical triplicates, error bars denote Standard Deviation. Two-way ANOVAs followed by Tukey tests for multiple comparisons was carried out: *p<0.05, **p<0.01, ***p<0.001, n.s. = not significant. Stars directly above the bars indicate a significant difference to the CAI4 wild type in the same CO_2 environment. **(B)** Graphs represent biological triplicates, error bars denote Standard Deviation. XTT readouts for the TFKO mutants in 0.03% and 5% CO_2 have been normalised to the 0.03% and 5% CO_2 SN152 wild type controls respectively. One-way ANOVAs followed by Dunnett's Tests for multiple comparisons to a control were performed to compare the TFKO mutant biofilms to the SN152 wild type controls (for both 0.03% and 5% CO_2). *p<0.05, **p<0.01, ***p<0.001, n.s. = not significant.

The TFKO screen also revealed that mutants lacking transcription factors associated with metal ion homeostasis, specifically iron homeostasis, had altered biofilm-formation in 0.03% and/or 5% CO_2 (Figure 3.4A and Supplementary Table S3.2). Mutants lacking genes expressing components of the HAP complex; *hap2Δ/Δ*, *hap3Δ/Δ*, *hap5Δ/Δ*, and *hap43Δ/Δ*, exhibited significantly reduced biofilm growth after 48h compared to wild type in 0.03% CO_2. However, their biofilm growth was significantly higher in 5% CO_2, reaching wild type levels in the cases of the *hap3Δ/Δ*, *hap5Δ/Δ*, and *hap43Δ/Δ* mutants (Figure 3.4A). This is an important observation as it indicates that an increase in CO_2 concentration is sufficient to compensate for the loss of these transcription factors. The HAP complex in *C. albicans* is responsible for the regulation of iron homeostasis [57]. Sef1 acts downstream of this complex and the *sef1Δ/Δ* mutant displayed significantly reduced biofilm growth in both 0.03% and 5% CO_2 after 48h growth (Figure 3.4A). These data suggest that the elevation of CO_2 can bypass the requirement for HAP complex activity in biofilm formation in a Sef1 dependent manner.

To further determine whether elevated CO_2 enhanced *C. albicans* ability to appropriate iron from the environment biofilms were grown in the presence of the Fe^{2+} chelator 3-(2-Pyridyl)-5,6-diphenyl-1,2,4-triazine-p,p'-disulfonic acid monosodium salt hydrate (Ferrozine). Iron chelation was observed to have a marked effect on biofilm growth at and above 350µM Ferrozine (Figure 3.4B). As had been observed with TFKO strains of the HAP complex, the elevation of CO_2 counteracted the effects of iron limitation (Figure 3.4B) providing further evidence of a role for CO_2 in enhancing iron uptake or utilisation capability. This tolerance to iron sequestration of *C. albicans* biofilms grown in 5% CO_2 was also exhibited by *tpk1Δ/Δ* and *tpk2Δ/Δ* mutants (Supplementary Figure S3.4), indicating these PKA isoforms are functionally redundant with respect to iron homeostatic pathways. Clinical strains of *C. albicans* isolated

from failed voice prostheses displayed the same phenotype with biofilm formation rescued in 5% CO_2 when grown in the presence of 500µM Ferrozine (Figure 3.4C). A transcriptomic analysis comparing biofilms grown in 0.03% and 5% CO_2 (described below) revealed that several genes related to iron acquisition were upregulated in 5% CO_2 CAI-4 biofilms after 48h, possibly explaining the tolerance to iron sequestration in high CO_2 (Figure 3.4B and 3.4C). *FTR2*, which encodes the high affinity iron permease Ftr2, had increased expression (0.97 log2 fold change). In addition, *CFL4* which encodes a putative ferric reductase, is regulated by Sef1 and induced in low-iron conditions [56] was upregulated (2.29 log2 fold change) in high CO_2 biofilms after 48h. Finally, the *CSA2* and *RBT5* genes, which encode proteins involved in the acquisition of iron from haem groups, were also upregulated (2.95 and 0.95 log2 fold changes respectively). Csa2 and Rbt5 have both previously been found to be required for normal biofilm formation in RPMI-1640 media [282][283].



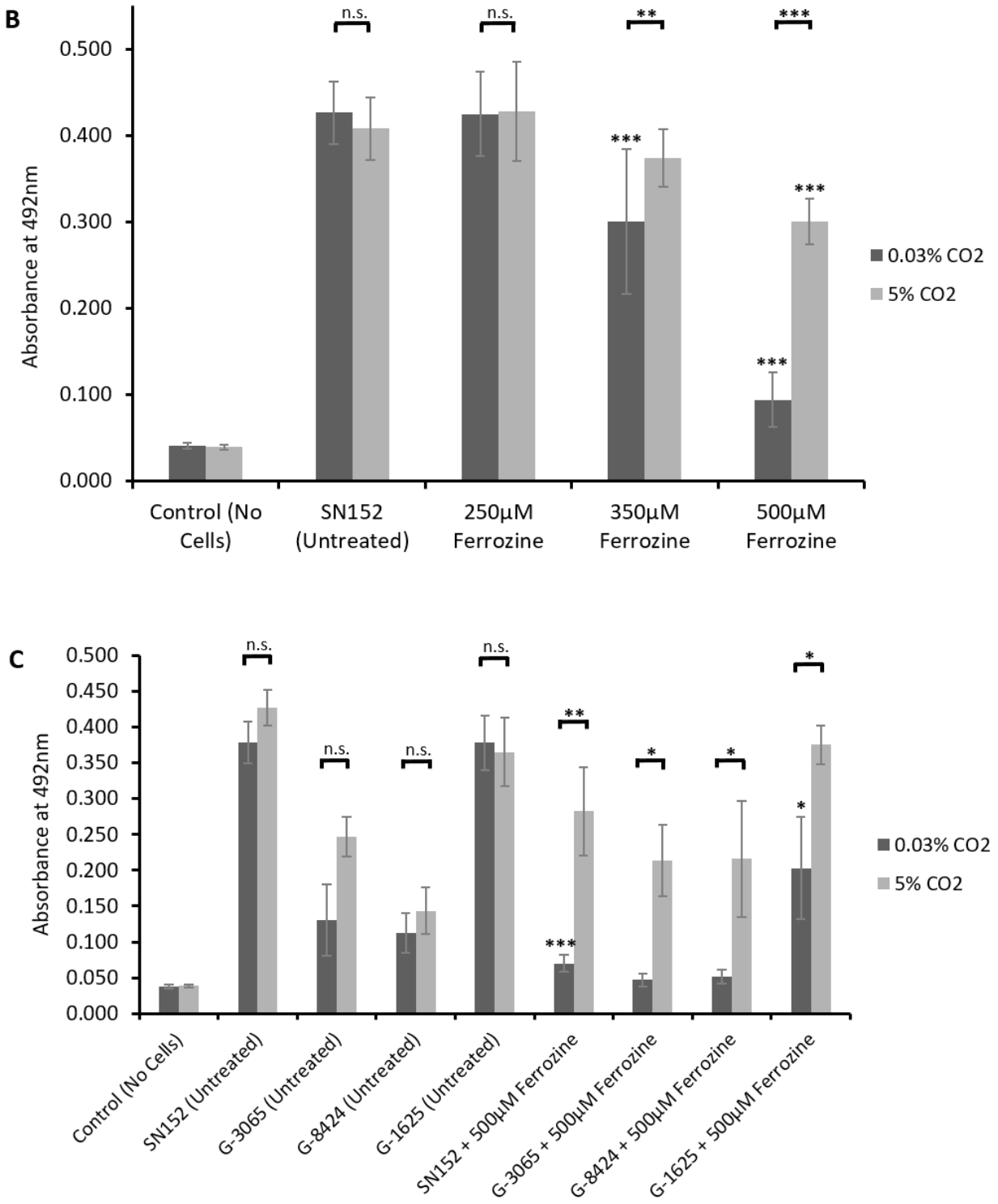


Figure 3.4: The effect of high (5%) CO_2 on iron homeostasis in *C. albicans* biofilms. Biofilms were seeded and grown for 48h before XTT quantification. Control wells with no cells were set up as media controls to monitor for contamination as well as to ensure there was no reaction of the silicone squares with the XTT reagents. **(A)** Biofilm growth assay using TFKO mutants lacking iron homeostatic transcription factors. Graph represents three biological replicates each containing technical triplicates, error bars denote Standard Deviation. **(B)** Iron starvation biofilm growth assay of SN152 in the presence of the Fe^{2+} chelator Ferrozine. Graph represents six biological replicates each containing technical triplicates, error bars denote Standard Deviation. **(C)** Iron starvation biofilm growth assay of clinical isolates in the presence of Ferrozine. Graph represents two biological replicates each containing technical triplicates, error bars denote Standard Deviation. Two-way ANOVAs followed by Tukey tests for multiple comparisons were carried out: *p<0.05, **p<0.01, ***p<0.001, n.s. = not significant. Stars directly above the bars indicate a significant difference to the SN152 wild type/untreated or untreated isolate in the same CO_2 environment.

3.5.4 Transcriptome analysis of *C. albicans* biofilms grown in high and low CO_2

To further investigate the effect of high CO_2 on *C. albicans* biofilm growth, we performed a genome-wide transcriptome analysis of *C. albicans* biofilms grown in 0.03% and 5% CO_2 to evaluate gene expression patterns in the two conditions. *C. albicans* biofilms were grown in biological triplicate in both 0.03% and 5% CO_2 for 48h. RNA was isolated and sequenced, generating an average of 58M reads per sample. Quality control analyses of the RNA-Seq reads were performed using FastQC and these can be found in Appendix 1. Using DESeq2 [276], the expression levels of each gene in the 5% CO_2 samples was compared to those in the 0.03% CO_2 samples. Growth in 5% CO_2 led to a global response resulting in the significant differential expression (false-discovery-rate adjusted p-value (q) ≤ 0.05) of 2875 genes, with roughly equal numbers of genes up- and downregulated (1441 up and 1434 down) (Figure 3.5A). 80 genes were strongly (log2 fold change >2) upregulated and 25 were strongly (log2 fold change <-2) downregulated. To investigate the cellular pathways which these differentially expressed genes are within we conducted Gene Set Enrichment Analysis (GSEA; Broad Institute) [277]. Briefly, GSEA takes a list of significantly (q ≤ 0.05) differentially expressed genes, ranked from the most upregulated to the most downregulated, and compares them to a gene set database [278] to determine whether the members of each gene set are randomly distributed throughout the ranked list or significantly overrepresented (enriched) at the top or the bottom. Gene sets with genes enriched at the top of the ranked list have a positive normalised enrichment score (NES) and gene sets with genes enriched at the bottom have a negative NES. This makes it possible to draw conclusions about biological processes/pathways which were up- or downregulated between the two conditions. Gene sets along with the position of the genes in the ranked list of significantly differentially expressed genes and the running enrichment scores can be found in Appendix 2.

GSEA revealed that biofilm formation pathways controlled by four of the nine 'core' biofilm regulator transcription factors [127][128] were upregulated in 5% CO_2 biofilms at 48h (Figure 5B). Genes downstream of Brg1, Efg1, Ndt80 and Bcr1 are enriched in the upregulated genes at the top of the ranked list of differentially expressed genes (NES = +2.79, +2.66, +2.56, and +2.60 respectively) (Figure 3.5B), indicating high CO_2 drives expression of genes previously described as important in the biofilm-forming ability of *C. albicans*.

As GSEA can show enrichment profiles exhibiting correlations with several overlapping gene sets, we visualised networks of similar gene sets using the Cytoscape 3.7.1 EnrichmentMap plug-in [281]. Upregulated gene sets included those encoding membrane transporters, ribosome biogenesis, peroxisomal β-oxidation and white-opaque switching (Figure 3.5C). Pathways involved in cytoskeleton organisation, cell-cycle progression and membrane biosynthesis were downregulated in high CO_2 conditions (Figure 3.5C), indicating cells within biofilms in high CO_2 may have stopped dividing, consistent with such biofilms having moved more rapidly through the maturation process.

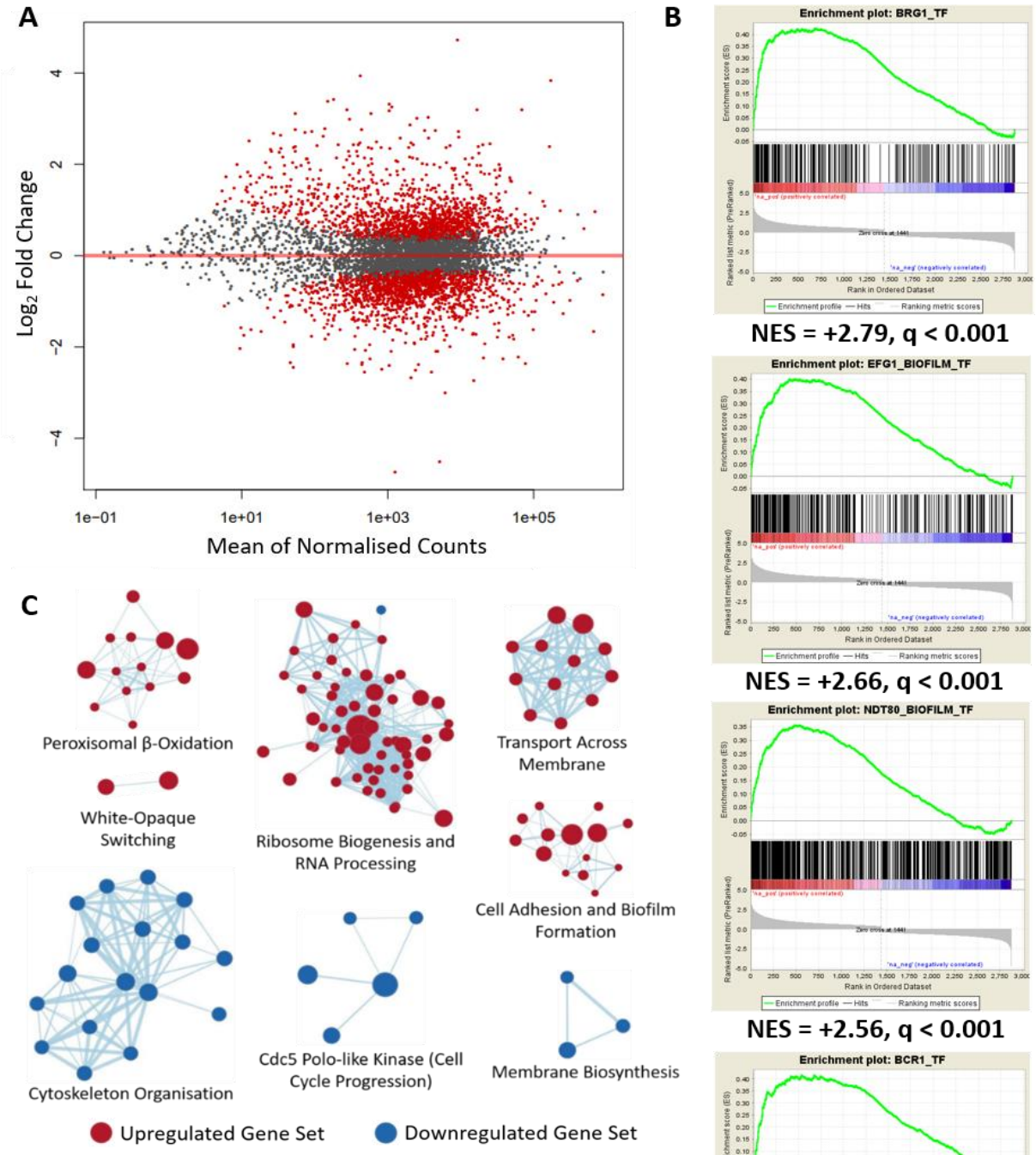


Figure 3.5: Global gene expression changes in 5% CO_2 vs. 0.03% CO_2 *C. albicans* biofilms. (A) Volcano plot of log_2 fold changes (5% CO_2 vs. 0.03% CO_2 biofilms) against mean of normalised counts for each gene; red dots = significantly differentially expressed (q≤0.05) genes, grey dots = not significant. 2875 genes showed significant differential expression. Normalised counts are the number of reads a particular gene has, thus the higher the mean of normalised count, the higher the expression of that gene. **(B)** GSEA enrichment plots of central biofilm regulator gene sets containing genes whose promoters have been shown by ChIP-chip experiments to be bound during biofilm formation by one or more of four (Brg1, Efg1, Ndt80, and Bcr1) of the nine 'core' biofilm regulators [27]. Vertical black lines represent individual genes in the significantly differentially expressed ranked gene list from upregulated (left) to downregulated (right). The enrichment score increases if there are lots of genes towards the beginning of the ranked list (upregulated). NES = normalised enrichment score, positive NES indicates enrichment in the upregulated group of genes. **(C)** Gene set cluster map showing the most upregulated and downregulated gene sets as determined by GSEA along with their cellular functions. Each circle is a gene set and the lines between them depict how much they overlap, thicker line = more genes in common.

GSEA suggested that cell adhesion processes were upregulated in high CO_2 biofilms (NES = +2.13) (Figures 3.6Ai). GO Slim process analysis also highlighted many genes associated with cell adhesion were upregulated in *C. albicans* biofilms grown in 5% CO_2 after 48h (Figure 3.6Bi). The second highest upregulated gene in 5% CO_2 biofilms compared to 0.03% CO_2 biofilms was *ALS1* with a 3.77 log2 fold change (Figure 3.6Bi). The Als1 cell surface adhesin has previously been shown to have important roles in biofilm formation [284], and its expression is controlled by the biofilm transcription regulation network composed of Brg1, Rob1, Tec1, Ndt80, Bcr1 and Efg1 [127]. Other genes encoding cell surface adhesins such as *ALS4* and *ALS2* had log2 fold increases in expression of 1.87 and 1.46 respectively in 5% CO_2 biofilms after 48h (Figure 3.6Bi).

GSEA has also identified genes involved in membrane transporter activity are enriched in the upregulated genes at the top of the ranked list of differentially expressed genes (NES = +2.22) (Figure 3.6Ai). Specifically, genes encoding amino acid transporters were enriched in the significantly upregulated genes of 5% CO_2 biofilms (NES = +2.62) (Figure 3.6Aii). Likewise, significantly differentially expressed genes possessing the GO term 'amino acid transport' were primarily upregulated (Figure 3.6Bii). The most highly upregulated of these was *GAP2* which encodes a general amino acid permease [285]. *GAP2* was in fact the highest upregulated gene of the entire RNA-Seq data set with a 4.60 log2 fold change. The basic amino acid permease genes *CAN1*, *CAN2*, and *CAN3* were also upregulated (Figure 3.6Bii).

Genes associated with carbohydrate transmembrane transport were also enriched in the significantly upregulated genes of 5% CO_2 biofilms as revealed by GSEA (NES = +1.88) (Figure 3.6Aii). Amongst these were 12 genes encoding putative major facilitator superfamily (MFS)

glucose transmembrane transporters present in the significantly differentially expressed gene list and these are almost all upregulated. The only exceptions are *HGT9* and *HGT18* with log2 fold changes of -1.24 and -1.70 respectively (Figure 3.6Bii).

Intriguingly, the *TPK1* gene, which encodes the PKA catalytic subunit isoform Tpk1, was upregulated in 5% CO_2 biofilms (1.04 log2 fold change) (Supplementary Figure S3.5B), whereas the other isoform encoding gene *TPK2* was downregulated (-0.80 log2 fold change) (Figure 3.6Bi and Supplementary Figure S3.4B). This could suggest a preference for Tpk1 instead of Tpk2 under high CO_2 conditions, although there was not a significant biofilm growth defect of a *TPK1* null mutant in any CO_2 environment (Figure 3.3A).

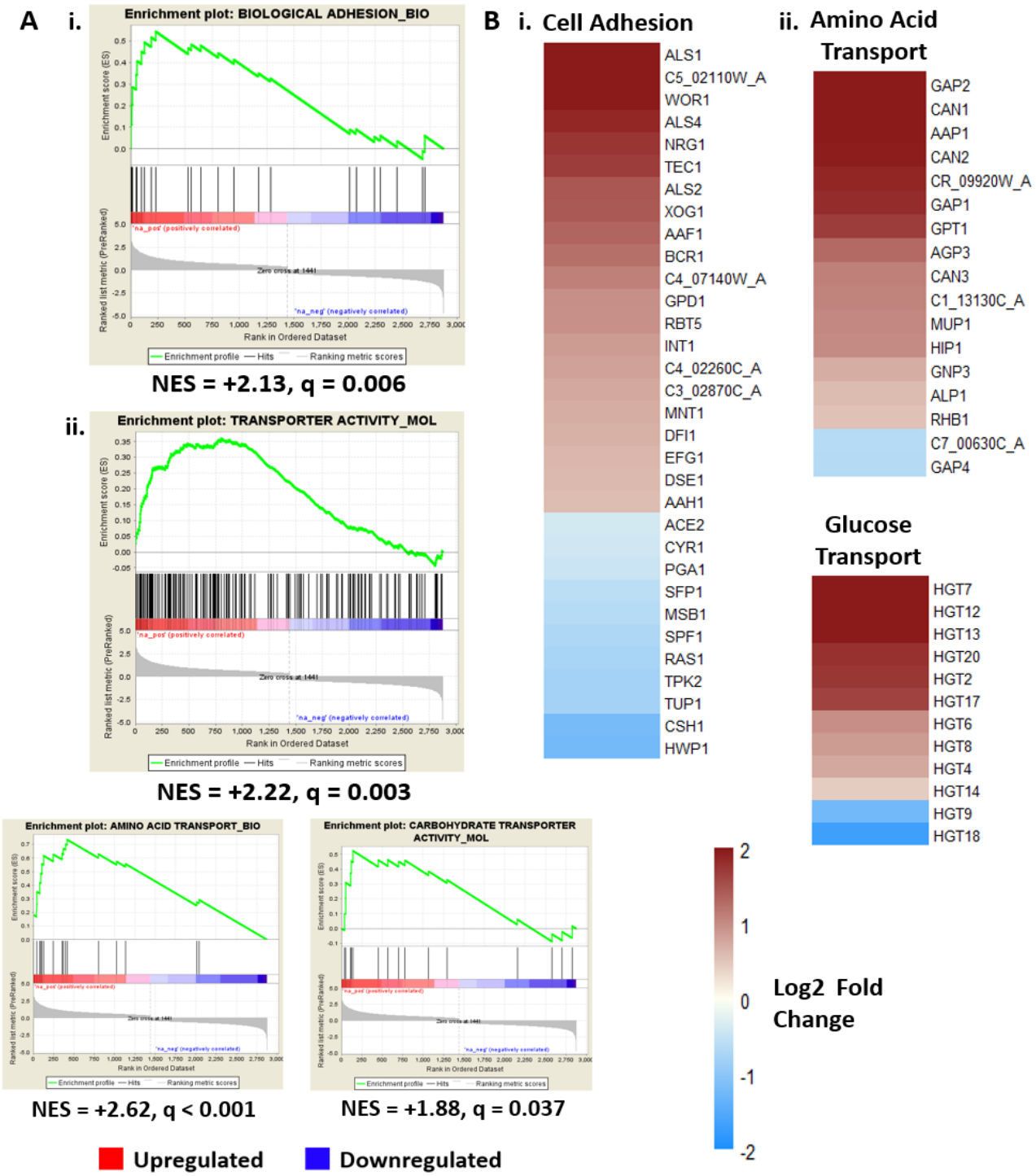


Figure 3.6: Adhesion and transport processes are predicted to be upregulated in 5% CO_2 vs. 0.03% CO_2 *C. albicans* biofilms. (Ai) GSEA enrichment plot of the BIOLOGICAL ADHESION_BIO gene set containing genes under the GO term 'biological adhesion'. **(Aii)** Enrichment plots of the TRANSPORTER ACTIVITY_MOL, AMINO ACID TRANSPORT_BIO and CARBOHYDRATE TRANSPORTER ACTIVITY_MOL gene sets containing genes under the GO terms 'transporter activity', 'amino acid transport' and 'carbohydrate transmembrane transporter activity' respectively. NES = normalised enrichment score, positive NES indicates enrichment in the upregulated group of genes. **(Bi)** Heat map of significantly differentially expressed genes associated with cell adhesion as identified by GO Slim process analysis. The colours saturate at log2 fold change of 2 and -2; *ALS1*, C5_02110W, and *WOR1* have log2 fold changes of 3.77, 3.02 and 2.15 respectively. **(Bii)** Heat maps of significantly differentially expressed genes associated with amino acid and glucose transport as identified by GO Slim process analysis. The colours saturate at log2 fold change of 2 and -2; *GAP2*, *CAN1*, and *AAP1* have log2 fold changes of 4.60, 2.34 and 2.32 respectively. *HGT7*, *HGT12*, and *HGT13* actually have log2 fold changes of 2.39, 2.26 and 2.24.

The majority of gene sets predicted to be downregulated in 5% CO_2 biofilms after 48h growth were associated with cytoskeletal organisation, hyphal growth and cell division (Supplementary Figure S3.5A). Genes previously identified to be involved in hyphal formation in response to foetal bovine serum (FBS) exposure or 37^oC were enriched in the downregulated genes (NES = -3.41). Likewise, the majority of genes under the GO term 'hyphal growth' in the significantly differentially expressed gene list were downregulated in 5% CO_2 biofilms at 48h growth (Supplementary Figure S3.5B). Significantly differentially expressed genes associated with the cytoskeleton, as identified by GO term analysis, were enriched in the downregulated genes (NES = -2.69) (Supplementary Figure S3.5A). Cytoskeleton reorganisation is important for the growth of *C. albicans* hyphal cells [286] as well as cell division [287][288], indicating cell growth is lower in 48h old *C. albicans* biofilms grown in 5% CO_2 than in those grown in 0.03% CO_2. Consistent with this, genes involved in the transition through the G1/S checkpoint were also enriched in the significantly downregulated genes (NES = -2.83) (Supplementary Figure S3.5A). Together, these data suggest *C. albicans* biofilm cells exhibit greater growth and division at 48h in 0.03% CO_2 than in 5% CO_2. Initially, this appears to be contradictory to the previous data highlighting the increased biofilm formation of *C. albicans* under high CO_2 conditions. However, due to the increased biofilm formation in a 5% CO_2 environment, *C. albicans* biofilms reach full maturity much quicker in high CO_2, as observed via confocal microscopy (Figure 3.2B). Thus by 48h *C. albicans* biofilms grown in high CO_2 have been fully mature for several hours, and hence would contain fewer dividing cells or cells extending hyphae in comparison to low CO_2 biofilms.

3.5.5 CO_2 elevation enhances azole tolerance in *C. albicans* biofilms

In addition to the observed increase in expression of genes that drive biofilm formation and we observed an elevation in certain stress response pathways in *C. albicans* biofilms grown in 5% CO_2. Gene sets involved in the response of *C. albicans* to antifungals such as Ketoconazole [289] (Figure 3.7A) were upregulated as well as several drug transporters (Figure 3.7B), indicating that CO_2 elevation may lead to increased drug tolerance. Upregulated genes included the *MDR1* gene (2.56 log2 fold change) which encodes the multidrug resistance pump Mdr1 and is associated with tolerance to several antifungals such as azoles [161]. To test this, *C. albicans* biofilms were seeded and grown for 24h in 0.03% and 5% CO_2 before the addition of antifungals, after which they were grown for an additional 24h in both conditions to observe the effect of drug application. Antifungal concentrations were selected based upon previously reported MIC values for these antifungals against *C. albicans* biofilms [115]. Overall, Fluconazole and Miconazole treatment led to a significant reduction in biofilm growth in 0.03% CO_2 (Figures 7C and Supplementary Figure S3.6). Treatment with Fluconazole and Miconazole also significantly reduced biofilm formation in 5% CO_2, however, their effectiveness was markedly reduced (Figures 7C and Supplementary Figure S3.6). This suggests an increased tolerance of biofilms grown in 5% CO_2 to azole treatment. Interestingly, Nystatin was equally as effective against biofilms in either CO_2 environment (Figure 3.7D).

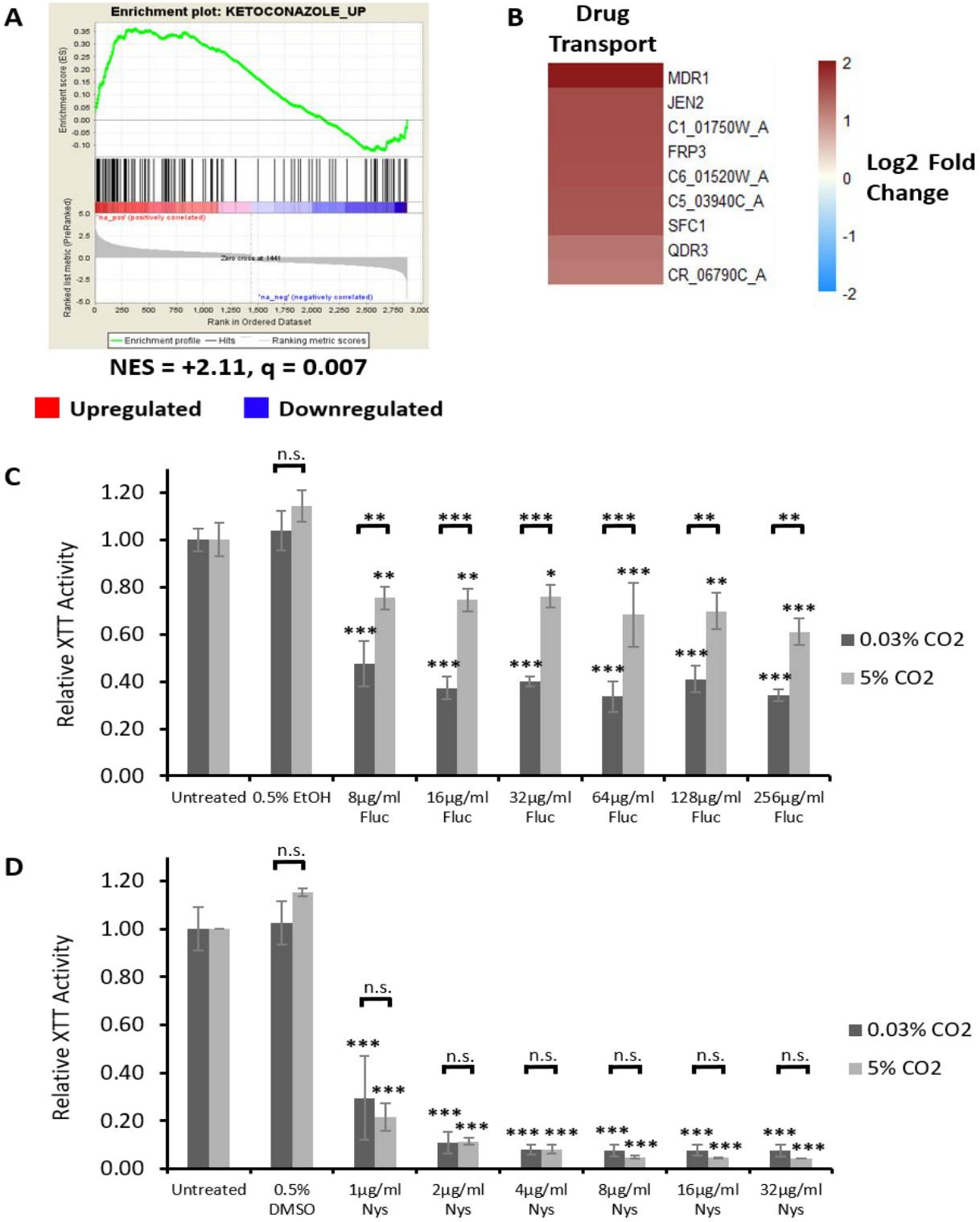


Figure 3.7: Antifungal sensitivity of *C. albicans* biofilms grown in high (5%) CO_2. (A) GSEA enrichment plot of the KETOCONAZOLE_UP gene set containing genes upregulated in *C. albicans* cells grown in the presence of Ketoconazole [62]. NES = normalised enrichment score, positive NES indicates enrichment in the upregulated group of genes. **(B)** Heat map of genes associated with drug transport, including the multidrug efflux pump gene *MDR1*. **(C)** Biofilm growth assay of CAI4pSM2 in the presence of Fluconazole. **(D)** Biofilm growth assay of CAI4pSM2 in the presence of Nystatin. Biofilms were seeded and grown for 24 hours before antifungal addition, they were then grown for a further 24 hours before quantification using the XTT assay. The relative XTT activity is presented with the 0.03% CO_2 biofilms being normalised to the 0.03% CO_2 untreated control and the 5% CO_2 biofilms being normalised to the 5% CO_2 untreated control. This prevents the general higher growth of 5% CO_2 biofilms impacting the analysis. Two-way ANOVAs followed by Tukey tests for multiple comparisons were carried out: *p<0.05, **p<0.01, ***p<0.001, n.s. = not significant. Stars directly above the bars indicate a significant difference to untreated in the same CO_2 environment.

3.5.6 Precision approaches to overcome CO_2 acceleration of *C. albicans* biofilm formation

Our data indicate that elevation of CO_2 leads to an increase in the ability to scavenge for iron and glucose, both essential for biofilm formation and growth. We therefore wished to test whether these represented potential targets to combat *C. albicans* growth in high CO_2 environments such as the airway. An Fe^{3+} chelator called Deferasirox, which is approved for treating patients with iron overload, has recently been shown to reduce infection levels in a murine oropharyngeal candidiasis model [290]. With this in mind, we repeated our previous iron starvation biofilm growth assay (Figure 3.4B) using Deferasirox in place of Ferrozine. We observed that Deferasirox treatment completely eradicates *C. albicans* biofilm growth in 0.03% CO_2 but has little effect on biofilm growth in 5% CO_2 (Figure 3.8A). Thus adding further evidence that exposure to high levels of CO_2 can enable *C. albicans* biofilms to overcome the effects of iron starvation. Deferasirox does not therefore appear to be an effective treatment against *C. albicans* biofilms in high CO_2 such as in the context of voice prostheses colonisation.

C. albicans biofilms grown in 5% CO_2 exhibited the upregulation of genes encoding glucose transporters. Accordingly, we contemplated whether treatment of *C. albicans* biofilms with the glucose analogue 2-deoxyglucose (a glycolytic inhibitor) may decrease biofilm growth in high CO_2 environments. 2-deoxyglucose (2-DG) has previously made it to Stage II clinical trials as an anti-prostate cancer treatment and is considered safe for use in humans [291]. Thus, it could be a potential therapeutic option to combat *C. albicans* biofilm formation on medical devices, specifically on voice prostheses. *C. albicans* biofilm formation was significantly reduced in the presence of 2-DG regardless of CO_2 environment (Figure 3.8B and Supplementary Figure S3.7). Interestingly, the biofilm reductions in all 2-DG concentrations were similar for biofilms in both low and high CO_2, despite the fact several glucose

transporters were upregulated in 5% CO_2 biofilms (Figure 3.6Bii). Treatment with 1% 2-DG reduced *C. albicans* SN152 biofilm formation by an average of 46% and 38% in 0.03% and 5% CO_2 respectively (Figure 3.8B). Likewise, 1% 2-DG reduced *C. albicans* CAI4pSM2 biofilm formation by an average of 33% and 30% in 0.03% and 5% CO_2 respectively (Supplementary Figure S3.7). This reduction was quite apparent and could be visually observed directly on the silicone surfaces (Figure 3.8C).

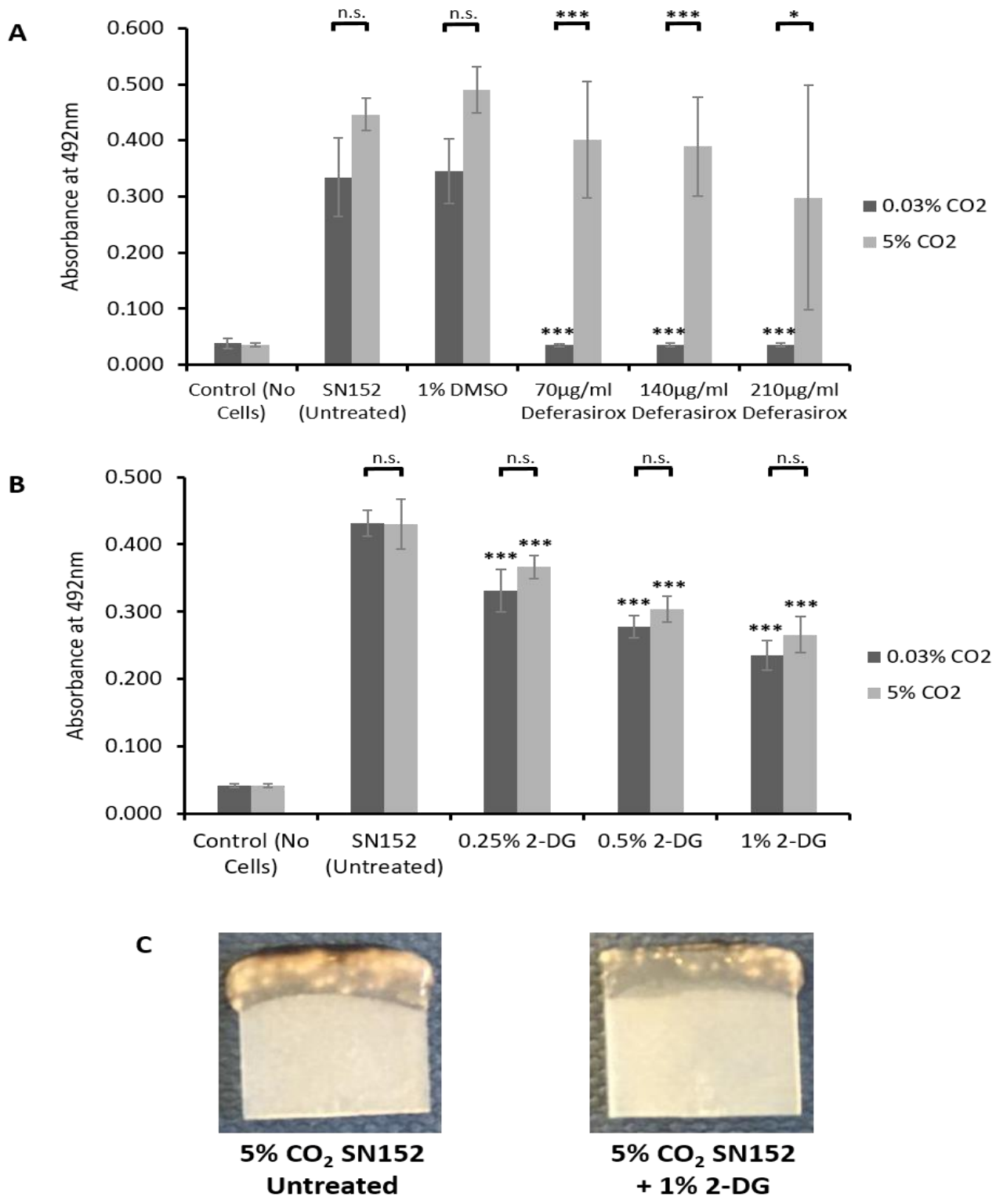


Figure 3.8: Efficacy of potential treatments to combat *C. albicans* biofilms grown in high (5%) CO_2. Biofilms were seeded and grown for 48h before XTT quantification. Control wells with no cells were set up as media controls to monitor for contamination as well as to ensure there was no reaction of the silicone squares with the XTT reagents. **(A)** Biofilm growth assay of SN152 in the presence of the Fe^{3+} chelator Deferasirox. Graph represents two biological replicates each containing technical triplicates, error bars denote Standard Deviation. **(B)** Biofilm growth assay of SN152 in the presence of the glycolytic inhibitor 2-DG. Graph represents three biological replicates each containing technical triplicates, error bars denote Standard Deviation. Two-way ANOVAs followed by Tukey tests for multiple comparisons were carried out: *p<0.05, **p<0.01, ***p<0.001, n.s. = not significant. Stars directly above the bars indicate a significant difference to the SN152 untreated in the same CO_2 environment. **(C)** Representative images of SN152 biofilms grown in 5% CO_2 ±2-DG for 48h (red coloration due to XTT assay).

3.6 Discussion

3.6.1 Physiological CO_2 levels increase *C. albicans* biofilm formation

Viewed together, the data presented here demonstrates for the first time that a physiologically relevant (5%) CO_2 environment acts as a trigger to increase the biofilm-forming ability of *C. albicans*. CO_2 is well established as a driver of the yeast-to-hyphal morphogenic switch in *C. albicans* [69][77][292], however, the effects of high CO_2 levels on biofilm formation were hitherto unknown. CO_2, in the form of bicarbonate ions (HCO_3^-), interacts with a lysine residue at position 1373 in the adenylate cyclase Cyr1 of the Ras1-Cyr1-PKA pathway, thereby activating it [77]. This Cyr1 activation is responsible for the CO_2-driven yeast-to-hyphal switch [69], and this morphogenesis is critical for biofilm formation [142]. A *cdc35Δ/Δ* null mutant is defective in hyphal formation [69], consistently our data demonstrates that this mutant was unable to make biofilms in either 0.03% or 5% CO_2. The lack of CO_2 response suggests Cyr1 is essential for the effect of CO_2 on *C. albicans* biofilms that we have characterised in this study. Further evidence for this argument comes from the *ras1Δ/Δ* null mutant which is hyphal deficient [66] and was unable to form biofilms in 0.03% CO_2 but formed equivalent biofilms to the wild type in 5% CO_2. This suggests a redundancy of Ras1 in this scenario as the HCO_3^- ions are able to bypass Ras1 and activate Cyr1 directly [77], restoring the ability to form hyphae [69] and hence biofilms.

Interestingly, from our data it appears that the ability of Cyr1 to respond to high CO_2 levels is reliant on the presence of its Ras-interacting RA domain since a *CDC35*$^{\Delta RA}$ mutant continued to have attenuated biofilm growth in 5% CO_2. This is not due to a hyphal defect as the *CDC35*$^{\Delta RA}$ strain displays normal hyphal growth in 5% CO_2 [293]. Furthermore, as Ras1 is not required for hyphal formation [69] or biofilm formation in high CO_2 (this study), the biofilm

deficiency of the *CDC35*$^{\Delta RA}$ strain cannot be explained by a requirement for the RA domain to mediate an interaction with Ras1. The role of the RA domain in biofilm growth remains elusive. Overall, these data suggest the response of *C. albicans* biofilms to physiological (5%) levels of CO_2 is dependent on Cyr1 but can bypass a requirement for Ras1.

Phenotypic analyses identified that the elevation of CO_2 enhances each stage of the *C. albicans* biofilm forming process, from attachment through maturation to dispersion. The observed increase in cell attachment is consistent with our transcriptome analysis as we observed an increase in the abundance of mRNA transcripts for *ALS1, ALS2* and *ALS4* which encode adhesins of the agglutinin-like sequence family that function in the cell-surface and cell-cell attachment of *C. albicans* [134]. Likewise, the increased dispersion also correlates with our transcriptome analysis since *NRG1* was upregulated (1.76 log2 fold change) in 5% CO2 biofilms after 48h. Overexpression of *NRG1* has previously been demonstrated to increase the dispersion of yeast cells from *C. albicans* biofilms [144], and so this possibly provides a mechanism to explain the increased dispersion from biofilms grown in high CO_2. This amplified dispersion could have important clinical implications since it suggests biofilms may not only form more rapidly on medical devices (e.g. voice prostheses) in high CO_2, but they may also have an increased propensity to disseminate and cause infection. Cells dispersing from mature biofilms have distinct characteristics compared to typical planktonic yeast cells; with enhanced adherence, an increased tendency to filament, and increased biofilm forming capability [126].

Overall, our transcriptome analysis identified that a number of hallmarks of the biofilm mode of growth – including increased cell adhesion, increased transport activity, and increased drug

tolerance – were upregulated in biofilms grown in high CO_2 conditions. Pathways governed by central regulators of biofilm formation – Efg1, Bcr1, Brg1, and Ndt80 [127] – were predicted by GSEA to be upregulated in *C. albicans* biofilms grown in 5% CO_2, possibly explaining the increased expression of genes related to hallmarks of biofilm growth.

Of the original 6 'core' biofilm regulators (Efg1, Bcr1, Brg1, Rob1, Ndt80 and Tec1) only 3 (Efg1, Brg1 and Rob1) were identified as required for normal biofilm growth in our TFKO screen. The original 6 were identified in a similar screen to ours and used the same TFKO library, however, their study was carried out using polystyrene surfaces [127] whereas we used silicone. This may suggest that attachment to silicone requires a more limited set of core transcription factors reflecting the importance of surface upon biofilm formation as has been observed previously [128]. CO_2 elevation appears to be able to compensate for the loss of some key regulators, as we observed its increase could bypass a requirement for Brg1 and Rob1. Intriguingly, of the four biofilm regulators whose gene sets were predicted to be upregulated in 5% CO_2 biofilms, only Efg1 and Brg1 were identified in our TFKO screen, and only *efg1Δ/Δ* had reduced biofilm growth in both 0.03% and 5% CO_2. This disparity may be explained by the degree of overlap in downstream target genes between the core regulators of biofilm formation [127] which implies significant potential for functional redundancy.

Many of the genes significantly upregulated in biofilms grown in high CO_2 after 48h were also found to be upregulated in other biofilm gene expression studies [130][294]. For instance, Nett, J. *et al.* observed an increase in the expression of adherence genes in an *in vivo* venous catheter biofilm model. Like us, this venous catheter biofilm study saw an increase in the transcript abundance of *ALS1* and *ALS2* however, this was only seen at earlier time point

biofilms [130]. This was also the case in a temporal gene expression analysis using *in vitro* denture and catheter models [294]. Interestingly, some pathways such as hexose transport, amino acid uptake, and stress responses that our differential gene expression analysis predicted to be upregulated in mature biofilms grown in high CO_2 were concluded to be upregulated only in early phase biofilms (12h) in this denture and catheter study [294]. The authors concluded the result of the induction of these pathways is the increase of intracellular pools of pyruvate, pentoses and amino acids, preparing for the large increase in biomass that occurs later in biofilm development [294]. We hypothesise that high CO_2 is stimulating these pathways and maintaining their activity even in mature biofilms, thus supporting the increased biomass and maturation rate of biofilms observed when grown in high CO_2.

Nearly all device-associated infections involve potential pathogens growing within a biofilm [4]. Previously, us and other laboratories have demonstrated *C. albicans* is the most prevalent fungal coloniser, in polymicrobial biofilms, of failed voice prostheses [195][204]. Due to the high CO_2 content of exhaled air and the fact voice prostheses are situated in the throat, the responses of *C. albicans* to CO_2 detailed here could provide an explanation for its competitive fitness in this scenario. More widely, this work could also be of importance to several *C. albicans* infections, for instance candidaemia, since CO_2 levels within mammalian hosts are up to 150x higher (~5% vs. 0.03%) than in atmospheric air [222][268].

3.6.2 *C. albicans* biofilms grown in 5% CO_2 exhibit increased drug tolerance

We observed an increase in azole antifungal tolerance within *C. albicans* biofilms grown in 5% CO_2. This, at least partly, could be explained by the increase in expression of drug transporter genes such as *MDR1* in 5% CO_2 biofilms which have previously been implicated in azole

tolerance [159][161]. However, *mdr1Δ/Δ*, as well as *cdr1Δ/Δ* and *cdr2Δ/Δ*, mutants only exhibit reduced azole tolerance in planktonic culture and early stage (6h) biofilms, while levels of tolerance are maintained in mature biofilms [161]. Therefore, we propose that it is more likely the increased azole tolerance phenotype of 5% CO_2 biofilms displayed is contributed to via another mechanism, possibly increased ECM deposition. β-1,3-glucan, a major component of biofilm ECM, can bind to azole antifungals and sequester them to prevent passage to the cells [157]. We have observed that after 48h, 5% CO_2 biofilms, while containing similar cell numbers to 0.03% CO_2 biofilms, often appear larger to the eye with a more bulbous appearance. This could suggest more ECM material being produced in high CO_2 environments, contributing to the increased azole tolerance. Furthermore, Miconazole treatment has been shown to generate superoxide radicals within *C. albicans* biofilms and leads to the increased expression of *SOD5* and *SOD6* (encode superoxide dismutase enzymes) in an attempt to protect against the toxic superoxides. A *sod4Δ/Δsod5Δ/Δsod6Δ/Δ* triple mutant is hypersensitive to Miconazole treatment when growing as a biofilm [183]. Our transcriptome analysis revealed *SOD6* is upregulated with a 1.52 log2 fold change (also *SOD4*; 1.02 log2 fold change) in 5% CO_2 biofilms, providing a potential further mechanism of the increased Miconazole tolerance.

3.6.3 CO_2 and iron homeostasis in *C. albicans* biofilms

Our TFKO library biofilm formation screen identified transcription factors involved in iron homeostasis as important for *C. albicans* biofilm growth. Principal among these were the Hap transcription factors which come together to form the HAP complex, a CCAAT box-binding transcriptional regulator, under iron-limiting conditions. Genetic studies have revealed a requirement of *HAP2, HAP3, HAP5* and *HAP43* for growth in low-iron media [269][295]. Thus,

the biofilm formation defect exhibited by the *hap2Δ/Δ*, *hap3Δ/Δ*, *hap5Δ/Δ*, and *hap43Δ/Δ* mutants in 0.03% CO_2 could be explained by this growth deficiency since RPMI-1640 media has a low iron content. Nevertheless, this makes it even more intriguing that simply an increase in ambient CO_2 levels was able to significantly increase the biofilm growth of these mutants.

The HAP complex represses a GATA-type transcription factor called Sfu1, Sfu1 is responsible for repressing iron-uptake genes along with *SEF1* under iron-replete conditions. Sef1 activates iron-uptake genes as well as *HAP43, HAP2* and *HAP3* [56], in this way the HAP complex is able to induce iron-uptake pathways while repressing iron-utilisation genes [56][57]. Deletion of Sef1 results in the aberrant downregulation of all the major iron-uptake pathways of *C. albicans* in low iron conditions [56]. Due to the fact the *sef1Δ/Δ* mutant had defective biofilm growth in both CO_2 conditions, we hypothesise that a high CO_2 environment may influence Sef1 directly, causing the HAP complex to become at least partially redundant under these conditions. It should be noted that we did not observe a significant effect on *SEF1* mRNA levels within 5% CO_2 biofilms after 48h. Thus, if it is influencing Sef1 activity, CO_2 must be acting at either the protein level or post-translational level as Sef1 is subject to a post-translational control loop consisting of Sfu1 and the cyclin-dependent kinase Ssn3 [58]. We do not believe the CO_2 effect on iron homeostasis is mediated through Ssn3 as this protein has recently been found to be dephosphorylated and thus inactive in 5% CO_2 [292]. Therefore, our current hypothesised model suggests that PKA can phosphorylate Sef1 and possibly also inhibit Sfu1 (Figure 3.9). This is currently under investigation and may possibly explain the tolerance to iron sequestration exhibited by *C. albicans* biofilms grown in high CO_2. We believe any potential phosphorylation of Sef1 by PKA to be Tpk1/Tpk2 redundant since the *tpk1Δ/Δ* and

the *tpk2Δ/Δ* mutants both exhibited a significant increase in biofilm growth in 5% CO_2 when in the presence of 500µM Ferrozine compared to 0.03% CO_2. This is supported by a Tpk1/Tpk2 phosphoproteomic study which predicted Sef1 to be a potential PKA target that can be phosphorylated by both Tpk1 and Tpk2 [75].

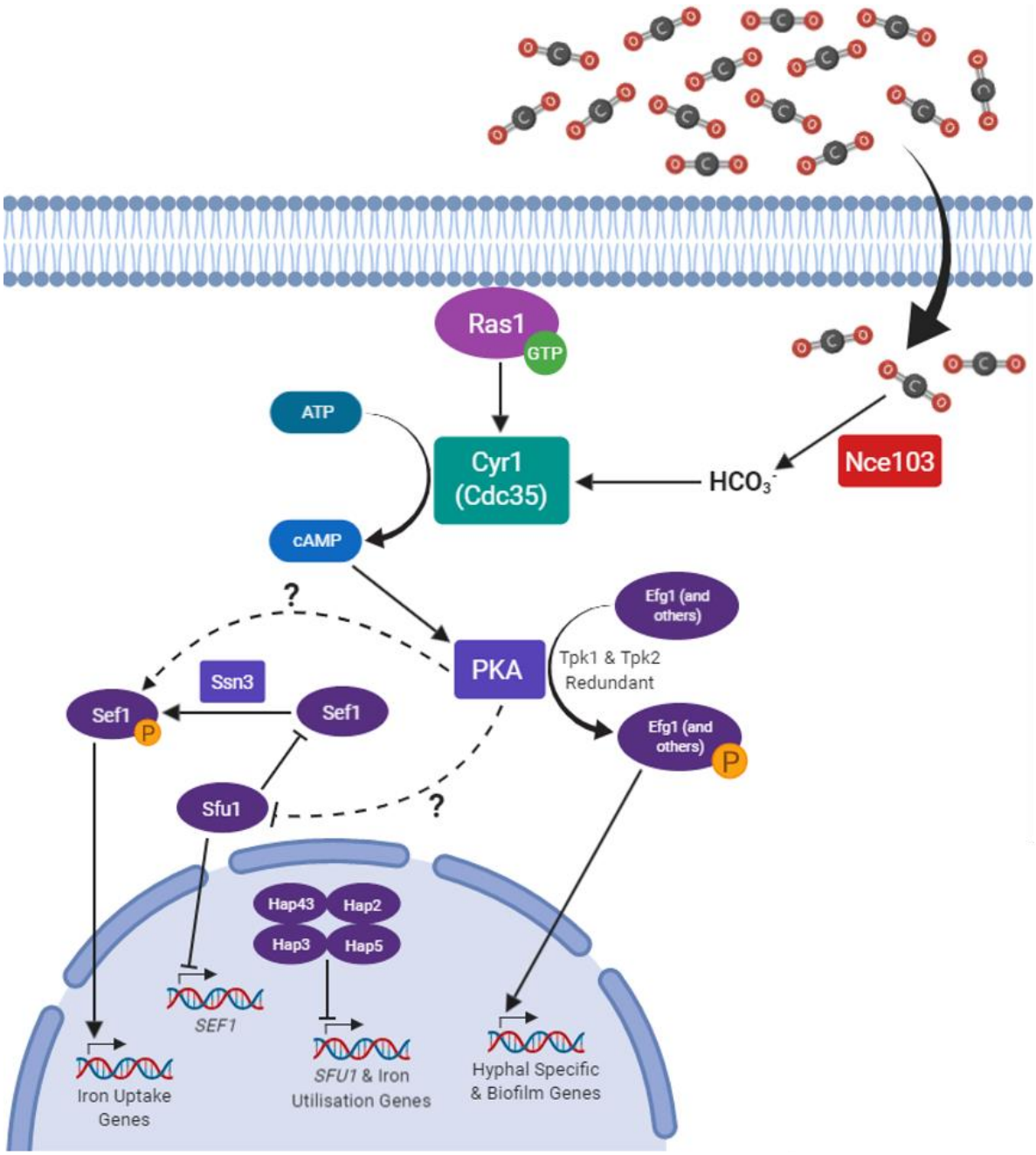


Figure 3.9: Predicted model of the interplay between CO_2 signalling and iron homeostasis in *C. albicans* biofilms on silicone surfaces. We hypothesise that the CO_2-mediated activation of PKA via Cyr1 will result in increased activity of Sef1 (via its phosphorylation and possibly the inhibition of Sfu1), thus increasing the expression of iron-uptake genes.

The increased azole tolerance of *C. albicans* biofilms in 5% CO_2 along with the observed iron starvation tolerance when treated with the Fe^{3+} chelator Deferasirox has important implications for the development of potential treatment strategies. This is especially true for those assessed *in vitro*, as it demonstrates that *C. albicans* can exhibit very different phenotypes in response to environmental changes, in our case CO_2 concentration. At a clinical level, this also indicates the location of a *C. albicans* biofilm within the body should be taken into consideration when deciding upon the most effective treatment. Encouragingly, 2-deoxyglucose (2-DG) was able to attenuate *C. albicans* biofilm growth in both 5% and atmospheric (0.03%) CO_2 environments. 2-DG has exhibited antimicrobial effects against fungal moulds [296] and bacterial biofilms [297]. This, together with its action against *C. albicans* biofilms presented here, highlights the potential for 2-DG to be used an anti-biofilm therapeutic. It may be particularly useful for medical devices such as voice prostheses which are situated in CO_2-rich environments in the body and are often colonised by a mixture of bacterial and fungal species [195][201][204]. It is important to note however that 2-DG was unable to eradicate *C. albicans* biofilm growth completely. It may be that 2-DG treatment is beneficial in combination with other compounds, such as iron chelators or traditional antifungals; this possibility is yet to be explored.

In conclusion, our data and others' indicate physiological (5%) levels of CO_2 can act as an important pathogenic signal for *C. albicans*. CO_2 drives many virulence factors such as yeast-to-hyphal morphogenesis [69], biofilm growth (this study), and iron acquisition (this study). These CO_2-mediated effects are likely to have important medical ramifications, primarily in the context of prosthetics as demonstrated with voice prosthetics, but also for host infections in CO_2-rich environments in the body.

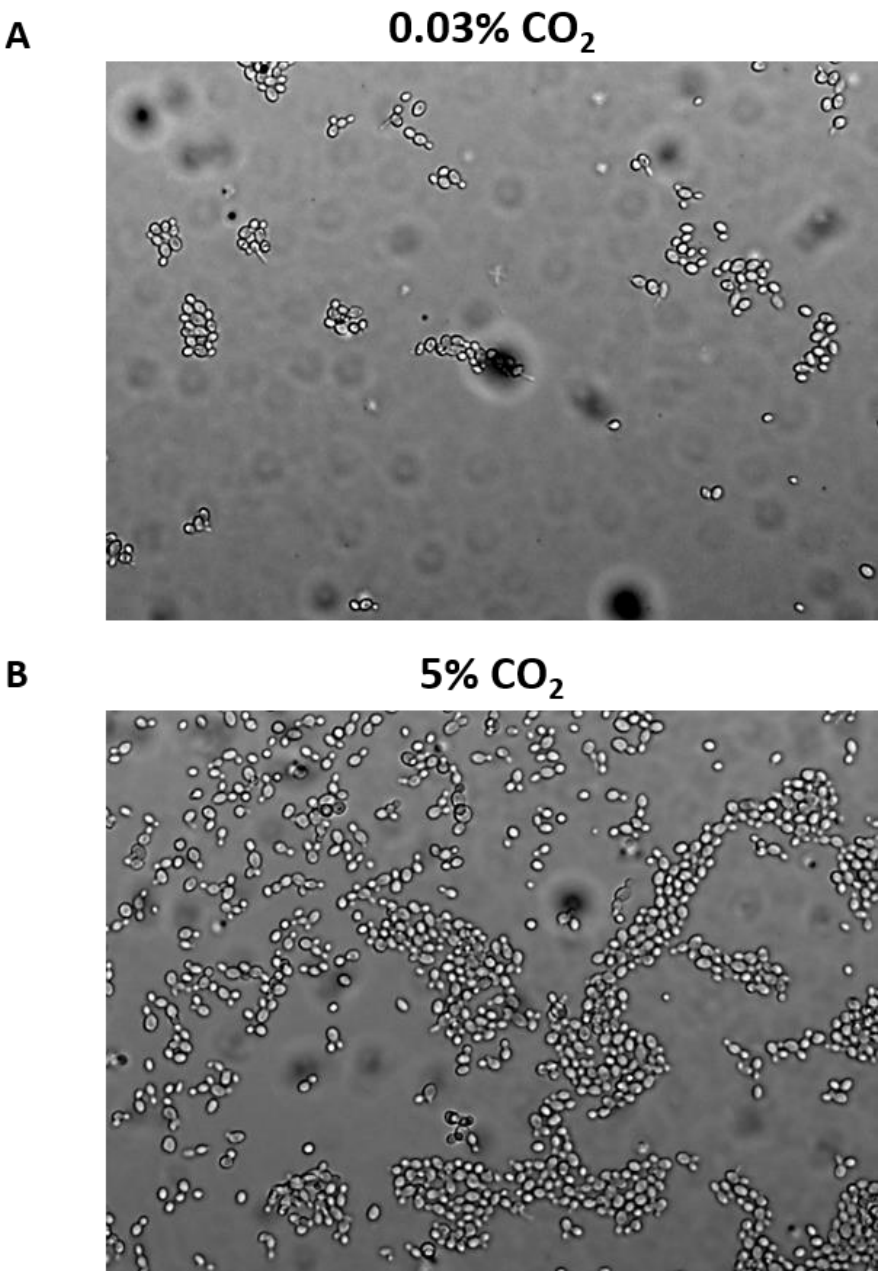
3.7 Supplementary Materials

Strain	Species	Genotype/Parent	Source/Reference
SN152	*C. albicans*	*ura3/*::imm434::*URA3/ura3*::imm434 *iro1::IRO1/iro1*::imm434 *his*1::hisG/*his1*::hisG *leu2/leu2 arg4/arg4*	[269]
CAI4	*C. albicans*	*ura3*::imm434/*ura3*::imm434 *iro1/iro1*::imm434	Mühlschlegel Lab
CAI4pSM2	*C. albicans*	CAI4 transformed with pSM2, *URA3* integrating plasmid	[77]
TFKO Library	*C. albicans*	SN152	[269]
CDH107 (*ras1Δ/Δ*)	*C. albicans*	CAI4	[69]
CR276 (*cdc35Δ/Δ*)	*C. albicans*	CAI4	[298]
WYF2 (*CDC35*$^{\Delta RA}$)	*C. albicans*	CR276 transformed with pClp-*cdc35*$^{\Delta RA}$	[293]
tpk1Δ/Δ	*C. albicans*	CAI4	Mühlschlegel Lab
tpk2Δ/Δ	*C. albicans*	CAI4	Mühlschlegel Lab
G-3065	*C. albicans*	Clinical Isolate	Failed Voice Prosthesis
G-8424	*C. albicans*	Clinical Isolate	Failed Voice Prosthesis
G-1625	*C. albicans*	Clinical Isolate	Failed Voice Prosthesis

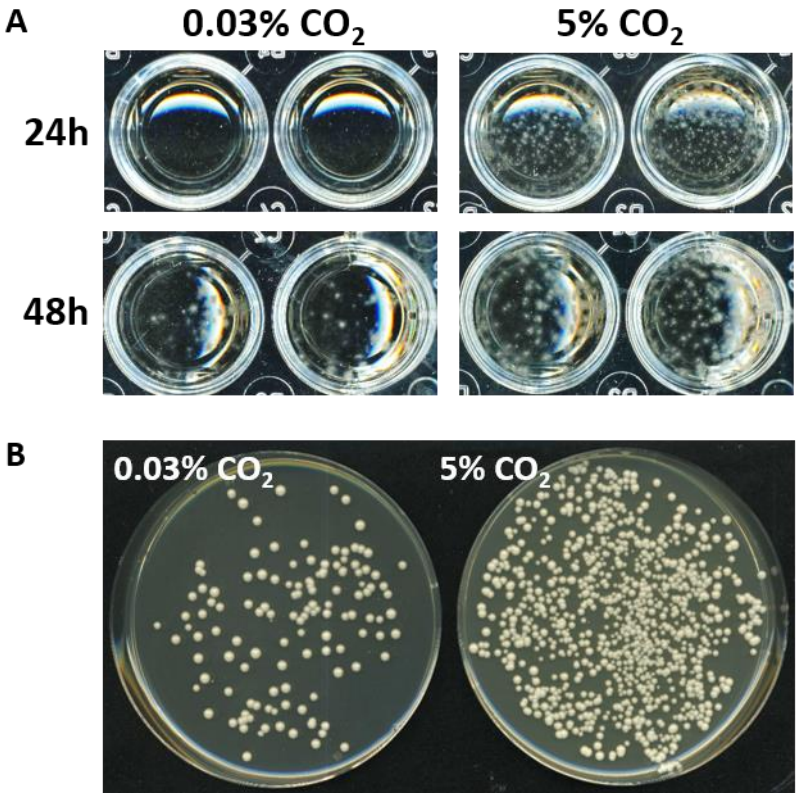
Supplementary Table S3.1: *Candida albicans* strains used in this study.

TFKO Mutant	Biofilm Growth	
	0.03% CO_2	5% CO_2
tup1Δ/Δ	– – – (p < 0.001)	– – – (p < 0.001)
sef1Δ/Δ	– – (p = 0.002)	– – (p < 0.001)
swi4Δ/Δ	– – (p < 0.001)	– – (p = 0.002)
pho4Δ/Δ	– – – (p < 0.001)	– (p = 0.049)
efg1Δ/Δ	– – (p = 0.007)	– – – (p = 0.044)
hap2Δ/Δ	– – – (p < 0.001)	n.s. (p = 0.561)
rbf1Δ/Δ	– – (p < 0.001)	n.s. (p = 0.873)
rob1Δ/Δ	– – (p < 0.001)	n.s. (p = 0.477)
fgr15Δ/Δ	– – (p = 0.005)	n.s. (p = 0.637)
dal81Δ/Δ	– – (p = 0.007)	n.s. (p = 0.682)
mig1Δ/Δ	– – (p = 0.014)	n.s. (p = 0.264)
brg1Δ/Δ	– – (p = 0.022)	n.s. (p = 0.998)
C4_00260WΔ/Δ	– – (p = 0.023)	n.s. (p = 0.915)
zcf27Δ/Δ	– – (p = 0.047)	n.s. (p = 0.870)
C1_13880CΔ/Δ	– (p = 0.009)	n.s. (p = 0.803)
crz1Δ/Δ	– (p = 0.022)	n.s. (p = 0.474)
hap43Δ/Δ	– (p = 0.030)	n.s. (p = 0.338)
leu3Δ/Δ	n.s. (p = 0.120)	– – (p < 0.001)
mbp1Δ/Δ	n.s. (p = 0.085)	– – (p = 0.007)
bas1Δ/Δ	n.s. (p = 0.563)	– (p = 0.016)
try6Δ/Δ	n.s. (p = 1.000)	– (p = 0.037)
mac1Δ/Δ	++ (p = 0.020)	n.s. (p = 0.847)
zcf30Δ/Δ	++ (p = 0.038)	n.s. (p = 0.640)
zcf17Δ/Δ	+ (p = 0.023)	n.s. (p = 0.735)

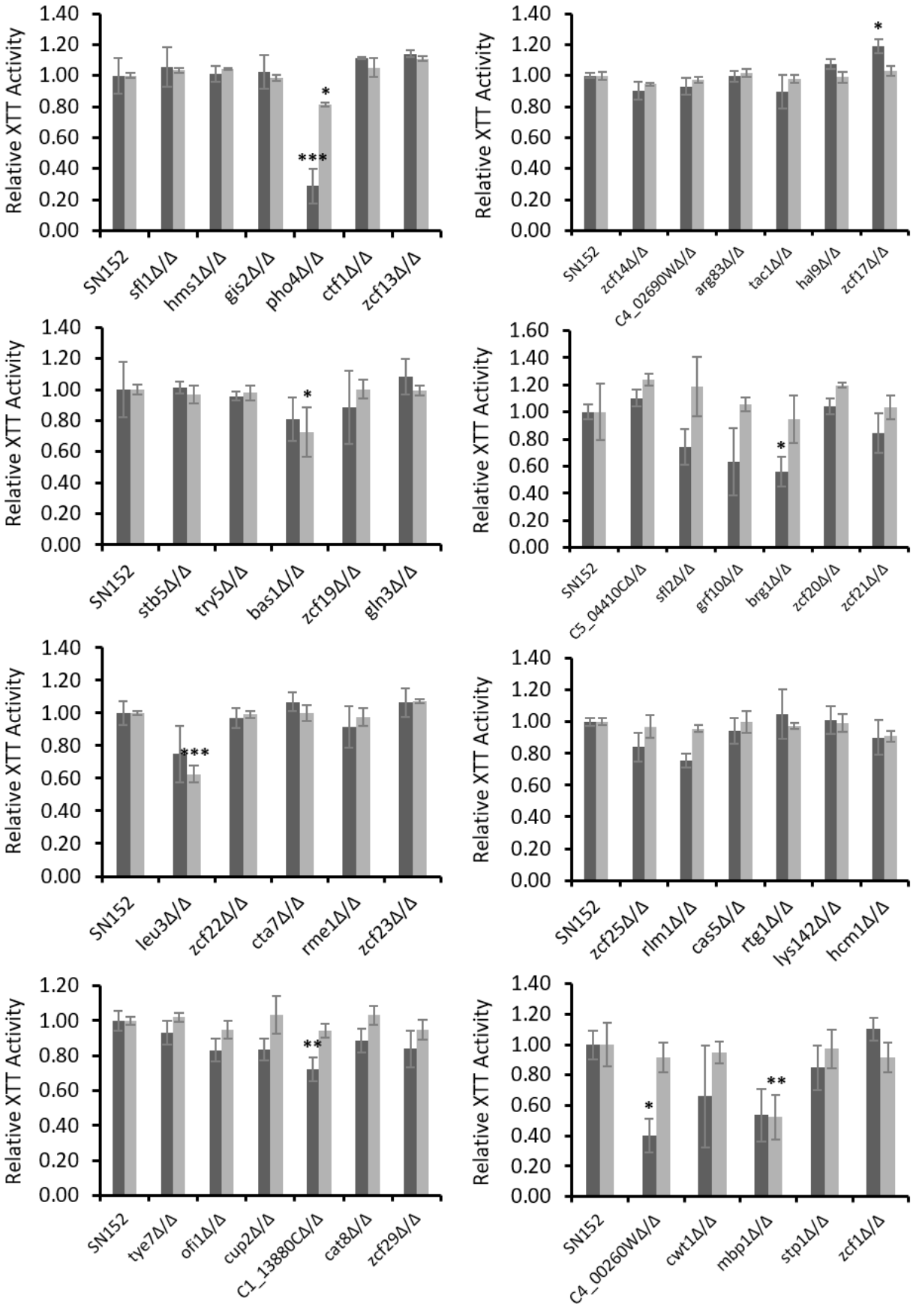
Supplementary Table S3.2: Summary of the transcription factor knockout (TFKO) mutants which had significantly altered biofilm growth in 0.03% and/or 5% CO_2 environments within our screen. Biofilms were quantified via XTT assays and normalised to the wild type XTT readout within each CO_2 environment; – – – <40% XTT activity relative to wild type, – – 40-70%, – >70%, + >110% ++ >130%, n.s. non-significant. Green indicates transcription factors previously known to have a role in biofilm regulation as per Gene Ontology analysis. Grey indicates transcription factors involved in maintaining cellular iron homeostasis.

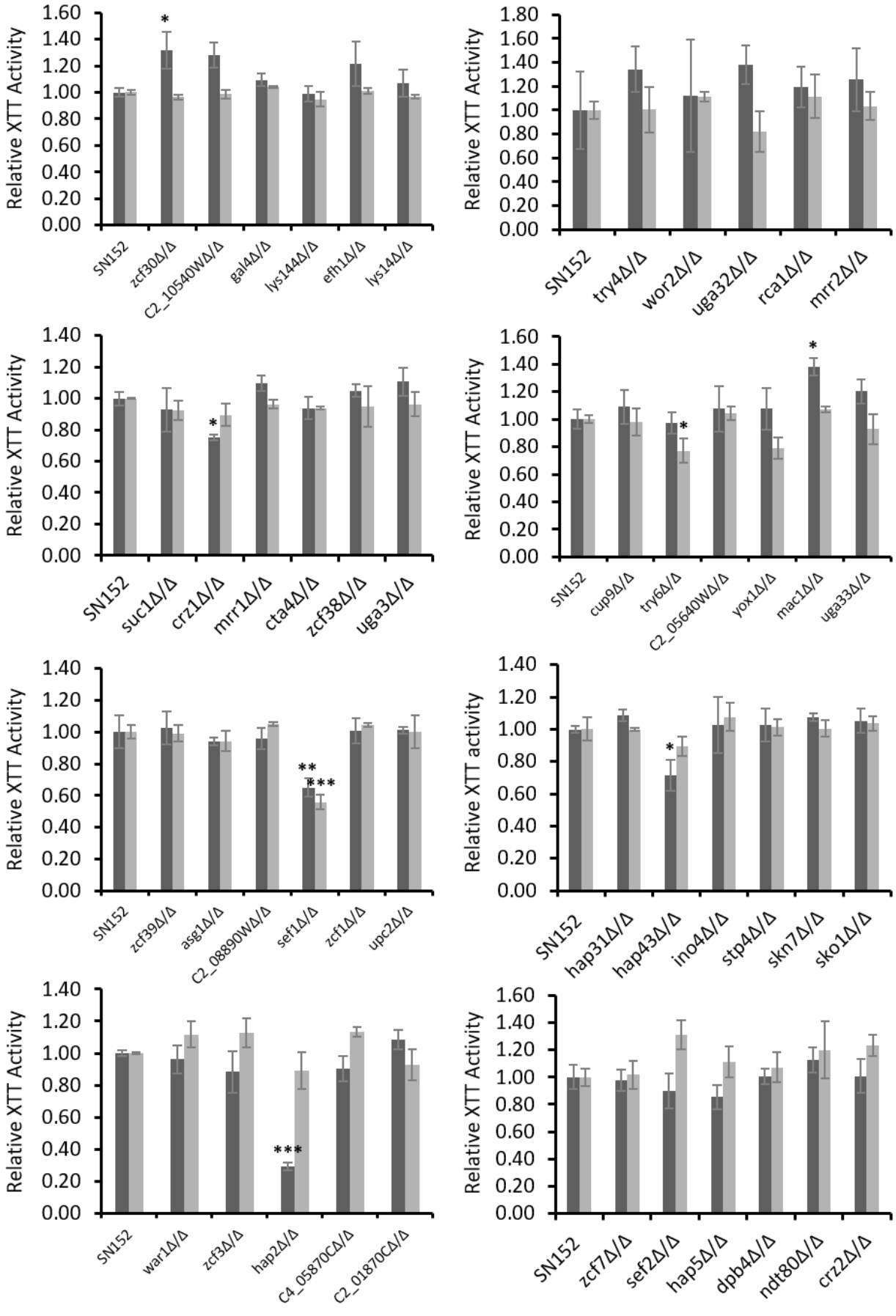


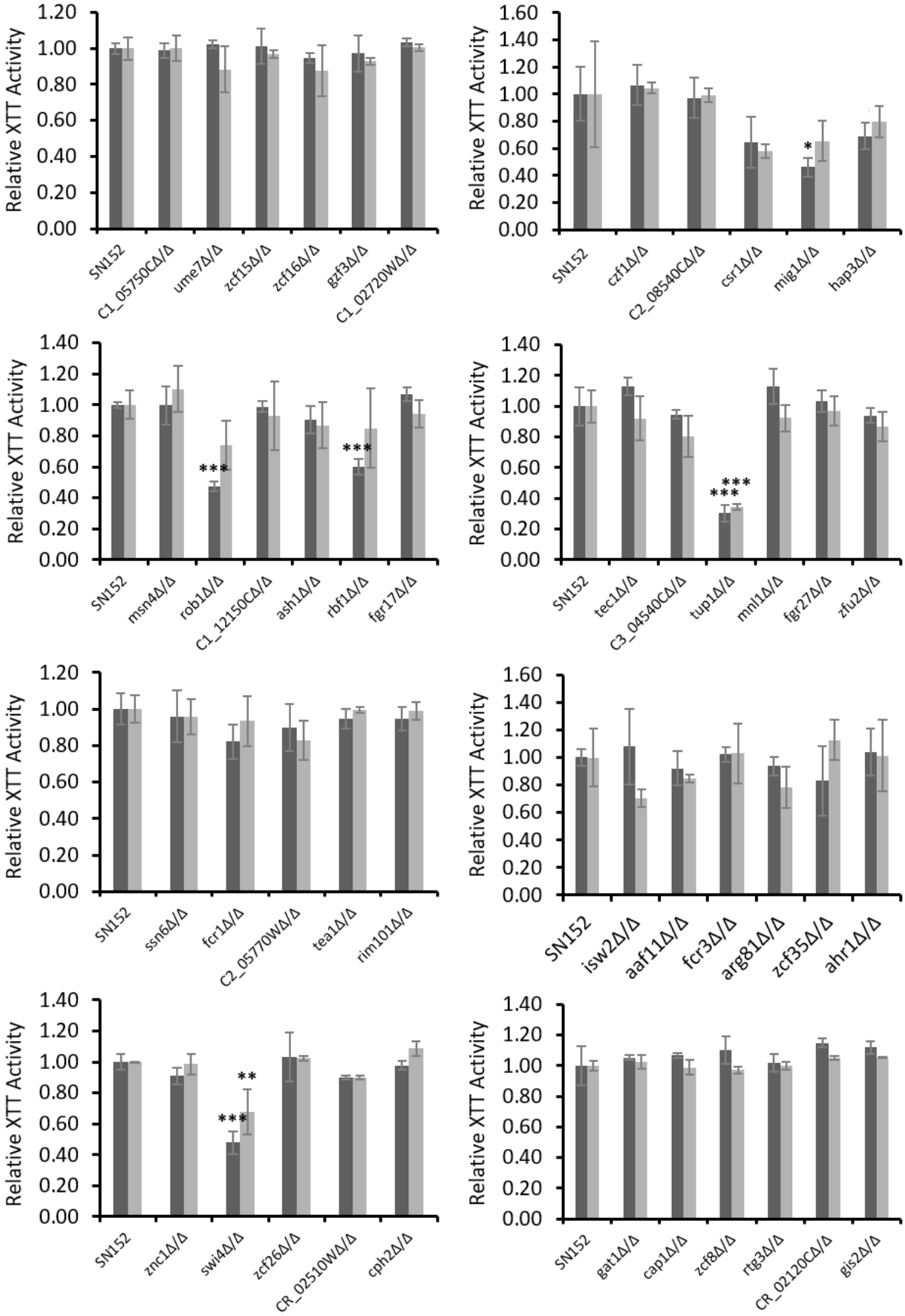
Supplementary Figure S3.1: Attachment of *C. albicans* CAI-4 cells to a silicone surface in 0.03% and 5% CO_2. *C. albicans* CAI-4 cells were seeded for 90 mins onto silicone-coated microscope slides in 0.03% CO_2 or 5% CO_2, unattached cells were washed off and images taken at 20x objective magnification. Several images were taken of both 0.03% and 5% CO_2 slides and representative examples are shown. **(A)** Representative image of a slide section from 0.03% CO_2. **(B)** Representative image of a slide section from 5% CO_2.

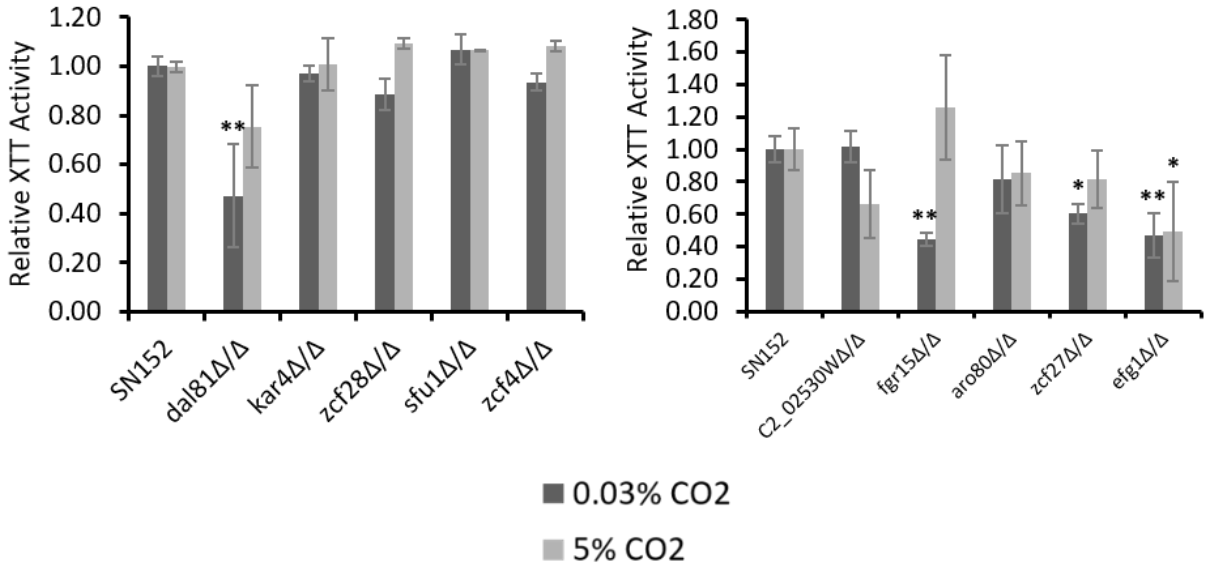


Supplementary Figure S3.2: Dispersion of *C. albicans* CAI4pSM2 cells from biofilms grown in 0.03% and 5% CO_2. (A) Wells containing RPMI-1640 media after biofilm growth, *C. albicans* cells can be seen as white clumps formed from hyphal cells. **(B)** Representative CFU plates from a 1:10 dilution of the spent RPMI-1640 media after 48h biofilm growth in both CO_2 conditions.

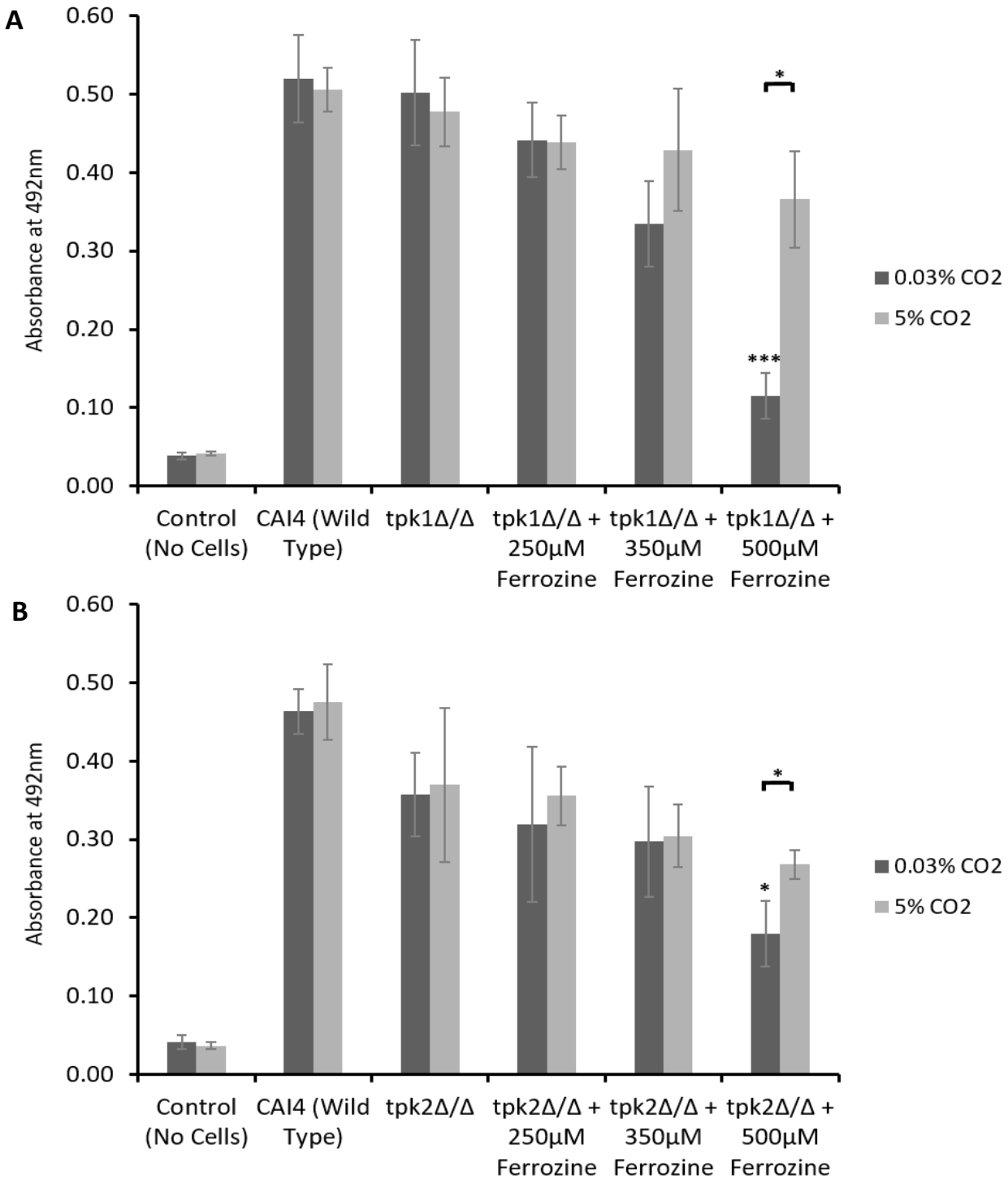

Relative XTT Activity
SN152
sfl1Δ/Δ
hms1Δ/Δ
gis2Δ/Δ
pho4Δ/Δ
ctf1Δ/Δ
zcf13Δ/Δ
zcf14Δ/Δ
C4_02690WΔ/Δ
arg83Δ/Δ
tac1Δ/Δ
hal9Δ/Δ
zcf17Δ/Δ
stb5Δ/Δ
try5Δ/Δ
bas1Δ/Δ
zcf19Δ/Δ
gln3Δ/Δ
C5_04410CΔ/Δ
sfl2Δ/Δ
grf10Δ/Δ
brg1Δ/Δ
zcf20Δ/Δ
zcf21Δ/Δ
leu3Δ/Δ
zcf22Δ/Δ
cta7Δ/Δ
rme1Δ/Δ
zcf23Δ/Δ
zcf25Δ/Δ
rlm1Δ/Δ
cas5Δ/Δ
rtg1Δ/Δ
lys142Δ/Δ
hcm1Δ/Δ
tye7Δ/Δ
ofi1Δ/Δ
cup2Δ/Δ
C1_13880CΔ/Δ
cat8Δ/Δ
zcf29Δ/Δ
C4_00260WΔ/Δ
cwt1Δ/Δ
mbp1Δ/Δ
stp1Δ/Δ
zcf1Δ/Δ
0.03% CO2
5% CO2


Relative XTT Activity
SN152
zcf30Δ/Δ
C2_10540WΔ/Δ
gal4Δ/Δ
lys144Δ/Δ
efh1Δ/Δ
lys14Δ/Δ
Relative XTT Activity
SN152
try4Δ/Δ
wor2Δ/Δ
uga32Δ/Δ
rca1Δ/Δ
mrr2Δ/Δ
Relative XTT Activity
SN152
suc1Δ/Δ
crz1Δ/Δ
mrr1Δ/Δ
cta4Δ/Δ
zcf38Δ/Δ
uga3Δ/Δ
Relative XTT Activity
SN152
cup9Δ/Δ
try6Δ/Δ
C2_05540WΔ/Δ
yox1Δ/Δ
mac1Δ/Δ
uga33Δ/Δ
Relative XTT Activity
SN152
zcf39Δ/Δ
asg1Δ/Δ
C2_08890WΔ/Δ
sef1Δ/Δ
zcf1Δ/Δ
upc2Δ/Δ
Relative XTT activity
SN152
hap31Δ/Δ
hap43Δ/Δ
ino4Δ/Δ
stp4Δ/Δ
skn7Δ/Δ
sko1Δ/Δ
Relative XTT Activity
SN152
war1Δ/Δ
zcf3Δ/Δ
hap2Δ/Δ
C4_05870CΔ/Δ
C2_01870CΔ/Δ
Relative XTT Activity
SN152
zcf7Δ/Δ
sef2Δ/Δ
hap5Δ/Δ
dpb4Δ/Δ
ndt80Δ/Δ
crz2Δ/Δ
0.03% CO2
5% CO2

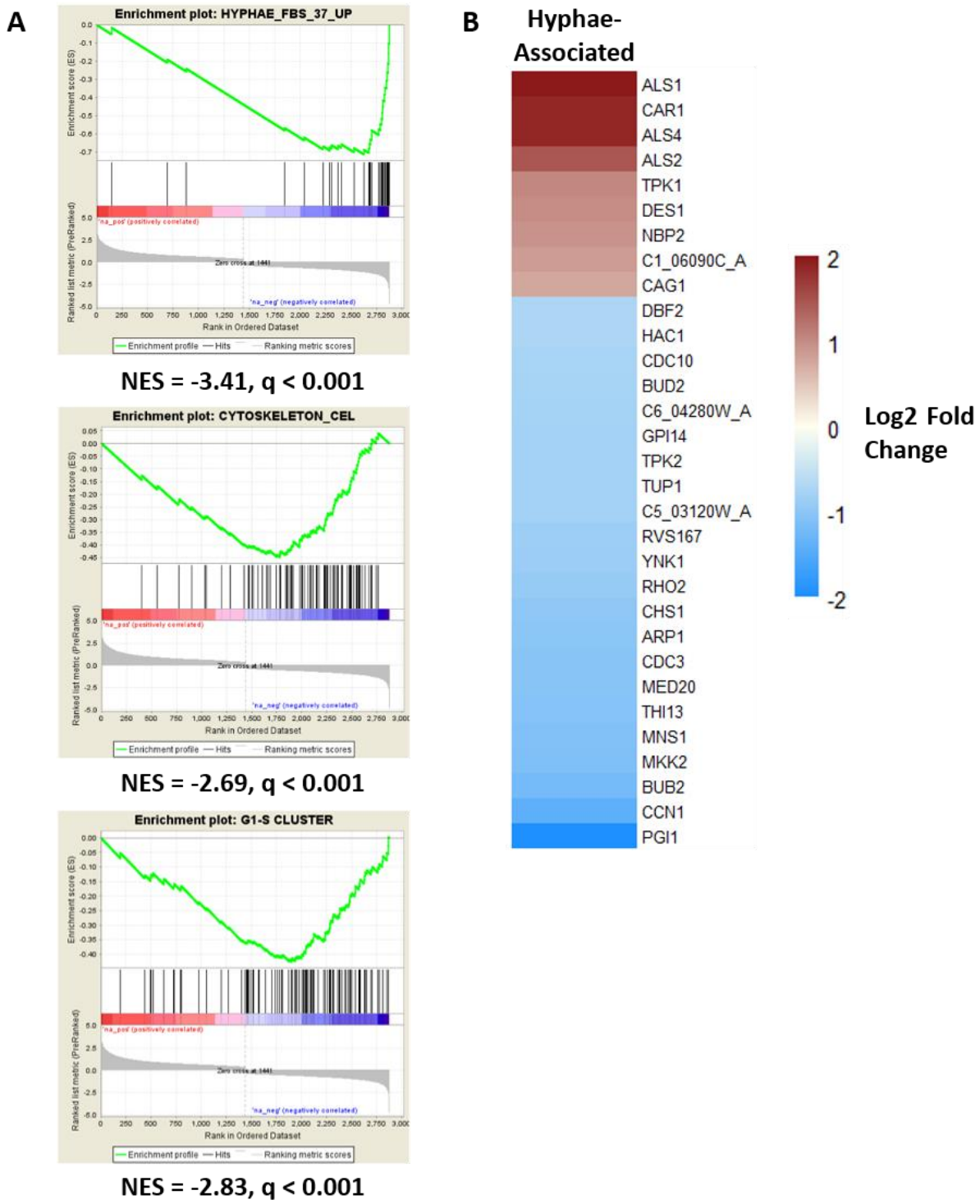

Relative XTT Activity
SN152
C1_05750CΔ/Δ
ume7Δ/Δ
zcf15Δ/Δ
zcf16Δ/Δ
gzf3Δ/Δ
C1_02720WΔ/Δ
czf1Δ/Δ
C2_08540CΔ/Δ
csr1Δ/Δ
mig1Δ/Δ
hap3Δ/Δ
msn4Δ/Δ
rob1Δ/Δ
C1_12150CΔ/Δ
ash1Δ/Δ
rbf1Δ/Δ
fgr17Δ/Δ
tec1Δ/Δ
C3_04540CΔ/Δ
tup1Δ/Δ
mnl1Δ/Δ
fgr27Δ/Δ
zfu2Δ/Δ
ssn6Δ/Δ
fcr1Δ/Δ
C2_05770WΔ/Δ
tea1Δ/Δ
rim101Δ/Δ
isw2Δ/Δ
aaf11Δ/Δ
fcr3Δ/Δ
arg81Δ/Δ
zcf35Δ/Δ
ahr1Δ/Δ
znc1Δ/Δ
swi4Δ/Δ
zcf26Δ/Δ
CR_02510WΔ/Δ
cph2Δ/Δ
gat1Δ/Δ
cap1Δ/Δ
zcf8Δ/Δ
rtg3Δ/Δ
CR_02120CΔ/Δ
gis2Δ/Δ
0.03% CO2
5% CO2



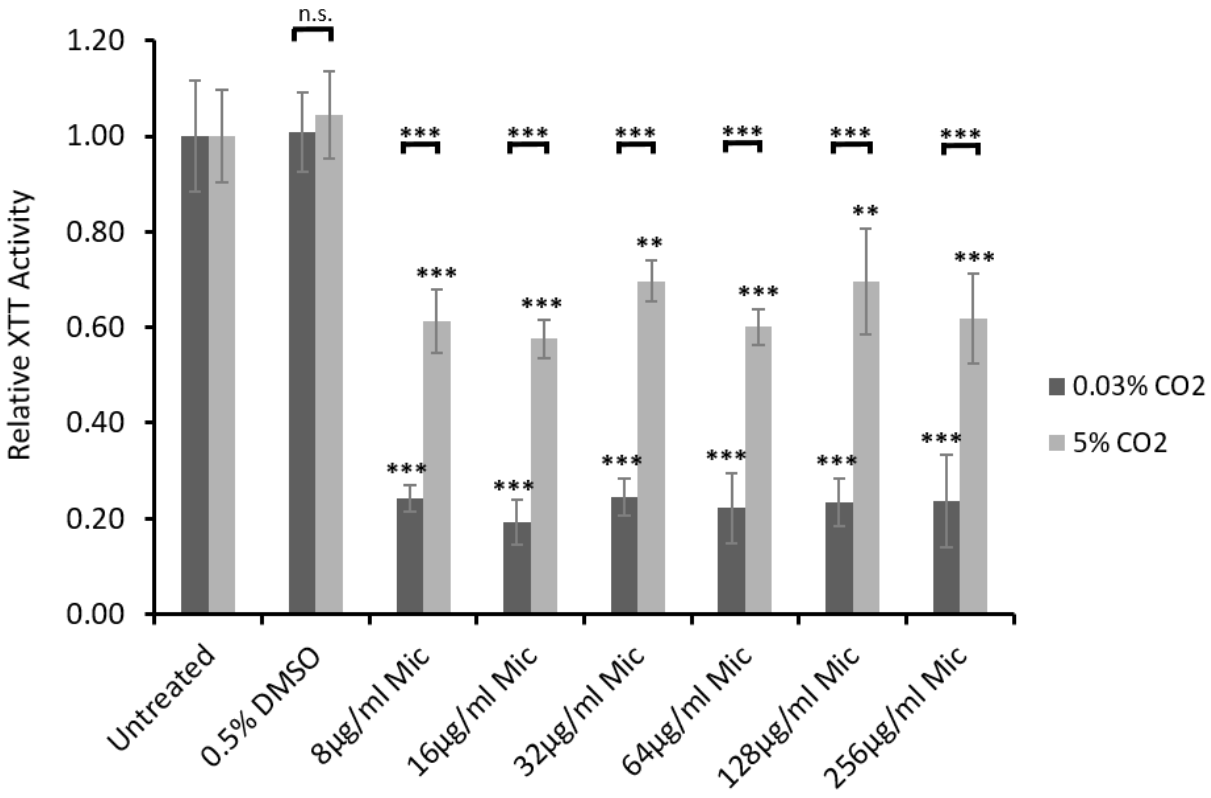
Supplementary Figure S3.3: Transcription Factor Knockout Screen of *C. albicans* biofilm-forming ability. Biofilms were seeded and grown before quantification via XTT assay. Graphs represent three biological replicates for each mutant. The XTT assay absorbances at 492nm for the 0.03% and 5% CO_2 biofilms have been normalised to the 0.03% and 5% CO_2 SN152 wild type controls respectively. This removes any day-to-day variation, thus allowing TFKO mutants grown on different days to be compared. One-way ANOVAs followed by Dunnett's Tests for multiple comparisons to a control were performed to compare the TFKO mutant biofilms to the SN152 wild type controls (for both 0.03% and 5% CO_2); *p<0.05, **p<0.01, ***p<0.001.



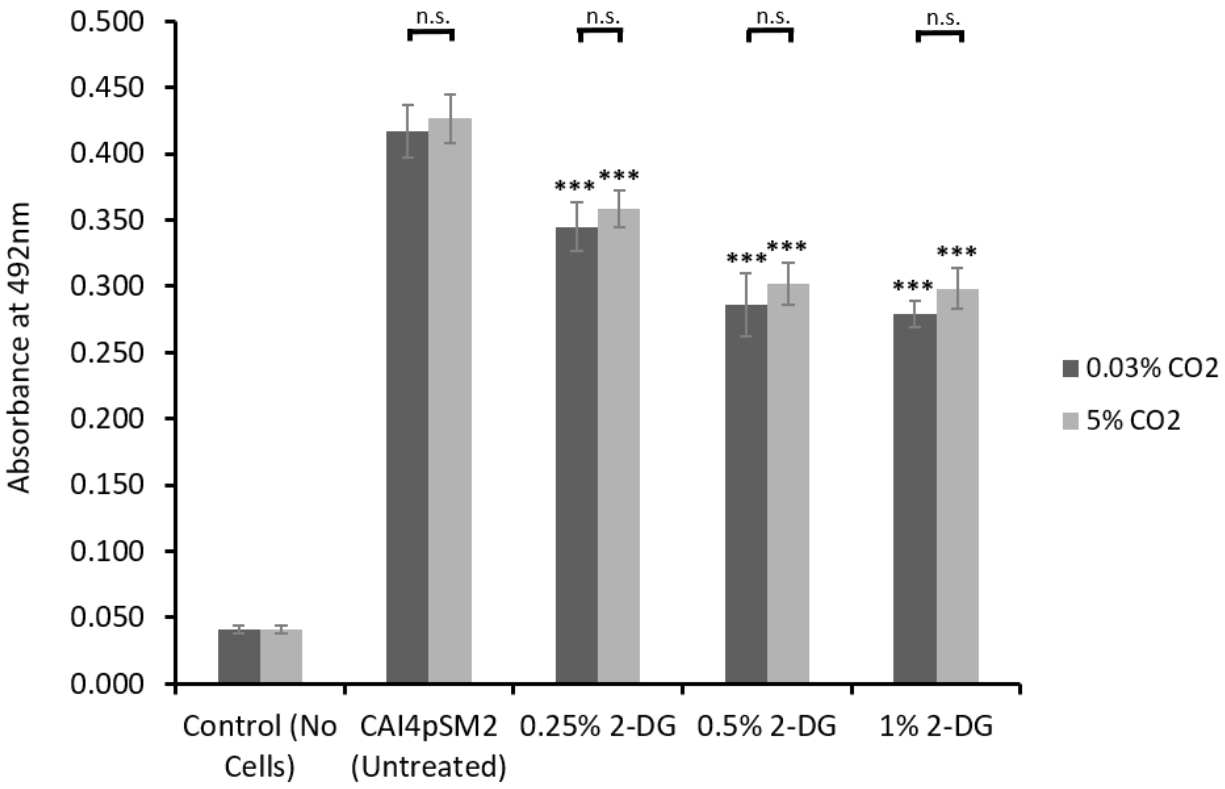
Supplementary Figure S3.4: The effect of high (5%) CO_2 on tolerance to iron starvation in *tpk1Δ/Δ* and *tpk2Δ/Δ* PKA mutants. Biofilms using **(A)** *tpk1Δ/Δ* and **(B)** *tpk2Δ/Δ* mutants were seeded and grown for 48h in the presence of the Fe^{2+} chelator Ferrozine before XTT quantification. Graphs represents two biological replicates each containing technical triplicates, error bars denote Standard Deviation. Two-way ANOVAs followed by Tukey tests for multiple comparisons were carried out: *p<0.05, **p<0.01, ***p<0.001, n.s. = not significant. Stars directly above the bars indicate a significant difference to the SN152 wild type/untreated or untreated isolate in the same CO_2 environment.



Supplementary Figure S3.5: Gene expression profiles of genes/gene sets downregulated in 5% CO_2 vs. 0.03% CO_2 *C. albicans* biofilms. (A) GSEA enrichment plots of the HYPHAE_FBS_37_UP gene set containing genes upregulated after 6h of exposure to FBS and 37°C (hyphal inducing conditions), the CYTOSKELETON_CEL gene set containing genes under the GO term 'cytoskeleton', and the G1-S CLUSTER gene set containing genes involved in the transition through the G1/S checkpoint. Vertical black lines represent individual genes in the ranked gene list from upregulated (left) to downregulated (right). NES = normalised enrichment score, negative NES indicates enrichment in the downregulated group of genes. **(B)** Heatmap of genes associated with hyphal growth as identified by GO term analysis. Colours saturate at log2 fold change of 2 and -2; *ALS1* actually has a log2 fold change of 3.77.



Supplementary Figure S3.6: Miconazole sensitivity of *C. albicans* biofilms grown in high (5%) CO_2. Biofilm growth assay of CAI4pSM2 in the presence of Nystatin. Biofilms were seeded and grown for 24 hours before antifungal addition, they were then grown for a further 24 hours before quantification using the XTT assay. The relative XTT activity is presented with the 0.03% CO_2 biofilms being normalised to the 0.03% CO_2 untreated control and the 5% CO_2 biofilms being normalised to the 5% CO_2 untreated control. This prevents the general higher growth of 5% CO_2 biofilms impacting the analysis. Two-way ANOVAs followed by Tukey tests for multiple comparisons were carried out: *p<0.05, **p<0.01, ***p<0.001, n.s. = not significant. Stars directly above the bars indicate a significant difference to untreated in the same CO_2 environment.



Supplementary Figure S3.7: Treatment of CAI4pSM2 *C. albicans* biofilms with 2-DG in 0.03% and 5% CO_2. Biofilms were seeded and grown for 48h in the presence of the glycolytic inhibitor 2-DG before XTT quantification. Control wells with no cells were set up as media controls to monitor for contamination as well as to ensure there was no reaction of the silicone squares with the XTT reagents. Graph represents three biological replicates each containing technical triplicates, error bars denote Standard Deviation. Two-way ANOVAs followed by Tukey tests for multiple comparisons were carried out: *p<0.05, **p<0.01, ***p<0.001, n.s. = not significant. Stars directly above the bars indicate a significant difference to the SN152 untreated in the same CO_2 environment.

Discussion

4.0 Discussion

Within this study we confirmed that *C. albicans* is the most prevalent fungal microorganism isolated from early failing VPs within our patient cohort. From our study it appears that the yeast burden contributes most to the loss of mechanical function that underlies early VP failure. This is demonstrated by the success our novel VP treatment guidelines which focus on the attenuation of fungal colonisation. Implementation of this management strategy resulted in 2.7-fold increase in device overall lifespan in a 20 patient cohort. Our study also supports a major role for the environment in promoting yeast colonisation and in particular we observed that 5% CO_2 (as found in exhaled breath) can drive the biofilm-formation of C. albicans. This may provide an explanation for its success in the VP setting. However, as expected, other bacterial (e.g. *S. aureus* and *P. aeruginosa*) and yeast (e.g. non-albicans *Candida* species) were also commonly found. Thus biofilms found on VPs represent complex and varied multi-species assemblies, each of which may contribute to VP deterioration.

4.1 Polymicrobial Nature of Voice Prosthesis Biofilms

Ours and previous studies [195][201][204] have observed the polymicrobial landscape of biofilms colonising failed VPs. The implications of polymicrobial biofilms and the interactions of the microbes within them in human disease are gaining increased interest [299]. Many diseases which were traditionally considered to be the result of a single microbial species, including infections of the oral cavity, otitis media and cystic fibrosis lung infections, have since been reassessed and recognised as true polymicrobial infections [299]. Interactions between microbes within polymicrobial infections can make them far more difficult to treat. For instance, it has been observed that physical interactions between yeast and hyphal *C.*

albicans cells and bacterial coccal cells in the oral mucosa result in increased antimicrobial tolerance of polymicrobial biofilms as well as enhanced biomass [299].

The two most commonly isolated species in our study were *S. aureus* (found on 64.2% of VPs) and *C. albicans* (found on 56.0% of VPs). These two organisms are normal members of the oral microflora and synergistic relationships between them have previously been recognised. For instance, within polymicrobial biofilms *S. aureus* cells have been observed to be coated in *C. albicans* ECM material, increasing their tolerance to antibiotics such as Vancomycin [241]. In fact, *S. aureus* is poor at forming biofilms on abiotic surfaces on its own, however, it has been suggested that the hyphal *C. albicans* cells provide a scaffold on which the *S. aureus* cells can attach within a mixed species biofilm [247][300]. This is likely a major reason why *S. aureus* is found with *C. albicans* and other *Candida* species in such high frequencies on the same VP, as well as probably being very important to the success of our treatment startegy focussing on combatting the fungal colonisers.

The attachment of *S. aureus* to *C. albicans* could also be a mechanism which the bacteria uses to invade human tissues during host infections, being carried on the hyphae as they penetrate the epithelial layers [258]. *S. aureus* is the third most commonly isolated organism with *C. albicans* in polymicrobial infections (a significant proportion of which are nosocomial infections) [257], demonstrating the importance of understanding interactions between these microorganisms. Carlson E. *et al.* demonstrated the potential dangers of co-infection with *S. aureus* and *C. albicans* over 30 years ago; intraperitoneal co-innoculation of immunocompetent mice with sublethal doses of *C. albicans* and *S. aureus* resulted in 100% mortality [259]. A further study discovered up to a 70000-fold decrease in the LD_{50} (inoculum

dose required to kill 50% of mice) for some *S. aureus* strains when co-innoculated with *C. albicans* compared to innoculation with *S. aureus* alone [260].

The second most common bacterial species isolated from early failing voice prostheses in our study was *P. aeruginosa*. In a previous study, *P. aeruginosa* was found to be the most prevalent bacteria on failed VPs [201]. Traditionally, *P. aeruginosa* and *C. albicans* were considered to have an antagonistic relationship because *in vitro* experiments have demonstrated *P. aeruginosa* is capable of binding to the surface of *C. albicans* hyphal cells and induce cell lysis [301]. Moreover, *P. aeruginosa* and *Candida* species exhibited a mutual inhibition of biofilm formation in dual-species biofilms *in vitro* [302]. However, it may not be this simple as they have been found together in polymicrobial biofilms on medical devices such as VPs (this study – all VPs with *P. aeruginosa* also had one or more *Candida* species), as well as being commonly co-isolated in the sputum of cystic fibrosis patients [303]. In fact, the presence of *C. albicans* in cystic fibrosis sputum is a strong predictor of co-colonisation with *Pseudomonas* species [304]. Similar to *S. aureus* and *C. albicans*, co-infection of murine models with sublethal doses of *P. aeruginosa* and *C. albicans* resulted in significantly higher mortality than either species alone [305]. The discrepancies between *in vitro* and *in vivo* findings with regards to interactions between *P. aeruginosa* and *Candida* are not fully understood, but are likely to be a result of host interactions as well these species' abilities to adapt to a variety of different niches. *In vivo* interactions between *P. aeruginosa* and *C. albicans* on medical devices and within polymicrobial biofilm infections are clinically very relevant and certainly warrant further investigations.

We identified many other *Candida* species in addition to *C. albicans* colonising failed VPs; *C. glabrata*, *C. tropicalis,* and *C. parapsilosis* were the third, fourth and fifth most commonly isolated species respectively. With the exception of *C. parapsilosis*, which was only co-isolated with another *Candida* species on one occassion, the other *Candida* species were commonly found together - most often *C. albicans* with one or more of the others. There has been limited work investigating potential synergistic/anatagonistic interactions within the *Candida* genus. We investigated whether the lack of *Candida* co-isolation with *C. parapsilosis* was due to a competitive advantage of *C. parapsilosis* over *C. albicans*. However, we found that *in vitro C. albicans* made much larger biofilms and outcompeted *C. parapsilosis* in a mixed biofilm, indicating other factors, such as patient diet, flora, and lifestyle which we were unable to mimic in our *in vitro* assay, are probably contributing to the success of *C. parapsilosis in vivo*. This is similar to previous studies; Kuhn, D. *et al.* found *C. albicans* isolates formed larger biofilms than *C. parapsilosis* isolates on silicone *in vitro* [237], whereas an investigation into *Candida* biofilms grown on catheters *in vivo* found little difference between *C. albicans* and *C. parapsilosis* biofilms [306].

C. glabrata was the second most common fungal species; it was isolated from 23 failed VPs and 19 of these had another *Candida* species present, most commonly *C. albicans*. This implies a potential synergistic relationship between these species. It has previously been observed that *C. glabrata* and *C. albicans* are frequently co-isolated from patients with denture stomatitis and their combined presence was often associated with severe inflammation [307]. Unlike *C. albicans*, *C. glabrata* is unable to form hyphae, and as a result forms smaller biofilms composed solely of yeast cells [308]. The authors of the denture stomatitis study hypothesised that the hyphal cells of *C. albicans* help to maintain the

structural integrity of denture-associated biofilms and provide a protective network for the smaller *C. glabrata* cells [307]. This may also be the case with VP-associated biofilms. Further evidence for a possible synergy between *C. albicans* and *C. glabrata* during infection comes from experiments which demonstrated *C. albicans* was able to enhance the invasiveness of *C. glabrata* in a RHE model, possibly as a result of *C. glabrata* 'hitchhiking' on *C. albicans* hyphae [309]. For most strains tested, tissue damage was also significantly increased during co-infection compared to single infection with either species [309].

We have demonstrated *C. albicans* biofilm growth in enhanced within a 5% CO_2 environment (see Section 4.2). It is possible that metabolically derived CO_2 generated by microorganisms in polymicrobial biofilms could create a microenvironment which supports biofilm formation. Hall, R. *et al*. observed that metabolic CO_2 within *C. albicans* biomasses can accumulate to induce filamentous growth via activation of Cyr1 [77]. The work presented here shows that CO_2 activation of Cyr1 also stimulates *C. albicans* biofilm growth. Thus, it is likely that once a polymicrobial biofilm reaches a critical size it enters a positive-feedback scenario where self-derived CO_2 drives further expansion which in turn provides more CO_2. Furthermore, *C. albicans* biofilms create a hypoxic microenvironment which can support the growth of anaerobic bacteria such as *Clostridium perfringens* and *Bacteroides fragilis*; *C. perfringens* is even able to induce *C. albicans* cells to form biofilm-like aggregations in liquid culture where it can survive in the normally toxic aerobic environment [310]. The combination of metabolically-derived CO_2 and hypoxia within growing biofilms is likely to substantially support polymicrobial biofilm formation on medical devices and biotic surfaces within the host.

While our antifungal treatment strategy was successful at extending VP *in situ* lifespans, inter-species interactions should not be underestimated. In addition to the interactions discussed above, it would also be interesting to explore possible viral or phage influences as these are not often considered in polymicrobial studies. This is also the case with non-fungal eukaryotic microorganisms such as protozoa. It is important to understand the synergistic and antagonistic relationships between microorganisms in this setting as they could provide insights for the development of further therapeutic strategies. These strategies could potentially be beneficial, not just for VP management, but also in the context of other prosthetic devices as well as polymicrobial host infections in general which are associated with enhanced pathogenicity.

4.2 Physiological Levels of CO_2 (5%) Enhance the Biofilm-Forming Ability of *Candida albicans*

A key finding in our study is that a CO_2 concentration of 5% increases the biofilm-forming ability of *C. albicans*. It has been well established that 5% CO_2 is a morphogenic signal for *C. albicans*, driving the yeast-to-hyphal switch via the Ras1-Cyr1-PKA pathway [69][77]. Despite this switch being known to be central to *C. albicans* biofilm formation, the effects of 5% CO_2 on *C. albicans* biofilm formation hitherto had not been explored. We demonstrate that all aspects of *C. albicans* biofilm growth – adhesion, maturation and dispersal – are enhanced in 5% CO_2. This CO_2-mediated increase in biofilm growth is specific to the biofilm scenario as planktonic *C. albicans* cells exhibited no significant growth rate difference in RPMI-1640 between 0.03% and 5% CO_2 environments (Figure 4.1). Transcriptome analysis revealed that several pathways governed by key regulators of *C. albicans* biofilm growth (Efg1, Brg1, Bcr1,

and Ndt80) were upregulated in biofilms grown in 5% CO_2. This provides an explanation for *C. albicans* success in colonising VPs, as observed in this study and others [195][201][204], since the CO_2 content of exhaled breath which the VP is consistently exposed to when *in situ* is approximately 5%. In mammals, physiological concentrations of CO_2 are up to 150x higher than atmospheric air [222][268], thus this data could have wider implications with regards to colonisation of other medical prosthetic devices, several of which are commonly colonised with *C. albicans* (see Section 4.3).

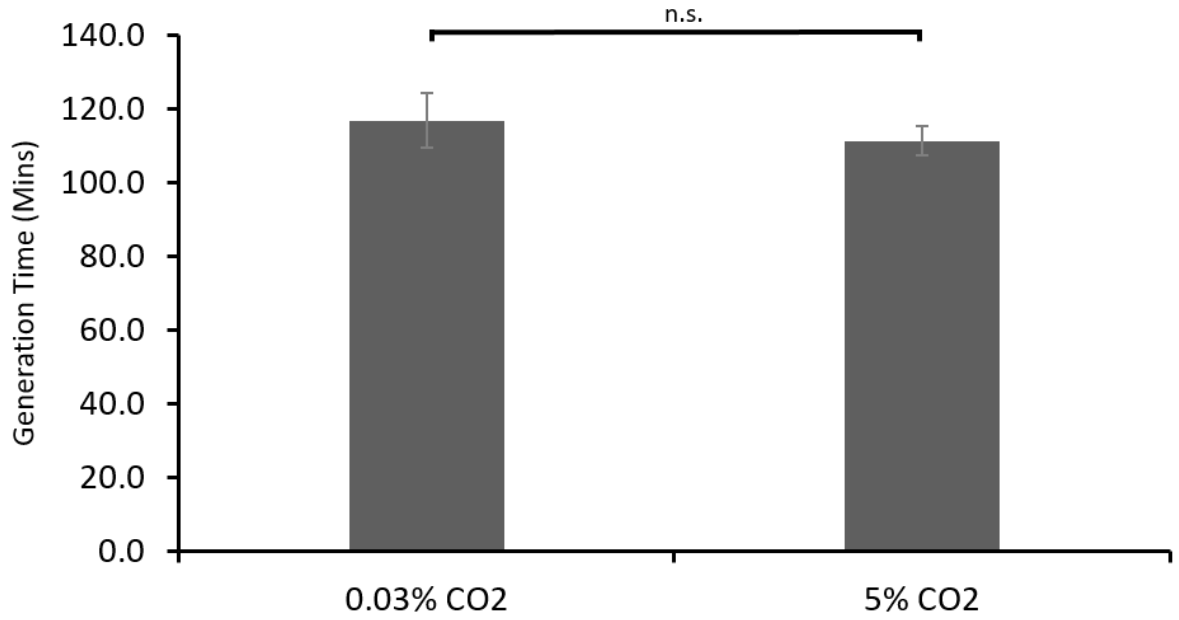


Figure 4.1: Planktonic growth of *C. albicans* CAI-4 in RPMI-1640 in 0.03% and 5% CO_2. Overnight cultures were inoculated to OD_{600} 0.1 in RPMI-1640 in 24-well plates. They were grown for 48 hours with 400rpm double orbital shaking in a BMG LABTECH SPECTROstar^{Nano} plate reader for 0.03% CO_2 conditions and a BMG LABTECH CLARIOstar plate reader for 5% CO_2 conditions. Growth was measured by OD_{600} readings taken every 10 mins. Graph represents three biological replicates each containing technical triplicate. A paired two-tail t test was carried out; n.s. = not significant.

In addition to *C. albicans,* we also frequently isolated several non-*albicans Candida* species, including *C. dubliniensis*, *C. glabrata*, *C. parapsilosis* and *C. krusei,* from failed VPs. This is consistent with other studies [195][201][204]. However, these other *Candida* species, do not

undergo a yeast-to-hyphae transition in response to elevated CO_2 levels [78]. In fact, other than *C. dubliniensis,* they do not form true hyphae at all and have been shown to form biofilms composed solely of yeast cells *in vitro* [237] and *in vivo* [306]. Therefore, elevated CO_2 is unlikely to directly explain their prevalence on VPs, though we cannot rule out that the adenylate cyclase of these latter species is activated by CO_2/bicarbonate ions. We did not observe an increase in the biofilm-forming ability of *C. parapsilosis* in 5% CO_2, although this may simply be due to the fact that the *C. parapsilosis* isolate we used generally did not form biofilms well in our *in vitro* model. One hypothesis is that the effect CO_2 has on species such as *C. albicans* can aid colonisation by other species – *C. glabrata* and the bacteria *S. aureus* have both been observed to attach to *C. albicans* hyphal cells in biofilms [247][300][309]. As discussed in Section 4.1, further investigations into interactions between species on medical devices are necessary and it would be interesting to determine if CO_2 has any effect on these.

4.2.1 The effect of high CO_2 on *C. albicans* biofilm growth relies on the adenylate kinase Cyr1

The Ras1-Cyr1-PKA pathway is crucial for the transduction of environmental cues from the exterior to the interior of the cell and integrates these signals with morphogenesis [6]. As discussed in Paper 2, CO_2 is able to directly activate the adenylate cyclase Cyr1 (Cdc35) and this Cyr1 activation is responsible for the CO_2-driven yeast-to-hyphal switch [69]. A *cdc35Δ/Δ* null mutant is defective in hyphal formation [69], consistently we found this mutant was unable to make biofilms in either 0.03% or 5% CO_2. The *ras1Δ/Δ* null mutant is also hyphal deficient [66] and was unable to form biofilms in 0.03% CO_2 but formed equivalent biofilms to the wild type in 5% CO_2. Overall, our data suggests the response of *C. albicans* biofilms to physiological (5%) levels of CO_2 is dependent on Cyr1 but can bypass a requirement for Ras1.

Our transcriptome analysis revealed the *RAS1, CYR1* (*CDC35*), and *TPK2* (encodes a catalytic subunit isoform of PKA) genes are significantly downregulated after 48 hours within 5% CO_2 biofilms in comparison to 0.03% CO_2. This could be explained by the fact the Ras1-Cyr1-PKA pathway can be considered most important for the earlier stages of biofilm formation when hyphal cells begin to form; indeed the Efg1 transcription factor, a key effector downstream of the pathway, principally functions in the initiation stage of biofilm growth [129]. We propose that *C. albicans* biofilms mature quicker in high CO_2 compared to low CO_2. Thus, as the 5% CO_2 biofilms have reached full maturity faster, the Ras1-Cyr1-PKA signalling pathway may be more active in the 0.03% CO_2 biofilms after 48h growth as they are still maturing or have matured more recently. The enrichment of hyphal related genes in the significantly downregulated genes in 5% CO_2 biofilms as revealed by GSEA is consistent with this. Moreover, upon progression to dispersion, the final stage of biofilm formation, several hyphal-specific genes downstream of Ras1-Cyr1-PKA pathway signalling are actively suppressed by transcriptional repressors such as Nrg1 [102]. Nrg1 is a positive regulator of biofilm dispersion and the *NRG1* gene was upregulated in 5% CO_2 biofilms, providing one explanation of hyphal gene repression and adding further evidence to the increased *C. albicans* biofilm maturation rate in 5% CO_2.

Finally, unlike other components of the Ras1-Cyr1-PKA pathway, *TPK1* is significantly upregulated (1.04 log2 fold change) in 5% CO_2 biofilms. The Tpk1 and Tpk2 isoforms have some redundant functions in *C. albicans*, demonstrated by no difference in biofilm formation compared to wild type of either the *tpk1Δ/Δ* or the *tpk2Δ/Δ* mutant (this study). However, they have also been shown to have specific roles, for example, recent transcriptomic and phosphoproteomic analyses using *tpk1Δ/Δ*, *tpk2Δ/Δ* and *tpk1Δ/Δtpk2Δ/Δ* mutants predicted

31 phosphorylation target sites specifically mediated by Tpk1 and 27 by Tpk2. Cell wall, membrane and signalling-related proteins were enriched in the Tpk1-specific targets, whereas filamentation and transporter-related proteins were enriched in the Tpk2-specific targets [75]. Given the apparent roles of Tpk2 in filamentation and transport, two very important processes for biofilm formation, it is quite surprising that *TPK1* expression is up and *TPK2* down in 5% CO_2 biofilms. However, the downregulation of *TPK2* is consistent with the enrichment of hyphal related genes in the significantly downregulated genes in 5% CO_2 biofilms which we propose is due to the faster maturation rate of high CO_2 biofilms. We should also highlight that the surface upon which a *C. albicans* biofilm is forming appears to exert a major influence on which signalling pathways are utilised. Indeed, a *tpk2Δ/Δ* mutant has exhibited attenuated adhesion and biofilm formation on a polystyrene surface [74], whereas on a silicone surface we observed *tpk2Δ/Δ* biofilm formation equivalent to an isogenic wild-type. This has previously been observed in *C. albicans* gene expression profiles using different biofilm models [294].

4.2.2 CO_2 and iron homeostasis in *C. albicans* biofilms

Our TFKO library biofilm formation screen identified iron homeostatic transcription factors including Sef1, and the HAP complex components Hap2, Hap3, Hap5, and Hap43. All four of the *hap* mutants – *hap2Δ/Δ*, *hap3Δ/Δ*, *hap5Δ/Δ*, and *hap43Δ/Δ* – exhibited a biofilm growth defect in 0.03% CO_2 but intriguingly had significantly higher biofilm growth in 5% CO_2. However, the *sef1Δ/Δ* mutant had defective biofilm growth in both CO_2 conditions. Since Sef1 functions downstream of the HAP complex, we hypothesise that a high CO_2 environment may influence Sef1 directly, causing the HAP complex to become at least partially redundant under these conditions.

It should be noted that we did not observe a significant effect on *SEF1* mRNA levels within 5% CO_2 biofilms after 48h. Thus, if it is influencing Sef1 activity, CO_2 must be acting at either the protein level or post-translational level as Sef1 is subject to a post-translational control loop consisting of Sfu1 and the cyclin-dependent kinase Ssn3 [58]. We do not believe the CO_2 effect on iron homeostasis is mediated through Ssn3 as this protein has been recently found to be dephosphorylated and thus inactive in 5% CO_2 [292]. Therefore, our current hypothesised model suggests that PKA, in a Tpk1/Tpk2 redundant manner can phosphorylate Sef1 and possibly also inhibit Sfu1. Our model is supported by the Tpk1/Tpk2 phosphoproteomic study discussed previously as it predicted Sef1 to be a potential PKA target that can be phosphorylated by both Tpk1 and Tpk2 [75].

The influence of CO_2 on the iron status of *C. albicans* cells could have wider implications regarding host infections and nutritional immunity. The transition from a commensal to a pathogenic lifestyle, especially in regards to entry into the bloodstream, is associated with rapid cellular reprogramming to adapt to the new environment [56]. A critical challenge *C. albicans* must overcome during infection is the maintenance of adequate iron levels, demonstrated by the high induction of several iron homeostatic genes in animal-infection models [311]. Most iron within the host is sequestered from potential pathogens either in the form of haemoglobin, bound to transferrin in the blood or bound to ferritin in tissues [44]. This provides a 'nutritional immunity' to combat infection with iron-dependent pathogens [38][312].

We observed *C. albicans* biofilms in high CO_2 overcoming the effects of iron starvation/sequestration *in vitro*. While *in situ* in the throat, VPs are coated in saliva which

contains the iron-chelating protein lactoferrin. Through its iron-sequestration properties, as well as other more direct antimicrobial actions, lactoferrin forms an important part of innate immune defence [313]. Consequently, it's possible that the CO_2 content of exhaled breath that VPs are exposed to could provide a competitive advantage to *C. albicans* in coping with lactoferrin-mediated iron-sequestration. Furthermore, the blood contains relatively high levels of CO_2 [222], and thus it is possible that high CO_2 is one (of many) signals *C. albicans* uses to increase iron acquisition in this environment. Consistent with this, our transcriptome analysis revealed mRNA transcript levels of *CSA2* and *RBT5* which encode proteins involved in the acquisition of iron from haem groups [41][314] were significantly increased in biofilms grown in 5% CO_2. Rbt5 in particular appears to be important in the acquisition of iron during host blood infection as *RBT5* is one of the most highly induced genes in murine and *Galleria mellonella* infection models [311], and anti-Rbt5 antibodies are prominent in the serum of patients following candidaemia [315].

In conclusion, our data and others' indicate physiological (5%) levels of CO_2 can act as an important pathogenic signal for *C. albicans*. CO_2 drives many virulence factors such as yeast-to-hyphal morphogenesis [69], biofilm growth (this study), and iron acquisition (this study). These CO_2-mediated effects are likely to have important medical ramifications, primarily in the context of prosthetics as demonstrated with voice prosthetics, but also for host infections in CO_2-rich environments in the body.

4.3 Potential Therapeutic Options to Combat *Candida albicans* Biofilms

In light of the characterised CO_2 effect on *C. albicans* biofilm formation, we investigated some potential therapeutic options for biofilms grown in high CO_2 environments which could be useful for VP management in the future.

We have demonstrated that 2-deoxyglucose (2-DG) is able to attenuate *C. albicans* biofilm growth in both 5% and atmospheric (0.03%) CO_2 environments. A 2-DG concentration of 1% reduced biofilm growth of the SN152 wild-type strain by 46% and 38% in 5% and 0.03% CO_2 respectively. 2-DG is actively taken up by hexose transporters on eukaryotic cell surfaces and our transcriptome analysis showed genes encoded several of these were upregulated in 5% CO_2 biofilms. Upon its phosphorylation, the resulting 2-DG-6-phosphate is a glycolytic inhibitor, inhibiting phosphoglucose isomerase and hexokinase in a competitive and non-competitive manner respectively [316][317]. Although more recent studies using *S. cerevisiae* have proposed that a glycolytic block does not sufficiently explain its growth inhibition effects, concluding the interplay between glycolysis and the pentose phosphate pathway is important as the separation of these pathways through genetic deletions results in increased 2-DG resistance [318]. 2-DG has been widely studied as a potential anti-cancer drug to combat Warburg metabolism; it has previously reached Stage II clinical trials as an anti-prostate cancer drug but was ultimately deemed unsuccessful [291]. The potential of repurposing 2-DG as a biofilm-treating antifungal agent for pathogenic yeasts has not previously been explored. 2-DG has exhibited antifungal effects against the moulds *Botrytis cinerea*, *Penicillium expansum*, and *Rhizopus stolonifer* [296]. It has also been observed to inhibit biofilm growth of *Escherichia coli* [297]. This, together with its action against *C. albicans*

biofilms presented in our study, could mean it is particularly useful against VP-associated biofilms which as we have demonstrated are often a mixture of bacterial and fungal species.

2-DG is considered safe for use in humans at low doses and besides we would envisage it to be applied directly to the VP surface in a similar way to the antifungals in our newly implemented treatment guidelines so host cell exposure would be minimal. It is important to note that 2-DG treatment was unable to eradicate *C. albicans* biofilm formation entirely, although it is encouraging that it is equally effective against both high and low CO_2 biofilms. Combination therapy using traditional antifungals and other compounds has previously been demonstrated to be effective against *C. albicans* biofilms [178][180][181]. It may be that 2-DG treatment is beneficial in combination with other compounds, such as iron chelators (see below) or traditional antifungals; this possibility is yet to be explored.

We also explored the possibility of using the Fe^{3+} chelator Deferasirox, which is an approved drug for treating patients with iron overload, as a therapeutic to combat *C. albicans* biofilms on silicone surfaces. It was recently revealed that treatment with Deferasirox significantly reduced salivary iron levels in a murine oropharyngeal model and resulted in a reduction in oral fungal burden [290]. Moreover, Deferasirox treated *C. albicans* cells had reduced survival in phagosomes after phagocytosis by human neutrophils, as well as decreased adhesion and invasion of oral epithelial cells *in vitro* [290]. In our study, Deferasirox completely prevented *C. albicans* biofilm formation in atmospheric CO_2 conditions but had very little effect in 5% CO_2. This demonstrates that Deferasirox has potential as a fungal biofilm therapeutic, however, not in high CO_2 environments and consequently is probably not useful for the management/treatment of VP-associated biofilms. This data also highlights that the

environment where a *C. albicans* biofilm is found can have crucial implications regarding which treatments will be most effective, and hence should influence the choice of treatment.

Within our study, we have focussed on the potential for repurposing currently available compounds which are approved for human use. We believe that this is an important avenue to explore as already approved compounds will be able to be implemented in treatments significantly quicker than completely new antifungal compounds (although these of course need to be discovered too). We have also highlighted the importance of external factors such as CO_2 environment when testing potential antifungals; adding additional complexity such as this to *in vitro* tests will hopefully give a more representative account of the efficacy *in vivo*.

4.4 *Candida albicans* Biofilm Formation on Other Medical-Implant Devices

The findings we have detailed within this study could be more generally applicable to the colonisation of several implanted medical devices. In addition to VPs, *C. albicans* is a common coloniser of many medical devices including central venous catheters, dentures, tracheostomy tubes, and urinary catheters [4]. We hope that the findings detailed in our study can be applicable to other scenarios of *C. albicans* colonisation. Catheters such as central venous catheters are typically made of silicone and so these represent the most likely candidates for similar *C. albicans* interactions. Moreover, the CO_2 content of venous blood is relatively high [222], meaning some of the CO_2-mediated effects may also be relevant here. A study investigating denture stomatitis and the associated fungal colonisation found that *C. albicans* and *C. glabrata* were the two most frequently isolated yeasts [307]. Likewise, *C. albicans* and *C. glabrata* were also the two most common fungal VP colonisers isolated in this study. This overlap is expected due to the similar locations of the devices within the body and

hence dentures and VPs are exposed to the same oral cavity microflora. However, it is possible that although they are not made of silicone, denture colonisation could be influenced by the CO_2 content of exhaled breath in a similar way to what we are proposing for VPs.

4.5 Future Investigations

The results presented here confirm *C. albicans* as the most prevalent coloniser of VPs, often in a polymicrobial biofilm. A drawback of the microbiology data we and others present is that it is qualitative rather than quantitative as it relies on pre-culturing before species identification. While these data give a very good overview of the microbial landscape on early failing VPs, we should follow up these studies with assessments of the microorganisms directly from the VP surface. These future studies could utilise new sequencing technologies, such as NanoPore DNA sequencing, for microbial identification [319]. This would give a quantitative readout of the relative abundance of different microorganisms, as well as allowing the identification of species which cannot be cultured under laboratory conditions and so are often overlooked with traditional identification methodology.

In addition, further polymicrobial investigations should be carried out to investigate interactions between species in mixed biofilms as well as the order of colonisation of these species on voice prosthetic surfaces. Due to the success of our antifungal treatment guidelines we hypothesised that *Candida* species, particularly *C. albicans*, are likely to be early colonisers which enable colonisation with other species. However, we did not directly test this and so it would be interesting to determine if this is indeed true. The influence of patient diet on colonisation would also be useful to examine as this would enable clinicians to give evidence-based patient advice to hopefully aid in VP lifespan management. Preliminary experiments

exploring the effect of alcohol and glucose levels have been carried out within our laboratory but further investigations are needed.

We have shown that 5% CO_2 can drive the biofilm growth phenotype in *C. albicans* and increase its tolerance to iron starvation. We have proposed a model whereby PKA in the Ras1-Cyr1-PKA pathway (known to be activated by 5% CO_2 [69][77]) may possibly phosphorylate and activate the iron-uptake regulator Sef1. This can then increase the expression of iron-uptake genes to circumvent iron starvation, as well as causing a redundancy of the HAP complex. We are currently investigating the phosphorylation of Sef1 in 5% CO_2 through the use of Phos-tag SDS-PAGE gels which can detect the phosphorylation state of proteins [320]. Finally, we identified 2-DG as a potential therapeutic for *C. albicans* biofilms in high CO_2 environments. Further investigations into its use as a viable antifungal are warranted, along with its possible use in combination with traditional antifungals or other compounds.

References

1. Bryers JD (**2008**). Medical biofilms. **Biotechnol Bioeng**. 100(1): 1–18. doi: 10.1002/bit.21838.

2. Zheng Y, He L, Asiamah TK, and Otto M (**2018**). Colonization of medical devices by staphylococci. **Environ Microbiol**. 20(9): 3141–3153. doi: 10.1111/1462-2920.14129.

3. Sabir N, Ikram A, Zaman G, Satti L, Gardezi A, Ahmed A, and Ahmed P (**2017**). Bacterial biofilm-based catheter-associated urinary tract infections: Causative pathogens and antibiotic resistance. **Am J Infect Control**. 45(10): 1101–1105. doi: 10.1016/j.ajic.2017.05.009.

4. Kojic EM, and Darouiche RO (**2004**). Candida Infections of Medical Devices. **Clin Microbiol Rev**. 17(2): 255–267. doi: 10.1128/CMR.17.2.255-267.2004.

5. Kim J, and Sudbery P (**2011**). Candida albicans, a major human fungal pathogen. **J Microbiol**. 49(2): 171–177. doi: 10.1007/s12275-011-1064-7.

6. Berman J, and Sudbery PE (**2002**). Candida albicans: a molecular revolution built on lessons from budding yeast. **Nat Rev Genet**. 3(12): 918–930. doi: 10.1038/nrg948.

7. Ganguly S, and Mitchell AP (**2011**). Mucosal biofilms of Candida albicans. **Curr Opin Microbiol**. 14(4): 380–385. doi: 10.1016/j.mib.2011.06.001.

8. Douglas LJ (**2003**). Candida biofilms and their role in infection. **Trends Microbiol**. 11(1): 30–36. doi: 10.1016/S0966-842X(02)00002-1.

9. Berman J (**2012**). Candida albicans. **Curr Biol**. 22(16): 620–622. doi: 10.1016/j.cub.2012.05.043.

10. Talpaert MJ, Balfour A, Stevens S, Baker M, Muhlschlegel FA, and Gourlay CW (**2015**). Candida biofilm formation on voice prostheses. **J Med Microbiol**. 64: 199–208. doi: 10.1099/jmm.0.078717-0.

11. Finkel JS, and Mitchell AP (**2011**). Genetic control of Candida albicans biofilm development. **Nat Rev Microbiol**. 9(2): 109–118. doi: 10.1038/nrmicro2475.

12. Magee BB, and Magee PT (**1987**). Electrophoretic karyotypes and chromosome numbers in Candida species. **J Gen Microbiol**. 133(2): 425–30. 3309156.

13. Santos M a, and Tuite MF (**1995**). The CUG codon is decoded in vivo as serine and not leucine in Candida albicans. **Nucleic Acids Res**. 23(9): 1481–1486. doi: 10.1093/nar/23.9.1481.

14. Butler G et al. (**2009**). Evolution of pathogenicity and sexual reproduction in eight Candida genomes. **Nature**. 459(7247): 657–662. doi: 10.1038/nature08064.

15. Asakura K, Iwaguchi S, Homma M, Sukai T, Higashide K, and Tanaka K (**1991**). Electrophoretic karyotypes of clinically isolated yeasts of Candida albicans and C. glabrata. **J Gen Microbiol**. 137(11): 2531–8. 1783899.

16. Janbon G, Sherman F, and Rustchenko E (**1998**). Monosomy of a specific chromosome determines L-sorbose utilization: a novel regulatory mechanism in Candida albicans. **Proc**

Natl Acad Sci U S A. 95(9): 5150–5155. doi: 10.1073/pnas.95.9.5150.

17. Perepnikhatka V, Fischer FJ, Niimi M, Baker R a., Cannon RD, Wang YK, Sherman F, and Rustchenko E (**1999**). Specific chromosome alterations in fluconazole-resistant mutants of Candida albicans. **J Bacteriol**. 181(13): 4041–4049. 10383973.

18. Forche A, Alby K, Schaefer D, Johnson AD, Berman J, and Bennett RJ (**2008**). The parasexual cycle in Candida albicans provides an alternative pathway to meiosis for the formation of recombinant strains. **PLoS Biol**. 6(5): 1084–1097. doi: 10.1371/journal.pbio.0060110.

19. Herskowitz I (**1988**). Life cycle of the budding yeast Saccharomyces cerevisiae. **Microbiol Rev**. 52(4): 536–553. 3070323.

20. Miller MG, and Johnson AD (**2002**). White-opaque switching in Candida albicans is controlled by mating-type locus homeodomain proteins and allows efficient mating. **Cell**. 110(3): 293–302. doi: 10.1016/S0092-8674(02)00837-1.

21. Soll DR (**1997**). Gene regulation during high-frequency switching in Candida albicans. **Microbiology**. 143: 279–288. 9043104.

22. Pujol C, Daniels KJ, Lockhart SR, Srikantha T, Radke JB, Geiger J, and Soll DR (**2004**). The closely related species Candida albicans and Candida dubliniensis can mate. **Eukaryot Cell**. 3(4): 1015–1027. doi: 10.1128/EC.3.4.1015.

23. Kvaal C, Lachke SA, Srikantha T, Daniels K, Mccoy J, and Soll DR (**1999**). Misexpression of the opaque-phase-specific gene PEP1 (SAP1) in the white phase of Candida albicans confers increased virulence in a mouse model of cutaneous infection. **Infect Immun**. 67(12): 6652–6662.

24. Bennett RJ, and Johnson AD (**2003**). Completion of a parasexual cycle in Candida albicans by induced chromosome loss in tetraploid strains. **EMBO J**. 22(10): 2505–2515. doi: 10.1093/emboj/cdg235.

25. Daniels KJ, Srikantha T, Lockhart SR, Pujol C, and Soll DR (**2006**). Opaque cells signal white cells to form biofilms in Candida albicans. **EMBO J**. 25(10): 2240–2252. doi: 10.1038/sj.emboj.7601099.

26. Yi S, Sahni N, Daniels KJ, Lu KL, Srikantha T, Huang G, Garnaas AM, and Soll DR (**2011**). Alternative mating type configurations (a/α versus a/a or α/α) of candida albicans result in alternative biofilms regulated by different pathways. **PLoS Biol**. 9(8). doi: 10.1371/journal.pbio.1001117.

27. Wu W, Lockhart SR, Pujol C, Srikantha T, and Soll DR (**2007**). Heterozygosity of genes on the sex chromosome regulates Candida albicans virulence. **Mol Microbiol**. 64(6): 1587–1604. doi: 10.1111/j.1365-2958.2007.05759.x.

28. Gow NAR, van de Veerdonk FL, Brown AJP, and Netea MG (**2011**). Candida albicans morphogenesis and host defence: discriminating invasion from colonization. **Nat Rev Microbiol**. 10(2): 112–122. doi: 10.1038/nrmicro2711.

29. Klein R, Harris C, Small C, Moll B, Lesser M, and Friedland G (**1984**). Oral candidiasis in high-risk patients as the initial manifestation of the acquired immunodeficiency syndrome.

N Engl J Med. 311(6): 354–358.

30. Kibbler CC, Seaton S, Barnes RA, Gransden WR, Holliman RE, Johnson EM, Perry JD, Sullivan DJ, and Wilson JA (**2003**). Management and outcome of bloodstream infections due to Candida species in England and Wales. **J Hosp Infect**. 54: 18–24. doi: 10.1016/S0195-6701(03)00085-9.

31. Koh AY, Köhler JR, Coggshall KT, Van Rooijen N, and Pier GB (**2008**). Mucosal Damage and Neutropenia Are Required for Candida albicans Dissemination. **PLoS Pathog**. 4(2): e35. doi: 10.1371/journal.ppat.0040035.

32. Mikulska M, Del Bono V, Ratto S, and Viscoli C (**2012**). Occurrence, presentation and treatment of candidemia. **Expert Rev Clin Immunol**. 8(8): 755–765. doi: 10.1586/eci.12.52.

33. Blot SI, Vandewoude KH, Hoste EA, and Colardyn FA (**2002**). Effects of nosocomial candidemia on outcomes of critically ill patients. **Am J Med**. 113(6): 480–485. doi: 10.1016/S0002-9343(02)01248-2.

34. Philpott CC, Leidgens S, and Frey AG (**2012**). Metabolic remodeling in iron-deficient fungi. **Biochim Biophys Acta - Mol Cell Res**. 1823(9): 1509–1520. doi: 10.1016/j.bbamcr.2012.01.012.

35. Pierre JL, and Fontecave M (**1999**). Iron and activated oxygen species in biology: The basic chemistry. **BioMetals**. 12(3): 195–199. doi: 10.1023/A:1009252919854.

36. Raymond KN, Dertz EA, and Kim SS Enterobactin: An archetype for microbial iron transport. .

37. Miret S, Simpson RJ, and McKie AT (**2003**). Physiology and molecular biology of dietary iron absorption. **Annu Rev Nutr**. 23(1): 283–301. doi: 10.1146/annurev.nutr.23.011702.073139.

38. Weinberg ED (**1975**). Nutritional immunity. Host's attempt to withold iron from microbial invaders. **JAMA**. 231(1): 39–41. doi: 10.1001/jama.231.1.39.

39. Noble S (**2013**). Candida albicans specializations for iron homeostasis: from commensalism to virulence. **Curr Opin Microbiol**. 16(6): 1–13. doi: 10.1016/j.mib.2013.09.006.

40. Manns JM, Mosser DM, and Buckley HR (**1994**). Production of a Hemolytic Factor by Candida albicans. .

41. Weissman Z, and Kornitzer D (**2004**). A family of Candida cell surface haem-binding proteins involved in haemin and haemoglobin-iron utilization. **Mol Microbiol**. 53(4): 1209–1220. doi: 10.1111/j.1365-2958.2004.04199.x.

42. Weissman Z, Shemer R, Conibear E, and Kornitzer D (**2008**). An endocytic mechanism for haemoglobin-iron acquisition in *Candida albicans*. **Mol Microbiol**. 69(1): 201–217. doi: 10.1111/j.1365-2958.2008.06277.x.

43. Pendrak ML, Chao MP, Yan SS, and Roberts DD (**2004**). Heme oxygenase in Candida albicans is regulated by hemoglobin and is necessary for metabolism of exogenous heme and hemoglobin to alpha-biliverdin. **J Biol Chem**. 279(5): 3426–33. doi:

10.1074/jbc.M311550200.

44. Andrews NC (**1999**). Disorders of iron metabolism. **N Engl J Med**. 341(26): 1986–95. doi: 10.1056/NEJM199912233412607.

45. Knight SAB, Vilaire G, Lesuisse E, and Dancis A (**2005**). Iron Acquisition from Transferrin by Candida albicans Depends on the Reductive Pathway. **Infect Immun**. 73(9): 5482–5492. doi: 10.1128/IAI.73.9.5482-5492.2005.

46. Moraes TF, Yu R, Strynadka NCJ, and Schryvers AB (**2009**). Insights into the Bacterial Transferrin Receptor: The Structure of Transferrin-Binding Protein B from Actinobacillus pleuropneumoniae. **Mol Cell**. 35(4): 523–533. doi: 10.1016/j.molcel.2009.06.029.

47. Knight SAB, Lesuisse E, Stearman R, Klausner RD, and Dancis A (**2002**). Reductive iron uptake by Candida albicans: Role of copper, iron and the TUP1 regulator. **Microbiology**. 148(1): 29–40. doi: 10.1099/00221287-148-1-29.

48. Ziegler L, Terzulli A, Gaur R, McCarthy R, and Kosman DJ (**2011**). Functional characterization of the ferroxidase, permease high-affinity iron transport complex from Candida albicans. **Mol Microbiol**. 81(2): 473–485. doi: 10.1111/j.1365-2958.2011.07704.x.

49. Weissman Z, Shemer R, and Kornitzer D (**2002**). Deletion of the copper transporter CaCCC2 reveals two distinct pathways for iron acquisition in Candida albicans. **Mol Microbiol**. 44(6): 1551–1560. doi: 10.1046/j.1365-2958.2002.02976.x.

50. Almeida RS, Brunke S, Albrecht A, Thewes S, Laue M, Edwards JE, Jr, Filler SG, and Hube B (**2008**). The Hyphal-Associated Adhesin and Invasin Als3 of Candida albicans Mediates Iron Acquisition from Host Ferritin. **PLoS Pathog**. 4(11): e1000217. doi: 10.1371/JOURNAL.PPAT.1000217.

51. Zhao X, Oh S-H, Cheng G, Green CB, Nuessen JA, Yeater K, Leng RP, Brown AJP, and Hoyer LL (**2004**). ALS3 and ALS8 represent a single locus that encodes a Candida albicans adhesin; functional comparisons between Als3p and Als1p. **Microbiology**. 150(7): 2415–2428. doi: 10.1099/mic.0.26943-0.

52. Cleary IA, Reinhard SM, Miller CL, Murdoch C, Thornhill MH, Lazzell AL, Monteagudo C, Thomas DP, and Saville SP (**2011**). Candida albicans adhesin Als3p is dispensable for virulence in the mouse model of disseminated candidiasis. **Microbiology**. 157(6): 1806–1815. doi: 10.1099/mic.0.046326-0.

53. Neilands JB (**1995**). Siderophores: structure and function of microbial iron transport compounds. **J Biol Chem**. 270(45): 26723–6. doi: 10.1074/jbc.270.45.26723.

54. Heymann P, Gerads M, Schaller M, Dromer F, Winkelmann G, and Ernst JF (**2002**). The siderophore iron transporter of Candida albicans (Sit1p/Arn1p) mediates uptake of ferrichrome-type siderophores and is required for epithelial invasion. **Infect Immun**. 70(9): 5246–55. doi: 10.1128/iai.70.9.5246-5255.2002.

55. Haas H (**2003**). Molecular genetics of fungal siderophore biosynthesis and uptake: the role of siderophores in iron uptake and storage. **Appl Microbiol Biotechnol**. 62(4): 316–330. doi: 10.1007/s00253-003-1335-2.

56. Chen C, Pande K, French SD, Tuch BB, and Noble SM (**2011**). An iron homeostasis

regulatory circuit with reciprocal roles in candida albicans commensalism and pathogenesis. **Cell Host Microbe**. 10(2): 118–135. doi: 10.1016/j.chom.2011.07.005.

57. Singh RP, Prasad HK, Sinha I, Agarwal N, and Natarajan K (**2011**). Cap2-HAP complex is a critical transcriptional regulator that has dual but contrasting roles in regulation of iron homeostasis in Candida albicans. **J Biol Chem**. 286(28): 25154–25170. doi: 10.1074/jbc.M111.233569.

58. Chen C, and Noble SM (**2012**). Post-Transcriptional Regulation of the Sef1 Transcription Factor Controls the Virulence of Candida albicans in Its Mammalian Host. **PLoS Pathog**. 8(11). doi: 10.1371/journal.ppat.1002956.

59. Pande K, Chen C, and Noble SM (**2013**). Passage through the mammalian gut triggers a phenotypic switch that promotes Candida albicans commensalism. **Nat Genet**. 45(9): 1088–1091. doi: 10.1038/ng.2710.

60. Laprade L, Boyartchuk VL, Dietrich WF, and Winston F (**2002**). Spt3 plays opposite roles in filamentous growth in Saccharomyces cerevisiae and Candida albicans and is required for C. albicans virulence. **Genetics**. 161(2): 509–19. 12072450.

61. Braun BR, Head WS, Wang MX, and Johnson AD (**2000**). Identification and characterization of TUP1-regulated genes in Candida albicans. **Genetics**. 156: 31–44. 10978273.

62. Staab JF, Bradway SD, Fidel PL, and Sundstrom P (**1999**). Adhesive and mammalian transglutaminase substrate properties of Candida albicans Hwp1. **Science**. 283(5407): 1535–8. doi: 10.1126/science.283.5407.1535.

63. Bailey DA, Feldmann PJ, Bovey M, Gow NA, and Brown AJ (**1996**). The Candida albicans HYR1 gene, which is activated in response to hyphal development, belongs to a gene family encoding yeast cell wall proteins. **J Bacteriol**. 178(18): 5353–60. 8808922.

64. Gow N a R, Brown AJP, and Odds FC (**2002**). Fungal morphogenesis and host invasion. **Curr Opin Microbiol**. 5(4): 366–371. doi: 10.1016/S1369-5274(02)00338-7.

65. Uhl MA et al. (**2003**). Haploinsufficiency-based large-scale forward genetic analysis of filamentous growth in the diploid human fungal pathogen C.albicans. **EMBO J**. 22(11): 2668–2678. doi: 10.1093/emboj/cdg256.

66. Leberer E, Harcus D, Dignard D, Johnson L, Ushinsky S, Thomas DY, and Schröppel K (**2001**). Ras links cellular morphogenesis to virulence by regulation of the MAP kinase and cAMP signalling pathways in the pathogenic fungus Candida albicans. **Mol Microbiol**. 42(3): 673–687. doi: 10.1046/j.1365-2958.2001.02672.x.

67. Bell WM, and Chaffin WL (**1983**). Effect of yeast growth conditions on yeast-mycelial transition in Candida albicans. **Mycopathologia**. 84(1): 41–44. 6369144.

68. Shapiro RS, Uppuluri P, Zaas AK, Collins C, Senn H, Perfect JR, Heitman J, and Cowen LE (**2009**). Hsp90 Orchestrates Temperature-Dependent Candida albicans Morphogenesis via Ras1-PKA Signaling. **Curr Biol**. 19(8): 621–629. doi: 10.1016/j.cub.2009.03.017.

69. Klengel T, Liang W-J, Chaloupka J, Ruoff C, Schröppel K, Naglik JR, Eckert SE, Mogensen EG, Haynes K, Tuite MF, Levin LR, Buck J, and Mühlschlegel FA (**2005**). Fungal adenylyl

cyclase integrates CO2 sensing with cAMP signaling and virulence. **Curr Biol**. 15(22): 2021–2026. doi: 10.1016/j.cub.2005.10.040.

70. Mattia E, Carruba G, Angiolella L, and Cassone A (**1982**). Induction of Germ Tube Formation by N-Acetyl-D- Glucosamine in Candida albicans: Uptake of Inducer and Germinative Response. **J Bacteriol**. 152(2): 555–562. 6752114.

71. Feng Q, Summers E, Guo B, and Fink G (**1999**). Ras signaling is required for serum-induced hyphal differentiation in Candida albicans. **J Bacteriol**. 181(20): 6339–6346. 10515923.

72. Bockmühl DP, and Ernst JF (**2001**). A potential phosphorylation site for an A-Type kinase in the Efgl regulator protein contributes to hyphal morphogenesis of Candida albicans. **Genetics**. 157(4): 1523–1530. 11290709.

73. Bockmuhl DP, Krishnamurthy S, Gerads M, Sonneborn A, and Ernst JF (**2001**). Distinct and redundant roles of the two protein kinase A isoforms Tpk1p and Tpk2p in morphogenesis and growth of Candida albicans. **Mol Microbiol**. 42(5): 1243–1257. doi: 10.1046/j.1365-2958.2001.02688.x.

74. Giacometti R, Kronberg F, Biondi RM, and Passeron S (**2011**). Candida albicans Tpk1p and Tpk2p isoforms differentially regulate pseudohyphal development, biofilm structure, cell aggregation and adhesins expression. **Yeast**. 28(4): 293–308. doi: 10.1002/yea.1839.

75. Cao C, Wu M, Bing J, Tao L, Ding X, Liu X, and Huang G (**2017**). Global regulatory roles of the cAMP/PKA pathway revealed by phenotypic, transcriptomic and phosphoproteomic analyses in a null mutant of the PKA catalytic subunit in Candida albicans. **Mol Microbiol**. 105(1): 46–64. doi: 10.1111/mmi.13681.

76. Pohlers S, Martin R, Kruger T, Hellwig D, Hanel F, Kniemeyer O, Saluz HP, van Dijck P, Ernst JF, Brakhage A, Muhlschlegel FA, and Kurzai O (**2017**). Lipid Signaling via Pkh1/2 Regulates Fungal CO2 Sensing through the Kinase Sch9. **Am Soc Microbiol**. 8(1): 1–15. doi: 10.1128/mBio.02211-16.

77. Hall RA, de Sordi L, MacCallum DM, Topal H, Eaton R, Bloor JW, Robinson GK, Levin LR, Buck J, Wang Y, Gow NAR, Steegborn C, and Mühlschlegel FA (**2010**). CO2 acts as a signalling molecule in populations of the fungal pathogen Candida albicans. **PLoS Pathog**. 6(11). doi: 10.1371/journal.ppat.1001193.

78. Sheth CC, Johnson E, Baker ME, Haynes K, and Mühlschlegel FA (**2005**). Phenotypic identification of Candida albicans by growth on chocolate agar. **Med Mycol**. 43(8): 735–738. doi: 10.1080/13693780500265998.

79. Xu X-L, Lee RTH, Fang H-M, Wang Y-M, Li R, Zou H, Zhu Y, and Wang Y (**2008**). Bacterial Peptidoglycan Triggers Candida albicans Hyphal Growth by Directly Activating the Adenylyl Cyclase Cyr1p. **Cell Host Microbe**. 4(1): 28–39. doi: 10.1016/j.chom.2008.05.014.

80. Maidan M, De Rop L, Serneels J, Exler S, Rupp S, Tournu H, Thevelein J, and Van Dijck P (**2005**). The G protein-coupled receptor Gpr1 and the Ga protein Gpa2 act through the cAMP-protein kinase A pathway to induce morphogenesis in Candida albicans. **Mol Biol Cell**. 16(1): 1971–1986. doi: 10.1091/mbc.E04.

81. Ivey FD, and Hoffman CS (**2005**). Direct activation of fission yeast adenylate cyclase by

the Gpa2 Galpha of the glucose signaling pathway. **PNAS**. 102(17): 6108–6113. doi: 10.1073/pnas.0502270102.

82. Hollomon JM, Grahl N, Willger SD, Koeppen K, and Hogan DA (**2016**). Global Role of Cyclic AMP Signaling in pH-Dependent Responses in Candida albicans. **mSphere**. 1(6): e00283-16. doi: 10.1128/mSphere.00283-16.

83. Hudson DA, Sciascia QL, Sanders RJ, Norris GE, Edwards PJB, Sullivan PA, and Farley PC (**2004**). Identification of the dialysable serum inducer of germ-tube formation in Candida albicans. **Microbiology**. 150(9): 3041–3049. doi: 10.1099/mic.0.27121-0.

84. Rolland F, De Winde JH, Lemaire K, Boles E, Thevelein JM, and Winderickx J (**2000**). Glucose-induced cAMP signalling in yeast requires both a G-protein coupled receptor system for extracellular glucose detection and a separable hexose kinase-dependent sensing process. **Mol Microbiol**. 38(2): 348–358. doi: 10.1046/j.1365-2958.2000.02125.x.

85. Goswami R, Dadhwal V, Tejaswi S, Datta K, Paul A, Haricharan RN, Banerjee U, and Kochupillai NP (**2000**). Species-specific prevalence of vaginal candidiasis among patients with diabetes mellitus and its relation to their glycaemic status. **J Infect**. 41(2): 162–166. doi: 10.1053/jinf.2000.0723.

86. Guggenheimer J, Moore PA, Rossie K, Myers D, Mongelluzzo MB, Block HM, Weyant R, and Orchard T (**2000**). Insulin-dependent diabetes mellitus and oral soft tissue pathologies. II. Prevalence and characteristics of Candida and candidal lesions. **Oral Surgery, Oral Med Oral Pathol Oral Radiol Endodontology**. 89(5): 570–576. doi: 10.1067/moe.2000.104477.

87. Rodaki A, Bohovych IM, Enjalbert B, Young T, Odds FC, Gow NAR, and Brown AJP (**2009**). Glucose Promotes Stress Resistance in the Fungal Pathogen Candida albicans. **Mol Biol Cell**. 20: 4845–4855. doi: 10.1091/mbc.E09.

88. Zhu Y, Fang HM, Wang YM, Zeng GS, Zheng X De, and Wang Y (**2009**). Ras1 and Ras2 play antagonistic roles in regulating cellular cAMP level, stationary-phase entry and stress response in Candida albicans. **Mol Microbiol**. 74(4): 862–875. doi: 10.1111/j.1365-2958.2009.06898.x.

89. Biswas K, and Morschhäuser J (**2005**). The Mep2p ammonium permease controls nitrogen starvation-induced filamentous growth in Candida albicans. **Mol Microbiol**. 56(3): 649–669. doi: 10.1111/j.1365-2958.2005.04576.x.

90. Liu H, Köhler J, and Fink GR (**1994**). Suppression of hyphal formation in Candida albicans by mutation of a STE12 homolog. **Science (80-)**. 266(5191): 1723–1726. doi: 10.1126/science.7992058.

91. Köhler JR, and Fink GR (**1996**). Candida albicans strains heterozygous and homozygous for mutations in mitogen-activated protein kinase signaling components have defects in hyphal development. **Proc Natl Acad Sci U S A**. 93(23): 13223–13228. 8917572.

92. Leberer E, Harcus D, Broadbent I, Clark KL, Dignard D, Ziegelbauer K, Schmidt A, Gow NAR, Brown AJP, and Thomas DY (**1996**). Signal transduction through homologs of the Ste20p and Ste7p protein kinases can trigger hyphal formation in the pathogenic fungus Candida albicans. **Proc Natl Acad Sci U S A**. 93(23): 13217–13222. 8917571.

93. Csank C, Schroppel K, Leberer E, Harcus D, Mohamed O, Meloche S, Thomas DY, and

Whiteway M (**1998**). Roles of the Candida albicans Mitogen-Activated Protein Kinase Homolog, Cek1p, in Hyphal Development and Systemic Candidiasis†. **Infect Immun**. 66(6): 2713–2721. 9596738.

94. Sanchez-Martinez C, and Perez-Martin J (**2002**). Gpa2, a G-Protein alpha Subunit Required for Hyphal Development in Candida albicans. **Eukaryot Cell**. 1(6): 865–874. doi: 10.1128/EC.1.6.865-874.2002.

95. Hoyer LL, Payne TL, Bell M, Myers AM, and Scherer S (**1998**). Candida albicans ALS3 and insights into the nature of the ALS gene family. **Curr Genet**. 33(6): 451–459. doi: 10.1007/s002940050359.

96. Zheng X, Wang Y, and Wang Y (**2004**). Hgc1, a novel hypha-specific G1 cyclin-related protein regulates Candida albicans hyphal morphogenesis. **EMBO J**. 23(8): 1845–1856. doi: 10.1038/sj.emboj.7600195.

97. Davis D, Edwards J, Mitchell AP, Ibrahim AS, and Edwards JE (**2000**). Candida albicans RIM101 pH response pathway is required for host-pathogen interactions. **Infect Immun**. 68(10): 5953–5959. doi: 10.1128/IAI.68.10.5953-5959.2000.Updated.

98. Brown DH, Giusani AD, Chen X, and Kumamoto CA (**1999**). Filamentous growth of Candida albicans in response to physical environmental cues and its regulation by the unique CZF1 gene. **Mol Microbiol**. 34(4): 651–62. doi: 10.1046/j.1365-2958.1999.01619.x.

99. Shi Q-M, Wang Y-M, Zheng X-D, Teck Ho Lee R, and Wang Y (**2007**). Critical role of DNA checkpoints in mediating genotoxic-stress-induced filamentous growth in Candida albicans. **Mol Biol Cell**. 18: 815–826. doi: 10.1091/mbc.E06.

100. da Silva Dantas A, Patterson MJ, Smith D a, Maccallum DM, Erwig LP, Morgan B a, and Quinn J (**2010**). Thioredoxin regulates multiple hydrogen peroxide-induced signaling pathways in Candida albicans. **Mol Cell Biol**. 30(19): 4550–4563. doi: 10.1128/MCB.00313-10.

101. Braun BR, and Johnson AD (**1997**). Control of Filament Formation in Candida albicans by the Transcriptional Repressor TUP1. **Science (80-)**. 277(5322): 105–109. 9204892.

102. Murad AMA, Leng P, Straffon M, Wishart J, Macaskill S, MacCallum D, Schnell N, Talibi D, Marechal D, Tekaia F, D'Enfert C, Gaillardin C, Odds FC, and Brown AJP (**2001**). NRG1 represses yeast-hypha morphogenesis and hypha-specific gene expression in Candida albicans. **EMBO J**. 20(17): 4742–4752. doi: 10.1093/emboj/20.17.4742.

103. Braun BR, Kadosh D, and Johnson AD (**2001**). NRG1, a repressor of filamentous growth in C.albicans, is down-regulated during filament induction. **EMBO J**. 20(17): 4753–4761. doi: 10.1093/emboj/20.17.4753.

104. Khalaf RA, and Zitomer RS (**2001**). The DNA binding protein Rfg1 is a repressor of filamentation in Candida albicans. **Genetics**. 157(4): 1503–1512. 11290707.

105. Kadosh D, and Johnson AD (**2005**). Induction of the Candida albicans Filamentous Growth Program by Relief of Transcriptional Repression: A Genome-wide Analysis. **Mol Biol Cell**. 16: 2903–2912. doi: 10.1091/mbc.E05.

106. Lu Y, Su C, Wang A, and Liu H (**2011**). Hyphal development in Candida albicans requires

two temporally linked changes in promoter chromatin for initiation and maintenance. **PLoS Biol**. 9(7): e1001105. doi: 10.1371/journal.pbio.1001105.

107. Zarnowski R, Westler WM, Lacmbouh A, Marita JM, Bothe JR, Bernhardt J, Sahraoui AL, Fontaine J, Sanchez H, Hatfield RD, Ntambi JM, Nett JE, Mitchell AP, and Andes R (**2014**). Novel Entries in a Fungal Biofilm Matrix Encyclopedia. **MBio**. 5(4): 1–13. doi: 10.1128/mBio.01333-14.

108. Martins M, Uppuluri P, Thomas DP, Cleary IA, Henriques M, Lopez-Ribot JL, and Oliveira R (**2014**). Presence of extracellular DNA in the Candida albicans biofilm matrix and its contribution to biofilms. **Mycopathologia**. 169(5): 323–331. doi: 10.1007/s11046-009-9264-y.

109. Thomas DP, Bachmann SP, and Lopez-Ribot JL (**2006**). Proteomics for the analysis of the Candida albicans biofilm lifestyle. **Proteomics**. 6(21): 5795–5804. doi: 10.1002/pmic.200600332.

110. Costerton JW, Stewart PS, and Greenberg EP (**1999**). Bacterial biofilms: a common cause of persistent infections. **Science (80-)**. 284(5418): 1318–1322. doi: 10.1126/science.284.5418.1318.

111. Donlan RM (**2001**). Biofilm formation: a clinically relevant microbiological process. **Clin Infect Dis**. 33(8): 1387–1392. doi: 10.1086/322972.

112. Donlan RM (**2001**). Biofilms and Device-Associated Infections. **Emerg Infect Dis**. 7(2): 277–281. doi: 10.3201/eid0702.700277.

113. Nobile CJ, and Johnson AD (**2014**). Candida albicans Biofilms and Human Disease. **Annu Rev Microbiol**. doi: 10.1146/annurev-micro-091014-104330.

114. Donlan RM, and Costerton JW (**2002**). Biofilms: survival mechanisms of clinically relevant microorganisms. **Clin Microbiol Rev**. 15(2): 167–93. doi: 10.1128/CMR.15.2.167-193.2002.

115. Chandra J, Kuhn DM, Mukherjee PK, Hoyer LL, McCormick T, Mahmoud A, Cormick TMC, and Ghannoum MA (**2001**). Biofilm formation by the fungal pathogen Candida albicans: development, architecture, and drug resistance. **J Bacteriol**. 183(18): 5385–5394. doi: 10.1128/JB.183.18.5385-5394.2001.

116. Nett JE, Sanchez H, Cain MT, and Andes DR (**2010**). Genetic Basis of *Candida* Biofilm Resistance Due to Drug-Sequestering Matrix Glucan. **J Infect Dis**. 202(1): 171–175. doi: 10.1086/651200.

117. Nett JE, Crawford K, Marchillo K, and Andes DR (**2010**). Role of Fks1p and matrix glucan in Candida albicans biofilm resistance to an echinocandin, pyrimidine, and polyene. **Antimicrob Agents Chemother**. 54(8): 3505–3508. doi: 10.1128/AAC.00227-10.

118. Verma-Gaur J, Qu Y, Harrison PF, Lo TL, Quenault T, Dagley MJ, Bellousoff M, Powell DR, Beilharz TH, and Traven A (**2015**). Integration of Posttranscriptional Gene Networks into Metabolic Adaptation and Biofilm Maturation in Candida albicans. **PLoS Genet**. 11(10): 1–28. doi: 10.1371/journal.pgen.1005590.

119. Fanning S, and Mitchell AP (**2012**). Fungal biofilms. **PLoS Pathog**. 8(4): 1–4. doi:

10.1371/journal.ppat.1002585.

120. Ramage G, Saville SP, and Thomas DP (**2005**). Candida Biofilms: an Update. **Am Soc Microbiol**. 4(4): 633–638. doi: 10.1128/EC.4.4.633.

121. Willaert RG (**2018**). Adhesins of yeasts: Protein structure and interactions. **J Fungi**. 4(4): 1–28. doi: 10.3390/jof4040119.

122. Lin J, Oh SH, Jones R, Garnett JA, Salgado PS, Rusnakova S, Matthews SJ, Hoyer LL, and Cota E (**2014**). The peptide-binding cavity is essential for ALS3-mediated adhesion of Candida albicans to human cells. **J Biol Chem**. 289(26): 18401–18412. doi: 10.1074/jbc.M114.547877.

123. Beaussart A, Alsteens D, El-Kirat-Chatel S, Lipke PN, Kucharíková S, Van Dijck P, and Dufrêne YF (**2012**). Single-Molecule Imaging and Functional Analysis of Als Adhesins and Mannans during Candida albicans Morphogenesis. **ACS Nano**. 6(12): 10950–10964. doi: 10.1021/nn304505s.

124. Baillie G, and Douglas L (**1999**). Role of dimorphism in the development of Candida albicans biofilms. **J Med Microbiol**. 48(7): 671–679.

125. Lohse MB, Gulati M, Johnson AD, and Nobile CJ (**2017**). Development and regulation of single- and multi-species Candida albicans biofilms. **Nat Rev Microbiol**. 16(1): 19–31. doi: 10.1038/nrmicro.2017.107.

126. Uppuluri P, Chaturvedi AK, Srinivasan A, Banerjee M, Ramasubramaniam AK, Köhler JR, Kadosh D, and Lopez-Ribot JL (**2010**). Dispersion as an important step in the Candida albicans biofilm developmental cycle. **PLoS Pathog**. 6(3). doi: 10.1371/journal.ppat.1000828.

127. Nobile CJ, Fox EP, Nett JE, Sorrells TR, Mitrovich QM, Hernday AD, Tuch BB, Andes DR, and Johnson AD (**2012**). A Recently Evolved Transcriptional Network Controls Biofilm Development in Candida albicans. **Cell**. 148(1–2): 126–138. doi: 10.1016/j.cell.2011.10.048.

128. Fox EP, Bui CK, Nett JE, Hartooni N, Mui MC, Andes DR, Nobile CJ, and Johnson AD (**2015**). An expanded regulatory network temporally controls Candida albicans biofilm formation. **Mol Microbiol**. 96(6): 1226–1239. doi: 10.1111/mmi.13002.

129. Chong PP, Chin VK, Wong WF, Madhavan P, Yong VC, and Looi CY (**2018**). Transcriptomic and genomic approaches for unravelling Candida albicans biofilm formation and drug resistance—an update. **Genes (Basel)**. 9(11): 1–19. doi: 10.3390/genes9110540.

130. Nett JE, Lepak AJ, Marchillo K, and Andes DR (**2009**). Time Course Global Gene Expression Analysis of an In Vivo Candida Biofilm. **J Infect Dis**. 200(2): 307–313. doi: 10.1086/599838.

131. Nobile CJ, and Mitchell AP (**2005**). Regulation of cell-surface genes and biofilm formation by the C. albicans transcription factor Bcr1p. **Curr Biol**. 15(12): 1150–1155. doi: 10.1016/j.cub.2005.05.047.

132. Nobile CJ, Andes DR, Nett JE, Smith FJ, Yue F, Phan QT, Edwards JE, Filler SG, and Mitchell AP (**2006**). Critical role of Bcr1-dependent adhesins in C. albicans biofilm formation in vitro and in vivo. **PLoS Pathog**. 2(7): 0636–0649. doi: 10.1371/journal.ppat.0020063.

133. Nobile CJ, Nett JE, Andes DR, and Mitchell AP (**2006**). Function of Candida albicans adhesin hwp1 in biofilm formation. **Eukaryot Cell**. 5(10): 1604–1610. doi: 10.1128/EC.00194-06.

134. Nobile CJ, Schneider HA, Nett JE, Sheppard DC, Filler SG, Andes DR, and Mitchell AP (**2008**). Complementary Adhesin Function in C. albicans Biofilm Formation. **Curr Biol**. 18(14): 1017–1024. doi: 10.1016/j.cub.2008.06.034.

135. Finkel JS, Xu W, Huang D, Hill EM, Desai J V., Woolford CA, Nett JE, Taff H, Norice CT, Andes DR, Lanni F, and Mitchell AP (**2012**). Portrait of Candida albicans adherence regulators. **PLoS Pathog**. 8(2). doi: 10.1371/journal.ppat.1002525.

136. Okshevsky M, and Meyer RL (**2015**). The role of extracellular DNA in the establishment, maintenance and perpetuation of bacterial biofilms. **Crit Rev Microbiol**. 41(3): 341–352. doi: 10.3109/1040841X.2013.841639.

137. Eckhart L, Fischer H, Barken KB, Tolker-Nielsen T, and Tschachler E (**2007**). DNase1L2 suppresses biofilm formation by Pseudomonas aeruginosa and Staphylococcus aureus. **Br J Dermatol**. 156(6): 1342–1345. doi: 10.1111/j.1365-2133.2007.07886.x.

138. Nobile CJ, Nett JE, Hernday AD, Homann OR, Deneault JS, Nantel A, Andes DR, Johnson AD, and Mitchell AP (**2009**). Biofilm matrix regulation by Candida albicans Zap1. **PLoS Biol**. 7(6). doi: 10.1371/journal.pbio.1000133.

139. Nett JE, Sanchez H, Cain MT, Ross KM, and Andes DR (**2011**). Interface of Candida albicans biofilm matrix-associated drug resistance and cell wall integrity regulation. **Eukaryot Cell**. 10(12): 1660–1669. doi: 10.1128/EC.05126-11.

140. Zarnowski R, Sanchez H, Covelli AS, Dominguez E, Heiss C, Azadi P, Mitchell A, Jaromin A, and Id RA (**2018**). Candida albicans biofilm – induced vesicles confer drug resistance through matrix biogenesis. **PLoS Biol**. 16(10): e2006872. doi: 10.1371/journal.pbio.2006872.

141. Desai J, and Mitchell A (**2015**). Candida albicans biofilm development and its genetic control. **Microbiol Spectr**. 3(3): MB-0005-2014. doi: 10.1128/microbiolspec.MB-0005-2014.

142. Ramage G, VandeWalle K, López-Ribot JL, and Wickes BL (**2002**). The filamentation pathway controlled by the Efg1 regulator protein is required for normal biofilm formation and development in Candida albicans. **FEMS Microbiol Lett**. 214(1): 95–100. doi: 10.1016/S0378-1097(02)00853-4.

143. Lu Y, Su C, Unoje O, and Liu H (**2014**). Quorum sensing controls hyphal initiation in *Candida albicans* through Ubr1-mediated protein degradation. **Proc Natl Acad Sci**. 111(5): 1975–1980. doi: 10.1073/pnas.1318690111.

144. Uppuluri P, Pierce CG, Thomas DP, Bubeck SS, Saville SP, and Lopez-Ribot JL (**2010**). The transcriptional regulator Nrg1p controls Candida albicans biofilm formation and dispersion. **Eukaryot Cell**. 9(10): 1531–1537. doi: 10.1128/EC.00111-10.

145. Nobile CJ, Fox EP, Hartooni N, Mitchell KF, Hnisz D, Andes DR, Kuchler K, and Johnson AD (**2014**). A Histone Deacetylase Complex Mediates Biofilm Dispersal and Drug Resistance in Candida albicans. **MBio**. 5(3): e01201-14. doi: 10.1128/mBio.01201-14.Editor.

146. Sellam A, Al-Niemi T, McInnerney K, Brumfield S, Nantel A, and Suci PA (**2009**). A

Candida albicans early stage biofilm detachment event in rich medium. **BMC Microbiol**. 9: 1–22. doi: 10.1186/1471-2180-9-25.

147. Hawser SP, and Douglas LJ (**1995**). Resistance of Candida albicans biofilms to antifungal agents in vitro. **Antimicrob Agents Chemother**. 39(9): 2128–2131. doi: 10.1128/AAC.39.9.2128.

148. Davis MR, Nguyen M-VH, Donnelley MA, and Thompson III GR (**2019**). Tolerability of long-term fluconazole therapy. **J Antimicrob Chemother**. 74(3): 768–771. doi: 10.1093/jac/dky501.

149. Tsui C, Kong EF, and Jabra-Rizk MA (**2016**). Pathogenesis of Candida albicans biofilm. **Pathog Dis**. 74(4): ftw018. doi: 10.1093/femspd/ftw018.

150. Geber A, Hitchcock CA, Swartz JE, Pullen FS, Marsden KE, Kwon-Chung KJ, and Bennett JE (**1995**). Deletion of the Candida glabrata ERG3 and ERG11 genes: Effect on cell viability, cell growth, sterol composition, and antifungal susceptibility. **Antimicrob Agents Chemother**. 39(12): 2708–2717. doi: 10.1128/AAC.39.12.2708.

151. Sanati H, Belanger P, Fratti R, and Ghannoum M (**1997**). A new triazole, voriconazole (UK-109,496), blocks sterol biosynthesis in Candida albicans and Candida krusei. **Antimicrob Agents Chemother**. 41(11): 2492–2496.

152. Ghannoum MA, and Rice Louis B. (**1999**). Antifungal Agents: Mode of Action, Mechanisms of Resistance, and Correlation of These Mechanisms with Bacterial Resistance. **Clin Microbiol Rev**. 12(4): 501–517.

153. Mathé L, and Van Dijck P (**2013**). Recent insights into Candida albicans biofilm resistance mechanisms. **Curr Genet**. 59: 251–264. doi: 10.1007/s00294-013-0400-3.

154. Borecká-Melkusová S, Moran GP, Sullivan DJ, Kucharíková S, Chorvát D, and Bujdáková H (**2009**). The expression of genes involved in the ergosterol biosynthesis pathway in Candida albicans and Candida dubliniensis biofilms exposed to fluconazole. **Mycoses**. 52(2): 118–128. doi: 10.1111/j.1439-0507.2008.01550.x.

155. Nailis H, Markéta Ř, Dijck P Van, Deforce D, Nelis H, and Coenye T (**2010**). Real-time PCR expression profiling of genes encoding potential virulence factors in Candida albicans biofilms: identification of model-dependent and -independent gene expression. **BMC Microbiol**. 10(114): 1–11.

156. Vediyappan G, Rossignol T, and D'Enfert C (**2010**). Interaction of Candida albicans biofilms with antifungals: Transcriptional response and binding of antifungals to beta-glucans. **Antimicrob Agents Chemother**. 54(5): 2096–2111. doi: 10.1128/AAC.01638-09.

157. Nett J, Lincoln L, Marchillo K, Massey R, Holoyda K, Hoff B, VanHandel M, and Andes D (**2007**). Putative role of β-1,3 glucans in Candida albicans biofilm resistance. **Antimicrob Agents Chemother**. 51(2): 510–520. doi: 10.1128/AAC.01056-06.

158. Mateus C, Crow SA, and Ahearn DG (**2004**). Adherence of Candida albicans to silicone induces immediate enhanced tolerance to fluconazole. **Antimicrob Agents Chemother**. 48(9): 3358–3366. doi: 10.1128/AAC.48.9.3358-3366.2004.

159. Sanglard D, Kuchler K, Ischer F, Pagani JL, Monod M, and Bille J (**1995**). Mechanisms of

resistance to azole antifungal agents in Candida albicans isolates from AIDS patients involve specific multidrug transporters. **Antimicrob Agents Chemother**. 39(11): 2378–86. doi: 10.1128/AAC.39.11.2378.

160. Calabrese D, Sanglard D, and Bille J (**2000**). A novel multidrug efflux transporter gene of the major facilitator superfamily from Candida albicans (FLU1) conferring resistance to fluconazole. **Microbiology**. 146(11): 2743–2754. doi: 10.1099/00221287-146-11-2743.

161. Mukherjee PK, Chandra J, Kuhn DM, and Ghannoum MA (**2003**). Mechanism of fluconazole resistance in Candida albicans biofilms: Phase-specific role of efflux pumps and membrane sterols. **Infect Immun**. 71(8): 4333–4340. doi: 10.1128/IAI.71.8.4333-4340.2003.

162. Perumal P, Mekala S, and Chaffin WLJ (**2007**). Role for cell density in antifungal drug resistance in Candida albicans biofilms. **Antimicrob Agents Chemother**. 51(7): 2454–2463. doi: 10.1128/AAC.01237-06.

163. Knot PD, Suci PA, Miller RL, Nelson RD, and Tyler BJ (**2006**). A small subpopulation of blastospores in Candida albicans biofilms exhibit resistance to amphotericin B associated with differential regulation of ergosterol and β-1,6-glucan pathway genes. **Antimicrob Agents Chemother**. 50(11): 3708–3716. doi: 10.1128/AAC.00997-06.

164. Gale EF (**1986**). Nature and development of phenotypic resistance to amphotericin B in Candida albicans. **Adv Microb Physiol**. 27: 277–320. 3532717.

165. Al-Fattani MA, and Douglas LJ (**2006**). Biofilm matrix of Candida albicans and Candida tropicalis: Chemical composition and role in drug resistance. **J Med Microbiol**. 55(8): 999–1008. doi: 10.1099/jmm.0.46569-0.

166. Denning DW (**2003**). Echinocandin antifungal drugs. **Lancet**. 362(9390): 1142–1151. doi: 10.1016/S0140-6736(03)14472-8.

167. Kuhn DM, George T, Chandra J, Mukherjee PK, and Ghannoum MA (**2002**). Antifungal susceptibility of Candida biofilms: unique efficacy of amphotericin B lipid formulations and echinocandins. **Antimicrob Agents Chemother**. 46(6): 1773–80. doi: 10.1128/AAC.46.6.1773.

168. Hacioglu M, Birteksoz Tan AS, Dosler S, Inan N, and Otuk G (**2018**). In vitro activities of antifungals alone and in combination with tigecycline against Candida albicans biofilms . **PeerJ**. 6: e5263. doi: 10.7717/peerj.5263.

169. Kucharíková S, Sharma N, Spriet I, Maertens J, Van Dijck P, and Lagrou K (**2013**). Activities of systemically administered echinocandins against in Vivo mature Candida albicans biofilms developed in a rat subcutaneous model. **Antimicrob Agents Chemother**. 57(5): 2365–2368. doi: 10.1128/AAC.02288-12.

170. Vermes, A., Guchelaar, H. J., & Dankert J (**2000**). Flucytosine: a review of its pharmacology, clinical indications, pharmacokinetics, toxicity and drug interactions. **J Antimicrob Chemother**. 46(2): 171–179.

171. Polak A, and Scholer HJ (**1975**). Mode of action of 5-fluorocytosine and mechanisms of resistance. **Chemotherapy**. 21(3–4): 113–30. doi: 10.1159/000221854.

172. LaFleur MD, Kumamoto CA, and Lewis K (**2006**). Candida albicans biofilms produce

antifungal-tolerant persister cells. **Antimicrob Agents Chemother**. 50(11): 3839–3846. doi: 10.1128/AAC.00684-06.

173. Al-Dhaheri RS, and Douglas LJ (**2008**). Absence of amphotericin B-tolerant persister cells in biofilms of some Candida species. **Antimicrob Agents Chemother**. 52(5): 1884–1887. doi: 10.1128/AAC.01473-07.

174. Hawser SP, Baillie GS, and Douglas LJ (**1998**). Production of extracellular matrix by Candida albicans biofilms. **J Med Microbiol**. 47(3): 253–256. doi: 10.1099/00222615-47-3-253.

175. Uppuluri P, Chaturvedi AK, and Lopez-Ribot JL (**2009**). Design of a simple model of Candida albicans biofilms formed under conditions of flow: Development, architecture, and drug resistance. **Mycopathologia**. 168(3): 101–109. doi: 10.1007/s11046-009-9205-9.

176. Ramage G, Jose A, Sherry L, Lappin DF, Jones B, and Williams C (**2013**). Liposomal amphotericin b displays rapid dose-dependent activity against Candida albicans Biofilms. **Antimicrob Agents Chemother**. 57(5): 2369–2371. doi: 10.1128/AAC.02344-12.

177. Schinabeck MK, Long LA, Hossain MA, Chandra J, Mukherjee PK, Mohamed S, and Ghannoum MA (**2004**). Rabbit Model of Candida albicans Biofilm Infection: Liposomal Amphotericin B Antifungal Lock Therapy. **Antimicrob Agents Chemother**. 48(5): 1727–1732. doi: 10.1128/AAC.48.5.1727-1732.2004.

178. Gao Y, Zhang C, Lu C, Liu P, Li Y, Li H, and Sun S (**2013**). Synergistic effect of doxycycline and fluconazole against Candida albicans biofilms and the impact of calcium channel blockers. **FEMS Yeast Res**. 13(5): 453–462. doi: 10.1111/1567-1364.12048.

179. Stepanović S, Vuković D, Ješić M, and Ranin L (**2004**). Influence of acetylsalicylic acid (Aspirin) on biofilm production by Candida species. **J Chemother**. 16(2): 134–138. doi: 10.1179/joc.2004.16.2.134.

180. Zhou Y, Wang G, Li Y, Liu Y, Song Y, Zheng W, Zhang N, Hu X, Yan S, and Jia J (**2012**). In vitro interactions between aspirin and amphotericin B against planktonic cells and biofilm cells of Candida albicans and C. parapsilosis. **Antimicrob Agents Chemother**. 56(6): 3250–3260. doi: 10.1128/AAC.06082-11.

181. Bink A, Kucharíková S, Neirinck B, Vleugels J, Van Dijck P, Cammue BPA, and Thevissen K (**2012**). The nonsteroidal antiinflammatory drug diclofenac potentiates the in vivo activity of caspofungin against candida albicans biofilms. **J Infect Dis**. 206(11): 1790–1797. doi: 10.1093/infdis/jis594.

182. Rashki Ghalehnoo Z, Rashki A, Najimi M, and Dominguez A (**2010**). The role of diclofenac sodium in the dimorphic transition in Candida albicans. **Microb Pathog**. 48(3–4): 110–115. doi: 10.1016/j.micpath.2009.12.003.

183. De Cremer K, De Brucker K, Staes I, Peeters A, Van den Driessche F, Coenye T, Cammue BPA, and Thevissen K (**2016**). Stimulation of superoxide production increases fungicidal action of miconazole against Candida albicans biofilms. **Sci Rep**. 6(1): 27463. doi: 10.1038/srep27463.

184. Yan Y, Tan F, Miao H, Wang H, and Cao YY (**2019**). Effect of Shikonin against Candida albicans Biofilms. **Front Microbiol**. 10(MAY): 1–11. doi: 10.3389/fmicb.2019.01085.

185. Farkash Y, Feldman M, Ginsburg I, Steinberg D, and Shalish M (**2018**). Green Tea Polyphenols and Padma Hepaten Inhibit Candida albicans Biofilm Formation. **Evidence-based Complement Altern Med**. 2018. doi: 10.1155/2018/1690747.

186. Coenye T, and Nelis HJ (**2010**). In vitro and in vivo model systems to study microbial biofilm formation. **J Microbiol Methods**. 83(2): 89–105. doi: 10.1016/j.mimet.2010.08.018.

187. Niu C, and Gilbert ES (**2004**). Colorimetric Method for Identifying Plant Essential Oil Components That Affect Biofilm Formation and Structure. **Appl Environ Microbiol**. 70(12): 6951–6956. doi: 10.1128/AEM.70.12.6951.

188. Grubb SEW, Murdoch C, Sudbery PE, Saville SP, Lopez-Ribot JL, and Thornhill MH (**2009**). Adhesion of Candida albicans to endothelial cells under physiological conditions of flow. **Infect Immun**. 77(9): 3872–3878. doi: 10.1128/IAI.00518-09.

189. Richter L, Stepper C, Mak A, Reinthaler A, Heer R, Kast M, Brückl H, and Ertl P (**2007**). Development of a microfluidic biochip for online monitoring of fungal biofilm dynamics. **Lab Chip**. 7: 1723–1731. doi: 10.1039/b708236c.

190. Martinez LR, Mihu MR, Tar M, Cordero RJB, Han G, Friedman AJ, Friedman JM, and Nosanchuk JD (**2010**). Demonstration of antibiofilm and antifungal efficacy of chitosan against candidal biofilms, using an in vivo central venous catheter model. **J Infect Dis**. 201(9): 1436–1440. doi: 10.1086/651558.

191. Li F, Svarovsky MJ, Karlsson AJ, Wagner JP, Marchillo K, Oshel P, Andes D, and Palecek SP (**2007**). Eap1p, an adhesin that mediates Candida albicans biofilm formation in vitro and in vivo. **Eukaryot Cell**. 6(6): 931–939. doi: 10.1128/EC.00049-07.

192. Leonhard M, and Schneider-Stickler B (**2015**). Voice prostheses, microbial colonization and biofilm formation. **Adv Exp Med Biol**. 830: 123–36.

193. Cancer Research UK (**2018**). Head and neck cancers incidence statistics. Cancer Res. UK. Available at https://www.cancerresearchuk.org/health-professional/cancer-statistics/statistics-by-cancer-type/head-and-neck-cancers/incidence [Accessed 10/31/2018].

194. Brook I (**2013**). The Laryngectomee Guide. .

195. Ticac B, Ticac R, Rukavina T, Kesovija P, Pedisic D, Maljevac B, and Starcevic R (**2010**). Microbial colonization of tracheoesophageal voice prostheses (Provox2) following total laryngectomy. **Eur Arch Otorhinolaryngol**. 267(10): 1579–86.

196. Delank K, and Scheuermann K (**2008**). Practical aspects of voice prosthesis use after laryngectomy. **Laryngorhinootologie**. 87(3): 160–6.

197. Ceachir O, Hainarosie R, and Zainea V (**2014**). Total laryngectomy - Past, Present, Future. **Maedica (Buchar)**. 9(2): 210–6. 25705281.

198. Bunting GW (**2004**). Voice following laryngeal cancer surgery: Troubleshooting common problems after tracheoesophageal voice restoration. **Otolaryngol Clin North Am**. 37(3): 597–612. doi: 10.1016/j.otc.2004.01.007.

199. Holmes AR, Rodrigues E, van der Wielen P, Lyons KM, Haigh BJ, Wheeler TT, Dawes PJD,

and Cannon RD (**2014**). Adherence of Candida albicans to silicone is promoted by the human salivary protein SPLUNC2/PSP/BPIFA2. **Mol Oral Microbiol**. 29(2): 90–98. doi: 10.1111/omi.12048.

200. Neu T, Verkerke G, Herrmann I, Schutte H, Van der Mei H, and Busscher H (**1994**). Microflora on explanted silicone rubber voice prostheses: taxonomy, hydrophobicity and electrophoretic mobility. **J Appl Bacteriol**. 76(5): 521–8.

201. Sayed S, Kazi R, Sengupta S, Chowdhari A, and Jagade M (**2012**). Microbial colonization of Blom-Singer indwelling voice prostheses in laryngectomized patients: a perspective from India. **Ear, Nose Throat J**. 91(4): E19-22.

202. Bauters TGM, Moerman M, Vermeersch H, and Nelis HJ (**2002**). Colonization of voice prostheses by albicans and non-albicans Candida species. **Laryngoscope**. 112(4): 708–712. doi: 10.1097/00005537-200204000-00021.

203. Schafer P, Klutzke N, and Schwerdtfeger FP (**2001**). Voice restoration with voice prosthesis after total laryngectomy. Assessment of survival time of 378 Provox-1, Provox-2 and Blom Singer voice prosthesis. **Laryngorhinootologie**. 80: 677–681.

204. Buijssen KJDA, van der Laan BFAM, van der Mei HC, Atema-Smit J, van den Huijssen P, Busscher HJ, and Harmsen HJM (**2012**). Composition and architecture of biofilms on used voice prostheses. **Head Neck**. 34(6): 863–71. doi: 10.1002/hed.21833.

205. Chaturvedi P, Syed S, Pawar P, Kelkar R, Biswas S, Datta S, Nair D, Chaukar D, and D'cruz A (**2014**). Microbial colonization of Provox voice prosthesis in the Indian scenario. **Indian J Cancer**. 51(2): 184. doi: 10.4103/0019-509X.138303.

206. Arweiler-Harbeck D, Sanders A, Held M, Jerman M, Ehrich H, and Jahnke K (**2001**). Does metal coating improve the durability of silicone voice prostheses? **Acta Otolaryngol**. 121(5): 643–6. 11583401.

207. Dijk F, Westerhof M, Busscher HJ, van Luyn MJ, and van Der Mei HC (**2000**). In vitro formation of oropharyngeal biofilms on silicone rubber treated with a palladium/tin salt mixture. **J Biomed Mater Res**. 51(3): 408–12. 10880083.

208. Kress P, Schäfer P, and Schwerdtfeger F-P (**2006**). [Clinical use of a voice prosthesis with a flap valve containing silver oxide (Blom-Singer Advantage), biofilm formation, in-situ lifetime and indication] Article in German. **Laryngo-Rhino-Otologie**. 85(12): 893–896. doi: 10.1055/s-2006-925292.

209. Everaert EP, van de Belt-Gritter B, van der Mei HC, Busscher HJ, Verkerke GJ, Dijk F, Mahieu HF, and Reitsma A (**1998**). In vitro and in vivo microbial adhesion and growth on argon plasma-treated silicone rubber voice prostheses. **J Mater Sci Mater Med**. 9(3): 147–57. 15348904.

210. Everaert EPJM, Van Der Mei HC, and Busscher HJ (**1998**). Adhesion of yeasts and bacteria to fluoro-alkylsiloxane layers chemisorbed on silicone rubber. **Colloids Surfaces B Biointerfaces**. 10(4): 179–190. doi: 10.1016/S0927-7765(98)00003-4.

211. Everaert EP, Mahieu HF, van de Belt-Gritter B, Peeters AJ, Verkerke GJ, van der Mei HC, and Busscher HJ (**1999**). Biofilm formation in vivo on perfluoro-alkylsiloxane-modified voice prostheses. **Arch Otolaryngol Head Neck Surg**. 125(12): 1329–32. 10604410.

212. Gottenbos B, Van Der Mei HC, Klatter F, Nieuwenhuis P, and Busscher HJ (**2002**). In vitro and in vivo antimicrobial activity of covalently coupled quaternary ammonium silane coatings on silicone rubber. **Biomaterials**. 23(6): 1417–1423. doi: 10.1016/S0142-9612(01)00263-0.

213. Oosterhof JJH, Buijssen KJDA, Busscher HJ, Van Der Laan BFAM, and Van Der Mei HC (**2006**). Effects of quaternary ammonium silane coatings on mixed fungal and bacterial biofilms on tracheoesophageal shunt prostheses. **Appl Environ Microbiol**. 72(5): 3673–3677. doi: 10.1128/AEM.72.5.3673-3677.2006.

214. Free RH, Elving GJ, van Weissenbruch R, Busscher HJ, vander Mei HC, and Albers FWJ (**2001**). Biofilm Formation on Voice Prostheses: In vitro Influence of Probiotics. **Ann Otol Rhinol Laryngol**. 110(10): 946–951. doi: 10.1177/000348940111001010.

215. Busscher HJ, van Hoogmoed CG, Geertsema-Doornbusch GI, van der Kuijl-Booij M, and van der Mei HC (**1997**). Streptococcus thermophilus and its biosurfactants inhibit adhesion by Candida spp. on silicone rubber. **Appl Environ Microbiol**. 63(10): 3810–7. 9327543.

216. Busscher HJ, Bruinsma G, van Weissenbruch R, Leunisse C, van der Mei HC, Dijk F, and Albers FW (**1998**). The effect of buttermilk consumption on biofilm formation on silicone rubber voice prostheses in an artificial throat. **Eur Arch Otorhinolaryngol**. 255(8): 410–3. 9801860.

217. Mahieu HF, van Saene HKF, Rosingh HJ, and Schutte HK (**1986**). Candida Vegetations on Silicone Voice Prostheses. **Arch Otolaryngol - Head Neck Surg**. 112(3): 321–325. doi: 10.1001/archotol.1986.03780030085017.

218. Van Weissenbruch R, Nelis HJ, Bouckaert S, Aerts R, Remon J-P, and Albers FWJ (**1997**). Chemoprophylaxis of Fungal Deterioration of the Provox Silicone Tracheoesophageal Prosthesis in Postlaryngectomy Patients. **Ann Otol Rhinol Laryngol**. 106(4): 329–337. doi: 10.1177/000348949710600413.

219. Helmerhorst EJ, Reijnders IM, Van 'T Hof W, Simoons-Smit I, Veerman ECI, and Amerongen AVN (**1999**). Amphotericin B- and fluconazole-resistant Candida spp., Aspergillus fumigatus, and other newly emerging pathogenic fungi are susceptible to basic antifungal peptides. **Antimicrob Agents Chemother**. 43(3): 702–704.

220. Oosterhof JJH, Elving GJ, Stokroos I, Van Nieuw Amerongen A, Van Der Mei HC, Busscher HJ, Van Weissenbruch R, and Albers FWJ (**2003**). The Influence of Antimicrobial Peptides and Mucolytics on the Integrity of Biofilms Consisting of Bacteria and Yeasts as Affecting Voice Prosthetic Air Flow Resistances. **Biofouling**. 19(6): 347–353. doi: 10.1080/08927010310001612054.

221. Lewin JS, Baumgart LM, Barrow MP, and Hutcheson KA (**2017**). Device life of the tracheoesophageal voice prosthesis revisited. **JAMA Otolaryngol - Head Neck Surg**. 143(1): 65–71. doi: 10.1001/jamaoto.2016.2771.

222. Arthurs GJ, and Sudhakar M (**2005**). Carbon dioxide transport. **Contin Educ Anaesthesia, Crit Care Pain**. 5(6): 207–210. doi: 10.1093/bjaceaccp/mki050.

223. Busscher H, Geertsema-Doornbusch GI, and van der Mei HC (**1997**). Adhesion to silicone rubber of yeasts and bacteria isolated from voice prostheses: influence of salivary

conditioning films. **J Biomed Mater Res**. 34(2): 201–9. 9029300.

224. Leunisse C, van Weissenbruch R, Busscher HJ, van der Mei HC, Dijk F, and Albers FW (**2001**). Biofilm formation and design features of indwelling silicone rubber tracheoesophageal voice prostheses--an electron microscopical study. **J Biomed Mater Res**. 58(5): 556–63. 11505431.

225. Oosterhof JJH, Van Der Mei HC, Busscher HJ, Free RH, Kaper HJ, Van Weissenbruch R, and Albers FWJ (**2005**). In vitro leakage susceptibility of tracheoesophageal shunt prostheses in the absence and presence of a biofilm. **J Biomed Mater Res - Part B Appl Biomater**. 73(1): 23–28. doi: 10.1002/jbm.b.30167.

226. Hilgers FJM, Ackerstaff AH, Balm AJM, Van Den Brekel MWM, Tan IB, and Persson JO (**2003**). A New Problem-solving Indwelling Voice Prosthesis, Eliminating the Need for Frequent Candida- and "Underpressure"-related Replacements: Provox ActiValve. **Acta Otolaryngol**. 123(8): 972–979. doi: 10.1080/00016480310015371.

227. Hilgers FJM, Ackerstaff AH, Jacobi I, Balm AJM, Tan IB, and Van Den Brekel MWM (**2009**). Prospective clinical phase II study of two new indwelling voice prostheses (provox vega 22.5 and 20 Fr) and a novel anterograde insertion device (provox smart inserter). **Laryngoscope**. 120(6): 1135–1143. doi: 10.1002/lary.20925.

228. Kress P, Schäfer P, Schwerdtfeger FP, and Rösler S (**2014**). Are modern voice prostheses better? A lifetime comparison of 749 voice prostheses. **Eur Arch Oto-Rhino-Laryngology**. 271(1): 133–140. doi: 10.1007/s00405-013-2611-0.

229. Hu Z, Zhang J, Chen Z, Jin Z, Leng P, Zhou J, and Xie X (**2019**). Matrix-assisted laser desorption/ionization time-of-flight mass spectrometric identification and antifungal susceptibility analysis of Candida species isolated from patients with invasive yeast infections in five university hospitals. **Brazilian J Microbiol**. 50(1): 99–105. doi: 10.1007/s42770-018-0027-0.

230. Kumar K, Askari F, Sahu M, and Kaur R (**2019**). Candida glabrata: A Lot More Than Meets the Eye. **Microorganisms**. 7(2): 39. doi: 10.3390/microorganisms7020039.

231. Inácio CP, de Araújo PSR, Brayner FA, Alves LC, Veras DL, and Neves RP (**2019**). Invasive Candida tropicalis Infection Caused by Catheter Biofilm in a Patient with Tongue Cancer. **Mycopathologia**. 0123456789. doi: 10.1007/s11046-018-0316-z.

232. Wang J, Zhang Z, Zhang M, Yang B, Wang T, Sun X, Chen X, Zhang MY, Guo ZY, and Jiang X (**2019**). A rare primary Candida parapsilosis infection of the knee joint in a patient without predisposing factors. **Medicine (Baltimore)**. 98(6): e14327. doi: 10.1097/MD.0000000000014327.

233. Gobom J, Schuerenberg M, Mueller M, Theiss D, Lehrach H, and Nordhoff E (**2001**). α-Cyano-4-hydroxycinnamic Acid Affinity Sample Preparation . A Protocol for MALDI-MS Peptide Analysis in Proteomics. **Anal Chem**. 73(3): 434–438. doi: 10.1021/ac001241s.

234. European Committee on Antimicrobial Susceptibility Testing (**2018**). Clinical Breakpoints for Antifungals. EUCAST. Available at http://www.eucast.org/astoffungi/clinicalbreakpointsforantifungals/ [Accessed 01/16/2019].

235. The European Committee on Antimicrobial Susceptibility Testing (**2019**). EUCAST Reading Guide for Broth Microdilution. Version 1.(January).

236. European Committee on Antimicrobial Susceptibility Testing (**2019**). Clinical Breakpoints for Bacteria. EUCAST. Available at http://www.eucast.org/clinical_breakpoints/ [Accessed 01/16/2019].

237. Kuhn DM, Chandra J, Mukherjee PK, and Ghannoum M a (**2002**). Comparison of Biofilms Formed by Candida albicans and Candida parapsilosis on Bioprosthetic Surfaces. **Infect Immun**. 70(2): 878–888. doi: 10.1128/IAI.70.2.878.

238. Kim S, Lee D, Lee S-J V., Kim D, Son HG, Lee H, Yang J-S, and Han SK (**2016**). OASIS 2: online application for survival analysis 2 with features for the analysis of maximal lifespan and healthspan in aging research. **Oncotarget**. 7(35). doi: 10.18632/oncotarget.11269.

239. van Weissenbruch R, Albers F, Bouckaert S, Nelis H, Criel G, Remon J, and Sulter A (**1997**). Deterioration of the Provox silicone tracheoesophageal voice prosthesis: microbial aspects and structural changes. **Acta Otolaryngol**. 117(3): 452–8. 9199534.

240. Everaert E, Mahieu H, Wong Chung R, Verkerke G, van der Mei H, and Busscher H (**1997**). A new method for in vivo evaluation of biofilms on surface-modified silicone rubber voice prostheses. **Eur Arch Otorhinolaryngol**. 254(6): 261–3.

241. Kong EF, Tsui C, Kucharíková S, and Andes D (**2016**). Commensal Protection of Staphylococcus aureus against Antimicrobials by Candida albicans Biofilm Matrix. 7(5): 1–12. doi: 10.1128/mBio.01365-16.Editor.

242. Lin YJ, Alsad L, Vogel F, Koppar S, Nevarez L, Auguste F, Seymour J, Syed A, Christoph K, and Loomis JS (**2013**). Interactions between Candida albicans and Staphylococcus aureus within mixed species biofilms. **Bios**. 84(1): 30–39. doi: 10.1893/0005-3155-84.1.30.

243. Radford DR, Sweet SP, Challacombe SJ, and Walter JD (**1998**). Adherence of Candida albicans to denture-base materials with different surface finishes. **J Dent**. 26(7): 577–83. 9754746.

244. Nevzatoğlu EU, Özcan M, Kulak-Ozkan Y, and Kadir T (**2007**). Adherence of Candida albicans to denture base acrylics and silicone-based resilient liner materials with different surface finishes. **Clin Oral Investig**. 11(3): 231–236. doi: 10.1007/s00784-007-0106-3.

245. Tsoukias NM, Tannous Z, Wilson AF, and George SC (**1998**). Single-exhalation profiles of NO and CO2 in humans: effect of dynamically changing flow rate. **J Appl Physiol**. 85(2): 642–652. doi: 10.1152/jappl.1998.85.2.642.

246. Coates AR, Halls G, and Hu Y (**2011**). Novel classes of antibiotics or more of the same? **Br J Pharmacol**. 163(1): 184–194. doi: 10.1111/j.1476-5381.2011.01250.x.

247. Harriott MM, and Noverr MC (**2009**). Candida albicans and Staphylococcus aureus form polymicrobial biofilms: Effects on antimicrobial resistance. **Antimicrob Agents Chemother**. 53(9): 3914–3922. doi: 10.1128/AAC.00657-09.

248. Melkoumov A, Goupil M, Louhichi F, Raymond M, De Repentigny L, and Leclair G (**2013**). Nystatin nanosizing enhances in vitro and in vivo antifungal activity against Candida albicans. **J Antimicrob Chemother**. 68(9): 2099–2105. doi: 10.1093/jac/dkt137.

249. Ribeiro MA, Dietze R, Paula CR, Da Matta DA, and Colombo AL (**2001**). Susceptibility profile of vaginal yeast isolates from Brazil. **Mycopathologia**. 151(1): 5–10. doi: 10.1023/A:1010909504071.

250. Singh S, Bhargava P, Sobel JD, Boikov D, and Vazquez JA (**2002**). Vaginitis Due to Candida krusei: Epidemiology, Clinical Aspects, and Therapy. **Clin Infect Dis**. 35(9): 1066–1070. doi: 10.1086/343826.

251. Nenoff P, Krüger C, Neumeister C, Schwantes U, and Koch D (**2016**). In vitro susceptibility testing of yeasts to nystatin – low minimum inhibitory concentrations suggest no indication of in vitro resistance of Candida albicans, Candida species or non-Candida yeast species to nystatin. **Clin Med Investig**. 1(3). doi: 10.15761/CMI.1000116.

252. Havenaar R, and Huis In't Veld JHJ (**1992**). Probiotics: A General View. In: Lact. Acid Bact. Vol. 1. **Springer US, Boston, MA**; pp 151–170.

253. Soukka T, Tenovuo J, and Lenander-Lumikari M (**1992**). Fungicidal effect of human lactoferrin against Candida albicans. **FEMS Microbiol Lett**. 69(3): 223–8. 1555756.

254. Nikawa H, Samaranayake LP, Tenovuo J, Pang KM, and Hamada T (**1993**). The fungicidal effect of human lactoferrin on Candida albicans and Candida krusei. **Arch Oral Biol**. 38(12): 1057–63. 8141667.

255. Soukka T, Lumikari M, and Tenovuo J (**1991**). Combined inhibitory effect of lactoferrin and lactoperoxidase system on the viability of Streptococcus mutans, serotype c. **Scand J Dent Res**. 99(5): 390–6. 1754841.

256. McCormack MG, Smith AJ, Akram AN, Jackson M, Robertson D, and Edwards G (**2015**). Staphylococcus aureus and the oral cavity: An overlooked source of carriage and infection? **Am J Infect Control**. 43(1): 35–37. doi: 10.1016/j.ajic.2014.09.015.

257. Klotz SA, Chasin BS, Powell B, Gaur NK, and Lipke PN (**2007**). Polymicrobial bloodstream infections involving Candida species: analysis of patients and review of the literature. **Diagn Microbiol Infect Dis**. 59(4): 401–406. doi: 10.1016/j.diagmicrobio.2007.07.001.

258. Schlecht LM, Peters BM, Krom BP, Freiberg JA, Hänsch GM, Filler SG, Jabra-Rizk MA, and Shirtliff ME (**2015**). Systemic Staphylococcus aureus infection mediated by Candida albicans hyphal invasion of mucosal tissue. **Microbiol (United Kingdom)**. 161(1): 168–181. doi: 10.1099/mic.0.083485-0.

259. Carlson E (**1982**). Synergistic effect of Candida albicans and Staphylococcus aureus on mouse mortality. **Infect Immun**. 38(3): 921–924.

260. Carlson E (**1983**). Effect of Strain of Staphylococcus aureus on Synergism with Candida albicans Resulting in Mouse Mortality and Morbidity. **Infect Immun**. 42(1): 285–292.

261. Silva S, Henriques M, Martins A, Oliveira R, Williams D, and Azeredo J (**2009**). Biofilms of non-Candida albicans Candida species: Quantification, structure and matrix composition. **Med Mycol**. 47(7): 681–689. doi: 10.3109/13693780802549594.

262. Buijssen KJDA, Harmsen HJM, van der Mei HC, Busscher HJ, and van der Laan BFAM (**2007**). Lactobacilli: Important in biofilm formation on voice prostheses. **Otolaryngol - Head Neck Surg**. 137(3): 505–507. doi: 10.1016/j.otohns.2007.05.051.

263. Otoo HN, Kyeng GL, Qiu W, and Lipke PN (**2008**). Candida albicans Als adhesins have conserved amyloid-forming sequences. **Eukaryot Cell**. 7(5): 776–782. doi: 10.1128/EC.00309-07.

264. Lipke PN, Garcia MC, Alsteens D, Ramsook CB, Klotz SA, and Dufrêne YF (**2012**). Strengthening relationships: amyloids create adhesion nanodomains in yeasts. **Trends Microbiol**. 20(2): 59–65. doi: 10.1016/j.tim.2011.10.002.

265. Alsteens D, Garcia MC, Lipke PN, and Dufrêne YF (**2010**). Force-induced formation and propagation of adhesion nanodomains in living fungal cells. **Proc Natl Acad Sci U S A**. 107(48): 20744–20749. doi: 10.1073/pnas.1013893107.

266. Chan CXJ, Joseph IG, Huang A, Jackson DN, and Lipke PN (**2015**). Quantitative analyses of force-induced amyloid formation in Candida albicans Als5p: Activation by standard laboratory procedures. **PLoS One**. 10(6): 1–13. doi: 10.1371/journal.pone.0129152.

267. Garcia MC, Lee JT, Ramsook CB, Alsteens D, Dufrêne YF, and Lipke PN (**2011**). A role for amyloid in cell aggregation and biofilm formation. **PLoS One**. 6(3). doi: 10.1371/journal.pone.0017632.

268. Monnin E, Indermuhle A, Dallenbach A, Fluckiger J, Stauffer B, Stocker T, Raynaud D, and Barnola J (**2001**). Atmospheric CO2 Concentrations over the Last Glacial Termination. **Science (80-)**. 291(5501): 112–114. doi: 10.1126/science.291.5501.112.

269. Homann OR, Dea J, Noble SM, and Johnson AD (**2009**). A Phenotypic Profile of the Candida albicans Regulatory Network. **PLoS Genet**. 5(12): e1000783. doi: 10.1371/journal.pgen.1000783.

270. Afgan E, Baker D, Batut B, Van Den Beek M, Bouvier D, Ech M, Chilton J, Clements D, Coraor N, Grüning BA, Guerler A, Hillman-Jackson J, Hiltemann S, Jalili V, Rasche H, Soranzo N, Goecks J, Taylor J, Nekrutenko A, and Blankenberg D (**2018**). The Galaxy platform for accessible, reproducible and collaborative biomedical analyses: 2018 update. **Nucleic Acids Res**. 46(W1): W537–W544. doi: 10.1093/nar/gky379.

271. Andrews S (**2010**). FASTQC: a quality control tool for high throughput sequence data. Babraham Bioinforma. Available at http://www.bioinformatics.babraham.ac.uk/projects/fastqc .

272. Krueger F (**2012**). TrimGalore: A wrapper tool around Cutadapt and FastQC to consistently apply quality and adapter trimming to FastQ files. Babraham Bioinforma. Available at https://www.bioinformatics.babraham.ac.uk/projects/trim_galore/ .

273. Kim D, Langmead B, and Salzberg SL (**2015**). HISAT: A fast spliced aligner with low memory requirements. **Nat Methods**. 12(4): 357–360. doi: 10.1038/nmeth.3317.

274. Candida Genome Database (**2017**). Index of /download/gff/C_albicans_SC5314/Assembly21. Available at http://www.candidagenome.org/download/gff/C_albicans_SC5314/Assembly21/ [Accessed 03/22/2018].

275. Anders S, Pyl PT, and Huber W (**2015**). HTSeq-A Python framework to work with high-throughput sequencing data. **Bioinformatics**. 31(2): 166–169. doi: 10.1093/bioinformatics/btu638.

276. Love MI, Huber W, and Anders S (**2014**). Moderated estimation of fold change and dispersion for RNA-seq data with DESeq2. **Genome Biol**. 15(12): 1–21. doi: 10.1186/s13059-014-0550-8.

277. Subramanian A, Tamayo P, Mootha VK, Mukherjee S, Ebert BL, Gillette M a, Paulovich A, Pomeroy SL, Golub TR, Lander ES, and Mesirov JP (**2005**). Gene set enrichment analysis: a knowledge-based approach for interpreting genome-wide expression profiles. **Proc Natl Acad Sci U S A**. 102(43): 15545–50. doi: 10.1073/pnas.0506580102.

278. Sellam A, van het Hoog M, Tebbji F, Beaurepaire C, Whiteway M, and Nantelc A (**2014**). Modeling the transcriptional regulatory network that controls the early hypoxic response in Candida albicans. **Eukaryot Cell**. 13(5): 675–690. doi: 10.1128/EC.00292-13.

279. Inglis DO, Arnaud MB, Binkley J, Shah P, Skrzypek MS, Wymore F, Binkley G, Miyasato SR, Simison M, and Sherlock G (**2012**). The Candida genome database incorporates multiple Candida species: Multispecies search and analysis tools with curated gene and protein information for Candida albicans and Candida glabrata. **Nucleic Acids Res**. 40(D1): 667–674. doi: 10.1093/nar/gkr945.

280. Cherry JM, Hong EL, Amundsen C, Balakrishnan R, Binkley G, Chan ET, Christie KR, Costanzo MC, Dwight SS, Engel SR, Fisk DG, Hirschman JE, Hitz BC, Karra K, Krieger CJ, Miyasato SR, Nash RS, Park J, Skrzypek MS, Simison M, Weng S, and Wong ED (**2012**). Saccharomyces Genome Database: the genomics resource of budding yeast. **Nucleic Acids Res**. 40(Database issue): D700-5. doi: 10.1093/nar/gkr1029.

281. Merico D, Isserlin R, Stueker O, Emili A, and Bader GD (**2010**). Enrichment map: A network-based method for gene-set enrichment visualization and interpretation. **PLoS One**. 5(11). doi: 10.1371/journal.pone.0013984.

282. Srikantha T, Daniels KJ, Pujol C, Kim E, and Soll DR (**2013**). Identification of genes upregulated by the transcription factor bcr1 that are involved in impermeability, impenetrability, and drug resistance of Candida albicans a/α biofilms. **Eukaryot Cell**. 12(6): 875–888. doi: 10.1128/EC.00071-13.

283. Pérez A, Pedrós B, Murgui A, Casanova M, López-Ribot JL, and Martínez JP (**2006**). Biofilm formation by Candida albicans mutants for genes coding fungal proteins exhibiting the eight-cysteine-containing CFEM domain. **FEMS Yeast Res**. 6(7): 1074–1084. doi: 10.1111/j.1567-1364.2006.00131.x.

284. O'Connor L, Lahiff S, Casey F, Glennon M, Cormican M, and Maher M (**2005**). Quantification of ALS1 gene expression in Candida albicans biofilms by RT-PCR using hybridisation probes on the LightCycler™. **Mol Cell Probes**. 19(3): 153–162. doi: 10.1016/j.mcp.2004.10.007.

285. Kraidlova L, Schrevens S, Tournu H, Van Zeebroeck G, Sychrova H, and Van Dijck P (**2016**). Characterization of the Candida albicans Amino Acid Permease Family: Gap2 Is the Only General Amino Acid Permease and Gap4 Is an S -Adenosylmethionine (SAM) Transporter Required for SAM-Induced Morphogenesis. **mSphere**. 1(6): 1–19. doi: 10.1128/mSphere.00284-16.

286. Yokoyama K, Kaji H, Nishimura K, and Miyaji M (**1990**). The role of microfilaments and microtubules in apical growth and dimorphism of Candida albicans. **J Gen Microbiol**. 136(6):

1067–1075. doi: 10.1099/00221287-136-6-1067.

287. Belmont LD, Hyman AA, Sawin KE, and Mitchison TJ (**1990**). Real-time visualization of cell cycle-dependent changes in microtubule dynamics in cytoplasmic extracts. **Cell**. 62(3): 579–589. doi: 10.1016/0092-8674(90)90022-7.

288. Gachet Y, Tournier S, Millar JBA, and Hyams JS (**2001**). A MAP kinase-dependent actin checkpoint ensures proper spindle orientation in fission yeast. **Nature**. 412(6844): 352–355. doi: 10.1038/35085604.

289. Synnott JM, Guida A, Mulhern-Haughey S, Higgins DG, and Butler G (**2010**). Regulation of the Hypoxic Response in Candida albicans. **Eukaryot Cell**. 9(11): 1734–1746. doi: 10.1128/ec.00159-10.

290. Puri S, Kumar R, Rojas IG, Salvatori O, and Edgerton M (**2019**). Iron Chelator Deferasirox Reduces Candida albicans Invasion of Oral Epithelial Cells and Infection Levels in Murine Oropharyngeal Candidiasis. **Antimicrob Agents Chemother**. 63(4). doi: 10.1128/AAC.02152-18.

291. DiPaola R (**2014**). A Phase I/II Trial of 2-Deoxyglucose (2DG) for the Treatment of Advanced Cancer and Hormone Refractory Prostate Cancer (2-Deoxyglucose). ClinicalTrials.gov. Available at https://clinicaltrials.gov/ct2/show/results/NCT00633087 [Accessed 08/05/2019].

292. Lu Y, Su C, Ray S, Yuan Y, and Haoping L (**2019**). CO2 Signaling through the Ptc2-Ssn3 Axis Governs Sustained Hyphal Development of Candida albicans by Reducing Ume6 Phosphorylation and Degradation. **Am J Med**. 10(1): e02320-18.

293. Fang HM, and Wang Y (**2006**). RA domain-mediated interaction of Cdc35 with Ras1 is essential for increasing cellular cAMP level for Candida albicans hyphal development. **Mol Microbiol**. 61(2): 484–496. doi: 10.1111/j.1365-2958.2006.05248.x.

294. Yeater KM, Chandra J, Cheng G, Mukherjee PK, Zhao X, Rodriguez-Zas SL, Kwast KE, Gannoum MA, and Hoyer LL (**2007**). Temporal analysis of Candida albicans gene expression during biofilm development. **Microbiology**. 153(8): 2373–2385. doi: 10.1099/mic.0.2007/006163-0.

295. Baek YU, Li M, and Davis DA (**2008**). Candida albicans ferric reductases are differentially regulated in response to distinct forms of iron limitation by the Rim101 and CBF transcription factors. **Eukaryot Cell**. 7(7): 1168–1179. doi: 10.1128/EC.00108-08.

296. El-Ghaouth A, Wilson CL, and Wisniewski M (**1997**). Antifungal activity of 2-deoxy-D-glucose on Botrytis cinerea, Penicillium expansum, and Rhizopus stolonifer: Ultrastructural and cytochemical aspects. **Phytopathology**. 87(7): 772–779. doi: 10.1094/PHYTO.1997.87.7.772.

297. Sutrina SL, Griffith MSJ, and Lafeuillee C (**2016**). 2-Deoxy-D-Glucose Is a Potent Inhibitor of Biofilm Growth in Escherichia Coli. **Microbiol (United Kingdom)**. 162(6): 1037–1046. doi: 10.1099/mic.0.000290.

298. Rocha CR, Schröppel K, Harcus D, Marcil a, Dignard D, Taylor BN, Thomas DY, Whiteway M, and Leberer E (**2001**). Signaling through adenylyl cyclase is essential for hyphal growth and virulence in the pathogenic fungus Candida albicans. **Mol Biol Cell**. 12(11):

3631–3643. doi: 10.1091/mbc.12.11.3631.

299. Peters BM, Jabra-Rizk MA, O'May GA, William Costerton J, and Shirtliff ME (**2012**). Polymicrobial interactions: Impact on pathogenesis and human disease. **Clin Microbiol Rev**. 25(1): 193–213. doi: 10.1128/CMR.00013-11.

300. Peters BM, Jabra-Rizk MA, Scheper MA, Leid JG, Costerton JW, and Shirtliff ME (**2010**). Microbial interactions and differential protein expression in Staphylococcus aureus -Candida albicans dual-species biofilms. **FEMS Immunol Med Microbiol**. 59(3): 493–503. doi: 10.1111/j.1574-695X.2010.00710.x.

301. Hogan DA, and Kolter R (**2002**). Pseudomonas-Candida interactions: An ecological role for virulence factors. **Science (80-)**. 296(5576): 2229–2232. doi: 10.1126/science.1070784.

302. Bandara HMHN, Yau JYY, Watt RM, Jin LJ, and Samaranayake LP (**2010**). Pseudomonas aeruginosa inhibits in-vitro Candida biofilm development. **BMC Microbiol**. 10(1): 125. doi: 10.1186/1471-2180-10-125.

303. Haiko J, Saeedi B, Bagger G, Karpati F, and Özenci V (**2019**). Coexistence of Candida species and bacteria in patients with cystic fibrosis. **Eur J Clin Microbiol Infect Dis**. 38(6): 1071–1077. doi: 10.1007/s10096-019-03493-3.

304. Fourie, and Pohl (**2019**). Beyond Antagonism: The Interaction Between Candida Species and Pseudomonas aeruginosa. **J Fungi**. 5(2): 34. doi: 10.3390/jof5020034.

305. Neely AN, Law EJ, and Holder IA (**1986**). Increased susceptibility to lethal Candida infections in burned mice preinfected with Pseudomonas aeruginosa or pretreated with proteolytic enzymes. **Infect Immun**. 52(1): 200–204.

306. Paulitsch AH, Willinger B, Zsalatz B, Stabentheiner E, Marth E, and Buzina W (**2009**). In-vivo Candida biofilms in scanning electron microscopy. **Med Mycol**. 47(7): 690–696. doi: 10.3109/13693780802635237.

307. Coco BJ, Bagg J, Cross LJ, Jose A, Cross J, and Ramage G (**2008**). Mixed Candida albicans and Candida glabrata populations associated with the pathogenesis of denture stomatitis. **Oral Microbiol Immunol**. 23(5): 377–383. doi: 10.1111/j.1399-302X.2008.00439.x.

308. Kucharíková S, Neirinck B, Sharma N, Vleugels J, Lagrou K, and Van Dijck P (**2015**). In vivo Candida glabrata biofilm development on foreign bodies in a rat subcutaneous model. **J Antimicrob Chemother**. 70(3): 846–856. doi: 10.1093/jac/dku447.

309. Silva S, Henriques MC, Hayes A, Oliveira R, Azeredo J, and Williams DW (**2011**). Candida glabrata and Candida albicans co-infection of an in vitro oral epithelium. **J Oral Pathol Med**. 40(5): 421–427. doi: 10.1111/j.1600-0714.2010.00981.x.

310. Fox EP, Cowley ES, Nobile CJ, Hartooni N, Newman DK, and Johnson AD (**2014**). Anaerobic bacteria grow within candida albicans biofilms and induce biofilm formation in suspension cultures. **Curr Biol**. 24(20): 2411–2416. doi: 10.1016/j.cub.2014.08.057.

311. Amorim-Vaz S, Coste AT, Sanglarda D, Tran VDT, Pradervand S, and Pagni M (**2015**). RNA enrichment method for quantitative transcriptional analysis of pathogens in vivo applied to the fungus candida albicans. **MBio**. 6(5): 1–16. doi: 10.1128/mBio.00942-15.

312. Hennigar SR, and McClung JP (**2016**). Nutritional Immunity. **Am J Lifestyle Med**. 10(3): 170–173. doi: 10.1177/1559827616629117.

313. Jenssen H, and Hancock REW (**2009**). Antimicrobial properties of lactoferrin. **Biochimie**. 91(1): 19–29. doi: 10.1016/j.biochi.2008.05.015.

314. Nasser L, Weissman Z, Pinsky M, Amartely H, Dvir H, and Kornitzer D (**2016**). Structural basis of haem-iron acquisition by fungal pathogens. **Nat Microbiol**. 1(11): 1–10. doi: 10.1038/nmicrobiol.2016.156.

315. Brian Mochon A, Ye J, Kayala MA, Wingard JR, Clancy CJ, Hong Nguyen M, Felgner P, Baldi P, and Liu H (**2010**). Serological profiling of a Candida albicans protein microarray reveals permanent host-pathogen interplay and stage-specific responses during Candidemia. **PLoS Pathog**. 6(3). doi: 10.1371/journal.ppat.1000827.

316. Wick AN, Drury DR, Nakada HI, and Wolfe JB (**1957**). Localization of the primary metabolic block produced by 2-deoxyglucose. **J Biol Chem**. 224(2): 963–9. 13405925.

317. Chen W, and Guéron M (**1992**). The inhibition of bovine heart hexokinase by 2-deoxy-d-glucose-6-phosphate: characterization by 31P NMR and metabolic implications. **Biochimie**. 74(9–10): 867–873. doi: 10.1016/0300-9084(92)90070-U.

318. Ralser M, Wamelink MM, Struys EA, Joppich C, Krobitsch S, Jakobs C, and Lehrach H (**2008**). A catabolic block does not sufficiently explain how 2-deoxy-D-glucose inhibits cell growth. **Proc Natl Acad Sci U S A**. 105(46): 17807–11. doi: 10.1073/pnas.0803090105.

319. Juul S, Izquierdo F, Hurst A, Dai X, Wright A, Kulesha E, Pettett R, and Turner DJ (**2015**). What's in my pot? Real-time species identification on the MinION. **bioRxiv**. 030742. doi: 10.1101/030742.

320. Kinoshita E, Kinoshita-Kikuta E, and Koike T (**2012**). Phos-tag SDS-PAGE systems for phosphorylation profiling of proteins with a wide range of molecular masses under neutral pH conditions. **Proteomics**. 12(2): 192–202. doi: 10.1002/pmic.201100524.

321. Illumina (**2011**). Quality Scores for Next-Generation Sequencing. **Tech Note Seq**. 1–2.

322. Lever J, Krzywinski M, and Altman N (**2017**). Points of Significance: Principal component analysis. **Nat Methods**. 14(7): 641–642. doi: 10.1038/nmeth.4346.

Appendix 1 – Quality control analysis of RNA-Seq reads

Total RNA was extracted in biological triplicate from *C. albicans* CAI-4 biofilms grown for 48h in both 0.03% and 5% CO_2 using the E.Z.N.A.^{TM} Yeast RNA Kit as per the manufacturer's instructions with a few modifications as detailed in the Paper 2 Materials and Methods. After extraction, RNA purity was estimated using a NanoDrop ND-1000 spectrophotometer and sent to the Centre for Genome Enabled Biology and Medicine (Aberdeen, UK) for library preparation and sequencing. Sequencing was performed on the Illumina NextSeq500 platform, producing 75bp single-end reads.

The quality of the RNA sequencing reads was checked using FastQC [271] on the Galaxy web platform [270]. FastQC provides visual readouts of the quality of raw sequencing data; giving information on basic statistics (average sequence length, number of sequences and number of poor quality sequences), Phred score (the probability of a base being wrong), and adaptor content (the amount of adaptor contamination in the reads), among others. The information obtained from FastQC was used to determine if any trimming of the sequencing reads was required before further analysis. For all samples, low quality ends (Phred score < 20) and any adaptor sequences were trimmed using TrimGalore!. After trimming, 97.7% of initial reads remained and FastQC was run again to confirm the quality. Below are the FastQC outputs after trimming for the 3 replicates in each CO_2 condition.

Basic Statistics

The basic statistics reveal an average sequencing depth of 58M reads across the 3 replicates in each condition. They also conclude that there were no sequences flagged as poor quality in any of the samples after trimming. The sequence length of the reads after trimming was 40-52 bases in all samples (Appendix Table 1.1).



Basic Statistics

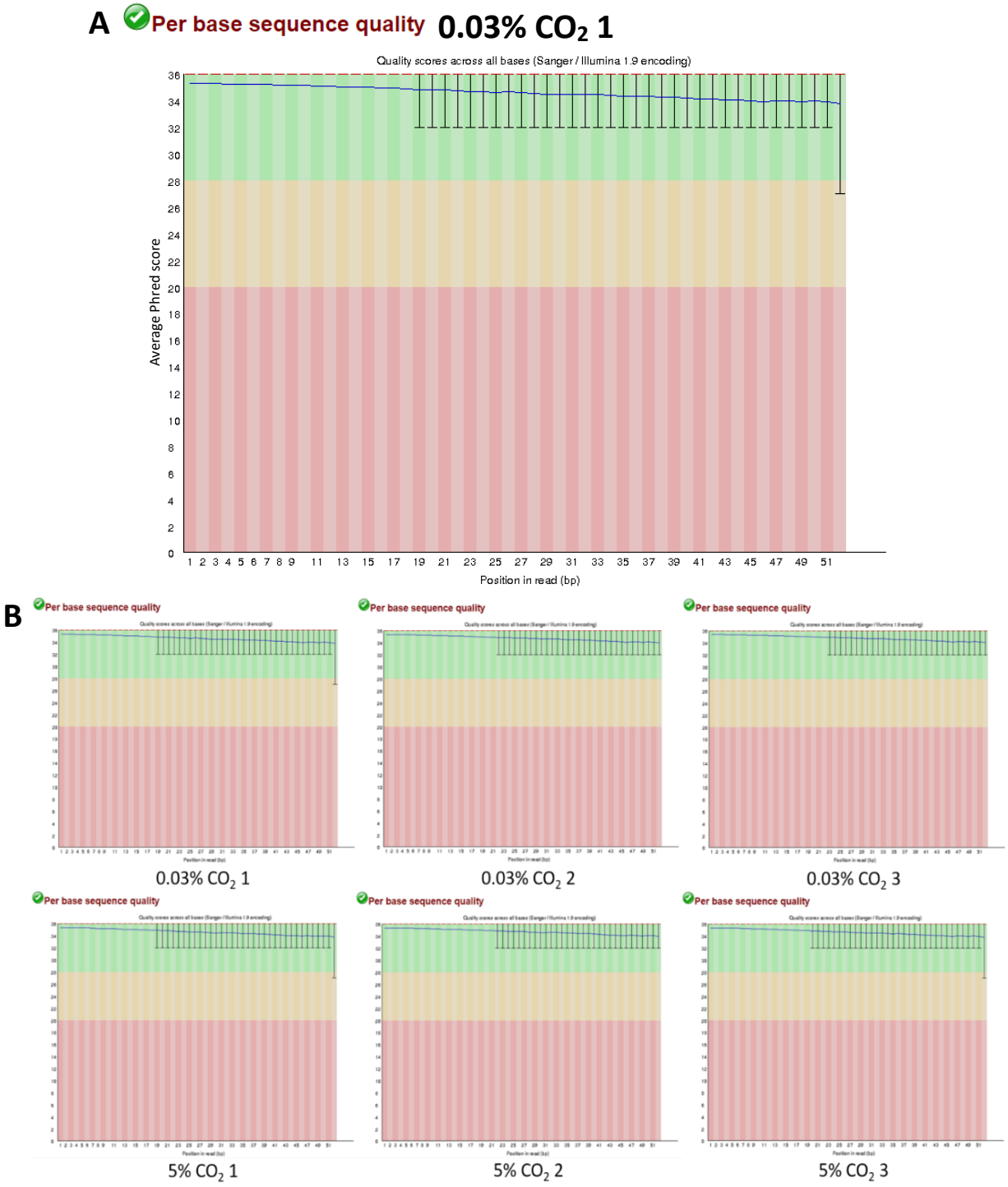
Measure	Value
Filename	Trim_Galore__on_data_233__trimmed_reads
File type	Conventional base calls
Encoding	Sanger / Illumina 1.9
Total Sequences	54050500
Sequences flagged as poor quality	0
Sequence length	40-52
%GC	41

Appendix Table 1.1: Basic statistics output from FastQC analysis of the RNA sequencing reads from the 0.03% CO_2 biofilm replicate 1 sample. This table is representative of all the samples.

Phred Score

The Phred score is a measure of the probability that a base within a sequencing read has been called wrong, thereby giving an estimation of the quality of the sequencing reaction and hence resulting reads. It is a logarithmic scale from 1-40, the higher the number the lower the probability of the base being wrong. A base with a Phred score of 30 indicates a 1 in 1000 probability of that base being identified incorrectly during the Illumina sequencing reaction. This corresponds to an accuracy of 99.9% and thus reads with Phred scores above 30 are generally considered good quality for next-generation sequencing (NGS) applications such as RNA-Seq [321]. For all 6 samples, the Phred scores were very high throughout the whole length of all the reads (Appendix Figure 1.1B). There is a natural reduction in Phred score

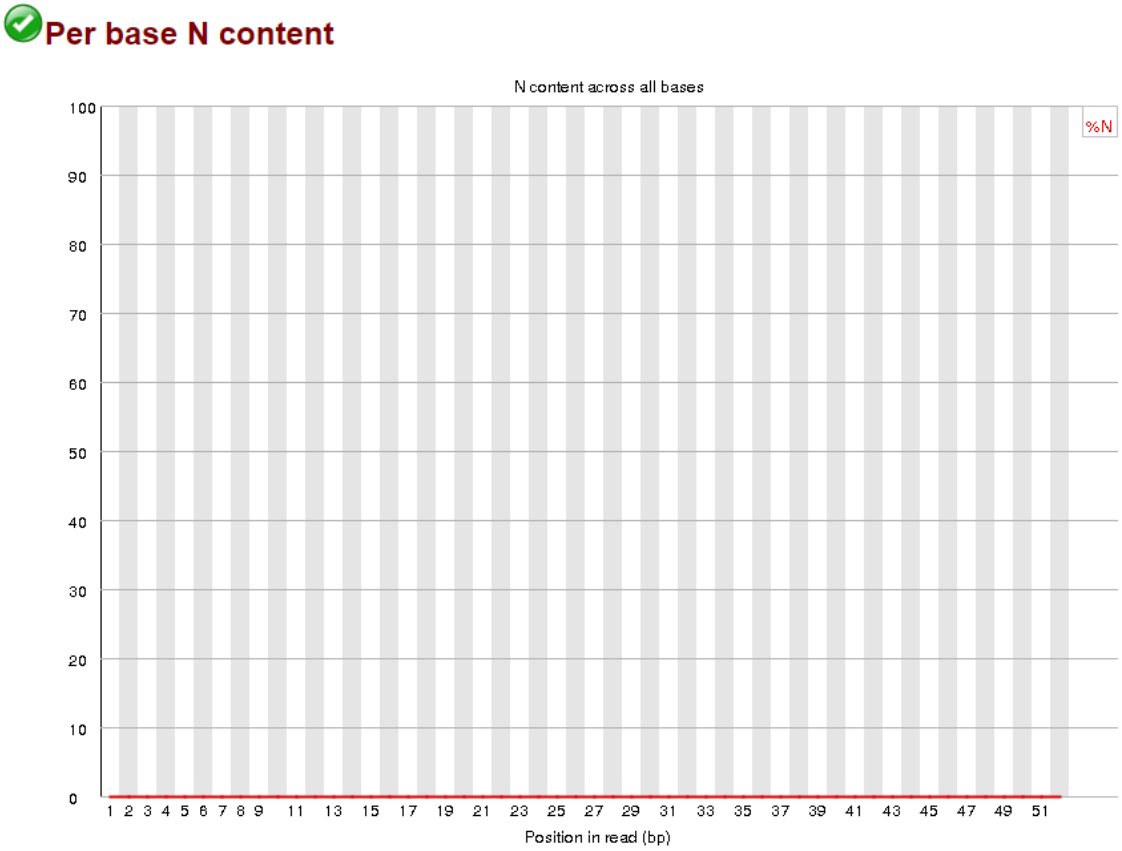
across the length of the read as an artefact of the sequencing reaction and this cannot be avoided. Despite this, even the last few bases in each read still had Phred scores above 30 (Appendix Figure 1.1A). The average Phred score per read across all 6 samples was 35.



Appendix Figure 1.1: Phred score visualisations giving the average Phred score for each base across the length of the sequencing reads. (A) Average Phred scores for bases within reads in the 0.03% CO_2 biofilm replicate 1 sample. **(B)** Average Phred scores for bases within reads for all 6 samples. Note: 0.03% CO_2 replicate 1 is included again.

N Content

The N content gives an indication of the number of ambiguous reads present in a sample, i.e. the number of reads which contain at least one base which was unable to be called and hence is denoted as N. There were no ambiguous reads in any of the 6 samples (Appendix Figure 1.2).

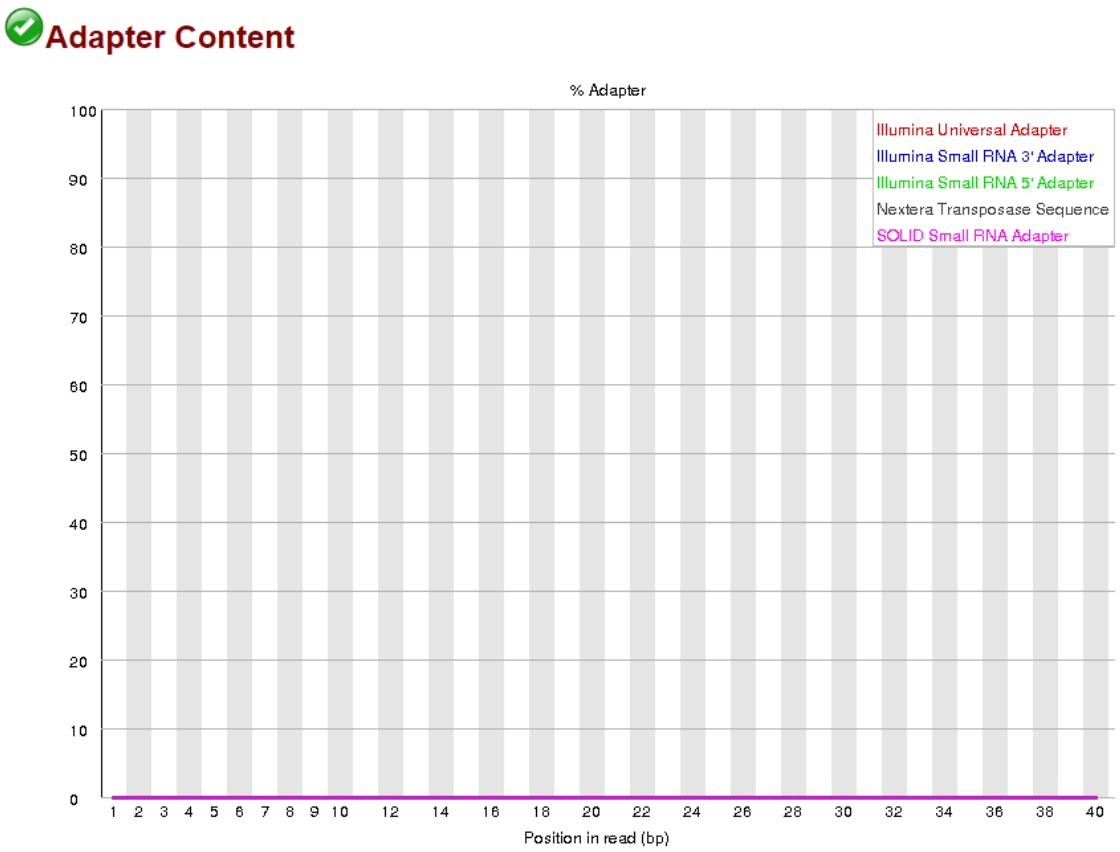


Appendix Figure 1.2: N content across all bases within the reads of the 0.03% CO_2 biofilm replicate 1 sample. Graph was identical to that above for all samples.

Adaptor Content

The adaptor content gives a quantification of any contamination of reads with adaptor sequences originating from the library preparation**.** Adaptor contamination can lead to alignment errors when aligning to a reference genome since the adaptor sequences will not appear in the genome. Thus, it is important to trim reads to remove any adaptor sequences

which could influence steps downstream. After trimming, there were no adaptor sequences remaining in reads from any of the samples (Appendix Figure 1.3).



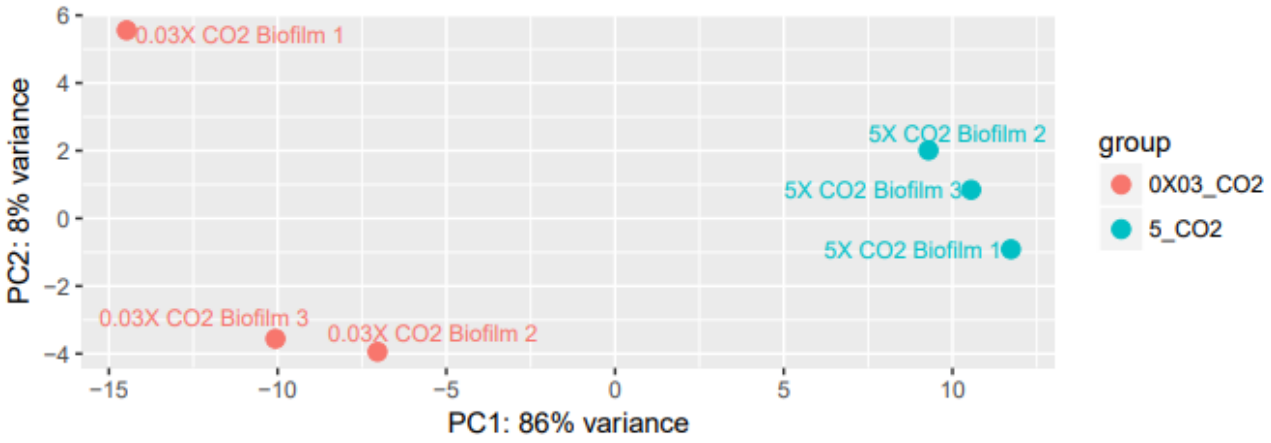
Appendix Figure 1.3: Adaptor content across bases within the reads of the 0.03% CO_2 biofilm replicate 1 sample. Graph was identical to that above for all samples.

Principal Component Analysis

Principal component analysis (PCA) is a useful method for visualising large data sets to determine how similar biological replicates of a sample are to each other, and how different they are to samples from other conditions. PCA was carried out within the DESeq2 package [276] as part of the differential gene expression analysis. The PCA reduces the dimensionality of the data by identifying directions (principal components) along which most variation occurs, simplifying very large data sets while retaining as much information as possible [322]. This allows for easier comparisons. The first principal component, PC1, is the direction along

which most of the variation occurs. The second principal component, PC2, covers as much as possible of the remaining variation.

Samples are displayed on a graph based on the two principal components (Figure 4); clustering indicates similarity, thus, the closer two points are together, the greater the similarity between those two samples. The biological replicates of the two conditions cluster well along the PC1 axis. The biological replicates of the 5% CO_2 biofilms also cluster well along the PC2 axis, whereas the 0.03% CO_2 Biofilm 2 and 0.03% CO_2 Biofilm 3 samples cluster along the PC2 axis but the 0.03% CO_2 Biofilm 1 sample does not (Appendix Figure 1.4). The reasons for this lack of clustering are unclear. However, we decided to retain the 0.03% CO_2 biofilm 1 sample in subsequent differential gene expression analysis because it still clusters with the other 0.03% CO_2 replicates along the PC1 axis which is the direction where most variation occurs. Thus, the 0.03% CO_2 biofilm 1 sample is still closer to the other 0.03% CO_2 replicates than the 5% CO_2 samples.



Appendix Figure 1.4: Principal component analysis of 0.03% CO_2 and 5% CO_2 RNA-Seq samples. Principal component analysis was performed using the DESeq2 package as part of the differential gene expression

Appendix 2 – Ranked GSEA gene set lists

Below are lists of genes which are significantly differentially expressed, false-discovery-rate (q) values ≤ 0.05, in *C. albicans* biofilms grown in 5% CO_2 compared to those grown in 0.03% CO_2 (atmospheric air). The genes are organised into the gene sets in which they appear within the gene set database used for Gene Set Enrichment Analysis.

Gene sets with genes enriched in the upregulated group of differentially expressed genes

These gene sets are for pathways which the GSEA concluded are significantly upregulated within 5% CO_2 biofilms. The rank in gene list refers to the position of the gene in the overall list of significantly differentially expressed genes in this study ranked with regards to log2 fold change. The running enrichment score is a running tally as a quantitative measure of how much each gene contributes to the overall gene set/pathway being upregulated as measured via GSEA. Genes which cause the running enrichment score to increase, known as the leading edge subset (green – prior to the highest score), are those which have the greatest contribution to the overall enrichment at the top of the ranked list.

BRG1_TF

Rank in Gene List	Gene Identifier	Gene Name	Log2 Fold Change	Running Enrichment Score
1	orf19.5741	ALS1	3.7669	0.0145
4	orf19.4934	OP4	3.3214	0.0268
5	orf19.4211	FET31	3.1690	0.0393
7	orf19.5267	C1_11990W_A	3.1051	0.0512
8	orf19.4438	RME1	3.0969	0.0634
9	orf19.3643	C6_00810C_A	3.0665	0.0755
13	orf19.849	MNN41	2.9716	0.0861
21	orf19.5728	C6_03600C_A	2.6549	0.0939
22	orf19.6715	C3_07720C_A	2.6148	0.1042
23	orf19.1286	C5_04040C_A	2.6036	0.1145

25	orf19.5604	MDR1	2.5564	0.1242
26	orf19.851	MNN42	2.5559	0.1343
30	orf19.4933	FAD3	2.4966	0.1430
37	orf19.6713	WOR4	2.4007	0.1502
39	orf19.2023	HGT7	2.3851	0.1592
40	orf19.7218	RBE1	2.3719	0.1686
41	orf19.97	CAN1	2.3381	0.1778
46	orf19.1932	CFL4	2.2907	0.1853
49	orf19.7094	HGT12	2.2631	0.1935
50	orf19.2332	C1_10850W_A	2.2465	0.2024
54	orf19.54	RHD1	2.2299	0.2100
55	orf19.2725	C4_02730C_A	2.2163	0.2188
59	orf19.6547	C7_01770W_A	2.1587	0.2262
60	orf19.4884	WOR1	2.1534	0.2347
62	orf19.2738	SUL2	2.1449	0.2427
65	orf19.5933	C3_04730C_A	2.1167	0.2503
69	orf19.218	BUD20	2.1019	0.2575
81	orf19.454	SFL1	1.9628	0.2611
83	orf19.3674	GAL102	1.9457	0.2684
85	orf19.6276	C1_06350W_A	1.9402	0.2757
86	orf19.6983	C3_05450C_A	1.9390	0.2833
92	orf19.4231	PTH2	1.8930	0.2889
93	orf19.2356	CRZ2	1.8902	0.2964
99	orf19.4555	ALS4	1.8730	0.3019
102	orf19.935	AGA1	1.8553	0.3084
103	orf19.5625	C6_03360C_A	1.8474	0.3157
104	orf19.258	C3_02660W_A	1.8340	0.3229
116	orf19.7150	NRG1	1.7552	0.3257
118	orf19.3668	HGT2	1.7445	0.3322
122	orf19.1743	ACS1	1.7279	0.3379
127	orf19.5908	TEC1	1.6893	0.3431
136	orf19.3182	GIS2	1.6607	0.3466
142	orf19.7054	C7_00650W_A	1.6351	0.3512
145	orf19.5302	PGA31	1.6212	0.3568
148	orf19.6488	C7_02250W_A	1.6081	0.3624
157	orf19.5307	JEN2	1.5563	0.3655
164	orf19.5070	C1_07990C_A	1.5436	0.3693
167	orf19.1224	FRP3	1.5343	0.3746
176	orf19.3368	C4_03420C_A	1.4951	0.3775
209	orf19.3675	GAL7	1.3944	0.3710
210	orf19.6736	C3_07550C_A	1.3852	0.3764
225	orf19.450	C1_05150C_A	1.3508	0.3765
229	orf19.5032	SIM1	1.3375	0.3806
231	orf19.7436	AAF1	1.3322	0.3855

240	orf19.1189	C6_00290W_A	1.3141	0.3877
241	orf19.5475	C3_00020W_A	1.3109	0.3928
246	orf19.3795	AGP3	1.2958	0.3965
258	orf19.7151	C7_04220W_A	1.2797	0.3974
271	orf19.3672	GAL10	1.2536	0.3978
279	orf19.723	BCR1	1.2419	0.4000
283	orf19.2781	C1_07640C_A	1.2380	0.4038
290	orf19.871	C2_03500W_A	1.2183	0.4063
301	orf19.4784	CRP1	1.1956	0.4073
306	orf19.6054	C1_00540C_A	1.1753	0.4104
315	orf19.2024	C2_00990W_A	1.1524	0.4119
317	orf19.918	CDR11	1.1521	0.4161
355	orf19.740	HAP41	1.0953	0.4065
363	orf19.5474	C3_00010C_A	1.0793	0.4081
373	orf19.6514	CUP9	1.0667	0.4089
375	orf19.7095	C7_00270W_A	1.0640	0.4128
389	orf19.3867	RPL7	1.0450	0.4120
405	orf19.5232	CSI2	1.0221	0.4104
408	orf19.1416	COX11	1.0184	0.4136
415	orf19.3195	HIP1	1.0059	0.4153
416	orf19.3670	GAL1	1.0030	0.4193
438	orf19.449	C1_05160C_A	0.9844	0.4153
462	orf19.6937	PTR22	0.9548	0.4104
468	orf19.674	C1_11280W_A	0.9483	0.4122
471	orf19.6486	LDG3	0.9477	0.4152
472	orf19.1971	TRY3	0.9474	0.4189
480	orf19.4942	C1_13150W_A	0.9421	0.4200
484	orf19.4783	C1_09240C_A	0.9391	0.4226
517	orf19.4459	C1_03870C_A	0.9121	0.4141
519	orf19.1736	CR_04680C_A	0.9104	0.4174
529	orf19.4056	BRG1	0.9001	0.4175
531	orf19.3618	YWP1	0.8988	0.4207
534	orf19.3969	SFL2	0.8950	0.4235
565	orf19.7374	CTA4	0.8713	0.4156
569	orf19.2893	C4_06410W_A	0.8674	0.4179
571	orf19.1662	C3_01850W_A	0.8659	0.4209
605	orf19.1314	C4_03600C_A	0.8390	0.4118
606	orf19.5992	WOR2	0.8387	0.4151
608	orf19.938	C5_00510W_A	0.8386	0.4180
630	orf19.7592	FAA4	0.8113	0.4133
639	orf19.2752	ADR1	0.8048	0.4135
651	orf19.7539	INO2	0.8011	0.4125
652	orf19.3967	PFK1	0.8007	0.4157
658	orf19.6548	ISU1	0.7951	0.4169

666	orf19.3895	CHT2	0.7864	0.4174
670	orf19.4210	C6_00490W_A	0.7844	0.4193
672	orf19.1957	CYC3	0.7839	0.4221
675	orf19.6487	C7_02260W_A	0.7824	0.4244
686	orf19.5284	CR_05420W_A	0.7745	0.4237
691	orf19.2639	C5_03410C_A	0.7654	0.4252
714	orf19.7306	CR_09100C_A	0.7531	0.4199
724	orf19.3193	FCR3	0.7434	0.4194
734	orf19.2892	C4_06420W_A	0.7377	0.4189
742	orf19.1735	CR_04710W_A	0.7319	0.4192
743	orf19.6781	ZFU2	0.7310	0.4221
760	orf19.1742	HEM3	0.7235	0.4189
768	orf19.1842	BUD5	0.7208	0.4191
782	orf19.1718	ZCF8	0.7132	0.4170
793	orf19.413.1	RPS27A	0.7090	0.4161
828	orf19.4528	C1_01950C_A	0.6879	0.4060
835	orf19.7521	REP1	0.6844	0.4064
844	orf19.5906	ADE2	0.6799	0.4061
846	orf19.6984	C3_05460W_A	0.6787	0.4084
863	orf19.4167	C4_00750C_A	0.6698	0.4050
895	orf19.3707	YHB1	0.6507	0.3959
897	orf19.6599.1	CR_09640C_A	0.6501	0.3981
912	orf19.5555	C6_02810C_A	0.6423	0.3953
940	orf19.5312	MET4	0.6309	0.3876
944	orf19.413	C1_05520W_A	0.6293	0.3890
948	orf19.610	EFG1	0.6283	0.3903
971	orf19.5626	C6_03370W_A	0.6154	0.3845
981	orf19.118	FAD2	0.6115	0.3835
1000	orf19.7027	C7_00880C_A	0.6017	0.3791
1013	orf19.4166	ZCF21	0.5938	0.3769
1017	orf19.3291	HMT1	0.5926	0.3781
1024	orf19.868	ADAEC	0.5876	0.3782
1026	orf19.1604	C2_09460C_A	0.5873	0.3801
1040	orf19.721	CR_06450W_A	0.5806	0.3775
1056	orf19.2825	DRE2	0.5683	0.3741
1071	orf19.7539.1	CR_00040C_A	0.5628	0.3711
1078	orf19.3369	MOH1	0.5601	0.3710
1081	orf19.6734	TCC1	0.5593	0.3725
1084	orf19.2751	C4_02510W_A	0.5586	0.3739
1089	orf19.96	TOP1	0.5545	0.3746
1124	orf19.7501	NAP1	0.5387	0.3639
1129	orf19.568	SPE2	0.5347	0.3645
1134	orf19.5994	RHB1	0.5315	0.3651
1168	orf19.5754	C6_03800C_A	0.5173	0.3547

1211	orf19.1047	ERB1	0.4868	0.3408
1216	orf19.2309	PET127	0.4852	0.3412
1221	orf19.6817	FCR1	0.4841	0.3416
1233	orf19.3706	CR_07780W_A	0.4753	0.3393
1271	orf19.7502	CR_00310C_A	0.4529	0.3272
1399	orf19.1285	C5_04050W_A	0.3691	0.2808
1496	orf19.1601	RPL3	-0.3736	0.2461
1567	orf19.6091	RIM8	-0.4230	0.2214
1581	orf19.1605	PMS1	-0.4303	0.2182
1585	orf19.1095	GLE2	-0.4323	0.2188
1600	orf19.2961	C1_02720W_A	-0.4415	0.2153
1618	orf19.1313	CDR3	-0.4519	0.2107
1648	orf19.5031	SSK1	-0.4651	0.2016
1658	orf19.3282	BMT3	-0.4723	0.2000
1666	orf19.2930	C1_02430C_A	-0.4773	0.1993
1675	orf19.1933	C5_01350W_A	-0.4847	0.1982
1716	orf19.3042	C1_03410W_A	-0.5056	0.1851
1724	orf19.1961	C5_01090C_A	-0.5101	0.1845
1727	orf19.4432	KSP1	-0.5124	0.1858
1757	orf19.7149	C7_04240C_A	-0.5236	0.1769
1766	orf19.2737	C4_02620C_A	-0.5281	0.1760
1795	orf19.7380	C3_05990C_A	-0.5410	0.1676
1817	orf19.1317	OSH3	-0.5537	0.1618
1820	orf19.3433	OYE23	-0.5552	0.1633
1829	orf19.3794	CSR1	-0.5640	0.1625
1842	orf19.2506	C3_01020W_A	-0.5699	0.1602
1846	orf19.342	BMT7	-0.5716	0.1613
1864	orf19.5763	C6_03880W_A	-0.5813	0.1572
1881	orf19.6118	CR_07470W_A	-0.5904	0.1535
1893	orf19.5953	SFP1	-0.5949	0.1517
1911	orf19.5384	CHS8	-0.6038	0.1477
1919	orf19.332.1	C3_03340C_A	-0.6062	0.1475
1924	orf19.6798	SSN6	-0.6080	0.1483
1934	orf19.4433	CPH1	-0.6125	0.1474
1965	orf19.7053	GAC1	-0.6218	0.1385
1973	orf19.6117	CR_07480W_A	-0.6246	0.1384
2011	orf19.7056	C7_00630C_A	-0.6409	0.1269
2024	orf19.5595	SHE3	-0.6492	0.1250
2036	orf19.405	VCX1	-0.6548	0.1234
2039	orf19.4456	GAP4	-0.6561	0.1253
2072	orf19.3010.1	ECM33	-0.6787	0.1159
2098	orf19.3999	C5_05070W_A	-0.6929	0.1092
2134	orf19.2724	C4_02740W_A	-0.7093	0.0988
2148	orf19.1223	DBF2	-0.7173	0.0967

2152	orf19.6512	EXO70	-0.7208	0.0985
2157	orf19.2638	C5_03430W_A	-0.7253	0.0998
2192	orf19.7337	CR_09410W_A	-0.7441	0.0899
2195	orf19.333	FCY2	-0.7456	0.0921
2247	orf19.4900	MNN12	-0.7687	0.0760
2257	orf19.4346	C5_03140C_A	-0.7731	0.0756
2296	orf19.4341	C5_03120W_A	-0.8019	0.0645
2300	orf19.4899	GCA1	-0.8036	0.0665
2317	orf19.691	GPD2	-0.8155	0.0637
2321	orf19.6757	GCY1	-0.8170	0.0658
2350	orf19.5268	MED10	-0.8366	0.0585
2369	orf19.6800	POS5	-0.8546	0.0551
2401	orf19.3180	C5_01920C_A	-0.8766	0.0469
2410	orf19.4245	C5_02370C_A	-0.8863	0.0474
2469	orf19.2184	C2_07980W_A	-0.9428	0.0293
2489	orf19.4943	PSA2	-0.9615	0.0259
2492	orf19.1075	C6_04190C_A	-0.9633	0.0289
2511	orf19.1048	IFD6	-0.9756	0.0260
2528	orf19.7563	BET2	-0.9932	0.0239
2598	orf19.675	C1_11270W_A	-1.0678	0.0021
2641	orf19.467	WOR3	-1.1183	-0.0093
2658	orf19.3767	PEP1	-1.1432	-0.0108
2694	orf19.4867	SWE1	-1.2140	-0.0192
2701	orf19.5716	SAP4	-1.2287	-0.0166
2734	orf19.3283	CR_00710C_A	-1.3219	-0.0234
2736	orf19.6816	C3_06860C_A	-1.3248	-0.0186
2766	orf19.7078	C7_00420C_A	-1.3949	-0.0240
2784	orf19.6277	C1_06340W_A	-1.4729	-0.0246
2804	orf19.5285	PST3	-1.5662	-0.0256
2818	orf19.6420	PGA13	-1.6448	-0.0240
2843	orf19.535	RBR1	-1.8774	-0.0256
2861	orf19.7077	C7_00430W_A	-2.3018	-0.0230
2869	orf19.5674	PGA10	-2.5161	-0.0157
2873	orf19.7336	CR_09390C_	-4.3577	0.0004

EFG1_BIOFILM_TF

Rank in Gene List	Gene Identifier	Gene Name	Log2 Fold Change	Running Enrichment Score
1	orf19.5741	ALS1	3.7669	0.0116
4	orf19.4934	OP4	3.3214	0.0214
5	orf19.4211	FET31	3.1690	0.0314
7	orf19.5267	C1_11990W_A	3.1051	0.0409

8	orf19.4438	RME1	3.0969	0.0507
13	orf19.849	MNN41	2.9716	0.0586
15	orf19.7279.1	CR_08830W_A	2.8212	0.0672
16	orf19.4921.1	C1_12910W_A	2.7644	0.0760
18	orf19.7585	INO1	2.7086	0.0842
21	orf19.5728	C6_03600C_A	2.6549	0.0919
22	orf19.6715	C3_07720C_A	2.6148	0.1002
23	orf19.1286	C5_04040C_A	2.6036	0.1085
34	orf19.4673	BMT9	2.4314	0.1123
37	orf19.6713	WOR4	2.4007	0.1192
39	orf19.2023	HGT7	2.3851	0.1264
50	orf19.2332	C1_10850W_A	2.2465	0.1296
54	orf19.54	RHD1	2.2299	0.1356
55	orf19.2725	C4_02730C_A	2.2163	0.1426
59	orf19.6547	C7_01770W_A	2.1587	0.1483
60	orf19.4884	WOR1	2.1534	0.1551
62	orf19.2738	SUL2	2.1449	0.1616
65	orf19.5933	C3_04730C_A	2.1167	0.1675
69	orf19.218	BUD20	2.1019	0.1730
80	orf19.2766	C4_02380W_A	1.9940	0.1755
81	orf19.454	SFL1	1.9628	0.1817
82	orf19.111	CAN2	1.9617	0.1880
83	orf19.3674	GAL102	1.9457	0.1941
86	orf19.6983	C3_05450C_A	1.9390	0.1995
87	orf19.1350	C2_08330W_A	1.9373	0.2057
92	orf19.4231	PTH2	1.8930	0.2102
93	orf19.2356	CRZ2	1.8902	0.2162
98	orf19.6687	C7_03550C_A	1.8746	0.2206
99	orf19.4555	ALS4	1.8730	0.2265
102	orf19.935	AGA1	1.8553	0.2316
103	orf19.5625	C6_03360C_A	1.8474	0.2375
104	orf19.258	C3_02660W_A	1.8340	0.2433
116	orf19.7150	NRG1	1.7552	0.2447
118	orf19.3668	HGT2	1.7445	0.2498
127	orf19.5908	TEC1	1.6893	0.2521
128	orf19.4936	C1_13090W_A	1.6835	0.2574
130	orf19.2430	C1_06150W_A	1.6813	0.2624
142	orf19.7054	C7_00650W_A	1.6351	0.2633
144	orf19.4682	HGT17	1.6299	0.2681
145	orf19.5302	PGA31	1.6212	0.2733
146	orf19.1996	CHA1	1.6194	0.2784
148	orf19.6488	C7_02250W_A	1.6081	0.2832
154	orf19.4833	MLS1	1.5673	0.2862
167	orf19.1224	FRP3	1.5343	0.2864

173	orf19.5114.1	C1_08350C_A	1.5195	0.2893
176	orf19.3368	C4_03420C_A	1.4951	0.2933
179	orf19.1105	C5_03910C_A	1.4741	0.2972
186	orf19.5203	C1_04350C_A	1.4653	0.2996
191	orf19.5288.1	CR_05330W_A	1.4527	0.3026
209	orf19.3675	GAL7	1.3944	0.3005
210	orf19.6736	C3_07550C_A	1.3852	0.3049
225	orf19.450	C1_05150C_A	1.3508	0.3038
229	orf19.5032	SIM1	1.3375	0.3069
231	orf19.7436	AAF1	1.3322	0.3107
240	orf19.1189	C6_00290W_A	1.3141	0.3118
241	orf19.5475	C3_00020W_A	1.3109	0.3159
243	orf19.1122	C5_03730W_A	1.3059	0.3197
246	orf19.3795	AGP3	1.2958	0.3231
249	orf19.4951	C1_13240W_A	1.2920	0.3264
256	orf19.3711	CR_07820W_A	1.2840	0.3281
257	orf19.4972	OFI1	1.2815	0.3322
258	orf19.7151	C7_04220W_A	1.2797	0.3363
264	orf19.2169	C2_08150W_A	1.2599	0.3384
265	orf19.4394	CR_03510W_A	1.2583	0.3424
271	orf19.3672	GAL10	1.2536	0.3444
279	orf19.723	BCR1	1.2419	0.3456
289	orf19.6343	FEN1	1.2191	0.3460
290	orf19.871	C2_03500W_A	1.2183	0.3499
292	orf19.4234	C5_02280C_A	1.2171	0.3534
294	orf19.3656	COX15	1.2085	0.3568
308	orf19.6169	ATO1	1.1735	0.3555
309	orf19.2397.3	CR_03260W_A	1.1715	0.3593
310	orf19.3337	C1_01510W_A	1.1671	0.3630
313	orf19.4793	C1_09330W_A	1.1571	0.3659
315	orf19.2024	C2_00990W_A	1.1524	0.3692
321	orf19.986	GLY1	1.1498	0.3709
326	orf19.85	GPX2	1.1465	0.3730
328	orf19.6288	CR_07610C_A	1.1430	0.3762
336	orf19.6555	C7_01690W_A	1.1259	0.3771
354	orf19.84	CAN3	1.0956	0.3740
355	orf19.740	HAP41	1.0953	0.3775
363	orf19.5474	C3_00010C_A	1.0793	0.3782
365	orf19.6530	C7_01910C_A	1.0781	0.3812
373	orf19.6514	CUP9	1.0667	0.3819
379	orf19.1978	GIT2	1.0578	0.3834
380	orf19.6661	C5_03520W_A	1.0555	0.3867
389	orf19.3867	RPL7	1.0450	0.3869
394	orf19.4892	TPK1	1.0386	0.3887

405	orf19.5232	CSI2	1.0221	0.3881
407	orf19.6529	CDC34	1.0202	0.3909
408	orf19.1416	COX11	1.0184	0.3942
416	orf19.3670	GAL1	1.0030	0.3946
420	orf19.3653	FAT1	0.9995	0.3967
421	orf19.7112	FRP2	0.9991	0.3998
438	orf19.449	C1_05160C_A	0.9844	0.3968
453	orf19.1756	GPD1	0.9626	0.3944
462	orf19.6937	PTR22	0.9548	0.3944
464	orf19.5636	RBT5	0.9526	0.3970
467	orf19.3439	C6_01450C_A	0.9497	0.3992
480	orf19.4942	C1_13150W_A	0.9421	0.3976
482	orf19.3413	FGR37	0.9415	0.4002
494	orf19.1687	C3_01560W_A	0.9292	0.3989
505	orf19.1906	C2_00130W_A	0.9200	0.3980
517	orf19.4459	C1_03870C_A	0.9121	0.3966
529	orf19.4056	BRG1	0.9001	0.3952
531	orf19.3618	YWP1	0.8988	0.3977
534	orf19.3969	SFL2	0.8950	0.3998
554	orf19.4856	LIP3	0.8759	0.3952
567	orf19.2021	HGT8	0.8705	0.3933
569	orf19.2893	C4_06410W_A	0.8674	0.3957
588	orf19.2398	CR_03250C_A	0.8512	0.3915
593	orf19.7314	CDG1	0.8470	0.3926
605	orf19.1314	C4_03600C_A	0.8390	0.3910
606	orf19.5992	WOR2	0.8387	0.3937
608	orf19.938	C5_00510W_A	0.8386	0.3960
625	orf19.4563	C4_02260C_A	0.8160	0.3924
630	orf19.7592	FAA4	0.8113	0.3934
651	orf19.7539	INO2	0.8011	0.3882
652	orf19.3967	PFK1	0.8007	0.3908
658	orf19.6548	ISU1	0.7951	0.3914
670	orf19.4210	C6_00490W_A	0.7844	0.3896
672	orf19.1957	CYC3	0.7839	0.3917
674	orf19.7296	SLP3	0.7825	0.3938
675	orf19.6487	C7_02260W_A	0.7824	0.3963
677	orf19.3190	HAL9	0.7820	0.3984
691	orf19.2639	C5_03410C_A	0.7654	0.3958
693	orf19.4792	C1_09320C_A	0.7627	0.3978
717	orf19.4941	TYE7	0.7516	0.3913
721	orf19.1815	CR_07080W_A	0.7444	0.3925
725	orf19.921	HMS1	0.7425	0.3937
734	orf19.2892	C4_06420W_A	0.7377	0.3930
740	orf19.908	FEN12	0.7328	0.3934

741	orf19.1727	PMC1	0.7324	0.3957
743	orf19.6781	ZFU2	0.7310	0.3976
768	orf19.1842	BUD5	0.7208	0.3907
769	orf19.4393	CIT1	0.7193	0.3929
782	orf19.1718	ZCF8	0.7132	0.3906
785	orf19.7488	CR_00460C_A	0.7123	0.3921
826	orf19.5635	PGA7	0.6885	0.3788
828	orf19.4528	C1_01950C_A	0.6879	0.3806
830	orf19.7084	DFI1	0.6877	0.3824
844	orf19.5906	ADE2	0.6799	0.3795
846	orf19.6984	C3_05460W_A	0.6787	0.3813
849	orf19.1345	LIP8	0.6774	0.3827
852	orf19.4936.1	C1_13100W_A	0.6750	0.3840
863	orf19.4167	C4_00750C_A	0.6698	0.3823
872	orf19.2198	FLC3	0.6670	0.3813
895	orf19.3707	YHB1	0.6507	0.3749
912	orf19.5555	C6_02810C_A	0.6423	0.3708
916	orf19.4967	COX19	0.6401	0.3716
940	orf19.5312	MET4	0.6309	0.3648
945	orf19.6385	ACO1	0.6292	0.3652
946	orf19.1562	C2_02390W_A	0.6284	0.3672
948	orf19.610	EFG1	0.6283	0.3688
964	orf19.3188	TAC1	0.6208	0.3650
971	orf19.5626	C6_03370W_A	0.6154	0.3646
981	orf19.118	FAD2	0.6115	0.3631
1004	orf19.4235	PDE1	0.5995	0.3565
1008	orf19.3278	GSY1	0.5973	0.3572
1013	orf19.4166	ZCF21	0.5938	0.3576
1024	orf19.868	ADAEC	0.5876	0.3556
1040	orf19.721	CR_06450W_A	0.5806	0.3516
1044	orf19.1264	CFL2	0.5783	0.3523
1056	orf19.2825	DRE2	0.5683	0.3499
1059	orf19.2199	PHO86	0.5673	0.3509
1062	orf19.475	CR_03940W_A	0.5661	0.3519
1071	orf19.7539.1	CR_00040C_A	0.5628	0.3506
1078	orf19.3369	MOH1	0.5601	0.3501
1081	orf19.6734	TCC1	0.5593	0.3511
1082	orf19.474	CR_03930C_A	0.5589	0.3529
1086	orf19.7341.1	CR_09460C_A	0.5566	0.3535
1124	orf19.7501	NAP1	0.5387	0.3409
1127	orf19.7312	ERG13	0.5359	0.3418
1129	orf19.568	SPE2	0.5347	0.3431
1130	orf19.732	CR_07170W_A	0.5343	0.3448
1134	orf19.5994	RHB1	0.5315	0.3453

1136	orf19.2178.1	C2_08060W_A	0.5308	0.3466
1143	orf19.3276	PWP2	0.5277	0.3460
1216	orf19.2309	PET127	0.4852	0.3197
1221	orf19.6817	FCR1	0.4841	0.3197
1225	orf19.814	SSY1	0.4791	0.3201
1271	orf19.7502	CR_00310C_A	0.4529	0.3041
1305	orf19.5903	RAX1	0.4393	0.2928
1330	orf19.2457	C1_05920W_A	0.4262	0.2849
1374	orf19.4028	RER2	0.3886	0.2695
1399	orf19.1285	C5_04050W_A	0.3691	0.2614
1422	orf19.3206	CCT7	0.3424	0.2540
1454	orf19.1777	C2_10050W_A	-0.3269	0.2430
1502	orf19.6840	C1_04470C_A	-0.3775	0.2261
1521	orf19.6873	RPS8A	-0.3944	0.2204
1526	orf19.4998	ROB1	-0.3985	0.2201
1533	orf19.314	C3_03150W_A	-0.4049	0.2190
1564	orf19.5210	C2_05860C_A	-0.4215	0.2088
1568	orf19.6408	CR_08420W_A	-0.4238	0.2090
1585	orf19.1095	GLE2	-0.4323	0.2042
1593	orf19.3334	RPS21	-0.4371	0.2029
1600	orf19.2961	C1_02720W_A	-0.4415	0.2019
1648	orf19.5031	SSK1	-0.4651	0.1853
1650	orf19.949	C5_00400C_A	-0.4656	0.1863
1666	orf19.2930	C1_02430C_A	-0.4773	0.1821
1685	orf19.3359	ARP8	-0.4915	0.1767
1690	orf19.4997	KIS2	-0.4932	0.1767
1706	orf19.90	C6_00890W_A	-0.5019	0.1725
1712	orf19.3340	SOD2	-0.5043	0.1722
1724	orf19.1961	C5_01090C_A	-0.5101	0.1695
1757	orf19.7149	C7_04240C_A	-0.5236	0.1588
1766	orf19.2737	C4_02620C_A	-0.5281	0.1574
1795	orf19.7380	C3_05990C_A	-0.5410	0.1483
1799	orf19.2747	RGT1	-0.5428	0.1489
1801	orf19.2765	PGA62	-0.5436	0.1502
1805	orf19.4280	C5_02640W_A	-0.5451	0.1508
1815	orf19.733	CR_07160C_A	-0.5513	0.1491
1817	orf19.1317	OSH3	-0.5537	0.1504
1826	orf19.7297	CR_09010C_A	-0.5614	0.1491
1829	orf19.3794	CSR1	-0.5640	0.1501
1833	orf19.4403	VPS11	-0.5655	0.1508
1846	orf19.342	BMT7	-0.5716	0.1480
1911	orf19.5384	CHS8	-0.6038	0.1252
1916	orf19.3325	C1_01360C_A	-0.6051	0.1255
1924	orf19.6798	SSN6	-0.6080	0.1248

1947	orf19.3002	RPS1	-0.6150	0.1182
1951	orf19.3325.3	RPS21B	-0.6157	0.1190
1961	orf19.4907	C1_10360C_A	-0.6207	0.1175
1965	orf19.7053	GAC1	-0.6218	0.1183
1985	orf19.7242	NCR1	-0.6295	0.1130
1986	orf19.1998	C2_01260W_A	-0.6300	0.1150
2011	orf19.7056	C7_00630C_A	-0.6409	0.1077
2039	orf19.4456	GAP4	-0.6561	0.0994
2064	orf19.6660	C5_03510C_A	-0.6730	0.0923
2072	orf19.3010.1	ECM33	-0.6787	0.0917
2098	orf19.3999	C5_05070W_A	-0.6929	0.0842
2134	orf19.2724	C4_02740W_A	-0.7093	0.0730
2145	orf19.5211	IDP1	-0.7162	0.0714
2148	orf19.1223	DBF2	-0.7173	0.0729
2152	orf19.6512	EXO70	-0.7208	0.0740
2157	orf19.2638	C5_03430W_A	-0.7253	0.0748
2171	orf19.3001	TEM1	-0.7323	0.0721
2192	orf19.7337	CR_09410W_A	-0.7441	0.0667
2195	orf19.333	FCY2	-0.7456	0.0683
2247	orf19.4900	MNN12	-0.7687	0.0511
2279	orf19.4153	C5_01590W_A	-0.7864	0.0416
2296	orf19.4341	C5_03120W_A	-0.8019	0.0379
2300	orf19.4899	GCA1	-0.8036	0.0393
2310	orf19.4858	VPS41	-0.8107	0.0384
2350	orf19.5268	MED10	-0.8366	0.0260
2351	orf19.1585	ZRT2	-0.8383	0.0287
2369	orf19.6800	POS5	-0.8546	0.0248
2383	orf19.3501	C6_02090C_A	-0.8633	0.0225
2387	orf19.6842	TUS1	-0.8656	0.0241
2392	orf19.4831	MTS1	-0.8688	0.0254
2396	orf19.3417	ACF2	-0.8713	0.0270
2404	orf19.1570	ERG7	-0.8790	0.0270
2410	orf19.4245	C5_02370C_A	-0.8863	0.0279
2433	orf19.6784	PGA32	-0.9057	0.0223
2441	orf19.2848	CR_02910W_A	-0.9119	0.0225
2484	orf19.6168	C3_00910W_A	-0.9551	0.0093
2489	orf19.4943	PSA2	-0.9615	0.0108
2509	orf19.395	ENO1	-0.9740	0.0066
2523	orf19.2049	C2_00750W_A	-0.9889	0.0047
2528	orf19.7563	BET2	-0.9932	0.0063
2537	orf19.3264.1	CR_00910W_A	-1.0028	0.0064
2549	orf19.860	BMT8	-1.0177	0.0054
2556	orf19.3358	LSC1	-1.0240	0.0063
2564	orf19.320	C3_03210W_A	-1.0341	0.0069

2625	orf19.113	CIP1	-1.1047	-0.0128
2641	orf19.467	WOR3	-1.1183	-0.0150
2650	orf19.1447	C2_01420C_A	-1.1370	-0.0145
2681	orf19.3374	ECE1	-1.1833	-0.0223
2694	orf19.4867	SWE1	-1.2140	-0.0231
2701	orf19.5716	SAP4	-1.2287	-0.0215
2725	orf19.5021	PDX1	-1.3069	-0.0263
2754	orf19.656	DPP1	-1.3641	-0.0328
2758	orf19.6084	C1_00190C_A	-1.3713	-0.0296
2766	orf19.7078	C7_00420C_A	-1.3949	-0.0278
2776	orf19.3207	CCN1	-1.4235	-0.0268
2804	orf19.5285	PST3	-1.5662	-0.0322
2806	orf19.2431	C1_06140C_A	-1.5766	-0.0276
2857	orf19.7111.1	SOD3	-2.2003	-0.0400
2861	orf19.7077	C7_00430W_A	-2.3018	-0.0338
2862	orf19.4975	HYR1	-2.3065	-0.0265
2868	orf19.3740	PGA23	-2.4731	-0.0206
2870	orf19.7544	TLO1	-2.5977	-0.0127
2873	orf19.7336	CR_09390C_A	-4.3577	0.0004

NDT80_BIOFILM_TF

Rank in Gene List	Gene Identifier	Gene Name	Log2 Fold Change	Running Enrichment Score
0	orf19.6993	GAP2	4.6048	0.0089
1	orf19.5741	ALS1	3.7669	0.0161
2	orf19.3904	MRV4	3.6966	0.0232
4	orf19.4934	OP4	3.3214	0.0292
5	orf19.4211	FET31	3.1690	0.0353
8	orf19.4438	RME1	3.0969	0.0404
9	orf19.3643	C6_00810C_A	3.0665	0.0463
12	orf19.2849	AQY1	2.9932	0.0512
13	orf19.849	MNN41	2.9716	0.0569
14	orf19.3117	CSA2	2.9491	0.0626
15	orf19.7279.1	CR_08830W_A	2.8212	0.0680
21	orf19.5728	C6_03600C_A	2.6549	0.0710
22	orf19.6715	C3_07720C_A	2.6148	0.0761
23	orf19.1286	C5_04040C_A	2.6036	0.0811
24	orf19.3906	MRV6	2.5814	0.0860
25	orf19.5604	MDR1	2.5564	0.0909
26	orf19.851	MNN42	2.5559	0.0959
29	orf19.3905	MRV5	2.5187	0.0999
30	orf19.4933	FAD3	2.4966	0.1047

34	orf19.4673	BMT9	2.4314	0.1081
37	orf19.6713	WOR4	2.4007	0.1119
39	orf19.2023	HGT7	2.3851	0.1160
40	orf19.7218	RBE1	2.3719	0.1206
46	orf19.1932	CFL4	2.2907	0.1229
49	orf19.7094	HGT12	2.2631	0.1264
50	orf19.2332	C1_10850W_A	2.2465	0.1307
55	orf19.2725	C4_02730C_A	2.2163	0.1333
56	orf19.3924	C5_04380C_A	2.1978	0.1375
58	orf19.2460	C1_05890W_A	2.1801	0.1413
60	orf19.4884	WOR1	2.1534	0.1450
65	orf19.5933	C3_04730C_A	2.1167	0.1474
67	orf19.1449	C2_01450C_A	2.1093	0.1511
69	orf19.218	BUD20	2.1019	0.1547
71	orf19.5735.3	C6_03670C_A	2.0931	0.1583
76	orf19.2177	C2_08090W_A	2.0332	0.1605
80	orf19.2766	C4_02380W_A	1.9940	0.1631
81	orf19.454	SFL1	1.9628	0.1669
84	orf19.936	C5_00530W_A	1.9408	0.1698
85	orf19.6276	C1_06350W_A	1.9402	0.1735
86	orf19.6983	C3_05450C_A	1.9390	0.1772
87	orf19.1350	C2_08330W_A	1.9373	0.1809
88	orf19.4568	ZCF25	1.9371	0.1847
91	orf19.4773	AOX2	1.9058	0.1875
92	orf19.4231	PTH2	1.8930	0.1911
93	orf19.2356	CRZ2	1.8902	0.1948
94	orf19.7566	CR_09920W_A	1.8869	0.1984
98	orf19.6687	C7_03550C_A	1.8746	0.2007
99	orf19.4555	ALS4	1.8730	0.2043
102	orf19.935	AGA1	1.8553	0.2071
103	orf19.5625	C6_03360C_A	1.8474	0.2106
104	orf19.258	C3_02660W_A	1.8340	0.2142
115	orf19.4551	CTN1	1.7587	0.2133
116	orf19.7150	NRG1	1.7552	0.2167
117	orf19.6518	C7_02010C_A	1.7499	0.2201
118	orf19.3668	HGT2	1.7445	0.2234
125	orf19.138	FIG1	1.6915	0.2242
126	orf19.4063	GPT1	1.6901	0.2274
127	orf19.5908	TEC1	1.6893	0.2307
128	orf19.4936	C1_13090W_A	1.6835	0.2339
130	orf19.2430	C1_06150W_A	1.6813	0.2367
131	orf19.6844	ICL1	1.6773	0.2399
132	orf19.6995	ATO6	1.6712	0.2432
134	orf19.6574	ALK6	1.6654	0.2459

140	orf19.3548.1	WH11	1.6394	0.2470
142	orf19.7054	C7_00650W_A	1.6351	0.2497
145	orf19.5302	PGA31	1.6212	0.2520
149	orf19.7514	PCK1	1.6074	0.2538
152	orf19.6998	GTT1	1.5874	0.2560
154	orf19.4833	MLS1	1.5673	0.2586
157	orf19.5307	JEN2	1.5563	0.2608
159	orf19.6997	ATO5	1.5554	0.2633
164	orf19.5070	C1_07990C_A	1.5436	0.2646
167	orf19.1224	FRP3	1.5343	0.2667
168	orf19.1541	C2_02230C_A	1.5341	0.2697
171	orf19.3432	C6_01520W_A	1.5218	0.2718
176	orf19.3368	C4_03420C_A	1.4951	0.2730
177	orf19.3218	C5_03940C_A	1.4817	0.2758
193	orf19.204	C2_09000C_A	1.4504	0.2723
199	orf19.2990	XOG1	1.4398	0.2730
204	orf19.1497	ZCF6	1.4097	0.2740
208	orf19.3440	FRP5	1.3962	0.2754
210	orf19.6736	C3_07550C_A	1.3852	0.2777
214	orf19.3209	FGR42	1.3727	0.2790
215	orf19.6267	C1_06430C_A	1.3724	0.2817
225	orf19.450	C1_05150C_A	1.3508	0.2805
229	orf19.5032	SIM1	1.3375	0.2818
231	orf19.7436	AAF1	1.3322	0.2840
236	orf19.5975	TRY4	1.3208	0.2848
237	orf19.7114	CSA1	1.3190	0.2874
240	orf19.1189	C6_00290W_A	1.3141	0.2890
244	orf19.1287	C5_04030W_A	1.3044	0.2903
245	orf19.77.1	C6_04150W_A	1.3027	0.2928
249	orf19.4951	C1_13240W_A	1.2920	0.2940
253	orf19.2691	C4_03000C_A	1.2884	0.2952
254	orf19.4567	C4_02230C_A	1.2867	0.2977
256	orf19.3711	CR_07820W_A	1.2840	0.2998
258	orf19.7151	C7_04220W_A	1.2797	0.3018
263	orf19.385	GCV2	1.2606	0.3025
264	orf19.2169	C2_08150W_A	1.2599	0.3050
271	orf19.3672	GAL10	1.2536	0.3048
279	orf19.723	BCR1	1.2419	0.3043
280	orf19.3071	MIH1	1.2400	0.3067
283	orf19.2781	C1_07640C_A	1.2380	0.3082
285	orf19.272	FAA21	1.2320	0.3102
286	orf19.4591	CAT2	1.2297	0.3125
290	orf19.871	C2_03500W_A	1.2183	0.3136
293	orf19.3733	IDP2	1.2096	0.3151

294	orf19.3656	COX15	1.2085	0.3174
295	orf19.3049	C1_03470C_A	1.2055	0.3197
301	orf19.4784	CRP1	1.1956	0.3199
308	orf19.6169	ATO1	1.1735	0.3197
309	orf19.2397.3	CR_03260W_A	1.1715	0.3219
310	orf19.3337	C1_01510W_A	1.1671	0.3242
313	orf19.4793	C1_09330W_A	1.1571	0.3256
315	orf19.2024	C2_00990W_A	1.1524	0.3274
322	orf19.7447	JEN1	1.1493	0.3270
323	orf19.2618	MET2	1.1493	0.3293
326	orf19.85	GPX2	1.1465	0.3306
329	orf19.787.1	C4_03960W_A	1.1375	0.3320
335	orf19.4689	PGA57	1.1259	0.3320
336	orf19.6555	C7_01690W_A	1.1259	0.3342
342	orf19.1599	C2_09410W_A	1.1128	0.3342
345	orf19.3831	C4_04520W_A	1.1070	0.3355
347	orf19.6996	MNN14	1.1027	0.3372
352	orf19.2881	MNN4	1.0963	0.3376
354	orf19.84	CAN3	1.0956	0.3393
358	orf19.7444	C3_06550C_A	1.0906	0.3402
373	orf19.6514	CUP9	1.0667	0.3363
375	orf19.7095	C7_00270W_A	1.0640	0.3380
379	orf19.1978	GIT2	1.0578	0.3387
380	orf19.6661	C5_03520W_A	1.0555	0.3408
389	orf19.3867	RPL7	1.0450	0.3394
394	orf19.4892	TPK1	1.0386	0.3397
400	orf19.1152	C1_11670W_A	1.0299	0.3396
408	orf19.1416	COX11	1.0184	0.3386
413	orf19.6520	C7_02000C_A	1.0105	0.3389
415	orf19.3195	HIP1	1.0059	0.3404
416	orf19.3670	GAL1	1.0030	0.3423
420	orf19.3653	FAT1	0.9995	0.3430
421	orf19.7112	FRP2	0.9991	0.3449
429	orf19.787	C4_03950C_A	0.9902	0.3439
433	orf19.3116	EXM2	0.9862	0.3445
434	orf19.1868	RNR22	0.9851	0.3464
438	orf19.449	C1_05160C_A	0.9844	0.3470
450	orf19.2020	HGT6	0.9702	0.3443
451	orf19.7231	FTR2	0.9694	0.3461
455	orf19.5094	BUL1	0.9611	0.3467
462	orf19.6937	PTR22	0.9548	0.3460
463	orf19.1581	C2_02560W_A	0.9534	0.3479
464	orf19.5636	RBT5	0.9526	0.3497
467	orf19.3439	C6_01450C_A	0.9497	0.3507

468	orf19.674	C1_11280W_A	0.9483	0.3525
474	orf19.4910	FGR41	0.9459	0.3522
480	orf19.4942	C1_13150W_A	0.9421	0.3519
482	orf19.3413	FGR37	0.9415	0.3533
484	orf19.4783	C1_09240C_A	0.9391	0.3547
485	orf19.6254	ANT1	0.9376	0.3565
494	orf19.1687	C3_01560W_A	0.9292	0.3549
505	orf19.1906	C2_00130W_A	0.9200	0.3525
509	orf19.968	PGA14	0.9144	0.3530
517	orf19.4459	C1_03870C_A	0.9121	0.3518
519	orf19.1736	CR_04680C_A	0.9104	0.3531
520	orf19.6017	C1_00880W_A	0.9077	0.3549
529	orf19.4056	BRG1	0.9001	0.3533
531	orf19.3618	YWP1	0.8988	0.3546
534	orf19.3969	SFL2	0.8950	0.3554
542	orf19.1543	OPI1	0.8881	0.3542
545	orf19.4716	GDH3	0.8862	0.3551
567	orf19.2021	HGT8	0.8705	0.3479
569	orf19.2893	C4_06410W_A	0.8674	0.3492
570	orf19.3954.1	C5_04690C_A	0.8667	0.3508
588	orf19.2398	CR_03250C_A	0.8512	0.3453
599	orf19.173	CR_02510W_A	0.8419	0.3427
603	orf19.4658	C4_01290W_A	0.8397	0.3431
606	orf19.5992	WOR2	0.8387	0.3439
608	orf19.938	C5_00510W_A	0.8386	0.3451
609	orf19.3040	EHT1	0.8371	0.3467
613	orf19.6686	ENP2	0.8327	0.3470
617	orf19.4768	C1_09110W_A	0.8266	0.3473
630	orf19.7592	FAA4	0.8113	0.3438
638	orf19.5079	CDR4	0.8049	0.3424
644	orf19.6928	SAP9	0.8038	0.3419
651	orf19.7539	INO2	0.8011	0.3409
652	orf19.3967	PFK1	0.8007	0.3425
666	orf19.3895	CHT2	0.7864	0.3385
670	orf19.4210	C6_00490W_A	0.7844	0.3387
672	orf19.1957	CYC3	0.7839	0.3398
692	orf19.6948	CCC1	0.7648	0.3333
693	orf19.4792	C1_09320C_A	0.7627	0.3348
697	orf19.7446	OPI3	0.7606	0.3350
698	orf19.2072	C2_00550W_A	0.7590	0.3364
705	orf19.1252	YME1	0.7556	0.3354
708	orf19.1233	ADE4	0.7546	0.3360
717	orf19.4941	TYE7	0.7516	0.3341
718	orf19.5959	NOP14	0.7472	0.3355

721	orf19.1815	CR_07080W_A	0.7444	0.3361
724	orf19.3193	FCR3	0.7434	0.3367
725	orf19.921	HMS1	0.7425	0.3381
731	orf19.6886	C2_05750W_A	0.7392	0.3374
734	orf19.2892	C4_06420W_A	0.7377	0.3380
740	orf19.908	FEN12	0.7328	0.3373
743	orf19.6781	ZFU2	0.7310	0.3379
764	orf19.1150	C1_11690W_A	0.7228	0.3309
769	orf19.4393	CIT1	0.7193	0.3306
782	orf19.1718	ZCF8	0.7132	0.3269
785	orf19.7488	CR_00460C_A	0.7123	0.3274
786	orf19.4769	IPT1	0.7122	0.3288
790	orf19.1837	TBP1	0.7097	0.3289
791	orf19.3370	DOT4	0.7095	0.3303
793	orf19.413.1	RPS27A	0.7090	0.3312
794	orf19.2073	C2_00540W_A	0.7088	0.3326
800	orf19.5672	MEP2	0.7055	0.3318
801	orf19.7565	GNP3	0.7050	0.3332
802	orf19.6311	CR_04820W_A	0.7049	0.3345
826	orf19.5635	PGA7	0.6885	0.3262
828	orf19.4528	C1_01950C_A	0.6879	0.3271
830	orf19.7084	DFI1	0.6877	0.3280
844	orf19.5906	ADE2	0.6799	0.3238
846	orf19.6984	C3_05460W_A	0.6787	0.3247
849	orf19.1345	LIP8	0.6774	0.3252
860	orf19.6852	C1_04580C_A	0.6704	0.3223
863	orf19.4167	C4_00750C_A	0.6698	0.3227
877	orf19.3682	CWH8	0.6637	0.3185
884	orf19.5449	C3_00210C_A	0.6595	0.3173
890	orf19.2459	C1_05900W_A	0.6547	0.3164
895	orf19.3707	YHB1	0.6507	0.3160
898	orf19.6143	CR_07250C_A	0.6483	0.3164
912	orf19.5555	C6_02810C_A	0.6423	0.3122
940	orf19.5312	MET4	0.6309	0.3020
944	orf19.413	C1_05520W_A	0.6293	0.3020
946	orf19.1562	C2_02390W_A	0.6284	0.3028
948	orf19.610	EFG1	0.6283	0.3035
971	orf19.5626	C6_03370W_A	0.6154	0.2955
973	orf19.6066	C1_00410C_A	0.6139	0.2962
974	orf19.4118	CNT	0.6136	0.2974
998	orf19.3544	C2_05130W_A	0.6020	0.2889
1000	orf19.7027	C7_00880C_A	0.6017	0.2896
1005	orf19.5291	C4_04180C_A	0.5995	0.2891
1013	orf19.4166	ZCF21	0.5938	0.2873

1019	orf19.4174	C4_00680W_A	0.5892	0.2863
1024	orf19.868	ADAEC	0.5876	0.2858
1026	orf19.1604	C2_09460C_A	0.5873	0.2865
1040	orf19.721	CR_06450W_A	0.5806	0.2821
1051	orf19.7551	ALO1	0.5703	0.2790
1056	orf19.2825	DRE2	0.5683	0.2784
1062	orf19.475	CR_03940W_A	0.5661	0.2774
1067	orf19.1424	C4_04250W_A	0.5648	0.2768
1068	orf19.7396	C3_06140W_A	0.5646	0.2779
1071	orf19.7539.1	CR_00040C_A	0.5628	0.2782
1073	orf19.1886	RCL1	0.5625	0.2788
1078	orf19.3369	MOH1	0.5601	0.2782
1081	orf19.6734	TCC1	0.5593	0.2785
1082	orf19.474	CR_03930C_A	0.5589	0.2795
1083	orf19.969	C5_00260W_A	0.5589	0.2806
1086	orf19.7341.1	CR_09460C_A	0.5566	0.2808
1105	orf19.1944	GPR1	0.5479	0.2743
1121	orf19.2876	CBF1	0.5415	0.2691
1124	orf19.7501	NAP1	0.5387	0.2692
1126	orf19.4274	PUT1	0.5375	0.2699
1129	orf19.568	SPE2	0.5347	0.2700
1134	orf19.5994	RHB1	0.5315	0.2694
1136	orf19.2178.1	C2_08060W_A	0.5308	0.2700
1151	orf19.1767	C2_10140W_A	0.5258	0.2651
1166	orf19.6747	C3_07430W_A	0.5179	0.2602
1168	orf19.5754	C6_03800C_A	0.5173	0.2608
1179	orf19.1426	C4_04240C_A	0.5114	0.2576
1203	orf19.4600	C4_01930C_A	0.4923	0.2489
1205	orf19.2604	CR_02030C_A	0.4915	0.2494
1206	orf19.6994	BAT22	0.4909	0.2503
1216	orf19.2309	PET127	0.4852	0.2475
1218	orf19.5550	MRT4	0.4850	0.2480
1221	orf19.6817	FCR1	0.4841	0.2481
1225	orf19.814	SSY1	0.4791	0.2477
1233	orf19.3706	CR_07780W_A	0.4753	0.2457
1248	orf19.7397	C3_06150W_A	0.4675	0.2407
1271	orf19.7502	CR_00310C_A	0.4529	0.2323
1295	orf19.386	SAM4	0.4444	0.2235
1305	orf19.5903	RAX1	0.4393	0.2206
1316	orf19.3666	C1_02090C_A	0.4348	0.2172
1328	orf19.1280	SUI1	0.4268	0.2134
1330	orf19.2457	C1_05920W_A	0.4262	0.2138
1344	orf19.1770	CYC1	0.4172	0.2091
1358	orf19.4851	TFA1	0.4056	0.2045

1369	orf19.7382	CAM1	0.3971	0.2010
1395	orf19.5861	KRE9	0.3722	0.1912
1399	orf19.1285	C5_04050W_A	0.3691	0.1907
1403	orf19.5563	RNH1	0.3650	0.1901
1404	orf19.7667	IAH1	0.3645	0.1908
1435	orf19.1279	CDS1	0.3237	0.1788
1453	orf19.4380.1	CR_03620C_A	-0.3267	0.1723
1456	orf19.6094	VPS53	-0.3291	0.1721
1461	orf19.5671	C4_00420C_A	-0.3409	0.1711
1466	orf19.1991	C2_01340W_A	-0.3453	0.1700
1472	orf19.4308	HSL1	-0.3497	0.1686
1478	orf19.1891	APR1	-0.3562	0.1672
1480	orf19.3813	C4_04670C_A	-0.3580	0.1675
1489	orf19.1836	APN2	-0.3683	0.1648
1496	orf19.1601	RPL3	-0.3736	0.1630
1502	orf19.6840	C1_04470C_A	-0.3775	0.1616
1511	orf19.1064	ACS2	-0.3837	0.1590
1521	orf19.6873	RPS8A	-0.3944	0.1560
1522	orf19.1793	C4_05350W_A	-0.3951	0.1567
1525	orf19.657	SAM2	-0.3979	0.1567
1526	orf19.4998	ROB1	-0.3985	0.1574
1536	orf19.3158	C3_01190C_A	-0.4074	0.1544
1564	orf19.5210	C2_05860C_A	-0.4215	0.1439
1568	orf19.6408	CR_08420W_A	-0.4238	0.1434
1576	orf19.2423	ZCF11	-0.4276	0.1413
1581	orf19.1605	PMS1	-0.4303	0.1405
1591	orf19.6092	KEL1	-0.4368	0.1375
1592	orf19.3744	CEX1	-0.4369	0.1383
1593	orf19.3334	RPS21	-0.4371	0.1392
1600	orf19.2961	C1_02720W_A	-0.4415	0.1375
1603	orf19.3469	C6_02280W_A	-0.4451	0.1375
1613	orf19.6259	C1_06540C_A	-0.4493	0.1346
1616	orf19.5450	ETR1	-0.4506	0.1346
1618	orf19.1313	CDR3	-0.4519	0.1351
1630	orf19.2175	C2_08100W_A	-0.4560	0.1313
1647	orf19.302	C3_03060W_A	-0.4643	0.1255
1648	orf19.5031	SSK1	-0.4651	0.1264
1652	orf19.7625	PGA1	-0.4676	0.1260
1658	orf19.3282	BMT3	-0.4723	0.1248
1661	orf19.139	TRA1	-0.4731	0.1249
1666	orf19.2930	C1_02430C_A	-0.4773	0.1241
1675	orf19.1933	C5_01350W_A	-0.4847	0.1217
1676	orf19.4381	VTC3	-0.4850	0.1226
1685	orf19.3359	ARP8	-0.4915	0.1202

1688	orf19.3087.1	C4_07170C_A	-0.4924	0.1203
1690	orf19.4997	KIS2	-0.4932	0.1209
1700	orf19.6197	DHH1	-0.4987	0.1180
1712	orf19.3340	SOD2	-0.5043	0.1144
1721	orf19.6027	C1_00790W_A	-0.5088	0.1120
1722	orf19.2474	PRC3	-0.5094	0.1130
1724	orf19.1961	C5_01090C_A	-0.5101	0.1135
1733	orf19.3572.3	C2_05410W_A	-0.5153	0.1112
1741	orf19.1334	C7_03410C_A	-0.5182	0.1092
1750	orf19.5015	MYO2	-0.5204	0.1069
1757	orf19.7149	C7_04240C_A	-0.5236	0.1053
1759	orf19.5337	UBC15	-0.5240	0.1059
1768	orf19.6146	CLG1	-0.5285	0.1036
1795	orf19.7380	C3_05990C_A	-0.5410	0.0937
1799	orf19.2747	RGT1	-0.5428	0.0935
1801	orf19.2765	PGA62	-0.5436	0.0941
1805	orf19.4280	C5_02640W_A	-0.5451	0.0939
1810	orf19.1926	SEF2	-0.5475	0.0932
1812	orf19.2515	C3_01130C_A	-0.5487	0.0939
1814	orf19.931	C5_00580W_A	-0.5511	0.0945
1820	orf19.3433	OYE23	-0.5552	0.0935
1828	orf19.2613	ECM4	-0.5638	0.0916
1833	orf19.4403	VPS11	-0.5655	0.0910
1834	orf19.779	HAT1	-0.5656	0.0921
1838	orf19.1186	C6_00270W_A	-0.5689	0.0920
1842	orf19.2506	C3_01020W_A	-0.5699	0.0918
1845	orf19.1994	C2_01310W_A	-0.5712	0.0920
1850	orf19.4911	C1_10410W_A	-0.5728	0.0915
1893	orf19.5953	SFP1	-0.5949	0.0749
1900	orf19.3667	C1_02100W_A	-0.5992	0.0736
1901	orf19.1120	FAV2	-0.5994	0.0747
1911	orf19.5384	CHS8	-0.6038	0.0721
1912	orf19.493	RPL15A	-0.6044	0.0733
1914	orf19.3727	PHO112	-0.6047	0.0740
1916	orf19.3325	C1_01360C_A	-0.6051	0.0748
1924	orf19.6798	SSN6	-0.6080	0.0730
1944	orf19.6196	C1_07080W_A	-0.6147	0.0662
1951	orf19.3325.3	RPS21B	-0.6157	0.0648
1960	orf19.3823	ZDS1	-0.6205	0.0627
1961	orf19.4907	C1_10360C_A	-0.6207	0.0639
1964	orf19.3840	SAK1	-0.6215	0.0642
1965	orf19.7053	GAC1	-0.6218	0.0654
1978	orf19.5265	KIP4	-0.6268	0.0616
1985	orf19.7242	NCR1	-0.6295	0.0603

1990	orf19.4772	SSU81	-0.6316	0.0598
2007	orf19.1451	SRB9	-0.6401	0.0543
2011	orf19.7056	C7_00630C_A	-0.6409	0.0543
2029	orf19.290	KRE5	-0.6520	0.0484
2031	orf19.382	TEF2	-0.6522	0.0492
2039	orf19.4456	GAP4	-0.6561	0.0475
2053	orf19.5141	C7_03140W_A	-0.6645	0.0433
2064	orf19.6660	C5_03510C_A	-0.6730	0.0404
2072	orf19.3010.1	ECM33	-0.6787	0.0388
2074	orf19.6760	MDS3	-0.6798	0.0397
2076	orf19.348	SKN2	-0.6814	0.0406
2082	orf19.5334	ZSF1	-0.6847	0.0398
2093	orf19.2280	ZCF10	-0.6900	0.0369
2098	orf19.3999	C5_05070W_A	-0.6929	0.0365
2113	orf19.6255	C1_06560W_A	-0.6996	0.0320
2119	orf19.1723	C3_01280W_A	-0.7032	0.0313
2134	orf19.2724	C4_02740W_A	-0.7093	0.0267
2145	orf19.5211	IDP1	-0.7162	0.0239
2148	orf19.1223	DBF2	-0.7173	0.0244
2152	orf19.6512	EXO70	-0.7208	0.0246
2155	orf19.2158	NAG3	-0.7250	0.0251
2157	orf19.2638	C5_03430W_A	-0.7253	0.0261
2164	orf19.3281	CR_00750C_A	-0.7287	0.0250
2166	orf19.5338	GAL4	-0.7298	0.0260
2172	orf19.1330	C7_03460W_A	-0.7331	0.0253
2182	orf19.3156	C3_01180C_A	-0.7407	0.0229
2188	orf19.4979	KNS1	-0.7426	0.0222
2192	orf19.7337	CR_09410W_A	-0.7441	0.0224
2215	orf19.5927	RPS15	-0.7529	0.0146
2216	orf19.1995	MNN24	-0.7530	0.0160
2219	orf19.5376	C3_00790W_A	-0.7557	0.0167
2233	orf19.1760	RAS1	-0.7643	0.0127
2247	orf19.4900	MNN12	-0.7687	0.0087
2271	orf19.5506	PLC1	-0.7826	0.0005
2287	orf19.5078	OFR1	-0.7950	-0.0043
2292	orf19.7610	PTP3	-0.7979	-0.0044
2300	orf19.4899	GCA1	-0.8036	-0.0058
2315	orf19.6658	C5_03490C_A	-0.8135	-0.0101
2317	orf19.691	GPD2	-0.8155	-0.0090
2346	orf19.1331	HSM3	-0.8341	-0.0192
2347	orf19.1368	C2_09820W_A	-0.8347	-0.0176
2351	orf19.1585	ZRT2	-0.8383	-0.0172
2363	orf19.1409.1	C4_04390W_A	-0.8458	-0.0202
2365	orf19.6349	RVS162	-0.8493	-0.0190

2369	orf19.6800	POS5	-0.8546	-0.0186
2371	orf19.6078	POL93	-0.8557	-0.0174
2383	orf19.3501	C6_02090C_A	-0.8633	-0.0203
2387	orf19.6842	TUS1	-0.8656	-0.0199
2392	orf19.4831	MTS1	-0.8688	-0.0200
2394	orf19.3225	CWH43	-0.8703	-0.0187
2409	orf19.4391	CR_03480W_A	-0.8853	-0.0229
2410	orf19.4245	C5_02370C_A	-0.8863	-0.0212
2414	orf19.3149	LSP1	-0.8914	-0.0207
2417	orf19.6028	HGC1	-0.8928	-0.0199
2429	orf19.1212	C6_04100W_A	-0.9020	-0.0227
2434	orf19.31	C2_06550W_A	-0.9065	-0.0227
2435	orf19.1825	C1_06250W_A	-0.9073	-0.0209
2448	orf19.4774	AOX1	-0.9207	-0.0242
2450	orf19.3839	SAP10	-0.9220	-0.0229
2465	orf19.1930	CFL5	-0.9393	-0.0269
2472	orf19.2551	MET6	-0.9462	-0.0276
2478	orf19.6763	SLK19	-0.9516	-0.0279
2481	orf19.7668	MAL2	-0.9534	-0.0269
2484	orf19.6168	C3_00910W_A	-0.9551	-0.0259
2487	orf19.1747	KIP2	-0.9596	-0.0249
2491	orf19.7350	RCT1	-0.9633	-0.0243
2492	orf19.1075	C6_04190C_A	-0.9633	-0.0225
2494	orf19.5209	C2_05850C_A	-0.9650	-0.0210
2498	orf19.2767	PGA59	-0.9671	-0.0204
2506	orf19.2163	C6_04650W_A	-0.9739	-0.0215
2509	orf19.395	ENO1	-0.9740	-0.0205
2528	orf19.7563	BET2	-0.9932	-0.0261
2531	orf19.6592	CR_09700W_A	-0.9951	-0.0251
2532	orf19.5142	DFR1	-0.9958	-0.0232
2563	orf19.2190	VRP1	-1.0340	-0.0338
2594	orf19.3572	C2_05400W_A	-1.0653	-0.0443
2598	orf19.675	C1_11270W_A	-1.0678	-0.0436
2604	orf19.7324	THI13	-1.0714	-0.0436
2607	orf19.2172	ARA1	-1.0785	-0.0424
2613	orf19.7323	CBP1	-1.0888	-0.0424
2623	orf19.2451	PGA45	-1.1021	-0.0440
2636	orf19.6594	PLB3	-1.1133	-0.0469
2641	orf19.467	WOR3	-1.1183	-0.0465
2642	orf19.1522	C2_02050C_A	-1.1228	-0.0443
2648	orf19.6229	CAT1	-1.1311	-0.0442
2649	orf19.854	UGA11	-1.1368	-0.0421
2659	orf19.4980	HSP70	-1.1449	-0.0436
2666	orf19.4651	PGA53	-1.1527	-0.0439

2681	orf19.3374	ECE1	-1.1833	-0.0476
2682	orf19.6081	PHR2	-1.1904	-0.0453
2687	orf19.251	GLX3	-1.2052	-0.0446
2694	orf19.4867	SWE1	-1.2140	-0.0448
2695	orf19.301	PGA18	-1.2171	-0.0425
2696	orf19.3802	PMT6	-1.2175	-0.0401
2702	orf19.1321	HWP1	-1.2354	-0.0399
2705	orf19.1505	C2_01930C_A	-1.2441	-0.0383
2716	orf19.4906	C1_10350C_A	-1.2763	-0.0401
2721	orf19.6527	C7_01940C_A	-1.2939	-0.0392
2723	orf19.2202	C2_07790C_A	-1.3015	-0.0372
2725	orf19.5021	PDX1	-1.3069	-0.0351
2729	orf19.6191	TLO8	-1.3148	-0.0338
2736	orf19.6816	C3_06860C_A	-1.3248	-0.0338
2745	orf19.7504	CR_00290W_A	-1.3445	-0.0346
2754	orf19.656	DPP1	-1.3641	-0.0353
2755	orf19.7436.1	ECM15	-1.3659	-0.0327
2758	orf19.6084	C1_00190C_A	-1.3713	-0.0309
2766	orf19.7078	C7_00420C_A	-1.3949	-0.0311
2784	orf19.6277	C1_06340W_A	-1.4729	-0.0354
2787	orf19.4652	C4_01350W_A	-1.4873	-0.0334
2791	orf19.5454	DAL1	-1.5048	-0.0318
2796	orf19.6350	C1_12720C_A	-1.5284	-0.0305
2801	orf19.6313	MNT4	-1.5540	-0.0292
2806	orf19.2431	C1_06140C_A	-1.5766	-0.0279
2814	orf19.4064	GPI7	-1.6003	-0.0277
2817	orf19.1539	C2_02220C_A	-1.6348	-0.0254
2818	orf19.6420	PGA13	-1.6448	-0.0223
2819	orf19.2837	ALG5	-1.6502	-0.0191
2820	orf19.3908	MRV8	-1.6621	-0.0159
2826	orf19.2425	HGT18	-1.7046	-0.0147
2828	orf19.2467	PRN1	-1.7191	-0.0118
2834	orf19.1153	GAD1	-1.7752	-0.0105
2844	orf19.7550	IFA14	-1.9115	-0.0106
2857	orf19.7111.1	SOD3	-2.2003	-0.0115
2861	orf19.7077	C7_00430W_A	-2.3018	-0.0083
2865	orf19.7017	YOX1	-2.3578	-0.0050
2873	orf19.7336	CR_09390C_A	-4.3577	0.0004

BCR1_TF

Rank in Gene List	Gene Identifier	Gene Name	Log2 Fold Change	Running Enrichment Score
1	orf19.5741	ALS1	3.7669	0.0198
5	orf19.4211	FET31	3.1690	0.0356
8	orf19.4438	RME1	3.0969	0.0515
13	orf19.849	MNN41	2.9716	0.0659
22	orf19.6715	C3_07720C_A	2.6148	0.0770
23	orf19.1286	C5_04040C_A	2.6036	0.0909
26	orf19.851	MNN42	2.5559	0.1038
37	orf19.6713	WOR4	2.4007	0.1130
39	orf19.2023	HGT7	2.3851	0.1254
41	orf19.97	CAN1	2.3381	0.1375
46	orf19.1932	CFL4	2.2907	0.1483
50	orf19.2332	C1_10850W_A	2.2465	0.1592
54	orf19.54	RHD1	2.2299	0.1701
55	orf19.2725	C4_02730C_A	2.2163	0.1819
59	orf19.6547	C7_01770W_A	2.1587	0.1924
60	orf19.4884	WOR1	2.1534	0.2039
65	orf19.5933	C3_04730C_A	2.1167	0.2137
81	orf19.454	SFL1	1.9628	0.2187
86	orf19.6983	C3_05450C_A	1.9390	0.2276
92	orf19.4231	PTH2	1.8930	0.2359
93	orf19.2356	CRZ2	1.8902	0.2460
99	orf19.4555	ALS4	1.8730	0.2542
102	orf19.935	AGA1	1.8553	0.2634
103	orf19.5625	C6_03360C_A	1.8474	0.2733
104	orf19.258	C3_02660W_A	1.8340	0.2831
116	orf19.7150	NRG1	1.7552	0.2884
118	orf19.3668	HGT2	1.7445	0.2974
127	orf19.5908	TEC1	1.6893	0.3035
128	orf19.4936	C1_13090W_A	1.6835	0.3125
136	orf19.3182	GIS2	1.6607	0.3188
142	orf19.7054	C7_00650W_A	1.6351	0.3257
145	orf19.5302	PGA31	1.6212	0.3336
148	orf19.6488	C7_02250W_A	1.6081	0.3415
157	orf19.5307	JEN2	1.5563	0.3469
210	orf19.6736	C3_07550C_A	1.3852	0.3350
214	orf19.3209	FGR42	1.3727	0.3413
225	orf19.450	C1_05150C_A	1.3508	0.3448
231	orf19.7436	AAF1	1.3322	0.3501
240	orf19.1189	C6_00290W_A	1.3141	0.3542
244	orf19.1287	C5_04030W_A	1.3044	0.3600
245	orf19.77.1	C6_04150W_A	1.3027	0.3670

258	orf19.7151	C7_04220W_A	1.2797	0.3694
271	orf19.3672	GAL10	1.2536	0.3717
279	orf19.723	BCR1	1.2419	0.3758
290	orf19.871	C2_03500W_A	1.2183	0.3786
310	orf19.3337	C1_01510W_A	1.1671	0.3778
315	orf19.2024	C2_00990W_A	1.1524	0.3825
326	orf19.85	GPX2	1.1465	0.3849
352	orf19.2881	MNN4	1.0963	0.3816
354	orf19.84	CAN3	1.0956	0.3871
355	orf19.740	HAP41	1.0953	0.3929
369	orf19.2652	TEF4	1.0727	0.3939
373	orf19.6514	CUP9	1.0667	0.3985
389	orf19.3867	RPL7	1.0450	0.3985
405	orf19.5232	CSI2	1.0221	0.3984
406	orf19.2062	SOD4	1.0219	0.4039
415	orf19.3195	HIP1	1.0059	0.4063
416	orf19.3670	GAL1	1.0030	0.4117
438	orf19.449	C1_05160C_A	0.9844	0.4092
462	orf19.6937	PTR22	0.9548	0.4058
464	orf19.5636	RBT5	0.9526	0.4106
480	orf19.4942	C1_13150W_A	0.9421	0.4100
517	orf19.4459	C1_03870C_A	0.9121	0.4016
519	orf19.1736	CR_04680C_A	0.9104	0.4061
529	orf19.4056	BRG1	0.9001	0.4076
531	orf19.3618	YWP1	0.8988	0.4121
534	orf19.3969	SFL2	0.8950	0.4161
569	orf19.2893	C4_06410W_A	0.8674	0.4082
606	orf19.5992	WOR2	0.8387	0.3994
608	orf19.938	C5_00510W_A	0.8386	0.4035
630	orf19.7592	FAA4	0.8113	0.4001
651	orf19.7539	INO2	0.8011	0.3970
652	orf19.3967	PFK1	0.8007	0.4012
658	orf19.6548	ISU1	0.7951	0.4036
666	orf19.3895	CHT2	0.7864	0.4053
670	orf19.4210	C6_00490W_A	0.7844	0.4084
672	orf19.1957	CYC3	0.7839	0.4122
675	orf19.6487	C7_02260W_A	0.7824	0.4156
724	orf19.3193	FCR3	0.7434	0.4019
734	orf19.2892	C4_06420W_A	0.7377	0.4025
740	orf19.908	FEN12	0.7328	0.4046
742	orf19.1735	CR_04710W_A	0.7319	0.4081
743	orf19.6781	ZFU2	0.7310	0.4120
768	orf19.1842	BUD5	0.7208	0.4070
802	orf19.6311	CR_04820W_A	0.7049	0.3986

826	orf19.5635	PGA7	0.6885	0.3938
828	orf19.4528	C1_01950C_A	0.6879	0.3971
844	orf19.5906	ADE2	0.6799	0.3952
846	orf19.6984	C3_05460W_A	0.6787	0.3984
852	orf19.4936.1	C1_13100W_A	0.6750	0.4002
863	orf19.4167	C4_00750C_A	0.6698	0.4001
884	orf19.5449	C3_00210C_A	0.6595	0.3962
895	orf19.3707	YHB1	0.6507	0.3960
911	orf19.76	SPB1	0.6423	0.3939
940	orf19.5312	MET4	0.6309	0.3869
948	orf19.610	EFG1	0.6283	0.3877
971	orf19.5626	C6_03370W_A	0.6154	0.3829
1000	orf19.7027	C7_00880C_A	0.6017	0.3757
1013	orf19.4166	ZCF21	0.5938	0.3745
1024	orf19.868	ADAEC	0.5876	0.3739
1026	orf19.1604	C2_09460C_A	0.5873	0.3767
1040	orf19.721	CR_06450W_A	0.5806	0.3750
1056	orf19.2825	DRE2	0.5683	0.3725
1066	orf19.3981	MAL31	0.5652	0.3722
1071	orf19.7539.1	CR_00040C_A	0.5628	0.3737
1081	orf19.6734	TCC1	0.5593	0.3734
1089	orf19.96	TOP1	0.5545	0.3738
1105	orf19.1944	GPR1	0.5479	0.3712
1124	orf19.7501	NAP1	0.5387	0.3674
1129	orf19.568	SPE2	0.5347	0.3688
1134	orf19.5994	RHB1	0.5315	0.3701
1136	orf19.2178.1	C2_08060W_A	0.5308	0.3726
1168	orf19.5754	C6_03800C_A	0.5173	0.3639
1176	orf19.6973	C3_05360C_A	0.5129	0.3641
1192	orf19.2653	C5_03260C_A	0.4987	0.3612
1221	orf19.6817	FCR1	0.4841	0.3534
1225	orf19.814	SSY1	0.4791	0.3549
1271	orf19.7502	CR_00310C_A	0.4529	0.3407
1305	orf19.5903	RAX1	0.4393	0.3308
1319	orf19.6071	NAA25	0.4337	0.3284
1496	orf19.1601	RPL3	-0.3736	0.2653
1521	orf19.6873	RPS8A	-0.3944	0.2585
1522	orf19.1793	C4_05350W_A	-0.3951	0.2606
1567	orf19.6091	RIM8	-0.4230	0.2466
1581	orf19.1605	PMS1	-0.4303	0.2441
1666	orf19.2930	C1_02430C_A	-0.4773	0.2156
1675	orf19.1933	C5_01350W_A	-0.4847	0.2153
1704	orf19.2992	RPP1A	-0.5005	0.2076
1712	orf19.3340	SOD2	-0.5043	0.2077

1724	orf19.1961	C5_01090C_A	-0.5101	0.2064
1749	orf19.6415.1	CR_08480C_A	-0.5204	0.2003
1757	orf19.7149	C7_04240C_A	-0.5236	0.2005
1768	orf19.6146	CLG1	-0.5285	0.1996
1795	orf19.7380	C3_05990C_A	-0.5410	0.1929
1820	orf19.3433	OYE23	-0.5552	0.1870
1829	orf19.3794	CSR1	-0.5640	0.1871
1833	orf19.4403	VPS11	-0.5655	0.1890
1842	orf19.2506	C3_01020W_A	-0.5699	0.1891
1846	orf19.342	BMT7	-0.5716	0.1911
1911	orf19.5384	CHS8	-0.6038	0.1706
1924	orf19.6798	SSN6	-0.6080	0.1694
1968	orf19.6147	CR_07230W_A	-0.6232	0.1569
2011	orf19.7056	C7_00630C_A	-0.6409	0.1448
2021	orf19.2994.1	RPS16A	-0.6462	0.1449
2036	orf19.405	VCX1	-0.6548	0.1432
2039	orf19.4456	GAP4	-0.6561	0.1460
2072	orf19.3010.1	ECM33	-0.6787	0.1378
2098	orf19.3999	C5_05070W_A	-0.6929	0.1323
2115	orf19.6872	C2_05590C_A	-0.7002	0.1301
2152	orf19.6512	EXO70	-0.7208	0.1207
2157	orf19.2638	C5_03430W_A	-0.7253	0.1231
2192	orf19.7337	CR_09410W_A	-0.7441	0.1145
2195	orf19.333	FCY2	-0.7456	0.1177
2247	orf19.4900	MNN12	-0.7687	0.1030
2300	orf19.4899	GCA1	-0.8036	0.0881
2369	orf19.6800	POS5	-0.8546	0.0675
2401	orf19.3180	C5_01920C_A	-0.8766	0.0607
2434	orf19.31	C2_06550W_A	-0.9065	0.0538
2489	orf19.4943	PSA2	-0.9615	0.0390
2498	orf19.2767	PGA59	-0.9671	0.0412
2528	orf19.7563	BET2	-0.9932	0.0358
2641	orf19.467	WOR3	-1.1183	0.0003
2694	orf19.4867	SWE1	-1.2140	-0.0124
2758	orf19.6084	C1_00190C_A	-1.3713	-0.0283
2766	orf19.7078	C7_00420C_A	-1.3949	-0.0234
2785	orf19.2768	AMS1	-1.4783	-0.0222
2786	orf19.3982	C5_04940W_A	-1.4788	-0.0143
2843	orf19.535	RBR1	-1.8774	-0.0249
2861	orf19.7077	C7_00430W_A	-2.3018	-0.0189
2873	orf19.7336	CR_09390C_A	-4.3577	0.0004

BIOLOGICAL ADHESION_BIO

Rank in Gene List	Gene Identifier	Gene Name	Log2 Fold Change	Running Enrichment Score
1	orf19.5741	ALS1	3.7668	0.1152
11	orf19.4216	C5_02110W_A	3.0229	0.2047
17	orf19.3160	HSP12	2.7155	0.2863
51	orf19.6001	SAP3	2.2455	0.3435
60	orf19.4884	WOR1	2.1534	0.4068
99	orf19.4555	ALS4	1.8730	0.4509
127	orf19.5908	TEC1	1.6893	0.4932
189	orf19.1097	ALS2	1.4598	0.5166
231	orf19.7436	AAF1	1.3322	0.5431
531	orf19.3618	YWP1	0.8988	0.4658
558	orf19.4257	INT1	0.8747	0.4835
644	orf19.6928	SAP9	0.8038	0.4783
805	orf19.1665	MNT1	0.7032	0.4438
948	orf19.610	EFG1	0.6283	0.4132
1174	orf19.5714	SAP1	0.5140	0.3501
1285	orf19.1671	UTR2	0.4467	0.3252
2015	orf19.1133	MSB1	-0.6427	0.0892
2072	orf19.3010.1	ECM33	-0.6787	0.0904
2239	orf19.548	CDC10	-0.7654	0.0556
2294	orf19.6109	TUP1	-0.8013	0.0612
2450	orf19.3839	SAP10	-0.9220	0.0352
2686	orf19.4477	CSH1	-1.2046	-0.0103
2701	orf19.5716	SAP4	-1.2287	0.0224
2702	orf19.1321	HWP1	-1.2353	0.0603

TRANSPORTER ACTIVITY_MOL

Rank in Gene List	Gene Identifier	Gene Name	Log2 Fold Change	Running Enrichment Score
0	orf19.6993	GAP2	4.6048	0.0272
3	orf19.4335	TNA1	3.3619	0.0463
12	orf19.2849	AQY1	2.9932	0.0610
25	orf19.5604	MDR1	2.5564	0.0717
39	orf19.2023	HGT7	2.3851	0.0810
41	orf19.97	CAN1	2.3381	0.0944
44	orf19.2810	AAP1	2.3154	0.1074
45	orf19.3120	C4_06910W_A	2.3040	0.1210
49	orf19.7094	HGT12	2.2631	0.1332
52	orf19.7093	HGT13	2.2362	0.1457

62	orf19.2738	SUL2	2.1449	0.1550
73	orf19.7071	FGR2	2.0821	0.1636
82	orf19.111	CAN2	1.9617	0.1723
94	orf19.7566	CR_09920W_A	1.8869	0.1794
106	orf19.4304	GAP1	1.8272	0.1861
108	orf19.3122	ARR3	1.8229	0.1965
111	orf19.1587	HGT20	1.7944	0.2064
118	orf19.3668	HGT2	1.7445	0.2144
126	orf19.4063	GPT1	1.6901	0.2218
139	orf19.3455	C6_02150C_A	1.6417	0.2271
144	orf19.4682	HGT17	1.6299	0.2353
151	orf19.1867	C2_07580W_A	1.5932	0.2425
155	orf19.2006.1	COX17	1.5667	0.2506
157	orf19.5307	JEN2	1.5563	0.2594
165	orf19.6570	NUP	1.5424	0.2659
184	orf19.3931	SFC1	1.4671	0.2680
203	orf19.700	SEO1	1.4102	0.2697
221	orf19.28	C2_06520C_A	1.3566	0.2714
246	orf19.3795	AGP3	1.2958	0.2702
278	orf19.23	RTA3	1.2449	0.2661
281	orf19.150	TIM17	1.2399	0.2727
301	orf19.4784	CRP1	1.1956	0.2727
304	orf19.5859	DAL8	1.1868	0.2790
305	orf19.1386	C2_09680W_A	1.1759	0.2860
314	orf19.1855	CR_06790C_A	1.1564	0.2898
317	orf19.918	CDR11	1.1521	0.2959
322	orf19.7447	JEN1	1.1493	0.3012
330	orf19.5121	OPT5	1.1367	0.3053
334	orf19.6532	C7_01880C_A	1.1270	0.3109
354	orf19.84	CAN3	1.0956	0.3104
362	orf19.1352	TIM22	1.0800	0.3142
372	orf19.4940	C1_13130C_A	1.0685	0.3171
379	orf19.1978	GIT2	1.0578	0.3212
399	orf19.5280	MUP1	1.0304	0.3203
415	orf19.3195	HIP1	1.0059	0.3207
420	orf19.3653	FAT1	0.9995	0.3251
424	orf19.5870	CTP1	0.9956	0.3299
441	orf19.5444	TIM44	0.9812	0.3297
450	orf19.2020	HGT6	0.9702	0.3325
451	orf19.7231	FTR2	0.9694	0.3383
462	orf19.6937	PTR22	0.9548	0.3402
483	orf19.5915	DUR35	0.9406	0.3384
485	orf19.6254	ANT1	0.9376	0.3435
504	orf19.309	DAL5	0.9209	0.3423

528	orf19.1393	C2_09610W_A	0.9008	0.3392
561	orf19.6956	DAL9	0.8726	0.3325
567	orf19.2021	HGT8	0.8705	0.3358
568	orf19.804	C2_04180C_A	0.8678	0.3409
579	orf19.6578	C7_01510W_A	0.8589	0.3423
615	orf19.2754	TIM13	0.8302	0.3343
635	orf19.5143	TIM54	0.8087	0.3321
638	orf19.5079	CDR4	0.8049	0.3361
655	orf19.2178	MRS4	0.7982	0.3349
667	orf19.5958	CDR2	0.7855	0.3355
671	orf19.1403	C2_09510C_A	0.7842	0.3390
698	orf19.2072	C2_00550W_A	0.7590	0.3339
703	orf19.5962	HGT4	0.7558	0.3369
726	orf19.7500	PXA1	0.7418	0.3332
733	orf19.1361	TIM23	0.7378	0.3353
737	orf19.2117	LEU5	0.7345	0.3385
741	orf19.1727	PMC1	0.7324	0.3418
748	orf19.4447	YMC1	0.7284	0.3439
754	orf19.941	SEC14	0.7263	0.3463
765	orf19.4583	C4_02080W_A	0.7224	0.3469
767	orf19.3700	TOM70	0.7212	0.3508
772	orf19.3234.1	SFT1	0.7184	0.3535
779	orf19.3526	ITR1	0.7151	0.3555
800	orf19.5672	MEP2	0.7055	0.3523
801	orf19.7565	GNP3	0.7050	0.3565
804	orf19.24	RTA2	0.7041	0.3599
832	orf19.6531.1	TOM7	0.6863	0.3540
853	orf19.4779	C1_09210C_A	0.6749	0.3506
858	orf19.2851	CR_02940C_A	0.6720	0.3531
872	orf19.2198	FLC3	0.6670	0.3522
875	orf19.7327	PHO88	0.6659	0.3554
915	orf19.4720	CTR2	0.6402	0.3448
916	orf19.4967	COX19	0.6401	0.3486
936	orf19.5599	MDL2	0.6316	0.3453
941	orf19.5720	C6_03540W_A	0.6297	0.3476
974	orf19.4118	CNT	0.6136	0.3394
989	orf19.3663	PHO91	0.6071	0.3378
991	orf19.6696	TIM9	0.6052	0.3410
997	orf19.1804	CR_04920W_A	0.6022	0.3427
1019	orf19.4174	C4_00680W_A	0.5892	0.3385
1023	orf19.2337	ALP1	0.5888	0.3408
1066	orf19.3981	MAL31	0.5652	0.3287
1084	orf19.2751	C4_02510W_A	0.5586	0.3257
1115	orf19.3696	TOM22	0.5433	0.3179

1242	orf19.3227	FTH2	0.4721	0.2742
1263	orf19.6209	C1_06980C_A	0.4553	0.2695
1272	orf19.6263	C1_06510C_A	0.4523	0.2692
1292	orf19.2633	HGT14	0.4453	0.2648
1325	orf19.3031	SEC62	0.4271	0.2555
1407	orf19.1027	PDR16	0.3576	0.2278
1425	orf19.2597	MRS2	0.3368	0.2235
1430	orf19.3900	C5_04170W_A	0.3313	0.2240
1446	orf19.6478	YCF1	-0.3083	0.2203
1494	orf19.1376	SSO2	-0.3734	0.2051
1514	orf19.3212	MID1	-0.3856	0.2004
1528	orf19.388	CAF16	-0.3992	0.1980
1546	orf19.5875	VAM3	-0.4110	0.1941
1554	orf19.1680	TFP1	-0.4179	0.1940
1570	orf19.3579	ATP4	-0.4249	0.1910
1618	orf19.1313	CDR3	-0.4519	0.1763
1699	orf19.2746	EMP70	-0.4987	0.1497
1730	orf19.1538	TLG2	-0.5139	0.1417
1745	orf19.2895	VMA8	-0.5188	0.1396
1792	orf19.7089	PMR1	-0.5400	0.1258
1798	orf19.1534	C2_02180W_A	-0.5426	0.1272
1809	orf19.1182	C6_00240C_A	-0.5468	0.1267
1877	orf19.5526	SEC20	-0.5880	0.1055
1897	orf19.2599	CRC1	-0.5979	0.1020
1929	orf19.2644	QCR2	-0.6107	0.0942
1933	orf19.459	ADP1	-0.6124	0.0967
1992	orf19.5880	C3_04360W_A	-0.6325	0.0790
2008	orf19.4954	C1_13280C_A	-0.6405	0.0773
2011	orf19.7056	C7_00630C_A	-0.6409	0.0803
2036	orf19.405	VCX1	-0.6548	0.0753
2039	orf19.4456	GAP4	-0.6561	0.0785
2055	orf19.7354	LAC1	-0.6662	0.0769
2083	orf19.7483	CRM1	-0.6851	0.0710
2086	orf19.5052	C1_07820W_A	-0.6879	0.0743
2092	orf19.645.1	VMA13	-0.6896	0.0765
2111	orf19.1866	VMA10	-0.6993	0.0740
2118	orf19.6634	VMA2	-0.7022	0.0759
2143	orf19.30	SPF1	-0.7144	0.0713
2155	orf19.2158	NAG3	-0.7250	0.0715
2187	orf19.7086	C7_00340C_A	-0.7426	0.0645
2195	orf19.333	FCY2	-0.7456	0.0663
2208	orf19.6656	C5_03480C_A	-0.7507	0.0663
2288	orf19.7578	CR_10020C_A	-0.7960	0.0419
2303	orf19.337	VTI1	-0.8058	0.0415

2351	orf19.1585	ZRT2	-0.8383	0.0291
2361	orf19.2598	VMA4	-0.8448	0.0307
2366	orf19.1614	MEP1	-0.8508	0.0343
2424	orf19.4733	YMC2	-0.8997	0.0186
2436	orf19.1979	GIT3	-0.9088	0.0199
2461	orf19.5926	ARG11	-0.9352	0.0166
2464	orf19.479.2	SEC22	-0.9387	0.0214
2475	orf19.806	VMA7	-0.9495	0.0233
2560	orf19.3249	LAG1	-1.0289	-0.0016
2567	orf19.4655	OPT6	-1.0420	0.0023
2582	orf19.4384	HXT5	-1.0530	0.0034
2627	orf19.2397	CR_03270W_A	-1.1058	-0.0063
2633	orf19.2587	HNM3	-1.1091	-0.0016
2656	orf19.4690	C4_00990W_A	-1.1405	-0.0030
2677	orf19.5428	C3_00390W_A	-1.1787	-0.0034
2704	orf19.644	HGT9	-1.2417	-0.0057
2807	orf19.3646	CTR1	-1.5788	-0.0340
2812	orf19.5017	DUR32	-1.5890	-0.0261
2816	orf19.4449	CCS1	-1.6287	-0.0176
2826	orf19.2425	HGT18	-1.7046	-0.0108
2859	orf19.7331	FCY24	-2.2699	-0.0092
2866	orf19.1395	C2_09590C_A	-2.4346	0.0030

AMINO ACID TRANSPORT_BIO

Rank in Gene List	Gene Identifier	Gene Name	Log2 Fold Change	Running Enrichment Score
0	orf19.6993	GAP2	4.6048	0.1824
41	orf19.97	CAN1	2.3381	0.2610
44	orf19.2810	AAP1	2.3154	0.3521
82	orf19.111	CAN2	1.9617	0.4168
94	orf19.7566	CR_09920W_A	1.8869	0.4877
106	orf19.4304	GAP1	1.8272	0.5563
126	orf19.4063	GPT1	1.6901	0.6166
246	orf19.3795	AGP3	1.2958	0.6263
354	orf19.84	CAN3	1.0956	0.6323
372	orf19.4940	C1_13130C_A	1.0685	0.6686
399	orf19.5280	MUP1	1.0304	0.7004
415	orf19.3195	HIP1	1.0059	0.7350
801	orf19.7565	GNP3	0.7050	0.6282
1023	orf19.2337	ALP1	0.5888	0.5742
1134	orf19.5994	RHB1	0.5315	0.5567
2011	orf19.7056	C7_00630C_A	-0.6409	0.2756

2039	orf19.4456	GAP4	-0.6561	0.2922

CARBOHYDRATE TRANSPORTER ACTIVITY_MOL

Rank in Gene List	Gene Identifier	Gene Name	Log2 Fold Change	Running Enrichment Score
39	orf19.2023	HGT7	2.3851	0.0994
49	orf19.7094	HGT12	2.2631	0.2035
52	orf19.7093	HGT13	2.2362	0.3088
111	orf19.1587	HGT20	1.7944	0.3736
118	orf19.3668	HGT2	1.7445	0.4541
144	orf19.4682	HGT17	1.6299	0.5226
450	orf19.2020	HGT6	0.9702	0.4619
567	orf19.2021	HGT8	0.8705	0.4626
703	orf19.5962	HGT4	0.7558	0.4512
779	orf19.3526	ITR1	0.7151	0.4589
1066	orf19.3981	MAL31	0.5652	0.3856
1292	orf19.2633	HGT14	0.4453	0.3280
2155	orf19.2158	NAG3	-0.7250	0.0609
2582	orf19.4384	HXT5	-1.0530	-0.0382
2704	orf19.644	HGT9	-1.2417	-0.0217
2826	orf19.2425	HGT18	-1.7046	0.0168

KETOCONAZOLE_UP

Rank in Gene List	Gene Identifier	Gene Name	Log2 Fold Change	Running Enrichment Score
0	orf19.6993	GAP2	4.6048	0.0318
3	orf19.4335	TNA1	3.3619	0.0542
18	orf19.7585	INO1	2.7086	0.0678
25	orf19.5604	MDR1	2.5564	0.0833
32	orf19.2701	C4_02930W_A	2.4462	0.0979
36	orf19.699	CR_06650C_A	2.4119	0.1135
38	orf19.670.2	C1_11320C_A	2.3900	0.1296
48	orf19.2809	CTN3	2.2853	0.1421
67	orf19.1449	C2_01450C_A	2.1093	0.1501
82	orf19.111	CAN2	1.9617	0.1585
83	orf19.3674	GAL102	1.9457	0.1720
94	orf19.7566	CR_09920W_A	1.8869	0.1813
96	orf19.5069	C1_07980C_A	1.8814	0.1940
101	orf19.1438	C4_03340C_A	1.8594	0.2053
115	orf19.4551	CTN1	1.7587	0.2127

118	orf19.3668	HGT2	1.7445	0.2240
131	orf19.6844	ICL1	1.6773	0.2312
140	orf19.3548.1	WH11	1.6394	0.2396
144	orf19.4682	HGT17	1.6299	0.2498
154	orf19.4833	MLS1	1.5673	0.2573
157	orf19.5307	JEN2	1.5563	0.2673
167	orf19.1224	FRP3	1.5343	0.2746
169	orf19.4539	C1_01840C_A	1.5256	0.2848
172	orf19.4445	C1_07220W_A	1.5197	0.2946
175	orf19.4506	LYS22	1.5066	0.3042
184	orf19.3931	SFC1	1.4671	0.3114
196	orf19.4041	PEX4	1.4462	0.3174
209	orf19.3675	GAL7	1.3944	0.3227
215	orf19.6267	C1_06430C_A	1.3724	0.3303
236	orf19.5975	TRY4	1.3208	0.3322
271	orf19.3672	GAL10	1.2536	0.3285
278	orf19.23	RTA3	1.2449	0.3349
285	orf19.272	FAA21	1.2320	0.3412
286	orf19.4591	CAT2	1.2297	0.3497
293	orf19.3733	IDP2	1.2096	0.3558
308	orf19.6169	ATO1	1.1735	0.3588
340	orf19.6306	CR_04870C_A	1.1171	0.3553
355	orf19.740	HAP41	1.0953	0.3578
369	orf19.2652	TEF4	1.0727	0.3604
416	orf19.3670	GAL1	1.0030	0.3506
438	orf19.449	C1_05160C_A	0.9844	0.3498
455	orf19.5094	BUL1	0.9611	0.3506
464	orf19.5636	RBT5	0.9526	0.3543
485	orf19.6254	ANT1	0.9376	0.3535
500	orf19.3684	C1_02270C_A	0.9253	0.3548
545	orf19.4716	GDH3	0.8862	0.3449
619	orf19.6838	C1_04460C_A	0.8236	0.3241
636	orf19.4894	C1_10240C_A	0.8084	0.3239
644	orf19.6928	SAP9	0.8038	0.3269
656	orf19.3661	C1_02040C_A	0.7964	0.3284
662	orf19.638	FDH1	0.7929	0.3320
674	orf19.7296	SLP3	0.7825	0.3334
682	orf19.7469	ARG1	0.7771	0.3362
703	orf19.5962	HGT4	0.7558	0.3342
704	orf19.278	C3_02870C_A	0.7557	0.3394
726	orf19.7500	PXA1	0.7418	0.3369
741	orf19.1727	PMC1	0.7324	0.3368
779	orf19.3526	ITR1	0.7151	0.3283
781	orf19.1704	FOX3	0.7134	0.3329

802	orf19.6311	CR_04820W_A	0.7049	0.3305
804	orf19.24	RTA2	0.7041	0.3350
806	orf19.6445	ECI1	0.7032	0.3395
807	orf19.5215	TES15	0.7027	0.3443
822	orf19.5806	ALD5	0.6926	0.3440
826	orf19.5635	PGA7	0.6885	0.3477
890	orf19.2459	C1_05900W_A	0.6547	0.3293
898	orf19.6143	CR_07250C_A	0.6483	0.3312
998	orf19.3544	C2_05130W_A	0.6020	0.2994
1018	orf19.1288	FOX2	0.5924	0.2966
1066	orf19.3981	MAL31	0.5652	0.2835
1075	orf19.1800	C4_05440C_A	0.5613	0.2844
1078	orf19.3369	MOH1	0.5601	0.2876
1125	orf19.1652	POX1-3	0.5383	0.2746
1126	orf19.4274	PUT1	0.5375	0.2783
1130	orf19.732	CR_07170W_A	0.5343	0.2809
1167	orf19.4504	C2_04480W_A	0.5177	0.2714
1178	orf19.2887	C4_06470W_A	0.5114	0.2713
1288	orf19.7520	POT1	0.4463	0.2348
1299	orf19.3770	ARG8	0.4428	0.2342
1502	orf19.6840	C1_04470C_A	-0.3775	0.1634
1658	orf19.3282	BMT3	-0.4723	0.1104
1739	orf19.2909	ERG26	-0.5168	0.0849
1812	orf19.2515	C3_01130C_A	-0.5487	0.0626
1840	orf19.4476	C1_04010C_A	-0.5694	0.0567
1841	orf19.260	SLD1	-0.5694	0.0606
1870	orf19.1631	ERG6	-0.5853	0.0545
1874	orf19.192	C2_04750W_A	-0.5875	0.0574
1896	orf19.1237	ARO9	-0.5971	0.0539
1973	orf19.6117	CR_07480W_A	-0.6246	0.0306
2000	orf19.4706	C4_00860C_A	-0.6382	0.0256
2042	orf19.1985	CR_07700W_A	-0.6587	0.0153
2044	orf19.2030	C2_00940W_A	-0.6589	0.0194
2068	orf19.7448	LYS9	-0.6746	0.0157
2158	orf19.5645	MET15	-0.7261	-0.0116
2188	orf19.4979	KNS1	-0.7426	-0.0170
2218	orf19.4135	PRC2	-0.7538	-0.0223
2321	orf19.6757	GCY1	-0.8170	-0.0537
2491	orf19.7350	RCT1	-0.9633	-0.1084
2504	orf19.3615	C2_08620W_A	-0.9711	-0.1061
2548	orf19.5379	ERG4	-1.0173	-0.1147
2571	orf19.5525	C6_02560W_A	-1.0454	-0.1155
2582	orf19.4384	HXT5	-1.0530	-0.1118
2587	orf19.428	C1_05370C_A	-1.0558	-0.1060

2598	orf19.675	C1_11270W_A	-1.0678	-0.1023
2648	orf19.6229	CAT1	-1.1311	-0.1123
2671	orf19.5614	C6_03260W_A	-1.1642	-0.1122
2682	orf19.6081	PHR2	-1.1904	-0.1077
2686	orf19.4477	CSH1	-1.2046	-0.1004
2687	orf19.251	GLX3	-1.2052	-0.0921
2692	orf19.1344	C7_03310W_A	-1.2123	-0.0852
2709	orf19.6139	FRE7	-1.2508	-0.0824
2728	orf19.2496	ATO2	-1.3134	-0.0799
2745	orf19.7504	CR_00290W_A	-1.3445	-0.0764
2756	orf19.677	CHO1	-1.3670	-0.0706
2796	orf19.6350	C1_12720C_A	-1.5284	-0.0743
2810	orf19.3932	C5_04470C_A	-1.5870	-0.0680
2813	orf19.4255	ECM331	-1.5893	-0.0578
2854	orf19.4082	DDR48	-2.1597	-0.0574
2857	orf19.7111.1	SOD3	-2.2003	-0.0430
2863	orf19.3210	C5_04010C_A	-2.3082	-0.0289
2874	orf19.1691	C3_01540W_A	-4.7146	0.0000

Gene sets with genes enriched in the downregulated group of differentially expressed genes

These gene sets are for pathways which the GSEA concluded are significantly downregulated within 5% CO_2 biofilms. The rank in gene list refers to the position of the gene in the overall list of significantly differentially expressed genes in this study ranked with regards to log2 fold change. The running enrichment score is a running tally as a quantitative measure of how much each gene contributes to the overall gene set/pathway being downregulated as measured via GSEA. Genes which cause the running enrichment score to increase, known as the leading edge subset (green – subsequent to the lowest enrichment score), are those which have the greatest contribution to the overall enrichment at the bottom of the ranked list.

HYPHAE_FBS_37_UP

Rank in Gene List	Gene Identifier	Gene Name	Log2 Fold Change	Running Enrichment Score
146	orf19.1996	CHA1	1.6194	-0.0158
694	orf19.3478	NIP7	0.7620	-0.1914
880	orf19.5025	MET3	0.6624	-0.2419
1848	orf19.4666	C4_01230C_A	-0.5718	-0.5694
2039	orf19.4456	GAP4	-0.6561	-0.6218
2224	orf19.7127	TLO16	-0.7578	-0.6699
2292	orf19.7610	PTP3	-0.7979	-0.6759
2309	orf19.2769	C4_02340W_A	-0.8076	-0.6638
2371	orf19.6078	POL93	-0.8557	-0.6665
2529	orf19.2903	AGO1	-0.9934	-0.6803
2625	orf19.113	CIP1	-1.1047	-0.6894
2675	orf19.3844	MRP8	-1.1741	-0.6809
2681	orf19.3374	ECE1	-1.1833	-0.6567
2691	orf19.2060	SOD5	-1.2121	-0.6333
2701	orf19.5716	SAP4	-1.2287	-0.6095
2702	orf19.1321	HWP1	-1.2354	-0.5824
2774	orf19.2274	C2_07180W_A	-1.4185	-0.5762
2788	orf19.3150	GRE2	-1.4957	-0.5479
2799	orf19.4054	CTA24	-1.5406	-0.5176
2808	orf19.2241	PST1	-1.5798	-0.4858
2811	orf19.125	EBP1	-1.5887	-0.4516
2815	orf19.3074	TLO10	-1.6051	-0.4175
2829	orf19.2685	PGA54	-1.7209	-0.3843
2833	orf19.6021	IHD2	-1.7682	-0.3465
2850	orf19.6601.1	YKE2	-2.0442	-0.3073
2854	orf19.4082	DDR48	-2.1597	-0.2610
2864	orf19.3460	C6_02200C_A	-2.3208	-0.2132
2869	orf19.5674	PGA10	-2.5161	-0.1594
2870	orf19.7544	TLO1	-2.5977	-0.1024
2874	orf19.1691	C3_01540W_A	-4.7146	0.0000

CYTOSKELETON_CEL

Rank in Gene List	Gene Identifier	Gene Name	Log2 Fold Change	Running Enrichment Score
402	orf19.6770	C3_07280C_A	1.0229	-0.1265
558	orf19.4257	INT1	0.8747	-0.1671
770	orf19.3115	C4_06940C_A	0.7191	-0.2304
776	orf19.712	KIP1	0.7156	-0.2201

896	orf19.670	SMT3	0.6502	-0.2516
1029	orf19.3295	C1_01070C_A	0.5854	-0.2889
1048	orf19.7450	C3_06610W_A	0.5722	-0.2857
1201	orf19.2925	C1_02380C_A	0.4943	-0.3317
1285	orf19.1671	UTR2	0.4467	-0.3538
1422	orf19.3206	CCT7	0.3424	-0.3966
1465	orf19.4927	BNI1	-0.3449	-0.4058
1472	orf19.4308	HSL1	-0.3497	-0.4020
1499	orf19.2911	SEC3	-0.3755	-0.4050
1516	orf19.7201	SLA2	-0.3884	-0.4041
1563	orf19.2519	CR_01360W_A	-0.4213	-0.4135
1607	orf19.4184	C4_00590C_A	-0.4463	-0.4213
1646	orf19.7537	BNR1	-0.4643	-0.4270
1663	orf19.3647	SEC8	-0.4737	-0.4247
1681	orf19.5007	ACT1	-0.4870	-0.4225
1750	orf19.5015	MYO2	-0.5204	-0.4381
1780	orf19.4557	C6_04120C_A	-0.5361	-0.4394
1784	orf19.1474	SLA1	-0.5389	-0.4313
1791	orf19.3251	ARC19	-0.5400	-0.4243
1836	orf19.4203	C6_00560W_A	-0.5675	-0.4304
1855	orf19.564	KAR3	-0.5771	-0.4271
1861	orf19.6598	WAL1	-0.5799	-0.4191
1880	orf19.5463	SEC6	-0.5893	-0.4155
1895	orf19.7377	ASE1	-0.5961	-0.4105
1900	orf19.3667	C1_02100W_A	-0.5992	-0.4017
1915	orf19.3013	CDC12	-0.6048	-0.3965
1917	orf19.6151	ARC15	-0.6057	-0.3866
1978	orf19.5265	KIP4	-0.6268	-0.3975
1980	orf19.7293	MPS1	-0.6269	-0.3872
1981	orf19.1698	C3_01510W_A	-0.6269	-0.3766
2002	orf19.3919	C5_04320C_A	-0.6391	-0.3729
2006	orf19.3680	SEP1	-0.6400	-0.3632
2024	orf19.5595	SHE3	-0.6492	-0.3583
2060	orf19.1418	SEC15	-0.6684	-0.3595
2085	orf19.5544	SAC6	-0.6878	-0.3564
2088	orf19.5691	CDC11	-0.6891	-0.3455
2110	orf19.6479	SEC1	-0.6991	-0.3411
2148	orf19.1223	DBF2	-0.7173	-0.3422
2152	orf19.6512	EXO70	-0.7208	-0.3311
2171	orf19.3001	TEM1	-0.7323	-0.3251
2226	orf19.6414.3	TPM2	-0.7599	-0.3316
2227	orf19.7292	ARP2	-0.7602	-0.3187
2235	orf19.3269	GSL2	-0.7648	-0.3083
2239	orf19.548	CDC10	-0.7654	-0.2964

2252	orf19.3873	ARC40	-0.7714	-0.2876
2256	orf19.505	SRV2	-0.7728	-0.2756
2283	orf19.2289	ARP3	-0.7895	-0.2716
2311	orf19.953.1	COF1	-0.8111	-0.2675
2313	orf19.2480.1	AUT7	-0.8121	-0.2541
2320	orf19.4395	CR_03520C_A	-0.8165	-0.2424
2332	orf19.3976	C5_04890C_A	-0.8273	-0.2324
2336	orf19.7308	TUB1	-0.8291	-0.2194
2356	orf19.2642	C5_03370C_A	-0.8402	-0.2120
2365	orf19.6349	RVS162	-0.8493	-0.2004
2400	orf19.1220	RVS167	-0.8758	-0.1978
2407	orf19.6148	CR_07220C_A	-0.8816	-0.1850
2457	orf19.6536	IQG1	-0.9316	-0.1868
2473	orf19.5664	HOF1	-0.9463	-0.1761
2484	orf19.6168	C3_00910W_A	-0.9551	-0.1635
2487	orf19.1747	KIP2	-0.9596	-0.1480
2499	orf19.486	NIP100	-0.9673	-0.1355
2517	orf19.2416.1	MLC1	-0.9818	-0.1250
2519	orf19.3086	SEC10	-0.9840	-0.1087
2547	orf19.6034	TUB2	-1.0160	-0.1012
2550	orf19.2641	ARP1	-1.0180	-0.0847
2563	orf19.2190	VRP1	-1.0340	-0.0714
2570	orf19.1055	CDC3	-1.0434	-0.0559
2578	orf19.2699	ABP1	-1.0507	-0.0406
2600	orf19.6010	CDC5	-1.0694	-0.0300
2632	orf19.2228	C2_06770W_A	-1.1086	-0.0224
2673	orf19.4837	DAM1	-1.1666	-0.0169
2693	orf19.7079	C7_00410C_A	-1.2125	-0.0032
2698	orf19.5827	BUB2	-1.2221	0.0161
2744	orf19.676	C1_11250W_A	-1.3444	0.0227
2763	orf19.6242	CYK3	-1.3834	0.0397

G1-S CLUSTER

Rank in Gene List	Gene Identifier	Gene Name	Log2 Fold Change	Running Enrichment Score
194	orf19.2133	LIP4	1.4493	-0.0522
438	orf19.449	C1_05160C_A	0.9844	-0.1277
495	orf19.7394	GDA1	0.9279	-0.1365
499	orf19.1880	HEM15	0.9255	-0.1263
519	orf19.1736	CR_04680C_A	0.9104	-0.1220
624	orf19.2302	C1_11140W_A	0.8169	-0.1495
629	orf19.1888	C2_07430C_A	0.8144	-0.1410

727	orf19.4959	C1_13320C_A	0.7415	-0.1669
729	orf19.3694	C1_02370C_A	0.7402	-0.1582
795	orf19.5551	MIF2	0.7086	-0.1729
799	orf19.2347	MNN2	0.7060	-0.1654
975	orf19.7564	DPB2	0.6134	-0.2209
1054	orf19.1666	C3_01800C_A	0.5686	-0.2421
1197	orf19.7083	DCC1	0.4972	-0.2872
1270	orf19.3715	ASF1	0.4536	-0.3076
1405	orf19.4603	ARL1	0.3596	-0.3514
1437	orf19.926	EXO1	0.3202	-0.3587
1454	orf19.1777	C2_10050W_A	-0.3269	-0.3605
1460	orf19.5147	LMO1	-0.3392	-0.3581
1463	orf19.5089	TERT	-0.3417	-0.3547
1472	orf19.4308	HSL1	-0.3497	-0.3533
1492	orf19.4105	CSM3	-0.3709	-0.3556
1518	orf19.2216	PDS5	-0.3915	-0.3598
1524	orf19.7224	C1_14170W_A	-0.3977	-0.3567
1569	orf19.5804	HYU1	-0.4241	-0.3674
1581	orf19.1605	PMS1	-0.4303	-0.3661
1643	orf19.1390	PMI1	-0.4633	-0.3824
1703	orf19.7186	CLB4	-0.5005	-0.3976
1742	orf19.7106	VPS70	-0.5184	-0.4049
1758	orf19.652	CR_05010W_A	-0.5240	-0.4039
1783	orf19.7065	PSF3	-0.5377	-0.4060
1803	orf19.771	LPG20	-0.5448	-0.4062
1811	orf19.7631	SLD5	-0.5479	-0.4020
1876	orf19.658	GIN1	-0.5877	-0.4178
1900	orf19.3667	C1_02100W_A	-0.5992	-0.4188
1908	orf19.4136	YBL053	-0.6030	-0.4140
1937	orf19.3319	C1_01300W_A	-0.6131	-0.4165
1943	orf19.3266	CR_00880W_A	-0.6147	-0.4108
1959	orf19.3322	DUT1	-0.6198	-0.4086
1977	orf19.4945	MSH6	-0.6250	-0.4071
2003	orf19.6049	C1_00570C_A	-0.6392	-0.4083
2005	orf19.1208	C4_03990C_A	-0.6397	-0.4009
2022	orf19.6671	LAP4	-0.6465	-0.3987
2024	orf19.5595	SHE3	-0.6492	-0.3911
2042	orf19.1985	CR_07700W_A	-0.6587	-0.3892
2045	orf19.4712	FGR6-3	-0.6599	-0.3818
2047	orf19.6434	PEX19	-0.6610	-0.3741
2057	orf19.1889	C2_07420W_A	-0.6673	-0.3692
2070	orf19.7634	MCD1	-0.6771	-0.3652
2091	orf19.262	SMC3	-0.6895	-0.3640
2096	orf19.7632	CR_10530W_A	-0.6922	-0.3570

2107	orf19.4616	POL30	-0.6973	-0.3521
2121	orf19.5775	C6_03990C_A	-0.7036	-0.3481
2122	orf19.6670	CAC2	-0.7039	-0.3395
2123	orf19.2267	RFA2	-0.7042	-0.3309
2167	orf19.7425	C3_06400C_A	-0.7301	-0.3375
2222	orf19.7409	ERV25	-0.7568	-0.3477
2237	orf19.5191	FGR6-1	-0.7650	-0.3434
2238	orf19.3239	CTF18	-0.7652	-0.3340
2239	orf19.548	CDC10	-0.7654	-0.3247
2257	orf19.4346	C5_03140C_A	-0.7731	-0.3213
2276	orf19.1340	C7_03350C_A	-0.7857	-0.3182
2282	orf19.7494	MMS22	-0.7892	-0.3103
2285	orf19.4162	MLH1	-0.7916	-0.3014
2288	orf19.7578	CR_10020C_A	-0.7960	-0.2924
2293	orf19.3581	C2_05510C_A	-0.7981	-0.2840
2312	orf19.5041	C4_03860C_A	-0.8118	-0.2806
2314	orf19.1823	C1_06270W_A	-0.8134	-0.2710
2322	orf19.5622	GLC3	-0.8172	-0.2635
2364	orf19.1427	C4_04230W_A	-0.8491	-0.2679
2380	orf19.6813	C3_06880W_A	-0.8617	-0.2628
2383	orf19.3501	C6_02090C_A	-0.8633	-0.2529
2384	orf19.5841	C2_02660W_A	-0.8644	-0.2424
2408	orf19.3296	C1_01080W_A	-0.8844	-0.2398
2435	orf19.1825	C1_06250W_A	-0.9073	-0.2381
2444	orf19.687	C6_01960W_A	-0.9151	-0.2298
2471	orf19.2093	RFA1	-0.9454	-0.2276
2479	orf19.338	C3_03410C_A	-0.9523	-0.2185
2485	orf19.2029	RFC5	-0.9578	-0.2086
2486	orf19.2863	CR_03000C_A	-0.9590	-0.1968
2503	orf19.4830	C1_09670C_A	-0.9706	-0.1907
2535	orf19.3490	FGR6-4	-1.0024	-0.1896
2539	orf19.727	CR_06380C_A	-1.0036	-0.1784
2540	orf19.6247	C1_06630W_A	-1.0064	-0.1661
2575	orf19.4664	NAT4	-1.0485	-0.1656
2581	orf19.3649	C6_00760W_A	-1.0528	-0.1545
2584	orf19.5579	C6_03000C_A	-1.0548	-0.1423
2626	orf19.7453	C3_06640W_A	-1.1051	-0.1436
2630	orf19.2657	C5_03210C_A	-1.1067	-0.1311
2634	orf19.3093	MSH2	-1.1103	-0.1186
2653	orf19.1738	UGP1	-1.1394	-0.1111
2694	orf19.4867	SWE1	-1.2140	-0.1107
2708	orf19.403	PCL2	-1.2505	-0.1001
2762	orf19.244	DCG1	-1.3790	-0.1023
2776	orf19.3207	CCN1	-1.4235	-0.0896

2808	orf19.2241	PST1	-1.5798	-0.0814
2813	orf19.4255	ECM331	-1.5893	-0.0634
2851	orf19.2649	PCL1	-2.0641	-0.0515
2865	orf19.7017	YOX1	-2.3578	-0.0274
2868	orf19.3740	PGA23	-2.4731	0.0022